

Choroidal Structure and Function in Chronic Retinal Diseases

Thesis submitted in accordance with the requirements of the University of Liverpool for the degree of Doctor in Philosophy

by

Nattapon Boonarpa

January 2016

To my mother

Abstract

Introduction

The choroid plays an important role in maintaining retinal homeostasis. Changes in choroidal structure and a failure of choroidal autoregulation (the ability of a vascular bed to maintain blood flow despite changes in perfusion pressure) may have a great consequence in the pathogenesis of several chronic chorioretinal diseases including diabetic retinopathy (DR) and central serous chorioretinopathy (CSCR).

Aim

The main aim of this thesis is to study the structure and function of the choroid and determine its role in the pathogenesis of DR and CSCR using enhanced depth imaging optical coherence tomography (EDI OCT) and laser Doppler flowmetry (LDF).

Methods

A protocol for standardising the choroidal thickness (ChT) measurement using topographical appearances of the choroidal posterior boundary was developed and validated on EDI OCT images from healthy volunteers and patients with DR. Extensive experiments were performed in order to validate the hardware and software of the LDF device.

Two controlled prospective studies were designed and performed; 1) Diabetic Retinopathy: Functional and Structural Study (DREFUS Study), and 2) Liverpool Central Serous Chorioretinopathy study (Liverpool CSCR Study). The DREFUS study involved diabetic patients with/without DR and healthy volunteers. DR patients were grouped using the presence or absence of clinically significant macular oedema (CSMO). The Liverpool CSCR study included patients presented with CSCR and healthy volunteers.

For both of the studies the ChT was measured using a single horizontal EDI OCT scan while the choroidal blood flow (ChBFlow) parameters (choroidal blood volume [ChBVolume] and velocity [ChBVelocity]) were measured by using LDF. Isometric exercise was used to test choroidal autoregulation function. Mean arterial BP (MAP), ocular perfusion pressure (OPP) and change in choroidal vascular resistance were calculated to evaluate the choroidal autoregulation. In addition, best corrected visual acuity (BCVA), blood pressure (BP), colour fundus photography, fluorescein angiography (FA), and OCT were performed. Other tests including indocyanine green angiography (ICG), volumetric EDI OCT scans, microperimetry, intraocular pressure, and axial length were only performed by the CSCR study.

Statistical analyses (correlation, t-test, ANOVA, ANCOVA, intraclass correlation coefficient [ICC], Fisher exact test, Mann-Whitney test) were performed as appropriate.

Results

The standardised protocol for ChT measurement was produced. ICC for interobserver and intraobserver agreements on ChT measurements using of the protocol were 0.96 and 0.99 respectively for healthy eyes (n = 12) and 0.97 and 0.99 respectively for eyes with DR (n = 46).

The mean subfoveal ChT (SfChT) was 304 μm (95% confidence interval (CI): 282 – 326) for patients with DR (N = 61). There were no significant differences in ChT between healthy eyes (N = 41; 351 μm (95% CI: 321 – 381)), diabetic eyes (N = 12; 299.9 μm (95% CI: 248.7 - 351.2) and eyes with DR ($P > 0.05$). A statistically significant increase in ChBVelocity by 8% was observed following an increase of MAP by 18% in DR with CSMO.

The mean SfChT of CSCR patients (N = 45) was 468.5 μm (95% CI: 437.1 – 499.9), approximately 30% thicker than in healthy eyes (N = 25; 361.4 μm (95% CI: 319.8 – 402.2) ($P < 0.05$). Hypertension was identified as the main risk factor affecting ChT in CSCR, particularly during the active stage of CSCR (normotensive CSCR: SfChT = 431 μm (95% CI: 378 – 485) vs hypertensive CSCR: SfChT = 521 μm (95% CI: 468 – 574): $P < 0.05$). An increase in OPP by 40% caused the ChT to increase significantly in CSCR patient (435.3 μm (95% CI: 378.2 - 492.4) at baseline vs 446.3 μm (95% CI: 393.4 - 499.2) at the end of exercise; $P < 0.05$). An increase of OPP by 31% caused significant change in ChBVolume in CSCR patients compared to healthy eyes ($P = 0.03$). Changes in ChBVolume in CSCR patients were negatively correlated with changes in choroidal vascular resistance ($r = -0.83$, $P < 0.05$).

Conclusions

In patients with diabetes, no significant changes in the ChT were observed in any group of DR patients. ChBVelocity regulation was impaired in patients with severe DR. These findings suggest that functional changes of the choroid may occur well before the structural changes in patients with DR.

In CSCR patients, increases in ChT and choroidal volume were observed in all CSCR phenotypes and also related with hypertension and the area of choroidal vascular hyperpermeability seen on ICG. The disruption of the regulation of choroidal structure and function was observed during isometric exercise in CSCR patients.

These findings highlight the significance of choroidal regulation in the pathogenesis of DR and CSCR.

Acknowledgements

The completion of this thesis would have not been possible without the help in one way or another from several contributors, some more professional, some more personal, who have made my journey and my time at the Department of Eye and Vision Science and St Paul's Eye Unit, Royal Liverpool University Hospital, easier.

First and foremost, I would like to express my sincere gratitude to my primary supervisor, Dr Yalin Zheng, and my secondary supervisors, Mrs Jayashree Sahni and Professor Simon Harding, for their knowledge and support throughout my PhD and their patience, guidance, and endless help to finish this thesis. Without their invaluable support, persistent help and critical advice, this thesis would not have been possible.

I would like to also sincerely thank Professor Martial Geiser and Professor Charles Riva for their advice and guidance with the LDF, especially for making me understand better how the instrument works and the interpretation of the results; without their advice, the LDF part of this thesis would not have been possible.

I would like to especially thank Mrs Valerie Tompkin, senior research optometrist, who has immensely helped me with the vision tests for my study and Dr Ankur Raj for allowing me to use parts of his DREFUS data to complete this thesis. I would like to thank Dr Gabriela Czanner for sharing her knowledge and guidance in the statistical analyses of the data, at times not straightforward!

I would also like to thank Annmarie and her team for keeping up with me and helping me with the patient's appointments and Steve, Jerry and the photographer team for the training and for providing me with their ophthalmic imaging knowledge and time off work for writing up my thesis. I would like to thank ophthalmologists and nurses at St Paul's Eye Unit, all of you have been there to support me when I recruited patients and collected data for my PhD.

This thesis and my PhD journey would not be possible without the support from my Thai and Spanish family and especially my partner, thank you for supporting me through my grumpy times!

Lastly, I would like to thank the Foundation for the Prevention of Blindness for the research funding throughout my PhD.

Table of contents

Abstract	II
Acknowledgement	IV
List of Figures	XII
List of Tables	XXII
List of Equations	XXV
Abbreviations	XXVI
1 Introduction	1
1.1 Background	3
1.2 The choroid	3
1.2.1 Choroidal anatomy	4
1.2.1.1 Bruch’s membrane (BM).....	4
1.2.1.2 The choroidal vascular system	5
1.2.1.3 Choriocapillaris.....	7
1.2.1.4 Suprachoroid.....	10
1.2.1.5 Choroidal nervous system	10
1.2.1.6 Choroidal lymphatic system.....	10
1.3 Choroidal function.....	11
1.3.1 Oxygen provision.....	11
1.3.2 Retinal temperature regulation.....	12
1.3.3 Retinal nutrient, waste and fluid transportation	14
1.3.4 Choroidal autoregulation.....	14
1.4 PhD research motivation	15
1.5 Aims	15
1.6 Outline of the thesis.....	16
1.7 Summary	16
2 Literature review	17
2.1 Background	18
2.2 How can the structure of the choroid be studied?	18
2.3 Optical coherence tomography	19
2.3.1 Time domain optical coherence tomography	22
2.3.2 Spectral domain optical coherence tomography (SD OCT).....	23
2.3.3 Enhanced depth imaging optical coherence tomography	24
2.3.3.1 Principles of EDI OCT	24

2.3.4	Swept-source optical coherence tomography	27
2.4	Choroidal imaging with EDI OCT	28
2.4.1	The appearance of the choroidal structure on EDI OCT scans	28
2.4.2	Measurement of choroidal thickness in healthy eyes	30
2.4.3	Asymmetric nature of the choroid	34
2.4.4	Diurnal variation of the choroid	35
2.4.5	Factors correlated with choroidal thickness	38
2.4.6	Summary of EDI OCT	39
2.5	How can the function of the choroid be studied?	40
2.6	Laser Doppler flowmetry	42
2.6.1	Basic principle of LDF	44
2.6.2	LDF systems	46
2.6.2.1	Fundus camera-based near infrared LDF	46
2.6.2.2	Compact LDF	48
2.6.2.3	Helmet-mounted LDF	49
2.6.3	Application of LDF to measure ChBFlow in response to physiological stimuli in healthy eyes	50
2.6.3.1	Effect of ocular perfusion pressure on ChBFlow	50
2.6.3.2	Effect of blood gases on ChBFlow	52
2.6.3.3	Effect of light on ChBFlow	53
2.6.3.4	Effect of postural changes on ChBFlow	55
2.6.3.5	Effect of ageing on ChBFlow	56
2.6.4	Response of ChBFlow to pharmaceutical agents	56
2.6.5	Other applications of LDF	59
2.6.6	Summary of LDF	59
2.7	Other ocular fundus imaging techniques for the ocular fundus	61
2.7.1	Indocyanine green angiography (ICGA)	61
2.7.2	Fundus autofluorescence imaging	61
2.7.3	Near infrared autofluorescence imaging	63
2.7.4	Microperimetry	64
2.8	Diabetic retinopathy	65
2.8.1	Study of choroidal structure using EDI OCT in diabetic retinopathy ...	69
2.8.2	Study of ChBFlow using LDF in diabetic retinopathy	71
2.9	Central serous chorioretinopathy	71
2.9.1	Studies of choroidal structure using EDI OCT in central serous chorioretinopathy	77

2.9.2	Studies of ChBFlow using LDF in central serous chorioretinopathy ...	78
2.10	Summary	79
3	Validation of EDI OCT and LDF.....	81
3.1	Background	82
3.2	Standardisation of choroidal thickness measurements using EDI OCT	82
3.2.1	Subjects and methods	83
3.2.1.1	Subjects	83
3.2.1.2	Standardised protocol for defining choroidal margins	84
3.2.1.3	Measurement of choroidal thickness.....	86
3.2.1.4	Statistical analysis	87
3.2.2	Results	88
3.2.2.1	Inter-observer agreement	88
3.2.2.2	Intra-observer agreement	90
3.2.2.3	Inter-method agreement	92
3.3	Validation of LDF measurements.....	95
3.3.1	Subjects and methods	95
3.3.1.1	The LDF system	95
3.3.1.2	Artificial eye	96
3.3.1.3	Subjects	97
3.3.2	Sub-study 1: To determine a working condition of the LDF device.....	97
3.3.2.1	Sub-study 1: Results	98
3.3.3	Sub-study 2: LDF system configuration	99
3.3.3.1	Sub-study 2: Results	99
3.3.3.2	Substudies 1 and 2 summary	100
3.3.3.3	LDF test after hardware and software modifications	102
3.3.4	Sub-study 3: validity of the LDF measurement	102
3.3.4.1	Experimental designs	102
3.3.4.2	Sub-study 3: Results	103
3.3.4.3	Sub-study 3 summary.....	105
3.3.5	Sub-study 4: The operational technique of using the LDF device	106
3.3.5.1	Experimental designs	106
3.3.5.2	Part 4: Results.....	107
3.3.5.3	Sub-study 4 summary.....	108
3.4	Summary	108
4	Patients and methods	110
4.1	Background	111

4.2	Diabetic Retinopathy: Functional and Structural Study (DREFUS study)	112
4.2.1	Patient recruitment criteria	112
4.2.2	Sample size estimation.....	114
4.2.3	Investigation procedures of DREFUS study.....	114
4.2.4	Detailed medical history.....	114
4.2.5	Vision tests	114
4.2.5.1	Best corrected visual acuity	114
4.2.5.2	Contrast sensitivity (CS)	115
4.2.6	Pupil dilatation and blood pressure measurement	116
4.2.7	Slit lamp examination.....	117
4.2.8	Choroidal blood flow parameters measurement and isometric exercise	117
4.2.9	EDI OCT.....	118
4.3	Liverpool Central Serous Chorioretinopathy Study (Liverpool CSCR Study)	119
4.3.1	Patient recruitment criteria	119
4.3.2	Sample size estimation.....	119
4.3.3	Investigational procedures for Liverpool CSCR study	119
4.3.4	Detailed medical history.....	120
4.3.4.1	Socio-economic classification.....	120
4.3.5	Quality of life impact and psychological profile questionnaires.....	121
4.3.6	Plasma and urine cortisol	121
4.3.7	Vision tests	121
4.3.8	Ocular biometric and axial length.....	122
4.3.9	Intra ocular pressure measurement	122
4.3.10	Ophthalmic imaging	122
4.3.10.1	EDI OCT volume scan.....	122
4.3.10.2	Single raster EDI OCT with isometric exercise	123
4.3.10.3	Choroidal thickness measurements.....	123
4.3.10.4	Colour fundus photography	124
4.3.10.5	Fundus fluorescein angiography (FFA) and indocyanine green angiography (ICGA)	124
4.3.10.6	Other fundus imaging	125
4.3.10.7	Relative grey value measurement	126
4.3.11	Choroidal blood flow parameter measurement with isometric exercise	127
4.3.12	Microperimetry	128
4.3.12.1	Fixation examination.....	128

4.3.12.2	Microperimetry examination.....	128
4.4	Statistical analyses	129
4.5	Summary	129
5	Healthy choroid	130
5.1	Background	131
5.2	Choroidal horizontal thickness	132
5.2.1	Difference of the choroidal thickness between right and left eyes	134
5.2.2	Difference of the choroidal thickness between male and female	136
5.2.3	Choroidal thickness and ageing.....	137
5.3	Choroidal thickness and volume under the macula.....	141
5.3.1	Differences of choroidal volume between two eyes	141
5.3.2	The pattern of thickness and volume of the choroid and the retina at the macula.....	144
5.4	Summary.....	146
6	Choroidal structure and function in DR	148
6.1	Background	149
6.2	Patient characteristics.....	151
6.3	Structure of the choroid in DR.....	154
6.3.1	Choroidal thickness in diabetic patients without any signs of retinopathy.....	154
6.3.2	Choroidal thickness in diabetic patients with retinopathy	155
6.3.3	The relationship between choroidal thickness and degree of retinopathy and maculopathy.....	158
6.4	Autoregulation ability of choroidal function in DR.....	160
6.5	Summary	165
7	Choroidal structure and function in CSCR	167
7.1	Background	168
7.2	Patient recruitment for the Liverpool CSCR study.....	171
7.3	Observational case controlled study	173
7.3.1	CSCR patient characteristics	173
7.3.1.1	The risks of developing CSCR.....	176
7.3.1.2	Socio-economic classification of CSCR patients in Liverpool and Merseyside.....	178
7.3.1.3	Quality of life impact and psychological profile questionnaires..	181
7.3.1.4	Cortisol level in CSCR	182
7.3.2	Vision and ocular biometry	183
7.4	Structure of the choroid in CSCR.....	185

7.4.1	Choroidal thickness and volume in patients with CSCR.....	186
7.4.2	Choroidal thickness and volume based on activity and duration of CSCR	188
7.4.2.1	Active and inactive CSCR.....	188
7.4.2.2	Acute and chronic CSCR.....	189
7.4.2.3	Choroidal thickness and volume in unilateral and bilateral CSCR	191
7.4.3	The relationship between choroidal structure and risks associated with CSCR	197
7.4.3.1	Impact of steroid usage on choroidal structure	197
7.4.3.2	Impact of hypertension on choroidal structure	198
7.4.3.3	The interaction of steroid use and hypertension in CSCR.....	200
7.4.4	The association between choroidal thickness and other imaging techniques.....	204
7.4.4.1	Fluorescein angiography appearance in CSCR	204
7.4.4.2	Indocyanine green angiography appearance in CSCR	206
7.4.4.3	The association between choroidal structure and choroidal vascular hyperpermeability seen on ICGA.....	207
7.4.4.4	Fundus autofluorescence imaging and its association with choroidal changes in CSCR	212
7.4.4.5	Fundus near-infrared autofluorescence imaging and its association with choroidal changes in CSCR	215
7.5	Choroidal autoregulation in CSCR	218
7.5.1	Autoregulatory ability of choroidal structure	218
7.5.2	Autoregulation ability of choroidal function.....	225
7.5.3	The relationship between choroidal structure and function	229
7.6	Retinal function in CSCR	231
7.6.1	Static and dynamic fixation	231
7.6.2	Retinal sensitivity.....	232
7.7	Summary	235
8	Discussions and conclusions.....	238
8.1	Standardisation of choroidal thickness measurements	239
8.2	The choroidal thickness in healthy eyes.....	242
8.3	Choroidal structure and function in diabetes	245
8.3.1	Changes of choroidal structure in DR	245
8.3.2	Choroidal blood flow regulation in DR.....	247
8.4	Choroidal structure and function in CSCR	249
8.4.1	Changes in the choroidal structure in CSCR.....	250

8.4.2	Choroidal autoregulation in CSCR.....	253
8.5	Future directions in choroidal ophthalmic imaging	257
8.5.1	<i>En face</i> imaging.....	257
8.5.2	Optical coherence tomography angiography.....	258
8.6	Future work	259
8.7	Conclusions.....	260
	References	261
	Appendices	278
	Appendix A. Ethic approval for Liverpool CSCR study.....	278
	Appendix B. The Liverpool CSCR study questionnaires	281
	Appendix C. Lists of publications.....	289

List of Figures

Figure 1.1: Cross-section of human eye showing the location of the choroid. Accompanying histological image shows the retina, the choroid and the sclera in the fovea region.....	4
Figure 1.2: Composited layers of Bruch's membrane; RPE: retinal pigment epithelium, ICL: inner collagenous layer, EL: elastin layer, OCL: outer collagenous layer (bm: basement membrane) (modified from ⁵)	5
Figure 1.3: Blood supply and drainage system of the choroid (Source: ¹⁰)	7
Figure 1.4: Choriocapillary functional unit of human choriocapillaris at different areas of the eye, from the peripapillary area (A), the submacular area (B), posterior pole (C), equator (D) and periphery (E) (Source: ¹⁵).....	9
Figure 1.5: Oxygen profile of the retina during dark adaptation. Layer 1 represents the distance from the choroid $x = 0$ to L, layer 2 represents the distance from L1 to L2 and layer 3 represents the distance from L2 to L. L1 is position between the inner and outer segment of photoreceptors. L2 is the position between the inner segment and the outer nuclear layer of photoreceptors. L is the interface between the inner and the outer retina (Source: ²²).....	12
Figure 1.6: Retinal-choroidal temperature recording at the macula during the intra ocular pressure (IOP) modification under ambient light and microscope light exposure (upper row) and the IOP modification (lower row) (increasing in IOP corresponding to decreasing choroidal blood flow). The macular temperature maintains closer to the body temperature in ambient light and decreases significantly when IOP approaches the mean blood pressure level (arrow) suggesting the heat source role of the choroid. The macular temperature maintains closer to the body temperature under the external heat and increases significantly when IOP approaches the mean blood pressure (arrow head) suggesting the heat sink role (Source: ²⁶)	13
Figure 2.1: Schematic structure of human retina (A) compared with a histological section (B) and an optical coherence tomography image (C), RNFL: retinal nerve fibre layer, GL: ganglion cell layer, IPL: inner plexiform layer, INL: inner nuclear layer, OPL: outer plexiform layer, ONL: outer nuclear layer	21
Figure 2.2: Concept of OCT, a B-scan is constructed from several A-scans (the intensity of reflected light vs the depth of tissue) across the retina (Source: ³⁶)	22
Figure 2.3: Concept of time domain OCT	23
Figure 2.4: Concept of SD OCT	24

Figure 2.5: Comparison between retinal cross sectional scans captured using different OCT modalities. A = TD OCT, B = SD OCT (ART = 9), C = EDI OCT (ART = 60) and D = EDI OCT (ART = 100)	26
Figure 2.6: Concept of swept-source OCT (Adapted from: ⁴⁰)	27
Figure 2.7: Comparison between histological cross section of the choroid (A) and EDI OCT scan (B). A schematic representation of normal anatomical landmarks (C). The thin black arrows (↑) indicate the choriocapillaris. The thick white arrows (⇧) indicate the small to medium hypo-reflective cores of Sattler's layer. The asterisks (*) indicate the large hypo-reflective cores of large choroidal vessels within Haller's layer. The triangles (△) indicate the suprachoroid and the red arrows (↑) indicate the suprachoroidal space.....	29
Figure 2.8: Measurements at different points showing the asymmetrical nature of the choroid using three SD OCT systems (A). ^{47, 50, 77} Difference in the mean thickness between children and adults at different locations (B) ⁶⁸	35
Figure 2.9: Diurnal variation of the ChT measurements over 24 hours (A) and 48 hour (B) (Adapted from: ^{79, 80, 82})	37
Figure 2.10: The relationship between ChT and age (Adapted from: ⁵²).....	38
Figure 2.11: Optical setup of laser Doppler velocimetry in rabbit's eye (top); (Adapted from: ¹⁰⁴) and laser Doppler flowmetry for ONH measurement (bottom); (Adapted from: ¹¹⁴) (L = lens , P = pinhole, PMT = photomultiplier tube, and CCD = charge-coupled device camera).....	43
Figure 2.12: Schematic diagram of the principle of LDF (Source: ¹⁰⁷).....	44
Figure 2.13: Doppler shift power spectrum, the spectrum is constituted from the power of shifted frequencies. The dotted line represents the noise level of the DSPS. The small arrow at around 160 Hz represents the velocity (Source: ¹⁰⁷)	45
Figure 2.14: Fundus camera based LDF system (Source: ¹¹⁶)	47
Figure 2.15: Compact LDF system (top) and optical arrangement (bottom) (Source: ¹¹⁷)	48
Figure 2.16: Helmet-mounted LDF system (Source: ¹¹⁸)	49
Figure 2.17: Changes in choroidal blood flow (ChBFlow), choroidal blood volume (ChBVolume), choroidal blood velocity (ChBVelocity), ocular pulsatile pressure (PP) and choroidal vascular resistance over time during isometric exercise (Source: ¹²²)	52
Figure 2.18: The response of choroidal blood flow parameters to different mixtures of O ₂ and CO ₂ : 100% O ₂ (open triangles), 97% O ₂ + 3% CO ₂ (circles), 95% O ₂ + 5% CO ₂ (solid up triangles) and 92% O ₂ + 8% CO ₂ (solid down triangles) (Source, ¹²⁶)	53

Figure 2.19: The effect of light and dark adaptation to the choroidal blood flow parameters (Source: ¹²⁸)	55
Figure 2.20: The chemical formula of indocyanine dyes (Source: ¹⁵⁴)	61
Figure 2.21: The ocular fundus blue wave autofluorescence images of a healthy eye (A) and of a patient with chronic CSCR (B).	63
Figure 2.22: The ocular fundus near infrared autofluorescence images of a healthy eye (A) and the left eye of a patient with chronic CSCR (B).	64
Figure 2.23: The display of microperimetry results from MP-1: symbolic (A), numeric (B) and interpolation (C) map.....	65
Figure 2.24: Fundus images of the left eye of a 55-year old patient with diabetic maculopathy without CSMO, colour fundus image (A), fundus fluorescein angiography image (B), blue wave autofluorescence image (C) and a cross sectional scan image (C)	67
Figure 2.25: Fundus images of the left eye of a 51-year old patient with diabetic maculopathy with CSMO. Figure A and B show the colour fundus image of the macula and the optic disc, respectively. Figure C and D show the microaneurysms on fundus fluorescein angiography at the macula and the optic disc, respectively. Figure E shows an area of macular oedema within the retina on a 3D volume scan.	68
Figure 2.26: Fundus images of the right eye of a 40-year old male patient with acute CSCR: colour fundus photograph (A), indocyanine green angiography showing an area of choroidal vessel dilatation (arrows) at 30 seconds (B) and an area of choroidal vessel hyperpermeability (arrows) at 10 minutes (C), a cross-sectional EDI OCT (D) showing the fluid accumulation beneath the retina (arrow), and the fluorescein angiography showing leakage of the fluorescein dye at 30 seconds (E), 5 minutes (F) and 10 minutes (G) after the injection.	75
Figure 2.27: Fundus images of the right eye of a 46-year old male patient with chronic CSCR: colour fundus photograph (A), a cross-sectional EDI OCT (B) showing fluid accumulation beneath the retina (arrow), fluorescein angiography showing a leakage of the fluorescein dye at 5 minutes (C), indocyanine green angiography showing an area of choroidal vessel hyperpermeability (arrows) at 5 minutes (D), near-Infrared autofluorescence (E), infrared reflectance image (F) and blue wave autofluorescence (G).	76
Figure 3.1: A single 9 mm horizontal line scan with enhanced depth imaging obtained from the right eye of a 55-year-old healthy male (A). The choroidal-scleral interface (CSI) (B) is indicated by a well demarcated hyper-reflective band (triangle heads) and the suprachoroidal space (SCS) (C) is indicated by the hypo-reflective	

band (arrows). The narrow arrows indicate the cross section of large choroidal vessels	85
Figure 3.2: Example of EDI OCT image classifications categories. Group A (A), the choroidal outer boundary consists of more than 80% of the CSI (triangle heads) and the SCS (narrow arrows) across the length of the scan. Group B (B) consists of less than 80% of the CSI and the SCS across the length of the scan. Group C (C) consists of a smooth line between the outer limit of large choroidal vessels and the sclera (wide arrows) and ungradeable (D) when the outer choroidal boundary is not identifiable on the scan	86
Figure 3.3: Bland-Altman plots showing inter-observer with mean difference (thick line) and 95% limits of agreement (dashed lines) for subfoveal choroidal thickness measurements (SfChT, left hand column) and total choroidal thickness measurements (ChT, right hand column) by classification: group A (A1 and A2), group B (B1 and B2), group C (C1 and C2), non-agreement (D1 and D2)	90
Figure 3.4: Bland-Altman plots showing intra-observer with mean difference (thick line) and 95% limits of agreement (dashed lines) for subfoveal choroidal thickness measurements (SfChT, left hand column) and the total choroidal thickness measurements (ChT, right hand column) by classification: group A (A1 and A2), group B (B1 and B2), group C (C1 and C2), non-agreement (D1 and D2)	92
Figure 3.5: Bland-Altman plots showing inter-method agreements with mean difference (thick line) and 95% limits of agreement (dashed lines) for subfoveal choroidal thickness measurements (SfChT, left hand column) and the total choroidal thickness measurements (ChT, right hand column) by classification: group A (A1 and A2), group B (B1 and B2), group C (C1 and C2)	94
Figure 3.6: The LDF device (A) and the user interface of the LabVIEW software (B)	96
Figure 3.7: The artificial eye device.....	97
Figure 3.8: Examples of LDF recordings from a healthy eye and the artificial eye set at 8.6 volts. The red arrows indicate the mean Doppler shifted frequency (Hz) representing the expected velocity.....	98
Figure 3.9: Examples of Doppler shift power spectrum (DSPS) from LDF recordings from 2 PMT of our fundus camera based LDF device. The red arrows indicate the mean Doppler shifted frequency (Hz) representing the expected velocity	98
Figure 3.10: The LDF system connections: the signal derived from the PMT fed to the Oculix and Flom-S signal processor (A) and the signal fed directly to the Flom-S signal processor (B), BNC: Bayonet Neill–Concelman cable	99

Figure 3.11: The DSPS from LDF recordings from 2 system connections, (A) the signal connected with the Oculix and Flom-S signal processor and (B) the signal fed directly to the Flom-S signal processor	100
Figure 3.12: Schematic design of the low pass filter.	101
Figure 3.13: Schematic of parameters considered for noise calculation and amplitude of the DSPS calculation	101
Figure 3.14: Comparison between the DSPS before and after the hardware modification. The DSPS derived from the artificial (A and B) and healthy (C and D) eyes before (A and C) and after (B and D) hardware modification.	102
Figure 3.15: Linearity of the blood flow parameters.....	104
Figure 3.16: The effect of PMT sensitivity	104
Figure 3.17: The blood flow parameters at different filter density	105
Figure 3.18: The different patterns of laser beam on the fovea: focus (A) and out of focus (B)	106
Figure 3.19: The position of the PMT (blue circle) and the laser beam (red circle)	106
Figure 3.20: The effect of focus of the laser beam	107
Figure 3.21: The DC levels (the amount of detected light on PMT) due to different PMT positions.....	108
Figure 4.1: Investigation procedures of DREFUS study, * represents the procedures included in the analyses for this thesis.....	114
Figure 4.2: Visual assessment charts. ETDRS chart “R” (A), ETDRS chart “1” (B) and EDTRS chart “2” (C).	115
Figure 4.3: Pelli-Robson contrast sensitivity charts. One set of chart consists of 2 charts: chart 1 (A) for right eye and chart 2 (B) for left eye.....	116
Figure 4.4: The sequence of choroidal blood flow measurement with isometric exercise for DREFUS study	118
Figure 4.5: Investigation procedures of Liverpool CSCR study	120
Figure 4.6: Type 1 and Type 2 M-chart.	122
Figure 4.7: The sequence of EDI OCT image acquisition with isometric exercise	123
Figure 4.8: Example of the area for measuring the mean grey values. The area marked as 1, 2, 3, 4 and 5 were assigned as the area of interest. The area marked as 6, 7, 8 and 9 were assigned as the reference area for each of the corresponding area (6 for 2, 7 for 3, 8 for 4 and 9 for 5). The average of the mean grey value from all reference area (6 + 7 + 8 + 9 4) was used as the reference for the central subfield (1). The area marked as 10 represents the mean grey value of optic disc.	126

Figure 4.9: The sequence of investigation of choroidal blood flow measurement with isometric exercise for the Liverpool CSCR study	127
Figure 4.10: The pattern of microperimetry examination used in the Liverpool CSCR study.....	129
Figure 5.1: Mean EDI OCT choroidal thickness at each location 500 µm apart across a 6 mm horizontal line scan centred on the foveal centre of 41 eyes of 41 healthy participants (error bars = 95% confidence interval, age: as continuous variable not shown).....	133
Figure 5.2: The mean (95% confidence interval; error bars) horizontal choroidal thickness at different locations between right (black) and left (grey) eyes	135
Figure 5.3: The mean (95% confidence interval, error bars) of the choroidal thickness at different locations between males (black) and females (grey)	137
Figure 5.4: The mean (95% confidence interval; error bars) choroidal thickness at different locations of each age group; < 40 years old (black), 41 – 50 years old (grey) and > 50 years old (gold). † represents $p = 0.073$ (< 41 vs > 50), ‡ represents $p = 0.066$ (41 – 50 vs > 50), ** represents $p < 0.05$ (< 41 vs > 50) and * represents $p < 0.05$ (41 – 50 vs > 50).....	139
Figure 5.5: Representative image of the mean ChT (top row) and ChVolume (bottom row) in each of the ETDRS subfield of right and left eyes	144
Figure 5.6: The mean choroidal thickness and retinal thickness in each of the ETDRS subfield of right (OD) and left (OS) eyes	145
Figure 5.7: The mean choroidal volume and retinal volume in each of the ETDRS subfield of right (OD) and left (OS) eyes	146
Figure 6.1: The outline of blood vessels stained with alkaline phosphatase (APase) showing the tortuosity of the choriocapillaris (A), area of diffuse (B) and complete loss (C) of choriocapillaris in diabetic patients. The cytochemical staining with nonspecific esterase (NSE) and the APase staining show the loss of capillary networks in a diabetic patient (E) compared to a healthy eye (F) (Source: ²³²).....	150
Figure 6.2: Mean choroidal thickness at each location 500 µm apart across 9 mm horizontal EDI OCT scans through the fovea of healthy and diabetic eyes. Error bars represent 95% confidence interval.....	155
Figure 6.3: Mean choroidal thickness at each location 500 µm apart across 9mm horizontal EDI OCT scans through the fovea of healthy, diabetic with and without retinopathy. Error bars represent 95% confidence interval.....	157
Figure 6.4: Mean choroidal thickness at each location 500 µm apart across 9mm horizontal EDI OCT scans through the fovea of healthy, diabetic with and without	

retinopathy. DR eyes are categorised as no CSMO and with CSMO and/or signs of significant ischaemic. Error bars represent 95% confidence interval	157
Figure 6.5: The association between ChT at each measured location and the grade of retinopathy	159
Figure 6.6: The association between ChT at each measured location and the grade of maculopathy	159
Figure 6.7: The mean DC, ChBVolume, ChBVelocity and ChBFlow at baseline and at the end of isometric exercise in diabetic patients without DR (group D), DR without CSMO (group A), DR with CSMO/ischaemia (group B/C) and healthy controls	164
Figure 6.8: Changes in DC, ChBVolume, ChBVelocity and ChBFlow from baseline in diabetic patients without DR (group D), DR without CSMO (group A), DR with CSMO/ischaemia (group B/C) and healthy controls	164
Figure 7.1: Mineralocorticoid receptor pathway (Adapted from ²⁴³)	170
Figure 7.2: The patient recruitment consort chart of the Liverpool CSCR study ...	172
Figure 7.3: Symptoms associated with CSCR.....	175
Figure 7.4: The Socio-economic classification of CSCR patients attending St Paul's Eye Unit and recruited into the Liverpool CSCR study	179
Figure 7.5: The socio-economic classification of CSCR patients attending St Paul's Eye Unit compared with Merseyside and the general population in England(* represents $P = 0.03$ and ** represents $P = 0.002$).....	180
Figure 7.6: Quality of life and psychological profile of CSCR patients (N = 13) and healthy controls (N = 22).....	182
Figure 7.7: The cortisol level in urine and plasma of CSCR patients and healthy controls.....	183
Figure 7.8: EDTRS maps of choroidal thickness (ChT) and volume of healthy controls and CSCR patients (all in microns). SfChT represents the subfoveal ChT. MChT and MChVolume represent the average of mean ChT and ChVolume of the 9-ETDRS subfields, respectively. (* and grey filled subfields denote subfields significantly different to those of healthy controls $P < 0.05$).....	187
Figure 7.9: EDTRS maps of choroidal thickness (ChT, all in microns) and volume (mm^3) of patients with active and inactive CSCR. SfChT represents the subfoveal ChT. MChT and MChVolume represent the average of mean ChT and ChVolume of the 9 ETDRS subfields, respectively	189
Figure 7.10: EDTRS maps of choroidal thickness (ChT, all in microns) and volume (mm^3) of patients with acute and chronic CSCR. SfChT represents the subfoveal	

ChT. MChT and MChVolume represent the average of mean ChT and ChVolume of the 9-ETDRS subfields, respectively	190
Figure 7.11: Age-adjusted subfoveal ChT (SfChT), mean macular ChT (MChT), the ChT value 9 ETDRS subfields (all in microns), mean macular ChVolume (MChVolume) and ChVolume of 9 ETDRS subfields (all in mm ³) of healthy controls (Left) and CSCR patients categorised as unilateral (middle) or bilateral (right) (* and grey filled subfields denote subfields significantly different to those of healthy controls $P < 0.05$, adjusted age = 45.4 years)	192
Figure 7.12: EDTRS maps of the differences of choroidal thickness (ChT, all in microns) and volume (mm ³) between the symptomatic eyes and the fellow eyes of patients with unilateral and bilateral CSCR. SfChT represents the subfoveal ChT. MChT and MChVolume represent the average of mean ChT and ChVolume of the 9-ETDRS subfields, respectively	194
Figure 7.13: EDTRS maps of choroidal thickness (ChT, all in microns) and volume (mm ³) of healthy controls and asymptomatic fellow eyes of unilateral CSCR patients. SfChT represents the subfoveal ChT. MChT and MChVolume represent the average of mean ChT and ChVolume of the 9-ETDRS subfields, respectively	195
Figure 7.14: EDTRS maps of choroidal thickness (ChT, all in microns) and volume (mm ³) of fellow eyes of unilateral CSCR patients with and without choroidal vascular hyperpermeability. SfChT represents the subfoveal ChT. MChT and MChVolume represent the average of mean ChT and ChVolume of the 9-ETDRS subfields, respectively	196
Figure 7.15: EDTRS maps of the differences in choroidal thickness (ChT, all in microns) and volume (mm ³) of CSCR patients and healthy controls with and without history of steroid usage. SfChT represents the subfoveal ChT. MChT and MChVolume represent the average of mean ChT and ChVolume of the 9 ETDRS subfields, respectively	198
Figure 7.16: Age-adjusted subfoveal ChT (SfChT), mean macular ChT (MChT), the ChT value 9 ETDRS subfields (all in microns), mean macular ChVolume (MChVolume) and ChVolume of 9 ETDRS subfields (all in mm ³) of healthy controls (left) and CSCR patients categorized as normotension (middle) or hypertension (right) (* and grey filled subfields denote subfields significantly different to those of healthy controls $P < 0.05$, adjusted age = 45.4 years)	199
Figure 7.17: Age-adjusted subfoveal ChT (SfChT), mean macular ChT (MChT), the ChT value 9 ETDRS subfields (all in microns), mean macular ChVolume (MChVolume) and ChVolume of 9 ETDRS subfields (all in mm ³) of CSCR patients categorised as normotension (left) or hypertension (right) who had SRF at the study	

entry (* and grey filled subfields denote subfields significantly different to those of normotension $P < 0.05$, adjusted age = 48.3 years).....	200
Figure 7.18: The age-adjusted subfoveal ChT (SfChT), mean macular ChT (MChT) and the ChT value of each of the 9 ETDRS subfield (all in microns) of healthy controls and CSCR patients who have had history of steroid usage (adjusted age = 45.4 years).....	203
Figure 7.19: Age- and steroid usage-adjusted subfoveal ChT (SfChT), mean macular ChT (MChT) and the ChT value of each of the 9 ETDRS subfield (all in microns) of healthy controls (left) and CSCR patients categorized as normotension (middle) or hypertension (right) (* and grey filled subfields denote subfields significantly different to those of healthy controls $P < 0.05$; adjusted age = 45.4 years)	203
Figure 7.20: FA patterns of CSCR eyes: A1-2 an early and late of pinpoint FA pattern; B1-2 early and late of ink blot FA pattern; C1-2 early and late of smoke stack FA pattern; D1-2 early and late of patchy FA pattern	205
Figure 7.21: Box plots of logMAR vision and duration of symptom of each FA pattern. The tinted box represents the inter quartile range and the whiskers represent lowest and the highest scores.....	206
Figure 7.22: The choroidal vascular hyperpermeability as seen on the ICGA of patients with unilateral CSCR (A) and bilateral CSCR (B).....	207
Figure 7.23: The representative 6 × 6 mm map of choroidal thickness (A) and choroidal vascular hyperpermeability (B)	208
Figure 7.24: The relationship between the percentage of choroidal vascular hyperpermeability and ChT within each 1 mm ² sector for the symptomatic eyes (A) and the asymptomatic fellow eyes (B).....	211
Figure 7.25: Examples of the mean grey scale values obtained from the FAF histogram of each location over the macula of the right eye of a healthy control (A) and the right eye of a CSCR patient (B).....	212
Figure 7.26: Relative FAF levels of the affected eyes of CSCR and the control eyes. The tinted box represents the inter quartile range and the whiskers represent the lowest and the highest scores.....	214
Figure 7.27: Relative FAF levels of the affected eyes of CSCR (categorised as acute and chronic) and the control eyes. The tinted box represents the inter quartile range and the whiskers represent the lowest and the highest scores.....	214
Figure 7.28: Examples of the mean grey scale values obtained from the NIR-AF histogram of each location over the macula of the left eye of a healthy control (A) and the left eye of a CSCR patient (B)	215

Figure 7.30: Relative NIR-AF levels of CSCR and control eyes. The tinted box represents the inter quartile range and the whiskers represent lowest and the highest scores	217
Figure 7.31: Relative NIR-AF levels of the affected CSCR eyes (categorised as acute and chronic) and the control eyes. The tinted box represents the inter quartile range and the whiskers represent the lowest and the highest scores.....	217
Figure 7.32: Example of differences in the retinal thickness (A) and choroidal thickness (B) measurements of the left eye of a CSCR patient between baseline and at the end of squatting	221
Figure 7.33: The mean (95% confidence interval; error bars) retinal thickness (RT) measured along the horizontal axis of the index eyes at baseline (marked as before) and at the end of squatting (marked as after) in controls (A) and CSCR patients (B)	222
Figure 7.34: The mean (95% confidence interval; error bars) choroidal thickness (ChT) measured along the horizontal axis of the index eyes at baseline (marked as before) and at the end of squatting (marked as after) in controls (A) and CSCR patients (B) (* represents $P < 0.05$).....	223
Figure 7.35: The mean (95% confidence interval; error bars) choroidal thickness (ChT) measured along the horizontal axis of the asymptomatic fellow eyes of patients with unilateral CSCR at baseline (marked as before) and at the end of squatting (marked as after) (* represents $P < 0.05$)	224
Figure 7.36: The mean DC (A), ChBVolume (B), ChBVelocity (C) and ChBFlow (D) at baseline (before isometric exercise) and after isometric exercise of CSCR patients and healthy controls. The tinted box represents the inter quartile range and the whiskers represent the lowest and the highest scores	228
Figure 7.37: Changes in DC, ChBVolume, ChBVelocity and ChBFlow in CSCR patients and healthy controls following the isometric exercise. The tinted box represents the inter quartile range and the whiskers represent the lowest and the highest scores	229
Figure 7.38: The scatter plot of changes in choroidal vascular resistance (Rm) after isometric exercise with changes in DC, ChBVolume, ChBVelocity and ChBFlow in CSCR patients and controls.....	231
Figure 8.1: The proposed pathogenesis mechanism of CSCR from the results obtained from the work in this thesis	257

List of Tables

Table 1.1: Diameters and dimensions of the choriocapillaris lobules at the different areas of the globe (Source: ¹⁵)	8
Table 2.1: Published estimates of subfoveal choroidal thickness in healthy eyes listed by year of publication.....	32
Table 2.2: Comparison of ChT measured in three different instruments (ICC and 95% limits of agreement) (Source: ^{61, 62})	34
Table 2.3: Advantages and disadvantages of non-invasive techniques used to measure choroidal blood circulation.....	41
Table 2.4: Summary of various pharmaceutical compounds showing the effect on choroidal blood flow using LDF	58
Table 2.5: Summary of previous research on choroidal thickness in various stages of DR	70
Table 2.6: Development of clinical terms used to describe CSCR (Source, ¹⁸⁴)	72
Table 3.1: Summary of inter-observer agreements on the total and subfoveal choroidal thickness measurements	89
Table 3.2: Summary of intra-observer agreements on the total and subfoveal choroidal thickness measurements	91
Table 3.3: Summary of inter-method agreements on the total and subfoveal choroidal thickness measurements	93
Table 4.1: Patient and healthy control inclusion and exclusion criteria in the DREFUS study	113
Table 4.2: NS-SEC analytic classes.....	121
Table 4.3: Fundus imaging modality.....	125
Table 4.4: Microperimetry parameters.....	128
Table 5.1: Mean ChT (95% confidence interval; CI) at each location 500 μ m apart across a 6 mm horizontal line scan (P = paired sample comparison to the SfChT)	134
Table 5.2: Mean difference in ChT (95% confidence interval; CI) between right and left eyes at each location 500 μ m apart across a 6 mm horizontal line scan (P = paired sample comparison).....	136
Table 5.3: The relationship between horizontal ChT, age and refraction	138
Table 5.4: The percentage of age accounted for the choroidal thickness at each location and regression coefficients between the ChT and age.....	140
Table 5.5: The demographical characteristics of healthy right and left eyes	142

Table 5.6: The choroidal thickness and choroidal volume distribution over the 9 ETDRS subfields of right and left eyes of 22 healthy participants	143
Table 6.1: Characteristics of 124 participants including healthy controls and DM patients categorised as diabetic controls and patients with diabetic maculopathy with and without CSMO. Eye specific data is provided for the study eye.	153
Table 6.2: The relationship between the horizontal ChT and systemic factors in diabetic patients (Pearson's r).....	158
Table 6.3: Systemic characteristics of healthy subjects, patients with diabetes and patients with DR (with 95% confidence interval) at baseline and after isometric exercise	161
Table 6.4: Mean differences in DC, ChBVolume, ChBVelocity and ChBFlow with 95% CI of healthy subjects, patients with diabetes and patients with DR	163
Table 6.5: Comparison of DC, ChBVolume, ChBVelocity and ChBFlow changes from baseline between DR patients and controls. Results are shown as a fraction of 1.	163
Table 6.6: Pearson's correlation coefficients between choroidal thickness and changes in choroidal blood flow parameters from baseline following isometric exercise.	165
Table 7.1: Number of participants available for analyses.....	173
Table 7.2: Characteristics of CSCR patients and healthy controls screened for the Liverpool CSCR study	174
Table 7.3: Risk factor (at any time point prior to the CSCR)	177
Table 7.4: Vision and ocular biometric characteristics of controls and CSCR patients	184
Table 7.5: Clinical characteristics of healthy subjects and CSCR patients (with 95% confidence interval).....	186
Table 7.6: The age-adjusted subfoveal ChT (SfChT), mean macular ChT (MChT) and the ChT value of each of the 9 ETDRS subfield (all in microns) of healthy controls and CSCR patients who had a history of steroid usage. CSCR patients were also categorised as normotension and hypertension (adjusted age = 45.4 years).	202
Table 7.7: Data available for fundus imaging analyses.....	204
Table 7.8: FA pattern (in %) seen in acute and chronic CSCR	205
Table 7.9: Mean ChT at the hyperpermeability area and non-hyperpermeability area of CSCR eyes.....	209
Table 7.10: Relative FAF level of controls and CSCR patients	213
Table 7.11: Relative NIR-AF level of controls and CSCR patients.....	216

Table 7.12: Systemic characteristics of controls and CSCR patients (with 95% confidence interval) at baseline and at the end of isometric exercise	219
Table 7.13: Systemic characteristics of healthy subjects and CSCR patients (with 95% confidence interval) at baseline and after isometric exercise	226
Table 7.14: The mean differences in DC, ChBVolume, ChBVelocity and ChBFlow between baseline and at the end of isometric exercise (with 95% confidence interval) of controls and CSCR patients	227
Table 7.15: Comparison of DC, ChBVolume, ChBVelocity and ChBFlow changes from baseline between DR patients and controls. Results are shown as a fraction of 1	227
Table 7.16: Pearson's correlation coefficients between changes in choroidal function and structure following isometric exercise	230
Table 7.17: Dynamic and static fixation of CSCR patients and controls.....	232
Table 7.18: The mean retinal sensitivity at the macula of controls and CSCR patients.....	233
Table 7.19: Pearson's correlation coefficients of retinal sensitivity and choroidal and retinal thickness and the level of FAF and NIR-AF in CSCR patients on each ETDRS subfield.	234

List of Equations

Equation 2.1: The proposed equation to predict the ChT from age and refraction .39	.39
Equation 2.2: The Doppler shift caused by moving RBCs; λ_i is the wavelength of the incident light and n is an index of the refraction of the light in the blood.44	44
Equation 2.3: Velocity (Vel) and volume (Vol) calculation; A_{dc} is the amplitude of the direct photocurrent (DC). The DC should be kept constant within 10% of the mean in order to ensure the variation of other parameters.46	46
Equation 2.4: Sensitivity of LDF measurement; sd is the standard deviation of the difference between measurements of all subjects, \bar{x} is the mean value of all measurements and k is the two-tail value of the t-distribution at the 0.05 level of significance.....46	46
Equation 2.5: Equation describing the relationship between ChBFlow and OPP; MOAP is a mean ophthalmic arterial pressure, defined by following equation: (MOAP = $BP_{diast} + 13(BP_{syst} - BP_{diast})$); R_m is the average resistance of blood vessels and OPP is the mean ocular perfusion pressure; IOP is the intraocular pressure50	50
Equation 4.1: MAP = mean arterial pressure; BP_{diast} = diastolic blood pressure; BP_{syst} = systolic blood pressure 117	117
Equation 4.2: Mean macular ChT (MChT) calculation..... 124	124
Equation 4.3: Equation describing the relative AF (both FAF and NIR AF) calculation..... 126	126
Equation 4.4: The ocular perfusion pressure formulation, MAP is calculated using Equation 4.1 127	127
Equation 4.5: Choroidal vascular resistance change formulation..... 127	127
Equation 5.1: The model predicting the ChT using age as a main predictor for the ChT at the centre of the fovea (A) and the total ChT (B) 138	138
Equation 7.1: The model for predicting the choroidal thickness (ChT) using the choroidal vascular hyperpermeability detected on ICGA (% of choroidal vascular hyperpermeability) as a main predictor for the symptomatic eyes (A) and the asymptomatic fellow eyes (B)210	210

Abbreviations

ACD = anterior chamber depth

AMD = age-related macular degeneration

AO = adaptive optics

APD = avalanche photodiode

ART = Automatic Real Time

AxL = axial length

BCEA = bicurve ellipse area

BCVA = best corrected visual acuity

BM = Bruch's membrane

BP = blood pressure

CDL = colour Doppler imaging

CERC = Clinical Eye Research Centre

ChBFlow = choroidal blood flow

ChBVelocity = choroidal blood velocity

ChBVolume = choroidal blood volume

ChT = choroidal thickness

ChVolume = choroidal volume

CNV = neovascularisation

CR = coefficient of repeatability

CSCR = central serous chorioretinopathy

CSI = choroidal-scleral interface

cSLO = confocal scanning laser ophthalmoscope

CSMO = clinically significant macular oedema

CV = coefficient of variance

DC = direct photocurrent

DMO = diabetic macular oedema

DR = diabetic retinopathy

DREFUS study = Diabetic Retinopathy Functional and Structural Study

DSPS = Doppler shift power spectrum

EDI OCT = enhanced depth imaging optical coherence tomography
EL = elastin layer
ETDRS = Early Treatment of Diabetic Retinopathy Study
FAF = fundus autofluorescence
FAZ = foveal avascular zone
FFA = fundus fluorescein angiography
GL = ganglion cell layer
HRA2 = Heidelberg Retina Angiograph 2
HSD2 = 11 β -hydroxysteroid dehydrogenase type II
ICC = Intraclass correlation coefficient
ICGA = indocyanine green angiography
ICL = inner collagenous layer
ILM = inner limiting membrane
INL = inner nuclear layer
IOP = intra ocular pressure
IPL = inner plexiform layer
IRF = Intra-retinal fluid
ISMO = isosorbide mononitrate
LCD = liquid crystal display
LDES = Liverpool Diabetic Eye Study
LDF = laser Doppler flowmetry
LDV = laser Doppler velocimetry
LEQ = The life events questionnaire
LF = lipofuscin
Liverpool CSCR Study = Liverpool Central Serous Chorioretinopathy Study
LP = laser photocoagulation
LSFG = laser speckle flowgraphy
LTA = laser-targeted angiography
LYVE-1 = lymphatic vessel endothelial hyaluronate receptor 1
MAP = mean arterial pressure
MChVolume = mean macular ChVolume

MP-1= Microperimeter-1
MRI = magnetic resonance imaging
M-score = degree of metamorphopsia
NIR AF = near-Infrared autofluorescence
NO = nitric oxide
NPDR = non-proliferative DR
NSC = national screening committee
NS-SEC = National Statistics Socio-economic classification
OCL = outer collagenous layer
OCT = optical coherence tomography
OCTA = Optical coherence tomography angiography
OMAG = optical micro-angiography
ONH = optic nerve head
ONL = outer neuclear layer
OPL = outer plexiform layer
OPP = ocular perfusion pressure
OSA = obstructive sleep apnoea
PCAs = posterior ciliary artery(ies)
PCI = partial coherence interferometry
pCO₂ = carbon dioxide tension
PCV = polypoidal choroidal vasculopathy
PDR = proliferative DR
PDT = photodynamic therapy
PED = pigment epithelium detachment
PED = pigment epithelium detachment
PHQ-15 = patient health questionnaire 15
PHQ-9 = patient health questionnaire 9
PMT = photomultiplier tube
pO₂ = O₂ tension
POBF = pulsatile ocular blood flow
PSS = perceived stress scale

QE = quantum efficiency
RBC = red blood cell
Rm = choroidal vascular resistance
RNFL = retinal nerve fibre layer
RPE = retinal pigment epithelium
SCS = suprachoroidal space
SD OCT = spectral-domain OCT
SfChT = subfoveal choroidal thickness
SPSS = Statistical Package for Social Scientists
SRF = sub-retinal fluid
SRLE = survey of recent life experience
SS OCT = Swept-source optical coherence tomography
SSADA = split-spectrum amplitude decorrelation angiography
TD OCT = time-domain OCT
VEGF = Vascular Endothelial Growth Factor
VPDT = verteporfin photodynamic therapy
WHO = World Health Organisation

Chapter 1 Introduction

The history of the study of the choroidal vasculature can be tracked back to the 1950s when Wybar ¹ described his first communication article on the vascular anatomy of the choroid in the British Journal of Ophthalmology. In this article, a neoprene vascular cast of the choroid was used to identify the anatomical variation of the choroid in different parts of the eye. The involvement of the choroid in ocular diseases during the first era of ophthalmology was mainly focused on its involvement in metastatic carcinoma or the localised damage of the choroid such as ocular histoplasmosis syndrome. During this period, assessing choroidal abnormalities remained an unsolved dilemma for most of ophthalmologists due to the lack of advanced imaging modalities that are capable of capturing the choroid.

Although fluorescein had been previously used to image retinal vessels, it was of limited value to delineate choroidal vessels. Flower and Hochheimer in 1974 ² introduced indocyanine green (ICG) in order to capture the choroidal circulation and summarised the application of ICG for choroidal imaging as:

“It seems to us that ICG has been demonstrated to be of comparable safety, although we would not recommend its use as an alternative to fluorescein. Fluorescein shows up the retinal vessels far better than ICG; however, ICG demonstrates the choroidal vessels whereas fluorescein cannot. We would hope that ICG infrared angiography will continue to be pursued as a potential clinical method of choroidal angiography”

Although, this revolutionised the field of choroidal imaging and gave new impetus to ophthalmic research, it was not until the early 1990s when ICG became an established method to investigate the choroid.

Although ICG is the gold standard to visualise the choroid, until recently its acceptance by researchers and clinicians was limited due to inadequate photographic quality and poor image resolution. The introduction of new ophthalmic imaging modalities such as enhanced depth imaging optical coherence tomography (EDI OCT) and laser Doppler flowmetry (LDF) allow the choroid to be studied non-invasively in real-time.

1.1 Background

In this chapter, I will first describe the choroidal anatomy and function with reference to the motivations, aims and objectives of my PhD thesis.

1.2 The choroid

The word “**choroid**” was derived in mid-17th century from the classical ancient Greek word “**choroeidēs (Χοριοειδής)**”. The word **χοριοειδής** comes from **chorion (χοριον)**, which refers to the “membrane that encloses the foetus”, and **eidōs (ειδος)** meaning form or shape.³

The choroid is the posterior part of the uveal system, consisting mainly of vessels situated between the smooth inner surface of the Bruch’s membrane (BM) and the sclera (**Figure 1.1**). On histology, the choroid is composed of 5 layers: the BM, the choriocapillaris, a medium sized vessel layer (the Sattler’s layer), a large sized vessel layer (the Haller’s layer) and the suprachoroidal space.

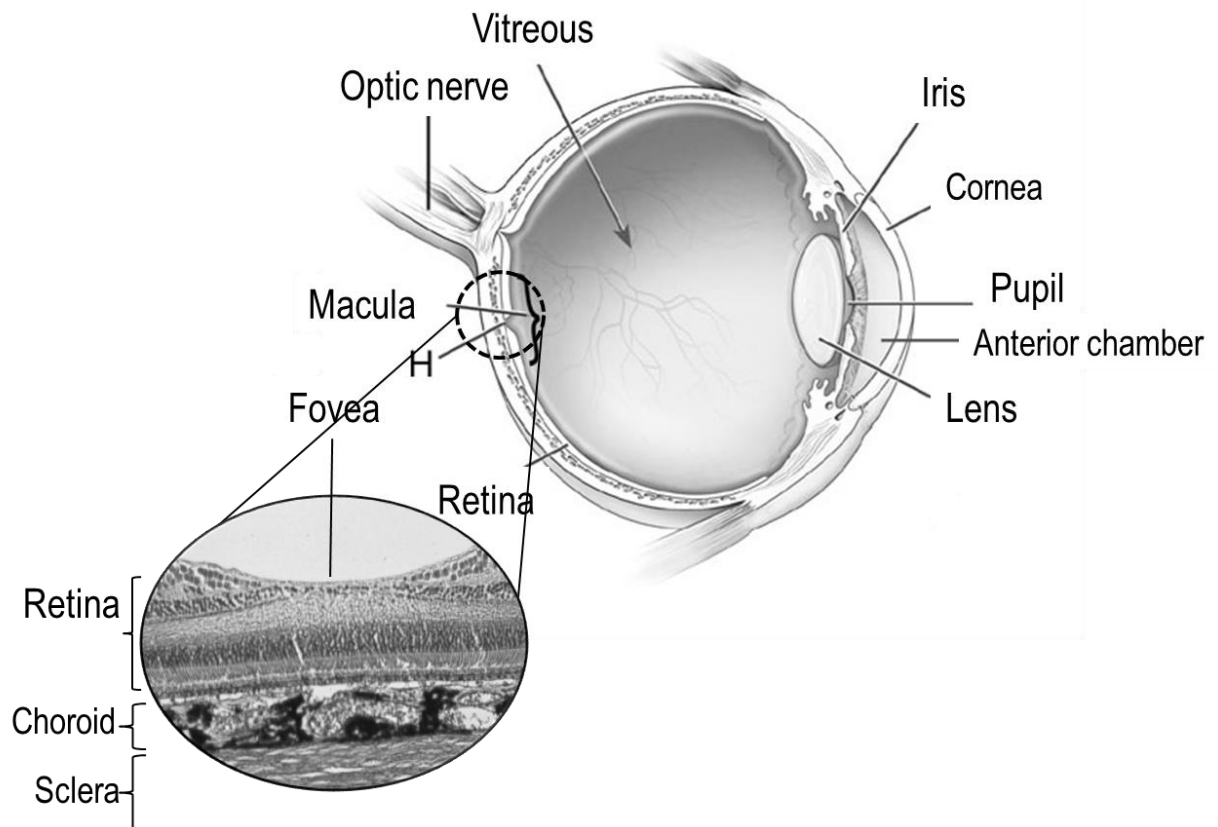


Figure 1.1: Cross-section of human eye showing the location of the choroid. Accompanying histological image shows the retina, the choroid and the sclera in the fovea region

1.2.1 Choroidal anatomy

1.2.1.1 Bruch's membrane (BM)

Histologically, the BM consists of 5 layers: the basement membrane of the retinal pigment epithelium (RPE; 0.14 – 0.15 μm thick), the inner collagenous layer (ICL, 1.4 μm thick), the elastin layer (EL; 0.8 mm thick), the outer collagenous layer (OCL; 0.7 μm thick) and the basement membrane of the choriocapillaris (0.14 μm thick) as shown in **Figure 1.2**.⁴ The main biological component of the BM is collagen and its content varies in each layer of the BM. Collagen types I and III are predominant in ICL and OCL, whereas type IV is the main component in the basement membrane of the RPE, the EL and the basement membrane of the choriocapillaris.⁴ The strongest adhesion force compared to other layers is found between the RPE cells and the basal lamina; this strong adhesion together with the tight collagen fibres and dense elastic layer of the BM acts as a stable platform to

support the RPE as well as a mechanic barrier to separate the RPE and the choriocapillaries.⁵ A weakened adhesion force between RPE cells and the basal lamina results in pigment epithelium detachment (PED). Occurrence of PED is often associated with several retinal disorders such as age-related macular degeneration (AMD) and central serous chorioretinopathy (CSCR).⁶

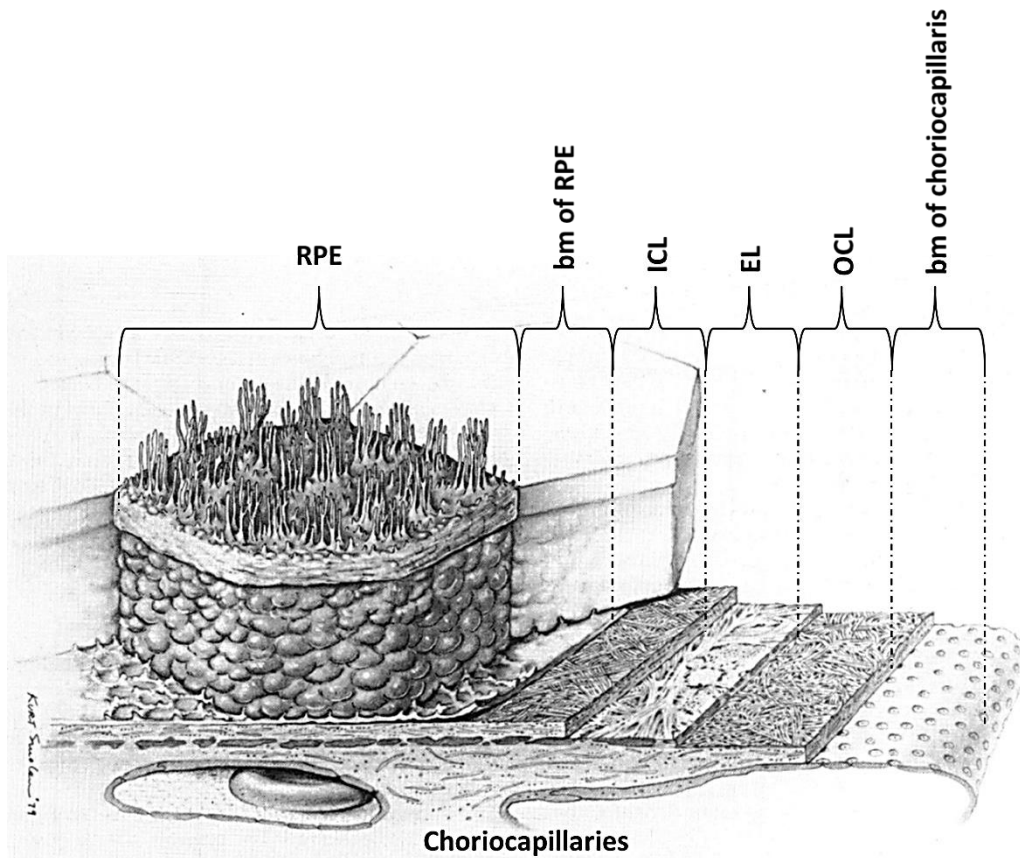


Figure 1.2: Composited layers of Bruch's membrane; RPE: retinal pigment epithelium, ICL: inner collagenous layer, EL: elastin layer, OCL: outer collagenous layer (bm: basement membrane) (modified from ⁵)

1.2.1.2 *The choroidal vascular system*

The blood supply to the eye originates from the ophthalmic artery, the first branch of the internal carotid artery. The ophthalmic artery then branches into the central retinal artery, the posterior ciliary artery(ies) (PCA) and the muscular branch. The branch that provides blood supply to the choroid is the PCA which further separates into 2 arterial systems: 1) short PCAs and 2) long PCAs.⁷

These arterial blood supply systems functionally divide the choroidal vasculature into 3 vascular layers: large vessels in the outer layer, medium vessels

in the intermediate layer and capillaries in the innermost layer. The large choroidal vessel layer receives blood supply from short and long PCAs as well as the branches of the Circle of Zinn, an annular ring of arteries surrounding the optic nerve. The medium sized vascular layer consists of an interdigitating arrangement of veins and arteries with different sizes according to location. These vessels run vertically to supply one or several lobules of the choriocapillaris.

Blood from the choroid drains through the vena vorticosa, also known as vortex veins. Usually around 7 vortex veins are present in the eye with at least one per each eye quadrant. The vortex veins pierce the sclera and empty into the superior and inferior ophthalmic veins.⁸ Obstruction of the blood flow of the vortex veins has been shown to be associated with thickening of the choroid and the area of choroidal hyperpermeability. This feature has been reported in patients with polypoidal choroidal vasculopathy (PCV).⁹

As the choroid is mainly a dense vascular network and receives a direct blood supply from the ophthalmic artery, systemic disorders such as severe hypertension may affect the vascular structure of the choroid. The effect of systemic factors and their association with choroidal structure will be explored in this thesis using EDI OCT and LDF techniques.

Figure 1.3: Blood supply and drainage system of the choroid (Source: ¹⁰)

1.2.1.3 ***Choriocapillaris***

The choriocapillaris is the single innermost layer of the choroidal arteries and veins external to the BM. The choriocapillaris vessels have a large lumen and thin walls. The choriocapillaris lumen is greater than conventional capillaries by 3 to 4 times allowing the flow of more than 1 red blood cell (RBC) at a time.¹¹

The arrangement of the choriocapillaris was proposed during the 70s and 80s using electron microscopy on post mortem tissue.¹²⁻¹⁴ Due to the complexity of the arrangement, there was little consensus amongst the experts.

The concept of the choroidal functional unit was introduced by Fryczkowski¹⁵ in his study of the choriocapillaris angioarchitecture on 36 human and 10 rhesus monkey eyes using a scanning electron microscopy. His study reported that the choriocapillaris network was supplied by feeding arterioles and drained into collecting venules. This study also showed that the structures were non-

homogenous throughout the eye. At the peripapillary and submacular areas, there was no evidence of a lobular arrangement but rather a dense honeycomb pattern of freely interconnected capillaries separated by small spaces (septae). At the posterior pole, the choriocapillaris was arranged in a lobular pattern, with either round or irregular lobules depending on the opening of both veins and arterioles. At the equator, the choriocapillaris was arranged in a similar pattern but larger in size compared to those at the posterior pole. In both posterior pole and equatorial areas, the collecting veins were predominantly at the centre of the lobule (86%), with only 14% of feeding arterioles at the centre of the lobule. Lastly, at the periphery, the choriocapillaris was arranged in a pale-like pattern ending at the ora serrata with the feeding arterioles and collecting veins running in the same plane as the capillary network.

Table 1.1: Diameters and dimensions of the choriocapillaris lobules at the different areas of the globe (Source: ¹⁵)

Area	Diameter of capillaries (µm)	Horizontal dimension (µm)
Peripapillary	15 - 25	-
Submacular	18 - 28	-
Posterior pole	20 - 35	400 × 650
Equator	20 - 38	500 × 750
Periphery	28 - 50	500 × 1100 (mid-periphery)

Figure 1.4: Choriocapillary functional unit of human choriocapillaris at different areas of the eye, from the peripapillary area (A), the submacular area (B), posterior pole (C), equator (D) and periphery (E) (Source: ¹⁵)

1.2.1.4 ***Suprachoroid***

The suprachoroid is the thin layer of interconnected lamellae of melanocytes, fibroblasts and connective tissue situated between the choroid and the sclera. It is approximately 30 µm thick. Outer to the suprachoroidal layer, there is also a thin space called the perichoroidal or suprachoroidal space.

1.2.1.5 ***Choroidal nervous system***

The choroid receives nerve supply from the long and short ciliary nerves. The long ciliary nerves carry sensory and sympathetic nerve fibres whilst the short ciliary nerves carry parasympathetic and sympathetic fibres.⁸ Moreover, in human choroid, there are approximately 2000 intrinsic choroidal neurons.¹⁶ The definite role of these intrinsic choroidal neurons is largely unknown. It has been suggested that these cells may play an important role in maintaining the choroidal thickness as well as the regulation of choroidal blood flow.

1.2.1.6 ***Choroidal lymphatic system***

In adult humans, the choroid does not contain any lymphatic vessels. However, a study carried out by Schroedl *et al*¹⁷ found lymphatic vessel endothelial hyaluronate receptor 1 (LYVE-1)-positive macrophages within the choroid using immunohistochemistry, suggesting the presence of immune cells within the choroid. They also suggested that these macrophages may contribute to the formation of temporary lymphatic channels in the choroid.

An increase in the number of choroidal macrophages has been shown to be associated with an increase in the level of nitric oxide (NO). NO plays an important role in regulating the blood flow of the choroid as well as modulating the angioarchitecture of choroidal vessels.¹⁸ Abnormal elevation of NO and the number of choroidal macrophages have been reported to be associated with the development of AMD¹⁹ and the severity of diabetic retinopathy (DR).²⁰

1.3 Choroidal function

Blood flow in the choroid is one of the highest within the body (800 - 1200 mL per 100 g tissue per minute) with 3 times more relative blood flow (per gram of tissue per minute) than the kidney²¹ and 40 to 70 times higher than the retina.²¹ The choroidal circulation is provided with approximately 85% of the total blood flow that the eye receives. This high blood flow circulation of the choroid suggests a crucial role of the choroid to maintain an adequate O₂ supply and a healthy outer retina.

1.3.1 Oxygen provision

Due to the high O₂ demand of the retina, a continuous supply is essential. *In vivo*, the O₂ profile in animal eyes has been recorded using the O₂ sensitive microelectrode. To construct the retinal O₂ profile, the microelectrode is advanced through the retina to the choroid. The microelectrode is then withdrawn at a rate of 2 µm per second while the O₂ profile is recording. An example of intraretinal O₂ profile is shown in **Figure 1.5**. By applying the mathematical models as described in Linsenmeier *et al* study²², the O₂ diffusion and consumption can be derived for each of the retinal layer. Birol *et al*²³ studied the O₂ distribution and consumption of the macaque retina using this microelectrode technique. They have shown that the choroid provides approximately 85% and 89% of the O₂ consumed by the photoreceptors during dark and light adaptation at the perifoveal area and approximately 77% of the O₂ consumption of the photoreceptors at the foveal area.

Although the choroid provides most of the O₂ for the retina, the O₂ extraction of the choroid is much lower than the retina. The arteriovenous O₂ extraction of the retina is approximately 35 – 40% whereas only 3 – 5% is reported in the choroid.

Figure 1.5: Oxygen profile of the retina during dark adaptation. Layer 1 represents the distance from the choroid $x = 0$ to L, layer 2 represents the distance from L1 to L2 and layer 3 represents the distance from L2 to L. L1 is position between the inner and outer segment of photoreceptors. L2 is the position between the inner segment and the outer nuclear layer of photoreceptors. L is the interface between the inner and the outer retina (Source: ²²)

1.3.2 Retinal temperature regulation

In addition to providing a continuous O_2 supply, maintaining a stable temperature of the macula is also provided by the choroid. This temperature modulating mechanism of the choroid is known to be controlled *via* active and passive regulation.²⁴

The retinal-choroidal temperature variation during recording experiments by Parver *et al* in cynomolgus monkey is illustrated in **Figure 1.6**. The results obtained from the thermoregulation experiment suggested that when the temperature of the macula was reduced, the choroid acted as a heat source to maintain the local temperature close to the central body. When the local temperature of the macula

was increased by exposing the eye to a microscope light, the choroid acted as a heat sink to dissipate exogenous heat produced by the external light.²⁵

Figure 1.6: Retinal-choroidal temperature recording at the macula during the intraocular pressure (IOP) modification under ambient light and microscope light exposure (upper row) and the IOP modification (lower row) (increasing in IOP corresponding to decreasing choroidal blood flow). The macular temperature maintains closer to the body temperature in ambient light and decreases significantly when IOP approaches the mean blood pressure level (arrow) suggesting the heat source role of the choroid. The macular temperature maintains closer to the body temperature under the external heat and increases significantly when IOP approaches the mean blood pressure (arrow head) suggesting the heat sink role (Source: ²⁶)

The passive temperature control mechanism of the choroid has also been shown using the cynomolgus monkey model. The macular retino-choroidal temperature was measured while the fellow eye was stimulated by external light. The choroidal blood flow (ChBFlow) was then measured using the hydrogen washout method. The results of this study showed an increase of the tissue temperature of the non-light-stimulated eye together with an increased ChBFlow confirming the passive mechanism of the choroid to maintain a stable tissue temperature environment of the outer retinal layers.²⁶

1.3.3 Retinal nutrient, waste and fluid transportation

Retinal photoreceptors are highly metabolically demanding cells, requiring sufficient O₂, nutrients and metabolites. Nearly 80% of the glucose delivered to the retina is provided from the choroid.²⁷ Due to the high protein permeability of choriocapillaris, the choroid also provides other low molecular weight metabolic molecules to the retina. The protein permeability coefficient of the choroid is approximately 50 to 80 times higher than that of skeletal muscle.²⁸ This allows more than 50% of metabolic molecules with size similar to that of glucose to pass through the capillary pores into the extracellular space.¹⁶ In order for these molecules to pass the blood retinal barrier of the RPE, an area with high glucose concentration is created within the extracellular space of the choroidal capillaries. This area of highly concentrated glucose facilitates the transport of the glucose into the retina.^{16, 28} The high protein permeability of the choroid also creates an area of high oncotic pressure which in turn allows metabolites from the retina to move across to the choroid.

In addition to O₂ and nutrient supply, the choroid also receives waste products produced from the RPE and photoreceptors via a passive diffusion of these waste molecules through the BM. Apart from the waste products, other biomolecules such as ions, CO₂, oxidised lipids and cholesterol produced by the RPE are also removed through the choroid.²⁹

1.3.4 Choroidal autoregulation

The choroidal circulation has a higher blood flow rate and a lower O₂ extraction than the retina. This special characteristic of the choroid is known to serve a high metabolic requirement of the retinal photoreceptors. In order to prevent these cells from ischaemia or oedema, a stable blood flow provided by the choroid is required. The choroid is also enriched with intrinsic neurons. Many researchers have argued and suggested that the choroid expresses some degree of autoregulation ability due to its crucial role and this enrichment of intrinsic neurons.

A recent study by Kiel and his group³⁰ have identified the autoregulatory capacity of the choroid. In their experimental setting, Kiel *et al* measured the ChBFlow of the eyes of albino rabbits while the IOP and mean arterial pressure (MAP) were manipulated independently. Their results demonstrated prominent ChBFlow compensation following adjustment of the choroidal perfusion pressure gradient over a range of 30 – 50 mmHg. Although these results demonstrated the

ability of the choroid to autoregulate its flow, their technique could not be used in living human eyes due to the invasive nature.

In the human eye, a novel technique of LDF has been introduced to study non-invasively the choroidal blood circulation. LDF has also been shown to be capable of detecting changes in ChBFlow under physiological stimuli as well as the autoregulatory response of the choroid. The study of the choroidal autoregulation using LDF will be discussed in more detail in the next chapter (Chapter 2).

1.4 PhD research motivation

The main role of the choroid is to supply blood circulation to the outer retina. More importantly, the high density of cones situated within the foveal avascular zone (FAZ) of the retina relies entirely on the choroid for its O₂, nutrition and blood supply. Despite the role of the choroid in the pathogenesis of a number of eye diseases, the alteration in choroidal haemodynamics is as yet poorly understood.

In the past decade the advent of new and sophisticated techniques including EDI OCT and LDF have enabled the study of both structure and function of the choroid. Using LDF and EDI OCT in conjunction will increase the understanding of the role of choroid in eye diseases, particularly the autoregulation of the choroid.

1.5 Aims

The overarching aim of my thesis is to investigate the role of the choroid in the pathogenesis of diabetic retinopathy (DR) and central serous chorioretinopathy (CSCR). The specific objectives of my thesis are as follows:

- To validate the applicability of LDF and EDI OCT in the ability to study the choroid
- To investigate the relationship between the choroidal structure and function in healthy adults using EDI OCT and LDF
- To describe changes in macular choroidal features of patients with DR and CSCR compared with healthy controls
- To assess the relationship between the choroidal morphology and function in healthy and diseased eyes
- To explore the association of presumed risk factors (such as age, duration of symptoms, ethnicity, smoking, exercise, blood pressure (BP), cortisol levels, personality traits) in CSCR and DR in order to determine whether these are associated with choroidal changes

1.6 Outline of the thesis

This thesis is structured in 8 main chapters. A brief outline of each chapter is detailed below:

Chapter 1 (Current chapter): Introduction to the choroidal structure and function

Chapter 2 (Literature review): Discussion of techniques used to determine the function and structure of the choroid as well as a review of previous structural and functional studies of the choroid with particular emphasis on LDF and EDI OCT.

Chapter 3 (Validation of the techniques used in this thesis): Validation of LDF and EDI OCT

Chapter 4 (Patients and methods): Presentation of the study details of two main projects (diabetic retinopathy: functional and structural study [DREFUS study] and Liverpool central serous chorioretinopathy study [Liverpool CSCR study]), including criteria for participant recruitment, common procedures and specific procedures.

Chapter 5 (Healthy choroid): Presentation of the choroidal structure within the context of the healthy eye.

Chapters 6 and 7 (Results): Presentation of detailed analyses of the results of the DREFUS and Liverpool CSCR studies in order to answer the research questions presented in this thesis.

Chapter 8 (Discussion and conclusions): Discussion of the results presented in Chapter 5, 6 and 7 of this thesis on choroidal structure and function and comparison with other techniques. A general discussion on the future direction and further studies in choroidal research will also be presented in this chapter.

1.7 Summary

The choroid is the posterior part of the uveal system extending from the ora serrata to the optic nerve. It locates between the sclera and the retina and it is mainly composed of blood vessels and connective tissue. The main role of the choroid is to maintain normal retinal homeostasis as well as providing nutrients to the retina. Choroidal dysfunction is thought to be responsible for the pathogenesis of several ocular disorders; however, the causes for the choroidal dysfunction remain elusive. In this thesis, I will explore the role of the choroid in the pathogenesis of some common chorioretinal diseases.

Chapter

2 Literature review

The choroid has an important role in maintaining the structure and function of the normal retina as described in Chapter 1.

Inadequate choroidal circulation may lead to impaired visual function; however, a clear understanding of the choroidal function in the human eye remains a great challenge in ophthalmology. The ability to visualise the choroid using conventional ophthalmic imaging such as fundus fluorescein angiography (FFA) and ultrasonography are often limited and obscured by the retinal pigment epithelium (RPE). With more recent technology such as enhanced depth imaging optical coherence tomography (EDI OCT) and choroidal blood flow (ChBFlow) assessment methods such as laser Doppler flowmetry (LDF), the choroid can be studied non-invasively in real-time with greater structural and functional detail.

2.1 Background

In this Chapter, I will discuss the methods used to study choroidal function and structure as well as some other aspects of retinal imaging. Previous techniques that were used to assess the function and structure of the choroid in diabetic retinopathy (DR) and central serous chorioretinopathy (CSCR) (used as models for ocular diseases in this thesis) are also analysed.

2.2 How can the structure of the choroid be studied?

Over the last 4 decades, indocyanine green angiography (ICGA) has been used as the main method for clinical study of the choroidal vasculature.³¹ However, the fine detailed structure of the choroid as well as a cross-sectional image of the choroid cannot be imaged using ICGA. In addition to this, the use of ICGA is limited

due to: 1) it is an invasive technique, requiring venous cannulation, 2) ICGA contains sodium iodide used to prevent its recrystallisation, which can cause an allergic reaction in patients allergic to iodine and 3) interpretation is complicated by the variability of choroidal vasculature and requires an experienced observer.

To visualise a cross-sectional image of the choroid, other conventional methods such as a B-scan ultrasonography and magnetic resonance imaging (MRI) have been used. However, the image quality obtained from these image modalities is relatively poor due to the loss of signal strength at deeper positions due to reflectance from the RPE and the low axial resolution.³ Only when the reflectivity of the tissue increases, for example, when there is a tumour, ultrasound becomes useful. The issues listed above result in a high demand for a new image modality that can produce a higher quality image of the choroid and its structures as well as overcoming the highly scattering RPE and the choroidal melanin.

Recent developments in optical coherence tomography (OCT) provide good quality cross sectional images of the retina. However, the visualisation of the choroid using a conventional OCT is more challenging arising from several aspects. 1) The maximum sensitivity of spectral domain (SD) OCT, the so called the zero-delay point, is usually between the posterior vitreous and the inner surface of the retina. Tissues further away from the zero-delay produce a weaker signal.³² Therefore, deeper structures, such as the choroid, appear darker in the image.³ 2) Scattering from the RPE reduces light penetration.

In the next section I will explain how the recent developments in OCT can be applied to image the choroid successfully.

2.3 Optical coherence tomography

The technique of OCT was first introduced by Haung in 1991 as a part of his PhD project.³³ It was first adapted to visualise human retina by Fercher and Swanson in 1993³⁴ and became commercially available in 1995 marketed by Humphrey Instruments, Inc.³⁵ OCT has become a standard of care for diagnosing and monitoring progression in several retinal diseases. OCT captures cross-sectional images of the retina that can be visualised in real time as well as providing a detailed outline of retinal layers from inner limiting membrane (ILM) to the RPE (**Figure 2.1**). Tissues anterior and posterior to the retina can also be visualised including the posterior vitreous and the choroid. OCT is not only used routinely in the clinic but also widely in ophthalmic research with more than 10,000 articles published over 2 decades.

The concept behind OCT is similar to that of B-scan ultrasonography. The difference is that OCT employs a coherent light in the near-infrared spectrum instead of an oscillating sound wave and the image obtained termed a tomograph.³⁶ The basic system consists of an interferometer and a low coherence light source split at the centre into two arms, sample and reference arms. The light in the sample arm undergoes changes as it travels across various biological tissues resulting in different time-to-flight/echo delay (deeper layer longer delay, superficial layer shorter delay) of the reflected light. Both, the delay and the amplitude of the reflected light from the sample arm and that from the reference arm form an interference signal which is detected by a photodetector. This interferometric signal constitutes an axial scan (A-scan). By moving the scan across the tissue, many A-scans are obtained and built up a 2-dimensional image or B-scan (**Figure 2.2**).³⁶ Two types of OCT are available for clinical use; 1) time-domain OCT (TD OCT) and 2) spectral-domain OCT (SD OCT), the latter of which has become the current standard.

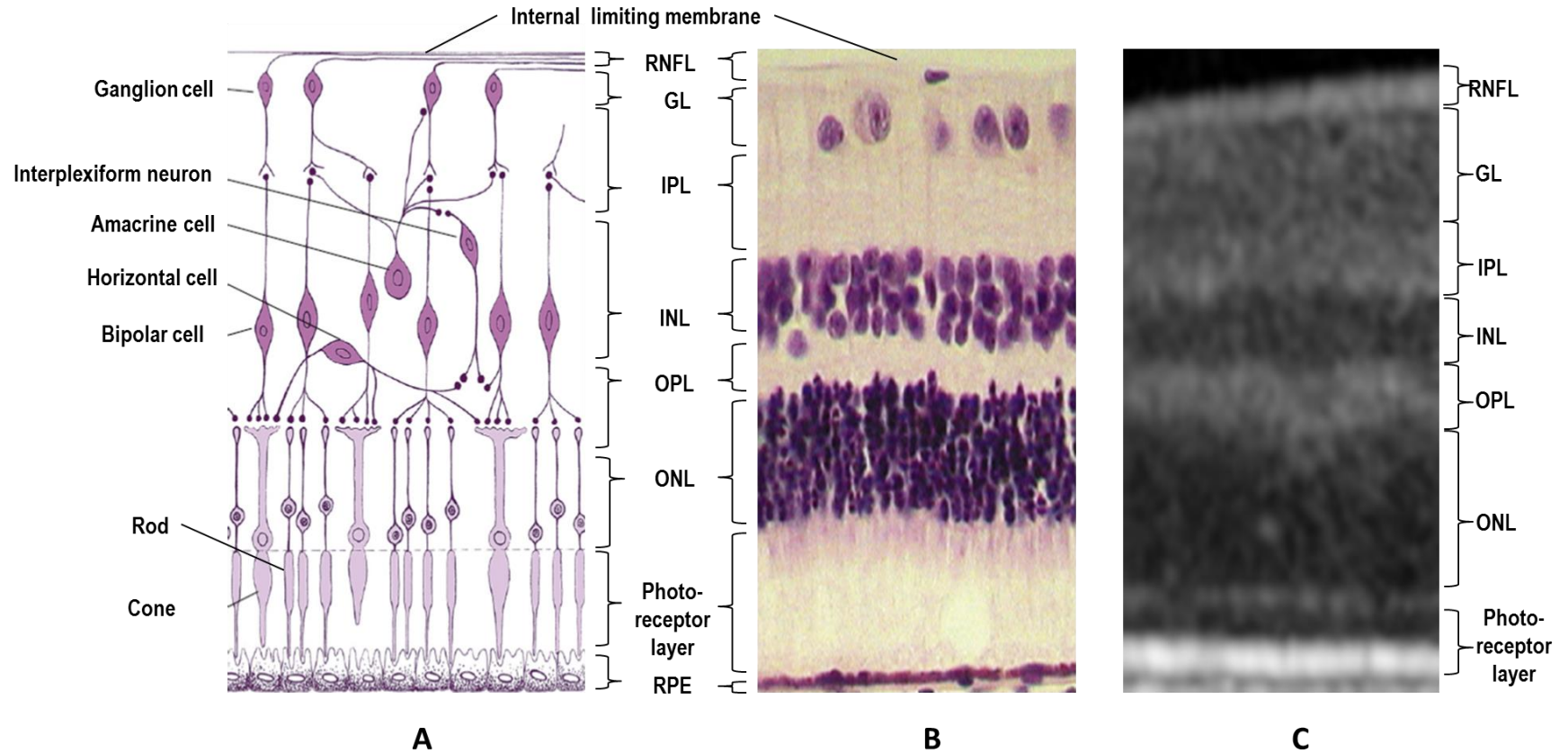


Figure 2.1: Schematic structure of human retina (A) compared with a histological section (B) and an optical coherence tomography image (C), RNFL: retinal nerve fibre layer, GL: ganglion cell layer, IPL: inner plexiform layer, INL: inner nuclear layer, OPL: outer plexiform layer, ONL: outer nuclear layer

Figure 2.2: Concept of OCT, a B-scan is constructed from several A-scans (the intensity of reflected light vs the depth of tissue) across the retina (Source: ³⁶)

2.3.1 Time domain optical coherence tomography

The first commercially available OCT instrument was the time domain (TD) OCT. In order to obtain a tomograph using TD OCT, the position of the reference mirror moves at different distances allowing the tissues from different depths to be sampled. TD OCT records 400 A-scans per second with an axial resolution of 8 – 10 μm in the tissue.³⁷ Although, in principle, TD OCT is simple and easy to manufacture, the time required for image acquisition and the resolution of the image are the great disadvantages of TD OCT (**Figure 2.5**).³ **Figure 2.3** shows a schematic diagram of TD OCT.

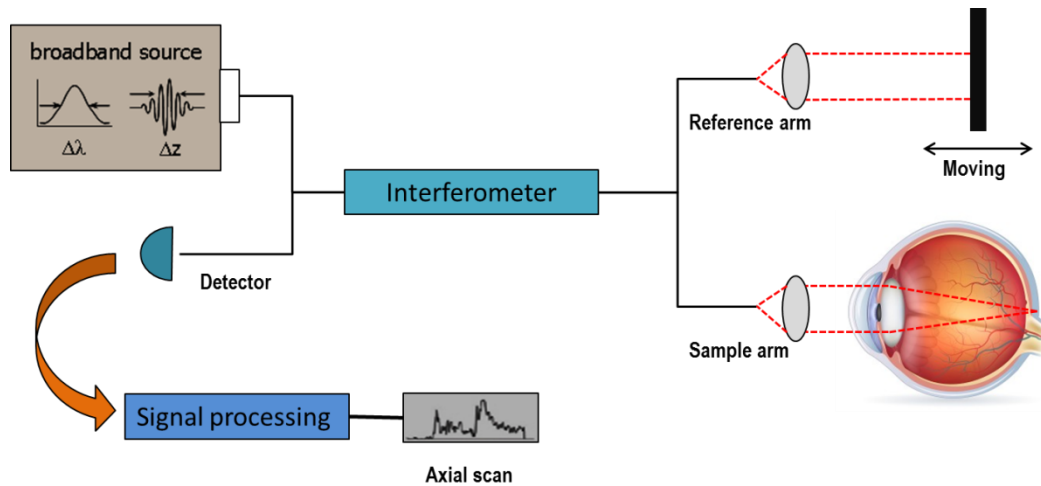


Figure 2.3: Concept of time domain OCT

2.3.2 Spectral domain optical coherence tomography (SD OCT)

Spectral domain (SD OCT) is a newer generation of OCT, first commercialised in 2006.³⁷ Unlike TD OCT, the reference arm of SD OCT is kept stationary. The combination of the light reflected from the sample and the reference arm is detected by a high-speed spectrometer as a spectrum. A Fourier transformation is then applied to the spectral interferogram to obtain the A-scans and consequently the B-scan (**Figure 2.5**). SD OCT is able to obtain 25,000 – 50,000 A-scans per second, 100 times faster acquisition than with TD OCT.³⁸ The axial resolution of SD OCT is 5 – 7 μm in tissue. **Figure 2.4** shows a schematic diagram of the SD OCT.

New OCT devices have an integrated eye tracking movement software used to stabilise the image against the patient's eye movement, allowing an increased reproducibility of the scans. Some examples of the tracking software integrated in commercial SD OCT systems are the infrared tracking and automatic motion correction software by Topcon, FastTrac™ by Carl Zeiss, VTRAC Eye-Tracking by Optovue and TruTrack by Heidelberg.

In addition to this, some OCT devices incorporate a digital image averaging technology to reduce the speckle noise caused by the use of coherent light to improve resolution. An example of this technology is the Automatic Real Time-function (ART) on Spectralis OCT device (Heidelberg engineering).

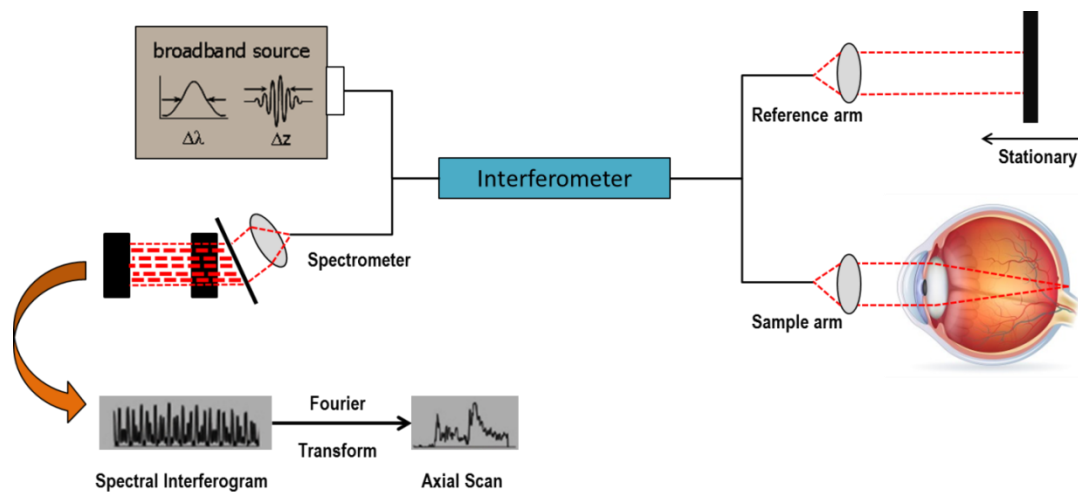


Figure 2.4: Concept of SD OCT

2.3.3 Enhanced depth imaging optical coherence tomography

In conventional OCT devices, a coherent light in the region of approximately 850 nm is commonly used. This light, however, penetrates less well into deeper tissues including through the RPE, giving a poorer image of the choroid as discussed in the preceding section.

To image the choroid, one would need to apply a broadband light source with a longer wavelength in the infrared region such as at 1060 nm or above. A simpler method for imaging the choroid using a conventional SD OCT has been proposed “enhanced depth imaging” OCT (EDI OCT). EDI OCT was first introduced by Spaide *et al* in 2008³² and since its introduction, it has been increasingly used in research with nearly 500 articles published to date.

2.3.3.1 Principles of EDI OCT

In conventional SD OCT, 2 conjugated images are developed: a real image and its inverted image; however, only the real image with the retina upwards (closer to the zero delay and greater detail) and the choroid at the bottom of the image is shown on the capturing screen³² while the other image is not shown. If the point of zero delay is placed posteriorly closer to the sclera, deeper structures such as the choroid can be visualised.

A standard procedure to displace the point of zero delay can be executed by moving the SD OCT instrument closer to the eye to obtain the inverted image, with

the choroid positioned upwards and the inner retina downwards.³² More recently, since 2010, EDI OCT has become simpler as some manufacturers have incorporated the EDI function in updated software giving non-inverted image (**Figure 2.5**). In this thesis, unless otherwise stated, I have used this platform implemented in the Heidelberg Spectralis unit.

During the EDI image acquisition, image clarity and signal-to-noise ratio can be improved by averaging several B-scans together (Automatic Real Time (ART)), typically > 25 frames for a volume scan³⁹ and 50 – 100 frames for a single scan.³ In order to determine the optimum ART several factors have been taken into account: lower ART settings do not produce images of good resolution and higher ART settings may produce blurred images since they take longer to acquire, allowing patient movement to occur. Taking these factors into account, the optimum setting for our experiments presented in this thesis was determined at 60, allowing acquiring both, single and volume EDI OCT scans.

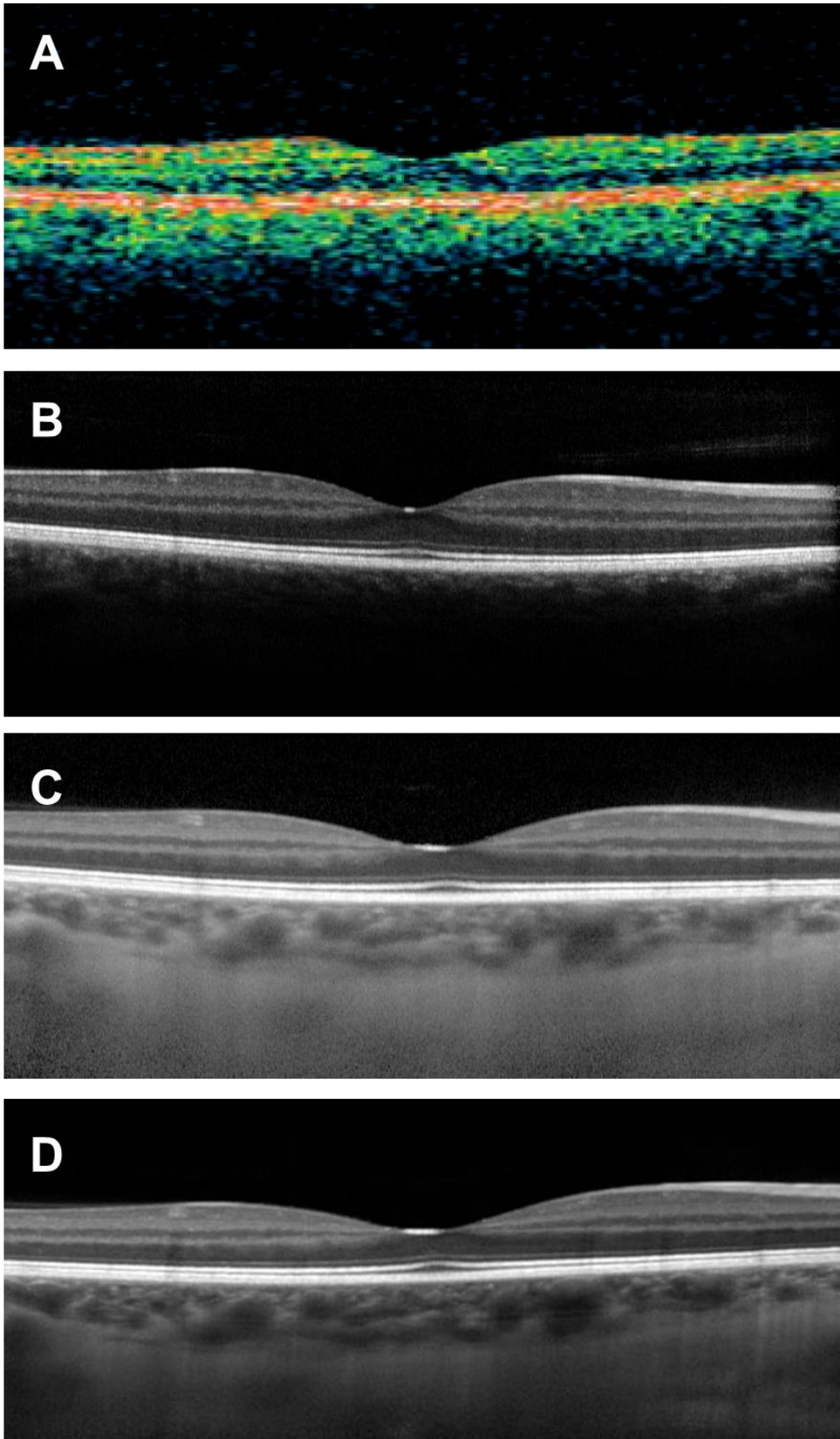


Figure 2.5: Comparison between retinal cross sectional scans captured using different OCT modalities. A = TD OCT, B = SD OCT (ART = 9), C = EDI OCT (ART = 60) and D = EDI OCT (ART = 100)

2.3.4 Swept-source optical coherence tomography

Swept-source OCT (SS OCT) is a new generation of OCT and is an extension of the SD OCT. SS OCT uses a narrow bandwidth swept laser source with a dual-balanced photo detector instead of the broadband light source and the spectrometer used in SD OCT. In SS OCT, the interference signal output is measured in nearly real-time by a photo detector as a function of the sweep time of the light source providing a much higher axial scan rate (~ 100000 A-scans/second) than a conventional SD OCT. The scan speed of SS OCT is two times faster than the SD OCT. SS OCT uses a longer wavelength centred at around 1050 nm^3 which increases the penetration of the laser for better visualisation of deeper structures. The axial resolution of SS OCT is approximately $5.3 \mu\text{m}$ in tissue. **Figure 2.6** shows a schematic diagram of the SS OCT.

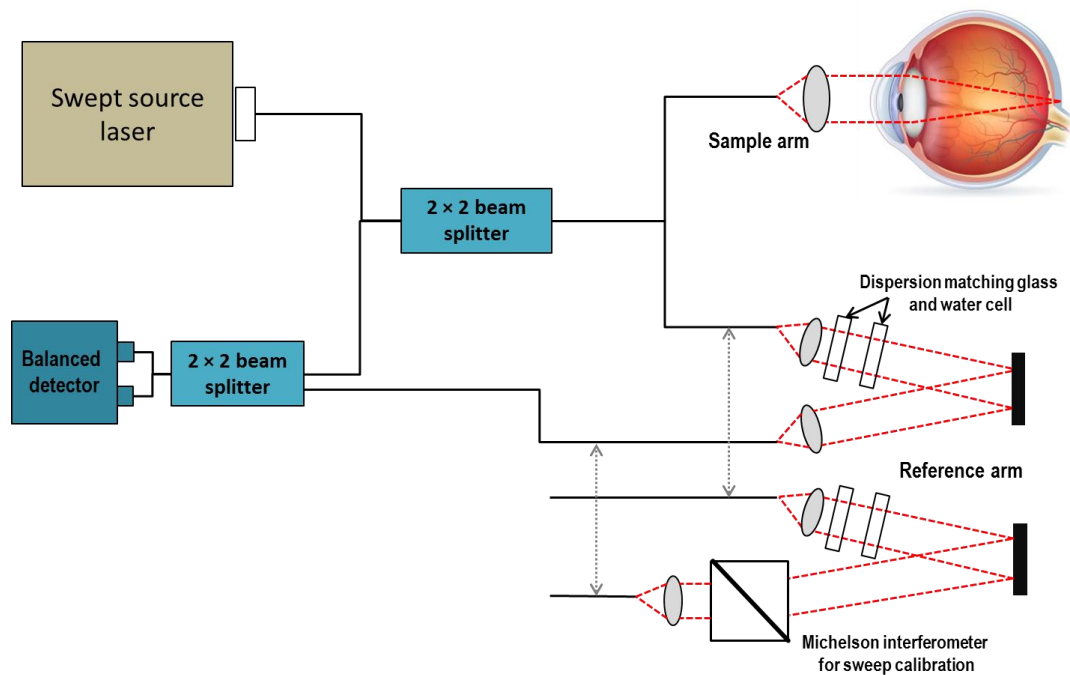


Figure 2.6: Concept of swept-source OCT (Adapted from: ⁴⁰)

2.4 Choroidal imaging with EDI OCT

2.4.1 The appearance of the choroidal structure on EDI OCT scans

In this section, I will describe how the anatomy of the choroidal structures defined in Section 1.2.1 appears on EDI OCT images (shown in **Figure 2.7**). The innermost layer of the choroid, the Bruch's membrane, appears as a hyper-reflective band, with the same intensity as the RPE. This layer cannot be separated from the RPE in scans of healthy eyes and so is termed the RPE/BM's complex. The BM only becomes visible when there is a separation of the RPE such as in serous pigment epithelium detachment (PED) or there is an area of RPE atrophy such as geographic atrophy.

The choroidal vasculature comprises the choriocapillaris, Sattler's and Haller's layers. The choriocapillaris has a relatively high reflectivity and can be observed as a thin layer with a hyper-reflective structure. It is located immediately posterior to the BM.⁴¹ The thickness of the choriocapillaris has been estimated at approximately 10 μm on EDI OCT scans.⁴²

Sattler's layer, a layer of medium sized vessels, can be seen as a layer of mixed reflectivity. It is situated approximately in the middle layer of the choroid containing oval shaped hyper-reflective spaces with hypo-reflective cores.⁴¹ Haller's layer, the large vessels layer, is located at the outer part of the choroid. Both, the Sattler's and the Haller's layers, have similar appearances on EDI OCT scans, therefore, many have used location to differentiate between these two layers. A cut-off value for the hypo-reflective core of approximately $> 100 \mu\text{m}$ has been proposed to identify Haller's layer.⁴³

The outer boundary of the choroid may have several appearances. The suprachoroid can be seen as a well demarcated hyper-reflective band outer to the large choroidal vessels called the choroidal-scleral interface (CSI).⁴⁴ A potential space between the sclera and the choroid called the suprachoroidal space (SCS) appears as a hypo-reflective band posterior to the choroidal-scleral interface. The differences in the appearance of the outer boundary will be used to standardise the protocol used for measuring choroidal thickness (ChT) in the next chapter.

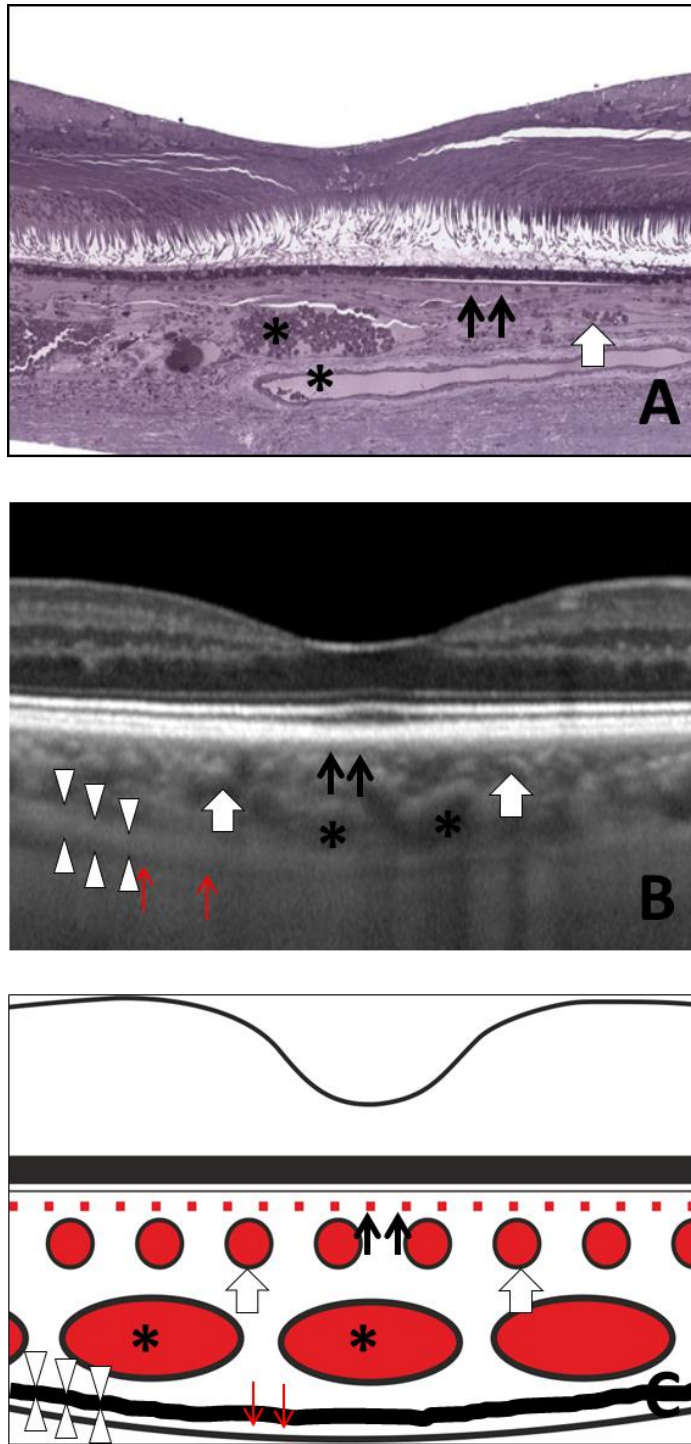


Figure 2.7: Comparison between histological cross section of the choroid (A) and EDI OCT scan (B). A schematic representation of normal anatomical landmarks (C).
 The thin black arrows (\uparrow) indicate the choriocapillaris. The thick white arrows (\uparrow) indicate the small to medium hypo-reflective cores of Sattler's layer. The asterisks (*) indicate the large hypo-reflective cores of large choroidal vessels within Haller's layer. The triangles (Δ) indicate the suprachoroid and the red arrows (\uparrow) indicate the suprachoroidal space

2.4.2 Measurement of choroidal thickness in healthy eyes

Prior to the OCT era, the thickness of the choroid was estimated in histological studies to be between 125 and 200 μm .^{45, 46} These histological profiles of the choroid, however, cannot be used to represent living human eyes, mainly due to the tissue volume loss during processing, which can account for as much as 33% of the total volume.⁴⁶

The choroidal thickness (ChT) is a common parameter used to represent one important aspect of the choroidal structure in healthy and diseased eyes. Two of the most common methods used to measure the ChT are 1) the software calliper and 2) the relocation of the automatic segmentation lines from the retina to the choroid. In both methods, the ChT is measured from the outer limit of the RPE/BM's complex to the choroidal–scleral interface. The most common location to measure the ChT reported in the majority articles is at the fovea centre. Margolis and Spaide⁴⁷ were the first to report the subfoveal choroidal thickness (SfChT) in their retrospective study on 54 non-myopic normal eyes (mean age of 50.4, range 19 – 85). The mean SfChT was 287 (standard deviation (SD); ± 76) μm . Since this first report, SfChT of normal healthy eyes has been reported by several groups using various SD OCT devices. **Table 2.1** shows the SfChT measurements from published studies using various OCT instruments, varying populations and ethnicities. Estimates of SfChT range from 253⁴⁸ to 448 μm ,⁴⁹ making it difficult to know what the actual range is. In the next few paragraphs I will review the factors that have caused this wide variation.

One of the reasons that the reported SfChT measurements vary among observers is due to the fact that different studies used different systemic and ophthalmic criteria to define “normal and/or healthy” eyes. For example, Margolis *et al*/based their definition of normal eyes entirely on the appearance on the selected scan. Eyes with mild vitreomacular changes and the fellow eyes of subjects with unioocular eye disease were also considered as normal. Some studies defined normal/healthy using the refractive error (within ± 6 or ± 3)⁵⁰⁻⁵⁴ while others defined normal/healthy using the participants' vision⁵⁵⁻⁵⁷ and axial length (AxL).⁵⁸ Some studies excluded participants with systemic diseases such as diabetes and hypertension while others did not mention these systemic factors in their study.

As mentioned above, measuring the ChT requires mostly manual annotation skills from the observer(s) and so validation is important. For ChT measurement using EDI, Spaide briefly reported a high correlation between independent

observers on a small group of healthy volunteers with no eye problems.³² Later, Rahman reported a high correlation of a single point manual measurement of SfChT between and within observers as well as between sessions. The study concluded that a variability of >32 μm could be observed despite using the same measurement method.⁵⁹ For the choroidal volume quantification, the differences in manual measurements between observers was approximately 0.42 mm^3 .³⁹ In addition to this study, Kim *et al* have suggested that a 1:1 μm image viewing mode should be used to perform the ChT measurement so as to give more accurate measurements of the ChT.⁶⁰ The general level of agreement shown in the above studies, however, did not account for the anatomical variation of the outer boundary of the choroid. Measuring the ChT using a precise location of the choroidal–scleral interface (SCI) is essential. The method I have used and developed to perform the ChT measurements is explained in detail in Chapter 3.

Another important point that needs to be considered for ChT measurements is the similarity of the ChT measurements across commercially available OCT systems. Branchini *et al*⁶¹ and Yamachita *et al*⁶² compared the mean ChT obtained from different SD OCT devices and found a near identical mean ChT and good reproducibility across the different SD OCT devices (**Table 2.2**). The reproducibility of the ChT measurements was also in good agreement when comparing the EDI OCT to the SS OCT.^{63, 64}

In summary, various SD OCT devices have been used to study the ChT. The most common reported location is at the foveal centre. This relatively large estimation is partly due to differences in devices and selective criteria used in previous studies. Also, some studies have included a relatively small number of subjects in their reports. The estimate range of SfChT on Spectralis OCT in Caucasian is approximately 334 to 342 μm and this will be used to compare with my healthy cohort in Chapter 5.

Table 2.1: Published estimates of subfoveal choroidal thickness in healthy eyes listed by year of publication

First author/year (reference)	Number of participants/ eyes	Mean age of participants (range)	Population/ race	SfChT	Model of the OCT device
Spaide (2008) ³²	17/34	33.4 (19 – 54)	Caucasian	318 (OD) and 335 (OS)	Spectralis*
Magolis (2009) ⁴⁷	30/54	50.4 (19 – 85)	Caucasian	287 ± 76	Spectralis*
Manjunath (2010)	34/34	51.1 (22 – 78)	Caucasian	272 ± 81	Cirrus HD OCT*
Ikuno (2010) ⁶⁵	79/43	39.4 (23 – 88)	Asian/Japanese	354 ± 111	SS OCT**
Benavente-Perez (2010) ⁴⁹	11/11	35.72	Caucasian	448.5 ± 82	SOCT Copernicus*
Rahman (2011) ⁵⁹	50/100	38 (30 – 49)	Mixed race	332 ± 90	Spectralis*
Ding (2011) ⁵¹	210/420	49.7 (20 – 85)	Asian/Chinese	261 ± 88.42	Spectralis*
Shin (2011) ⁵⁰	45/57	45.28 (23 – 80)	Asian/Korean	270.82 ± 51.4	3D OCT-1000 Mark II*
Li (2011) ⁶⁶	93/93	24 (19.6 – 33.4)	Caucasian	342 ± 118	Spectralis*
Ikuno (2011) ⁶⁷	12/24	37.6 (23.9 – 50.5)	Asian/Japanese	292.7 ± 77.3	SS OCT**
Ikuno (2011) ⁶⁷	12/24	37.6 (23.9 – 50.5)	Asian/Japanese	283.7 ± 84.1	Spectralis*
Fujiwara (2012) ⁵²	145/145	45.7 (5 – 88)	Asian/Japanese	265.5 ± 82.4	Spectralis*
Kim (2012) ⁵⁶	69/69	22.25 (20 – 25)	Asian/Korean	307.03 ± 91.27	Spectralis*
Chen (2012) ⁵⁸	50/100	38 (30 – 49)	Mainly Caucasian	334 ± 94 (OD) and 333 ± 90 (OS)	Spectralis*
Branchini (2012) ³⁹	28/28	35.2 (23 – 64)	Mainly Caucasian	347.51 ± 94.37	Cirrus HD OCT*
Branchini (2012) ³⁹	28/28	35.2 (23 – 64)	Mainly Caucasian	347.46 ± 97.92	Spectralis*

Table 2.1 (continue): Subfoveal choroidal thickness in healthy eyes

Branchini (2012) ³⁹	28/28	35.2 (23 – 64)	Mainly Caucasian	337.67 ± 89.01	RTVue*
Yamashita (2012) ⁶²	43/43	30.5 (19 – 40)	Asian/Japanese	272.6 ± 63.0	Spectralis*
Yamashita (2012) ⁶²	43/43	30.5 (19 – 40)	Asian/Japanese	272.8 ± 64.7	Cirrus HD OCT*
Yamashita (2012) ⁶²	43/43	30.5 (19 – 40)	Asian/Japanese	269.2 ± 61.0	3D OCT-1000 Mark II
Ruiz-Moreno (2013) ⁶⁸	43/83	10 (3 – 17)	Caucasian	312 ± 65.3	SS-OCT**
Ruiz-Moreno (2013) ⁶⁸	50/75	53 (25 – 85)	Caucasian	305.6 ± 102.6	SS-OCT**
Park (2013) ⁵⁴	48/48	6.7 (4 – 11)	Asian/Korean	348.4 ± 82.5	Spectralis*
Wei (2013) ⁴⁸	3233/3233	64.3 (50 – 93)	Asian/Chinese	253.8 ± 88.42	Spectralis*
Read (2013) ⁶⁹	194/194	8.2 (4 – 12)	Mainly Caucasian	330 ± 65	SOCT Copernicus*
Li (2014) ⁷⁰	1323/1323	11 – 12	Mainly Caucasian	369 ± 80.8 (boys) and 348 ± 72.1 (girls)	Spectralis*
Karaca (2014) ⁷¹	110/110	44.0 (18 – 70)	Asian/Turkish	315.5 ± 78.6	Spectralis*
Kim (2014) ⁵⁵	286/286	40.18 (13 – 75)	Asian/Korean	307.26 ± 95.18	Spectralis*
Ruiz-Medrano (2014) ⁵⁷	154/276	23 – 88	Caucasian	301.89 ± 80.53	SS OCT**
Copete (2014)	46/61	45 (5 – 86)	Caucasian	285.7 ± 88.8	3D-2000 OCT*
Copete (2014)	46/61	45 (5 – 86)	Caucasian	279.4 ± 96.6	SS OCT**

*Spectral domain OCT, **High-penetration, swept-source OCT (1060 nm)

Table 2.2: Comparison of ChT measured in three different instruments (ICC and 95% limits of agreement) (Source: ^{61, 62})

	Cirrus HD OCT®	Spectralis®	RTVue®
Cirrus HD OCT®	xx	0.976 (12.80 to -13.33)	0.965 (11.21 to -13.57)
Spectralis®	0.968 (31.89 to -32.35)	xx	0.964 (10.85 to -12.45)
Topcon 3D OCT-1000 Mark II®	0.958 (39.14 to -31.94)	0.975 (23.53 to -30.28)	xx

xx: not available

2.4.3 Asymmetric nature of the choroid

The information obtained from the choroidal profiles using only a single B-scan from various OCT imaging systems has revealed an asymmetrical nature on either side of the fovea. Margolis and Spaide ⁴⁷ showed this asymmetrical nature using an EDI horizontal scan across the fovea on a Spectralis® system. In this article, they reported that the thickest ChT point was at the fovea with mean ChT (\pm SD) of 287 μ m (\pm 76). The ChT became thinner temporally (261 \pm 77 μ m) and nasally, it was the thinnest (145 \pm 57 μ m). Similar results were also observed by other authors using different SD OCT devices (**Figure 2.8A**).^{50, 53} Although, this asymmetric pattern with the thickest point at the fovea is generally found in adults, a different pattern was found in healthy infants ⁶⁸ (**Figure 2.8B**) with the choroid being the thickest at the temporal macula. According to their findings, this was more obvious in the younger age group (3 – 9 years old).

The macular choroid also shows an asymmetrical nature on volumetric scans. One study that used SS OCT to study 31 eyes of healthy Japanese subjects with no ophthalmic or systemic symptoms showed a thicker choroid and greater choroidal volume temporally than nasally and superiorly than inferiorly.⁷² This pattern was also reported by other researchers using either the same SS OCT ^{73, 74} or the EDI OCT ^{75, 76} in both adults and infants.

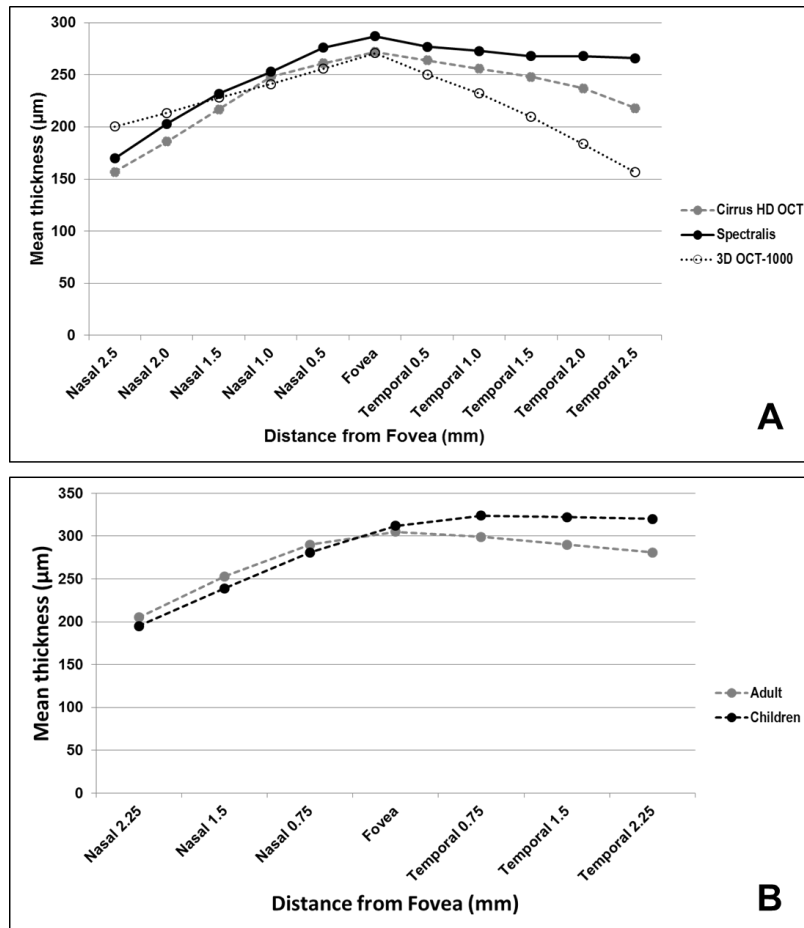


Figure 2.8: Measurements at different points showing the asymmetrical nature of the choroid using three SD OCT systems (A).^{47, 50, 77} Difference in the mean thickness between children and adults at different locations (B)⁶⁸

2.4.4 Diurnal variation of the choroid

In human eyes, the first evidence of diurnal changes in choroidal thickness was demonstrated by using a partial coherence interferometry (PCI, a dual laser beam version of optical coherence tomography).⁷⁸ The mean ChT obtained from the PCI data showed an antiphased fluctuation between the mean ChT and AxL but the sample size in this study was limited and 72% of the subjects had to be excluded from some aspects of the analysis.

The diurnal change in ChT has been shown more recently with EDI OCT.⁷⁹ Twelve healthy volunteers with mean age of 30 underwent EDI OCT scan every two hours from 9 am to 5 pm. The ChT was significantly decreased from 372.2 ± 100.4 µm at 9 am to 340.6 ± 82.9 µm at 5 PM with a mean change of 33.7 ± 21.5 µm. This changing amplitude was larger in eyes with thick and intermediate ChT compare to eyes with thin ChT.

The rhythm of ChT changes was also studied during day/night cycles in healthy eyes. In this study, the SfChT was thicker at night and became thinner during the day with the thickest at 3 AM ($290.8 \pm 110.8 \mu\text{m}$) and the thinnest at 6 pm ($271.9 \pm 103.5 \mu\text{m}$) with the average mean diurnal fluctuation of SfChT of $33 \mu\text{m}$.⁸⁰ This day/night choroidal cycle was shown to be independent from other systemic factors, except for the systolic blood pressure which showed an opposite rhythm to that of the ChT (correlation coefficient of -2.04 , $P = 0.02$).⁸⁰ The ChT from this study, however, only derived from mostly subjects with high myopia and could not represent emmetropic eyes. The pattern of diurnal variation was shown to be greater in men than that in women and also greater in those with a thicker choroid and shorter axial length.⁸¹ **Figure 2.9B** and **Figure 2.9C** show the measurements of the changes in diurnal rhythm of the ChT.

Several aspects need to be considered when a study of the diurnal rhythm of the choroid using EDI OCT is performed. 1) The position of the scan has to be at exactly the same location for each measurement. This can be done using the eye tracking technology mentioned in Section 2.3.2. The first scan at the first time point should be set as a reference scan. 2) Due to small amplitude changes of the ChT at each time point, the inter- and intra-observer agreements on the ChT measurement should be reported in these studies.

The theory behind the diurnal oscillation of the choroid may be explained as follows:

1) First, compensation of the choroidal structure according to the circadian variation of IOP and axial length. In human, IOP increases in the morning and decreases during the daytime to the lowest point at the nighttime. This pattern of IOP fluctuations are known to coincide with the axial length which exhibits the longest during the daytime and the shortest during the nighttime.⁸² Hence, the ChT may adjust to accompany the changes in IOP and the axial length as described above.

2) Second, control of the sympathetic nerve. The sympathetic nerve is more active during the daytime and becomes more relaxed during the nighttime.⁸³ This might be correlated with the ocular perfusion pressure which tends to be higher during the nighttime, resulting in higher diffusion of the fluid into the choroid.⁸⁴

3) Third, adjustment of amount of O_2 and nutrition supply to the activity of different photoreceptors during daytime and nighttime. The choroidal may become

stiffer to achieve higher blood flow rate during the daytime in response to the highly activated cones during the daytime.

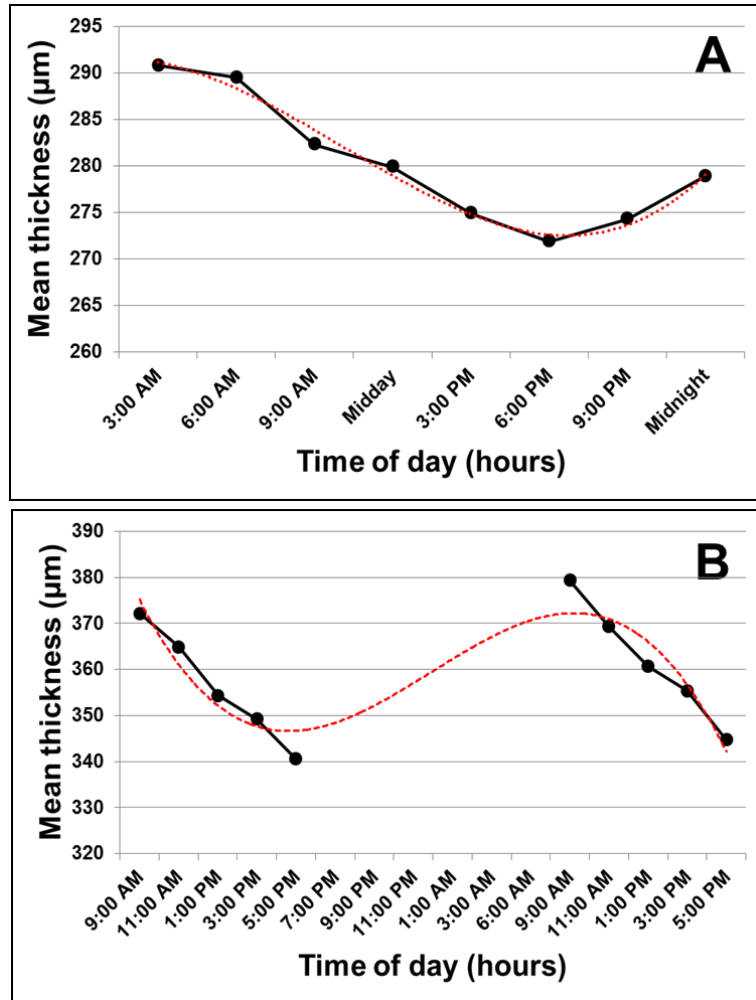


Figure 2.9: Diurnal variation of the ChT measurements over 24 hours (A) and 48 hour (B) (Adapted from: ^{79, 80, 82})

2.4.5 Factors correlated with choroidal thickness

Prior to the development of EDI OCT, knowledge of the correlations between the ChT and systemic and ophthalmic factors was limited. The only factor known to affect the choroidal vasculature was age. Thinning of the choroid, choroidal atrophy and the reduction of small and large choroidal vessels were the histological characteristics of ageing choroid.^{45, 46, 85} A negative correlation between the choroidal thickness at all the observed locations and age ($R = 0.424$; $P = 0.001$ for SfChT) was reported for the first time by Margolis *et al.*⁴⁷ In this retrospective study, it was also shown that the choroid at the foveal centre gets thinner approximately $1.56 \mu\text{m}$ per year. The limitation of Margolis's study was that the eyes included in the study do not represent normal as the authors had included eye with no significant observable pathological features and did not account for systemic or other ocular factors such as refraction and axial length.

Other groups have also found this strong negative correlation between age and ChT.^{50-53, 55, 57, 58, 65} The results reported for the average decrease per year between different studies vary quite significantly, however, from $1.31 \mu\text{m}$ ⁵⁰ to $4.80 \mu\text{m}$.⁴⁸ This wide range of variations is likely to derive from various factors such as participant profiles, type of OCT device, age range of participants and statistical method used for the analysis. **Figure 2.10** shows the relationship between ChT and age.

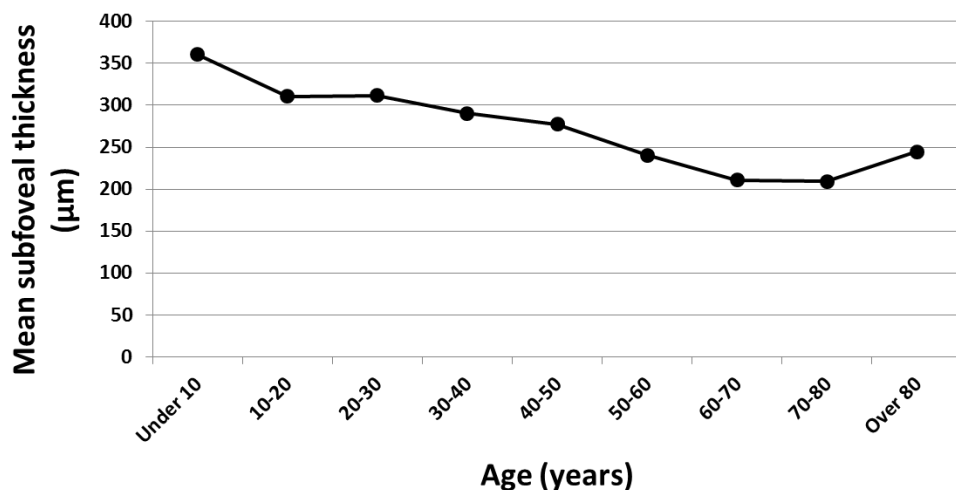


Figure 2.10: The relationship between ChT and age (Adapted from: ⁵²)

Several other factors affecting the ChT besides ageing have been more recently identified. Some studies found a negative correlation with AxL.^{48, 55, 56, 65, 86} Other studies found positive correlations with refractive error^{56, 86} while some found no correlation.^{52, 54} A decrease of the ChT by 15 µm for every increase of refraction of 1 dioptre (D) and 32 µm for every increase in AxL of 1 mm has been reported in an Asian/Chinese population⁴⁸ whereas a decrease of the ChT by 25.4 µm for every increase of 1 D and 58.2 µm for every increase in AxL of 1 mm has been reported in a healthy young Caucasian population.⁶⁶ With this complex relationship between ChT, age and other factors, Ruiz-Medrano⁵⁷ has proposed an equation to predict the ChT dependent on age and refractive error:

$$\text{Macular choroidal thickness } (\mu\text{m}) = 292.48 - 1.006 \times \text{age } (\text{yrs}) + 5.292 \times \text{refractive error } (D)$$

Equation 2.1: The proposed equation to predict the ChT from age and refraction

This equation however, cannot be used to represent other than the studied population as there was different participant selection criteria used in different studies.

2.4.6 Summary of EDI OCT

In this section, I have described how the anatomy of the choroidal structures appears on EDI OCT images. The appearance of the choroid on EDI OCT scans can be correlated to its histological structure; however, not all the choroidal vascular layers observed in its histological structure can be seen on EDI OCT scans, particularly the choriocapillaris. In addition, there is a considerable variation of the choroidal outer boundary observed on EDI OCT scans and this variation may affect the measurement of the choroidal thickness on EDI OCT scans.

The SfChT of normal eyes has also been previously estimated using EDI OCT from 253 to 448 µm. This relatively large estimation is partly due to differences in devices and selective criteria used in previous studies. In Caucasian ethnicity, the SfChT is likely to range between 334 to 342 µm; however, in order to report the ChT accurately, various factors need to be considered: age, refraction and axial length. There is, however, a wide discrepancy in the literature regarding how the refraction and axial length affect the ChT. The study of the function of the choroid is described in the next section.

2.5 How can the function of the choroid be studied?

In order to understand the function and vascular physiology of the choroid in normal and diseased eyes, several invasive and non-invasive techniques have been used over the years. Invasive methods used for determining choroidal circulation include hydrogen clearance,^{87, 88} fluorescent microspheres,^{89, 90} ICGA⁹¹ and lysosome-encapsulated heat-sensitive laser-targeted angiography (LTA).^{92, 93} Non-invasive methods include MRI,⁹⁴ colour Doppler imaging (CDI),⁹⁵ optical micro-angiography (OMAG),⁹⁶ laser speckle flowgraphy (LSFG),⁹⁷ ocular pulse amplitude (also known as pulsatile ocular blood flow (POBF))⁹⁸ and LDF.⁹⁹ The advantages and disadvantages of these non-invasive techniques are summarised in the **Table 2.3**.

LDF offers several advantages over other non-invasive techniques. Firstly, LDF provides the direct measurement of the choroidal circulatory parameters including velocity and volume at the fovea region. The LDF signal predominantly derived from blood circulation in the choriocapillaris. Secondly, LDF does not require the dilatation of the pupil or a tissue-instrument contact. More importantly, LDF measurements do not disturb the ocular environment and constitute a quick method to measure the sub-foveal choroidal blood flow without any interference from the retinal circulation.

Table 2.3: Advantages and disadvantages of non-invasive techniques used to measure choroidal blood circulation

Method	Direct/indirect	Description/concept	Advantage	Disadvantages	Reference
Magnetic resonance imaging (MRI)	Indirect	Technique based on the arterial spin labeling (ASL) of endogenous water content in blood	Provides a quantitative analysis in classic units (ml/100ml/min)	<ol style="list-style-type: none"> 1. High eye motion 2. Low resolution 3. High cost per measurement patient needs to be trained prior to the measurement 4. Long acquisition 	Zhang Y., 2012 ¹⁰⁰
Colour Doppler imaging (CDI)	Direct	This technique combines B-scan ultrasonography with Doppler effect	Provides detailed measurement of perfusion from different defined vessels	<ol style="list-style-type: none"> 1. Insufficient resolution 2. High variation due to anatomical differences in ocular structure 3. Acquisition takes 10 - 20 mins depending on the experience of the observer 	Stalmans, I., 2011 ¹⁰¹
Laser speckle flowgraphy (LSFG)	Direct	Technique based on the speckle pattern of the reflected light (wavelength 830 nm) from moving red blood cells, represented by mean blur rate (MBR) which is an index of relative blood flow velocity	Provides a 2-dimensional map of choroidal circulation	<ol style="list-style-type: none"> 1. Highly influenced by choroidal morphology 	Sugiyama, T., 2010 ⁹⁷
Pulsatile ocular blood flow (POBF)	Indirect	Technique based on the amount of blood entering the eye which corresponds to the changes of the IOP	Provides a function of time corresponding to the pulsatile component of intraocular blood flow (85% of which comes from the choroid)	<ol style="list-style-type: none"> 1. 20 seconds of instrument-corneal touch 2. 3-5 consecutive measurements are required for repeatable results 	Yu BS. and Lam AK., 2007 ¹⁰² Silver DM. and Farrell RA., 1994 ¹⁰³
Laser Doppler flowmetry (LDF)	Direct	Technique based on the Doppler effect of light scattered by moving red blood cells in the sampled volume	Provides measurements of relative blood flow in the fovea region without the need for dilatation and artefacts from retinal vessels	<ol style="list-style-type: none"> 1. High variability between the measurements 2. Highly influenced by the choroidal morphology 	Riva CE., 1994 ⁹⁹

2.6 Laser Doppler flowmetry

The study of the function of the choroid is relatively challenging. This is mainly due to the limitation of methods used to study choroidal circulation as well as the complexity of the choroidal vasculature and the position of the choroid, particularly the choriocapillaris. Several direct methods such as MRI and CDI have been used to study the choroidal function but the signals derived from the choroid are often affected by the signal from retinal circulation and patient's movements. More importantly, the choroidal function measured by the above methods cannot be used to study choroidal regulation. To date, only LDF has been used to determine the response of choroidal circulation to the physiological stimuli. In this section, previous studies on choroidal blood circulation using LDF will be discussed.

To measure ocular haemodynamic, Tanaka and colleagues (Riva and Ben-Sira) introduced a technique called laser Doppler velocimetry (LDV) in 1972, following a successful non-invasive measurement of blood velocity from rabbit eyes.¹⁰⁴ Ten years after the first measurement of LDV, Riva, Grunwald and Sinclair demonstrated the use of LDV to noninvasively measure blood flow of human optic nerve head (ONH).¹⁰⁵ However, LDV only provided a relative blood velocity at the area of observation, therefore, Riva and colleagues further developed and established a technique called "laser Doppler flowmetry (LDF)" that could be used to noninvasively measure and derive more parameters of relative blood flow of human eyes. They also studied bidirectional blood flow as a method for estimating blood flow in retinal vessels using two probes placed either side of the moving blood column.¹⁰⁶

LDF is based on the Doppler effect, first described by the Austrian physicist, Christian Doppler in 1842.¹⁰⁷ In the case of microvascular perfusion, the Doppler effect refers to the frequency shift caused by light scattered by moving red blood cells (RBC) as described by Bonner and Nossal.¹⁰⁸ LDF has been successfully established as a technique to measure blood flow in animals¹⁰⁹ and human ocular tissues such as the ONH¹¹⁰ and the iris.¹¹¹

Riva and co-workers have further demonstrated and validated the use of LDF to measure ChBFlow locally using cats as models.¹¹² In their first demonstration of non-invasive measurement, the ChBFlow remained stable for a long period of time. This stability of ChBFlow allowed the assessment of responses under various physiological and pharmaceutical stimuli.⁹⁹ An added advantage of LDF is that dilatation drops such as tropicamide do not interfere with the

measurements.¹¹³ **Figure 2.11** shows a schematic diagram of the optical setup of LDV and LDF.

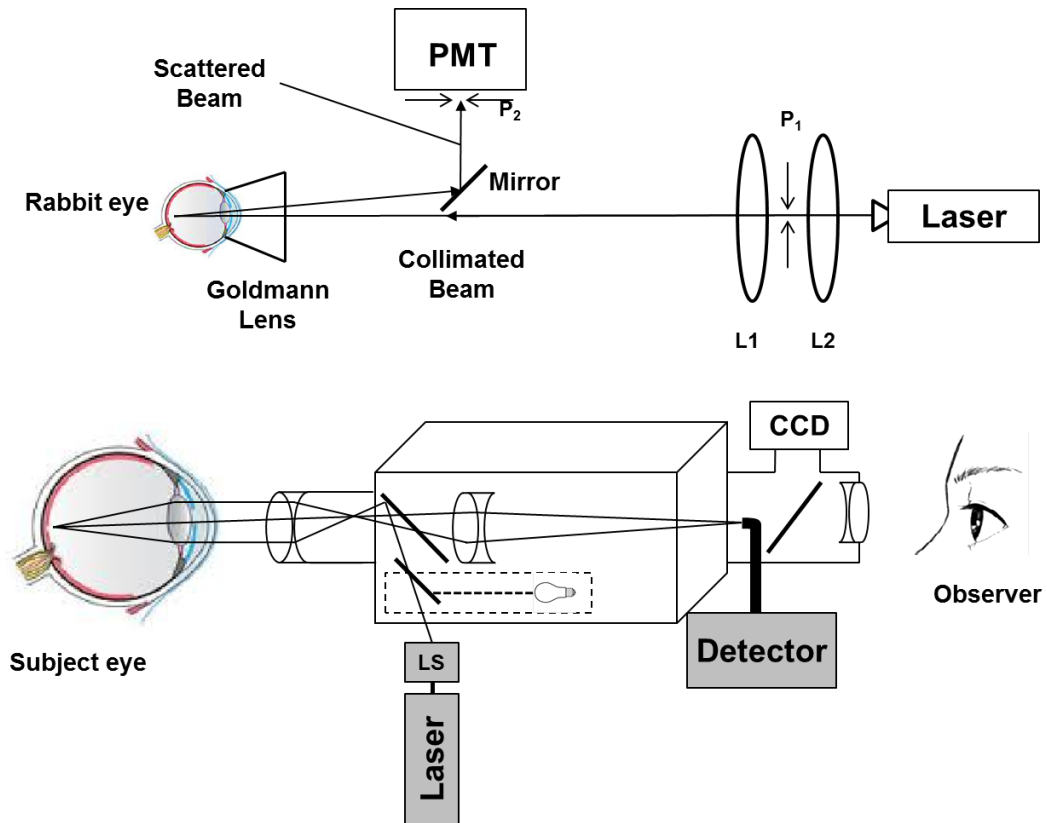


Figure 2.11: Optical setup of laser Doppler velocimetry in rabbit's eye (top); (Adapted from: ¹⁰⁴) and laser Doppler flowmetry for ONH measurement (bottom); (Adapted from: ¹¹⁴) (L = lens , P = pinhole, PMT = photomultiplier tube, and CCD = charge-coupled device camera)

2.6.1 Basic principle of LDF

In LDF, the monochromatic (single frequency; f_i) laser beam is produced by either a He-Ne (632.8 nm) or a diode (670.0 nm) source. **Figure 2.12** shows a schematic diagram of the incident laser with frequency (f_i) when it hits an RBC moving in direction (V) with velocity $|V|$ at an angle α_i . After hitting the RBC, the laser is scattered in various directions and angles (α_s) with associated frequency shifts denoted by Δf .

Figure 2.12: Schematic diagram of the principle of LDF (Source: ¹⁰⁷)

The Δf is called the Doppler shift and represents a shifted frequency of the laser beam. The Δf is described by the following equation:

$$\Delta f = nV(\cos \alpha_s - \cos \alpha_i)/\lambda_i$$

Equation 2.2: The Doppler shift caused by moving RBCs; λ_i is the wavelength of the incident light and n is an index of the refraction of the light in the blood.

Although, this Δf is very small compared to the incident laser frequency, Δf can be detected using optical mixing spectroscopy in the autodyne mode.¹⁰⁷

The light scattered by RBCs reflected back to the detector consists of various shifted frequencies (Δf_s) from the moving RBCs (around 1-5% of the total light is reflected) as well as the non-shifted light which emerges from the static components of tissue.¹⁰⁷ The non-shifted light acts as a reference signal at the detector surface. The output of the photodetector comprises only the oscillating components of various Δf_s according to the 'square law'. A Fourier transform is used

to analyse the power spectrum of these photocurrent Δf_s . The plot of the power of the photocurrent as a function of Δf_s constitutes the Doppler shift power spectrum (DSPS) as shown in **Figure 2.13**.¹¹⁴

Figure 2.13: Doppler shift power spectrum, the spectrum is constituted from the power of shifted frequencies. The dotted line represents the noise level of the DSPS. The small arrow at around 160 Hz represents the velocity (Source: ¹⁰⁷)

From the DSPS, blood flow parameters can be obtained. These parameters include the velocity (the mean speed of RBCs) and the volume (the number of moving RBCs). The velocity (Vel or choroidal blood velocity: ChBVelocity) is proportional to the mean Δf (Hz) and the volume (Vol or choroidal blood volume: ChBVolume) is proportional to the area under the DSPS curve (arbitrary units). The velocity and volume can be calculated as shown in **Equation 2.3**. The blood flow can be calculated as $\text{Vel} \times \text{Vol}$.

$$Vel = \frac{\int_{30Hz}^{\Delta f^{high}} \Delta f P(\Delta f) d\Delta f}{\int_{30Hz}^{\Delta f^{high}} P(\Delta f) d\Delta f},$$

$$Vol = \frac{1}{A_{dc}^2} \int_{30Hz}^{\Delta f^{high}} P(\Delta f) d\Delta f$$

Equation 2.3: Velocity (Vel) and volume (Vol) calculation; A_{dc} is the amplitude of the direct photocurrent (DC). The DC should be kept constant within 10% of the mean in order to ensure the variation of other parameters.

2.6.2 LDF systems

Before using any LDF devices, 2 important parameters need to be established in order to obtain reliable choriocapillaris flow measurements: reproducibility and sensitivity. The reproducibility of the test is defined using the coefficient of variance (CV) and the sensitivity of the test. The sensitivity of the test is calculated from **Equation 2.4** representing the minimum statistically significant change in blood flow parameters that can be detected.

$$S = \frac{sd}{\bar{x}} \times \frac{k}{\sqrt{N}}$$

Equation 2.4: Sensitivity of LDF measurement; sd is the standard deviation of the difference between measurements of all subjects, \bar{x} is the mean value of all measurements and k is the two-tail value of the t-distribution at the 0.05 level of significance.

2.6.2.1 Fundus camera-based near infrared LDF

The fundus camera-based LDF was first introduced by Riva and Petrig.¹¹⁵ The system consisted of a solid-state near-infrared diode laser ($\lambda = 811 \text{ nm}$) delivered through the illumination pathway of a fundus camera to the eye with $60 \mu\text{W}$ at the cornea.¹¹⁶ The reflected light returned back from the eye that served as the input to an aperture detector connected to a square-law photodetector such as a photomultiplier tube (PMT) or a silicon avalanche photodiode (APD); APD has a higher quantum efficiency (QE) and better spectral response compared to PMT.¹¹⁵ **Figure 2.14** shows a diagram of the fundus camera-based LDF. The LDF signal can then be analysed either using a commercially available skin blood perfusion software such as PeriFlux PF3 (Perimed Inc., Stockholm, Sweden) and BPM403A (Vasamedics, Minneapolis) or a custom-written computer-based software, Oculix,

developed by Petrig *et al.* I used a fundus camera LDF device with custom-written computer-based software (Flom-S device signal processor) to study the choroidal function in this thesis.

The sensitivity of the fundus camera-based LDF was reported in 15 healthy subjects based on 10 successive recording sections of 15 seconds at 8%.¹¹⁶

Figure 2.14: Fundus camera based LDF system (Source: ¹¹⁶)

2.6.2.2 **Compact LDF**

A second generation LDF, the compact LDF, was developed by Geiser and his team in 1999.¹¹⁷ This system was designed to overcome several drawbacks of the camera-based LDF and it was equipped with several advantages over the camera-based LDF, for example, it was mobile and the system had a better signal sensitivity due to the confocal arrangement of the optical system.

The system used a polarised laser source ($\lambda = 785 \text{ nm}$) and the laser passed to the eye through the confocal arrangement with a power of $90 \mu\text{W}$ at the cornea. A $\lambda/4$ plate was placed between the last lens and the eye in order to differentiate between the illumination light and the backscattered light. The backscattered light from the eye was then collected by a circularly-arranged bundle of 6 APD with a diameter of $180 \mu\text{m}$. The optical arrangement of the compact LDF is shown in **Figure 2.15**. The signal was then processed using Fourier transformation and analysed up to 10 kHz. The sensitivities of the test for choroidal blood velocity (ChBVelocity), choroidal blood volume (ChBVolume) and choroidal blood flow (ChBFlow) for human eyes were reported as 3.2 – 5.0%, 7.1 – 10.2 % and 7.4 – 13.6% respectively.¹¹⁷

Figure 2.15: Compact LDF system (top) and optical arrangement (bottom)
(Source: ¹¹⁷)

2.6.2.3 *Helmet-mounted LDF*

A helmet-mounted LDF was the 3rd generation of LDF and it was also developed by Geiser and colleagues.¹¹⁸ The instrument was designed for LDF during active physiological challenges such as biking and running. The system uses a polarised laser source ($\lambda = 780$ nm with a power of 100 μ W at the cornea). The optical arrangement of the helmet-mounted LDF is similar to that of the compact LDF, the main difference being that the helmet-mounted system used 2 achromats (or achromatic lenses) with focal length of 20 mm while the compact LDF used 2 lenses with focal length of 80 mm.

The sensitivities of the measurements for ChBVelocity, ChBVolume and ChBFlow were 5.7%, 8.6% and 5.7% respectively for the sitting position and 2.3%, 5.5% and 5.3% respectively for the standing position.¹¹⁸ **Figure 2.16** shows the schematic diagram of the helmet-mounted LDF system

Figure 2.16: Helmet-mounted LDF system (Source: ¹¹⁸)

2.6.3 Application of LDF to measure ChBFlow in response to physiological stimuli in healthy eyes

Riva *et al*⁹⁹ applied LDF for the first time to measure the subfoveal choroidal circulation noninvasively in human eyes. Subjects undertook physical manoeuvres such as breathing different gas mixtures. In Riva's O₂ breathing experiment, ChBFlow parameters were recorded using a Topcon camera based implementation of LDF. ChBVelocity and ChBFlow after 5 mins 100% O₂ did not change from baseline (0.5 ± 6% for ChBVelocity and 2 ± 7% for ChBFlow; *P* > 0.05 for both). Riva argued that this lack of response to O₂ indicated that the LDF signal and derived measurements were mainly from the choroid; blood flow would have reduced if the signal had been derived from the retinal vessels or optic nerve head by 33% and 37% respectively.¹¹⁹

Riva also demonstrated the response of the choroidal circulation to physical changes including the Valsalva manoeuvre and a rapid increase of IOP. Due to a small number of subjects in each experiment (n = 1 to 4), the results need to be interpreted with caution. However, these experiments opened a new avenue for researchers to quantify the subfoveal choroidal circulation in response to the effects of various physiological stimuli as well as pharmacological agents.

2.6.3.1 Effect of ocular perfusion pressure on ChBFlow

The relationship between the ocular perfusion pressure (OPP) (a parameter used to estimate perfusion pressure of the vascular layers of the eye) and ChBFlow was demonstrated by Kiel and Heuven¹²⁰ in experiments that corroborated the capability of the choroid to autoregulate (see Section 1.3.4).³⁰ Although the results obtained by Kiel and Heuven showed the autoregulation capability of the choroid, this invasive experiment could not be applied to human eyes. The relationship between the OPP and ChBFlow in humans at the fovea has also been studied by Riva using the LDF¹²¹ and the following assumption about the relationship between ChBFlow and OPP (**Equation 2.5**).

$$ChBF_m = \frac{\left(\frac{2}{3}MOAP - IOP\right)}{R_m} = \frac{OPP_m}{R_m}$$

Equation 2.5: Equation describing the relationship between ChBFlow and OPP; MOAP is a mean ophthalmic arterial pressure, defined by following equation: (MOAP = BP_{diast} + $\frac{1}{3}$ (BP_{syst} - BP_{diast})); R_m is the average resistance of blood vessels and OPP is the mean ocular perfusion pressure; IOP is the intraocular pressure

This equation shows that the difference between arterial pressure, venous pressure and vascular resistance reflects the amount of blood flow through the choroid.

In Riva's study, the OPP was manipulated in 2 experiments. The first was designed to rapidly increase IOP and the second to slowly increase IOP using a plastic suction cup. A decrease of OPP by 18% caused by an increase IOP from 12 to 29 mmHg, did not affect the ChBFlow. However, when the OPP was further decreased to 33%, the ChBVelocity, ChBVolume and ChBFlow reduced by 35%, 69% and 84% respectively. Interestingly, when the suction cup was released, the ChBFlow immediately increased, suggesting a refill response of the choroidal vasculature. Due to the non-linear response of ChBFlow to decreasing OPP, the authors suggested that the choroid may have the capability to autoregulate.

The effect of increasing OPP on the choroidal vasculature by isometric exercise was also studied by the same researchers.¹²² After 90 seconds of isometric exercise, the OPP increased by 67% while the ChBVelocity linearly increased but not the ChBVolume or the ChBFlow. This regulatory process of choroidal vasculature in response to increased OPP was caused by the changes of vascular resistance as shown in **Figure 2.17**. This capability of choroidal autoregulation has also been demonstrated in a study by Schmidl¹²³ and Polska.¹²⁴ Using isometric exercise combined with an artificially increased IOP, Polska showed that the regulatory mechanism of the choroidal vasculature was better when MAP was increased compared to when the IOP was increased. These results suggested a myogenic response of the choroidal vessels comprising of vasoconstriction to regulate the amount of blood supply to maintain flow when IOP was increased.

As well as isometric exercise, the autoregulation mechanism of the choroid to maintain its blood flow has been shown through dynamic exercise-induced changes in the OPP. Lovasik *et al*¹²⁵ demonstrated that while the OPP increased during biking exercise, the ChBFlow remained within 10% of its basal value. This finding was similar to that reported for isometric exercise.

Figure 2.17: Changes in choroidal blood flow (ChBFlow), choroidal blood volume (ChBVolume), choroidal blood velocity (ChBVelocity), ocular pulsatile pressure (PP) and choroidal vascular resistance over time during isometric exercise (Source: ¹²²)

2.6.3.2 *Effect of blood gases on ChBFlow*

Choroidal regulation has been shown to be affected by changes blood gases. This experimental design was used to demonstrate the sympathetic response of the choroidal innervation system which plays an important role in choroidal autoregulation. Gieser *et al*, used a mixture of gases and reported that breathing 100% O₂ (the model which exhibits vasoconstriction in the retinal vessels) did not affect the level of ChBVelocity and ChBFlow. On the other hand, when subjects were exposed to a mixture of gases with higher percentage of CO₂ (5% and 8%), a significant increase of ChBVelocity and ChBFlow was observed whereas the ChBVolume remained unchanged as shown in **Figure 2.18**. This experiment showed that the carbon dioxide tension (pCO₂) is an important determinant for the ChBVelocity and ChBFlow.¹²⁶ The authors also reported the dose response of ChBFlow at approximately 1.5% per 1 mmHg increase in pCO₂. The study, however, did not control for the systemic parameter changes after CO₂ breathing.

An increase in pCO₂ or hypercapnia is known to be associated with obstructive sleep apnoea (OSA), leading to several cardiovascular abnormalities,

hypertension and obesity. OSA has also been reported to be associated with ocular microvascular diseases such as CSCR.¹²⁷ This reported association, however, was only based purely on observation and after analysis of a questionnaire required to be filled in prior to the study; no direct methods such as sleep tests or transcutaneous pCO₂ monitoring were carried out.

Figure 2.18: The response of choridal blood flow parameters to different mixtures of O₂ and CO₂: 100% O₂ (open triangles), 97% O₂ + 3% CO₂ (circles), 95% O₂ + 5% CO₂ (solid up triangles) and 92% O₂ + 8% CO₂ (solid down triangles) (Source, ¹²⁶)

2.6.3.3 *Effect of light on ChBFlow*

The relationship between light and ChBFlow in human eyes has been investigated in order to corroborate the retinal temperature controlling role of choroid

as well as the changes of ChBFlow during the transitional stage between rod-dominated and s-cone-dominated retinal responses to light (cone domination during light adaptation and rod domination during dark). Longo *et al*¹²⁸ studied the ChBFlow of 12 healthy subjects (mean (\pm SD) age: 35 ± 10) during dark and light transition using a compact LDF device. The authors reported a decrease in choroidal flow parameters during dark adaptation by 2.8% ($p < 0.05$), 11% ($p < 0.01$) and 15% ($p < 0.001$) for ChBVelocity, ChBVolume and ChBFlow respectively (**Figure 2.19**). A reverse phenomena was observed during light adaption. From their results, the authors have suggested that vasoconstriction and vasodilatation of local choriocapillaris occurred during dark and light adaptation, respectively, in order to regulate retinal temperature (decrease in ChBFlow and ChBVolume in parallel with a decrease in heat production of the photoreceptors).¹²⁸ If this is the case, a direct stimulation of s-cones with strong visible light (Longo's experiment 4) should induce an increase in ChBFlow. The author, however, failed to recognise the changes in the ChBFlow following light adaptation experiment and a direct stimulation of s-cones on both the study and the contralateral eyes. Moreover, most of Longo's experiments used only 6 healthy subjects. Small number of subjects might lower the sensitivity to detect any statistical changes of ChBFlow parameters using LDF. Thus, further investigations are required to establish the relationship of the ChBFlow to the cone activation.

In several eye diseases, including DR, a decrease in O_2 tension (pO_2) has been reported to contribute to the pathogenesis of the disease. This hypoxic condition occurs when rods become active. Light therapy has been used to slow down disease progression.¹²⁹ This light therapy may also stimulate the vasodilatation effect of the choroid; however, further research is required in order to confirm this hypothesis.

Figure 2.19: The effect of light and dark adaptation to the choroidal blood flow parameters (Source: ¹²⁸)

2.6.3.4 ***Effect of postural changes on ChBFlow***

Alteration of human posture has been used as an alternative way to investigate responses of choroidal circulation. Longo *et al* ¹³⁰ and Kaeser *et al* ¹³¹ studied changes in ChBFlow in subjects in two different positions, standing and supine positions, were compared on 11 healthy subjects by Longo *et al* while the sitting and supine positions were compared on 22 healthy subjects by Kaeser *et al*. Both groups found a significant increase of IOP when subjects were supine (29% [$p = 0.001$] for Longo's study and 8% [$p < 0.05$] in Kaeser's study), which, corresponded to changes in OPP and ChBFlow. The change in ChBFlow was, however, different between these two studies. Longo found an increase in ChBFlow from standing to supine while Kaeser found a decrease in ChBFlow from sitting to supine. The discrepancy between the two studies may arise from different experimental designs; continuous measurement was used in Longo's study and intermittent measurement was used in Kaeser's study. The resting time period used

by the two studies was also different: 2 minutes in Longo's study and 30 minutes in Keaser's. Thus, further research is required in order to confirm this function of the choroid.

2.6.3.5 **Effect of ageing on ChBFlow**

The effect of ageing on choroidal circulation has been addressed by several investigators. Grunwald *et al* investigated the subfoveal ChBFlow on 29 healthy participants aged 15 to 76 using a fundus camera based LDF device. The authors found a negative correlation between both ChBVolume and ChBFlow and the subject's age ($R = -0.52$ [$p = 0.004$] and $R = -0.54$, [$p = 0.003$], respectively) but not the ChBVelocity.¹³² The authors then stratified subjects into two groups: younger group (15 – 45 years of age; $n = 18$) and older group (46 – 76 years of age; $n = 11$). Mean (\pm sd) of ChBFlow and ChBVolume was 18.9 ± 6 AU and 0.48 ± 0.2 AU, respectively for younger group. ChBFlow and ChBVolume were approximately 29% higher compared to the older group (13.3 ± 3.3 AU for ChBFlow [$p = 0.007$] and 0.34 ± 0.11 AU for ChBVolume [$p = 0.04$]) and these differences were statistically significant. The decreases of ChBVolume and ChBFlow suggest less choroidal circulation as we become older. However, there are several points to consider in this study: 1) the authors included subjects with hypertension (the highest systolic blood pressure was 181 mmHg and the highest diastolic blood pressure was 107 mmHg). Since hypertension has a direct effect on the microvasculature, including hypertensive patients in the normative data is very likely to interfere with the results. 2) The authors also failed to normalise the differences in BP during the age comparison of the LDF data. The study by Grunwald is also in direct conflict with a recent study by Straubhaar *et al*. Using the compact LDF device, Straubhaar reported that increasing age is associated with decreasing the ChBVelocity but not the ChBFlow and ChBVolume.¹³³ This discrepancy between the two groups might be due to different criteria for participant selection (Grunwald *et al* included patients on antihypertensive medication and 3 smokers [out of 29] while Straubhaar *et al* included 10 smokers [out of 70]). Moreover, the different LDF devices used in the two studies might have also contributed to the different results.

2.6.4 **Response of ChBFlow to pharmaceutical agents**

The ability of the choroid to autoregulate its circulation and the complex interaction between the choroidal regulation and OPP, MAP and IOP has been studied by several groups using various pharmacological interventions. The pharmacological agents include moxaverine, sildenafil citrate (Viagra), nitric oxide donor 5-isosorbide mononitrate (ISMO), indomethacin, cimetidine and histamine.

These medications exert either a vasodilation or vascular resistance modification on the choroidal vascular bed. Many researchers have also used certain pharmaceutical drugs in combination with isometric exercise to gain an insight into the complexity of the choroidal vascular regulation. **Table 2.4** shows a summary of the effect of several pharmaceutical compounds on the ChBFlow using LDF. Although the effect of the agents on the ocular haemodynamics *i.e.* IOP, MAP and OPP was different in each case, the choroid was still able to regulate its blood flow to a certain extent.

Table 2.4: Summary of various pharmaceutical compounds showing the effect on choroidal blood flow using LDF

Drugs	Effect of drug on vasculature	Dose	Route of administration	Number of subjects (mean age \pm SD)	References
Drug only					
Moxaverine	Vasodilatation and vessel relaxation	150 mg	IV	16 healthy (8 men (25 \pm 5) and 8 women (23 \pm 3))	Resch, H ¹³⁴
Sildenafil Citrate (Viagra)	Vasodilatation by enhancing the effect of nitric oxide	100 mg	PO	15 healthy men (39 \pm 8)	Grunwald, JE ¹³⁵
Nitric oxide donor 5-isosorbide mononitrate (ISMO)	Vasodilatation	20 mg	PO	12 healthy (29 \pm 6)	Grunwald, JE ¹³⁶
Indomethacin	Vasoconstriction	0.4 mg/kg (over 5 mins) 0.4 mg/kg/h (over 2 hrs)	IV	12 healthy men (25 \pm 5)	Weigert, G ¹³⁷
Cimetidine and histamine	Vasodilatation	Cimetidine 2.3 mg/min (over 50 mins) Histamine 0.32 μ g/kg/min (over 30 mins)	IV	18 healthy men (25 \pm 3)	Resch, H ¹³⁸
Drug and choroidal autoregulation					
Latanoprost	To lower the IOP	0.005% once daily (14 days)	Drop	24 healthy men	Boltz, A ¹³⁹
Nifedipine	Vasoconstriction	15 μ g/kg (over 5 mins) 0.2 μ g/kg/min (over 25 mins)	IV	15 healthy men (26 \pm 4)	Schmidl, D ¹⁴⁰
NG-monomethyl-L-arginine (L-NMMA)	Vasodilatation	6 mg/kg (over 5 mins) 60 μ g/kg/min (over 15 mins)	IV	14 healthy men (25 \pm 4)	Simader, C ¹⁴¹
Clonidine	Vasoconstriction	Isoglaucon 0.125%	Drop	12 healthy men	Weigert, G ¹⁴²
Brimonidine	Vasoconstriction	Alphagan 0.2%	Drop	12 healthy men	Weigert, G ¹⁴²

2.6.5 Other applications of LDF

LDF has also been used in studies of the function of the choroid in several eye diseases including age-related macular degeneration (AMD), DR, CSCR, rhegmatogenous retinal detachment,¹⁴³ myopia eye,¹⁴⁴ glaucoma,^{145, 146} retinitis pigmentosa,¹⁴⁷ retinal vein occlusion¹⁴⁸ and ocular adaptation in high altitude.¹⁴⁹

Many investigators have applied this non-invasive technique to assess the alterations of choroidal circulation in patients with higher risk of developing ocular diseases such as smoking and hypertension. For example, Wimpissinger and her colleagues studied the effects of smoking on the choroidal autoregulation and found abnormal ChBFlow regulation in smokers compared to the non-smokers.^{150, 151} Niknam *et al*¹⁵² compared ChBFlow in patients with systemic hypertension and age-matched controls. Their results showed a slightly lower ChBVolume and ChBFlow in hypertensive patients (n = 15) compared to healthy controls (n = 15) but these differences were not statistically significant. From their results, the authors suggested that systemic hypertension does not have the effect on choroidal circulation in patients that are well controlled by medication. This study, however, cannot be used to answer the effect of hypertension on choroidal autoregulation, further studies would need to be performed.

2.6.6 Summary of LDF

LDF has been used to directly determine the choroidal blood circulation as well as the regulation of ChBFlow under physiological and pharmacological challenges. The results obtained from the studies mentioned above, however, only apply to the ChBFlow at the fovea but not to the rest of the choroid.

Several factors also need to be considered when reviewing the literature on ChBFlow measurement using LDF:

- 1) The variation of the measurements: The scattering properties of different tissues often affect the amount of light returned back to the detector (measured as DC) and consequently affect the outcome of the LDF measurement. Thus, it is considered inappropriate to directly compare the LDF outputs between normal eyes and those with ocular disease.

- 2) In order to obtain reproducible results, the fixation ability of subjects is an important factor. Patients with less ability to fixate or loss of central vision such as geographic atrophy in AMD may not be suitable for LDF.

3) The sensitivity of LDF indicates the minimum statistically significant changes of ChBFlow parameters that can be detected. This value varies depending on the type of LDF device and the type of ocular disease. Therefore, the sensitivity of the measurement should be reported in all studies using LDF in order to assess the choroidal autoregulation.

4) Most of the research done previously reports the response of choroidal circulation to physiological stimuli in a limited number of subjects.

2.7 Other ocular fundus imaging techniques for the ocular fundus

In this section, a short description of other key techniques used in this thesis is provided.

2.7.1 Indocyanine green angiography (ICGA)

Indocyanine green (ICG) is an amphiphilic tricarbo-cyanine dye (see **Figure 2.20** for formula) which absorbs and emits light at the infrared region (peak absorption around 800 nm).

ICGA angiography (ICGA) was developed and used in medicine during the Second World War mainly used for hepatic and cardiac function analyses. In 1970, Hochheimer and Flower demonstrated the use of ICGA to image the choroidal vasculature. However, the potential of ICGA in ophthalmology was not fully recognised until Yannuzzi *et al* pointed out the value of ICGA for diagnosing occult choroidal neovascularization in 1992.¹⁵³ Since Yannuzzi's report, ICGA has been used in parallel with fundus angiography (FA) for investigating several ocular diseases particularly neovascular AMD and uveitis.

The advantage of ICGA over FA is that it uses light in the infrared region which can penetrate deeper into the retina. ICGA has a higher molecular weight (around 775) with nearly 98% binding to the plasma protein which allows it to remain within the highly fenestrated choroidal vasculature allowing better visualisation of the choroidal network.^{154, 155}

Figure 2.20: The chemical formula of indocyanine dyes (Source: ¹⁵⁴)

2.7.2 Fundus autofluorescence imaging

Ocular fundus autofluorescence (FAF) imaging is a method used to detect the natural fluorophores in normal human eyes. These human fluorophores can be

excited by light in the region around 440 – 510 nm and emit light in a relatively broad spectrum ranging between 500 and 700 nm (~600 nm).^{156, 157} The main fluorophores accumulate in lipofuscin (LF) granules located in the lysosomal compartment within the cytoplasm of RPE cells. The main component of LF is a di-retinal conjugate A2E (N-retinylidene-N-retinylethanol-amine) toxic to normal cells which is synthesised from vitamin A aldehyde and ethanolamine in a ratio of 2:1. Other LF components include the oxidised bisretinoid LF fluorophores. Oxidised LF by-products are also known to initiate photooxidation and photodegradation mechanisms as well as increase the formation of advanced glycation end products (AGE).¹⁵⁶

To capture the FAF, Delori *et al*¹⁵⁸ developed a modified fundus spectrophotometer to determine the topographical variation of the fluorophores along the horizontal line across the fovea. Their technique, however, could only capture a small area of retina with a limit of 13°. Later, the confocal scanning laser ophthalmoscope (cSLO) has been used to enhance the quality and contrast of FAF images. The current widely used commercial cSLO systems such as the Heidelberg Retina Angiograph 2 (HRA2) provides excitation of 488 nm with a barrier filter at 500 nm. The image resolution can be increased via image averaging. **Figure 2.21** shows the ocular FAF images of a healthy and the eye of a patient with chronic CSCR.

The association between FAF, progression of disease and visual outcome in CSCR is largely unknown. Hence, in this thesis, the FAF image will be used to determine the changes in the RPE of CSCR patients. The relationship between the FAF values and other factors, such as changes in the structure of the choroid, duration of the disease and the visual outcome will also be assessed in Chapter 7.

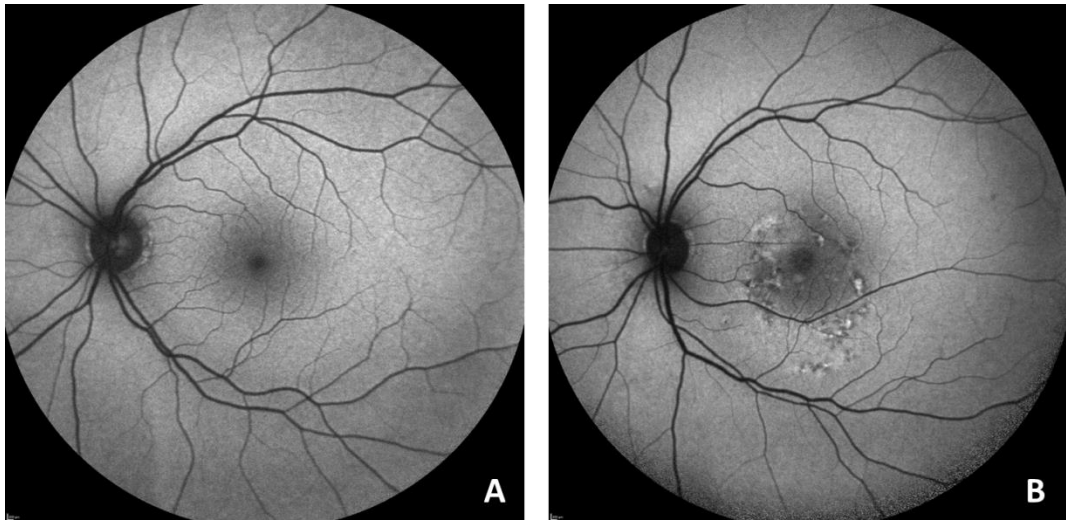


Figure 2.21: The ocular fundus blue wave autofluorescence images of a healthy eye (A) and of a patient with chronic CSCR (B).

2.7.3 Near infrared autofluorescence imaging

Another imaging technique closely related to the FAF is the near-Infrared autofluorescence (NIR AF) image. NIR AF originates from melanin and melanin related compounds such as oxidised melanin and melanolipofuscin in the RPE and choroid. These melanin and melanin related compounds produce a weaker autofluorescence around ~ 60 – 100 times less intense than that produced by LF.¹⁵⁹ Human melanin compounds can be excited at 790 nm with an emission spectrum above 800 nm. The NIR AF image can be captured using the same cSLO instrument as normal FAF images but instead with an excitation wavelength of 787 nm and a barrier filter above 810 nm. A NIR AF image obtained from a normal healthy eye has higher NIR AF signal at the centre corresponding to a higher concentration of melanin at the foveal centre. **Figure 2.22** shows the ocular NIR AF images of a healthy eye and the eye of a patient with chronic CSCR.

In Chapter 7, I will compare the changes in NIR AF levels in patients with CSCR and healthy eyes. I will also study the relationship between the changes in NIR AF level and other factors, such as changes in the structure of the choroid, duration of the disease and the visual outcome in patients with CSCR. This will help to understand more in detail of the pathogenesis of CSCR.

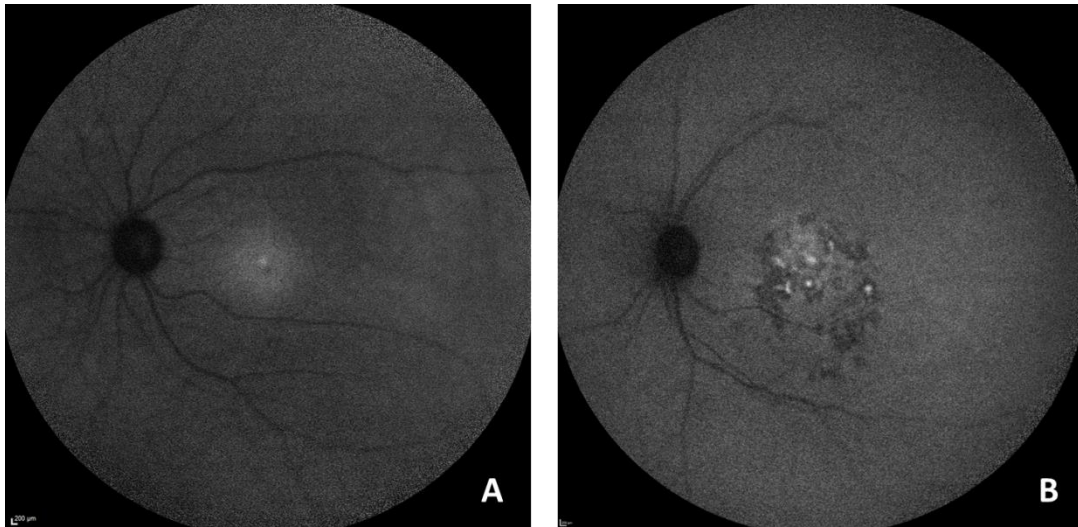


Figure 2.22: The ocular fundus near infrared autofluorescence images of a healthy eye (A) and the left eye of a patient with chronic CSCR (B).

2.7.4 Microperimetry

Microperimetry or fundus perimetry is a technique used to measure topographic correlation between fundus abnormalities. It was first pioneered by Nidek Instruments Inc., Padova, Italy in 2002¹⁶⁰ who developed their first commercial platform the Nidek Microperimeter-1 (MP-1). The MP-1 instrument uses SLO to integrate computerised perimetry into a colour fundus image. The perimetry of MP-1 is performed by an internal liquid crystal display (LCD) with an infrared camera covering a 45° field. Each stimulus uses light intensity ranging from 0 to 20 dB with the attenuation of a Goldmann standard stimulus sized I to IV. Two different threshold strategies of light within each stimulated retinal point are available depending on the accuracy required from the observer: 4-2-1 (more accurate but slower) and 4-2 (less accurate but faster). The results are colour coded and can be displayed using one of a selection of maps (symbolic, numeric or interpolation map) (Figure 2.23).¹⁶¹

During MP-1 measurement, the automatic eye-tracking system continuously registers pre-defined fundus landmarks in order to determine the patient's fixation location as well as calculating the relative shift of the subject's fixation. These results are automatically used by the instrument to estimate the fixation stability which is classified as stable, relatively unstable or unstable fixation.^{160, 161}

Although the distance visual acuity test remains the gold standard to assess retinal function, MP-1 offers several advantages: MP-1 allows the detection of small

functional defects of the macula; MP-1 sensitivity test allows the topographical location of specific structural changes.

In many chorioretinal diseases, including CSCR, a long term structural damage remains even after the recovery of distance high contrast visual acuity. Thus, in this thesis the alteration of the macular function will be assessed using MP-1.

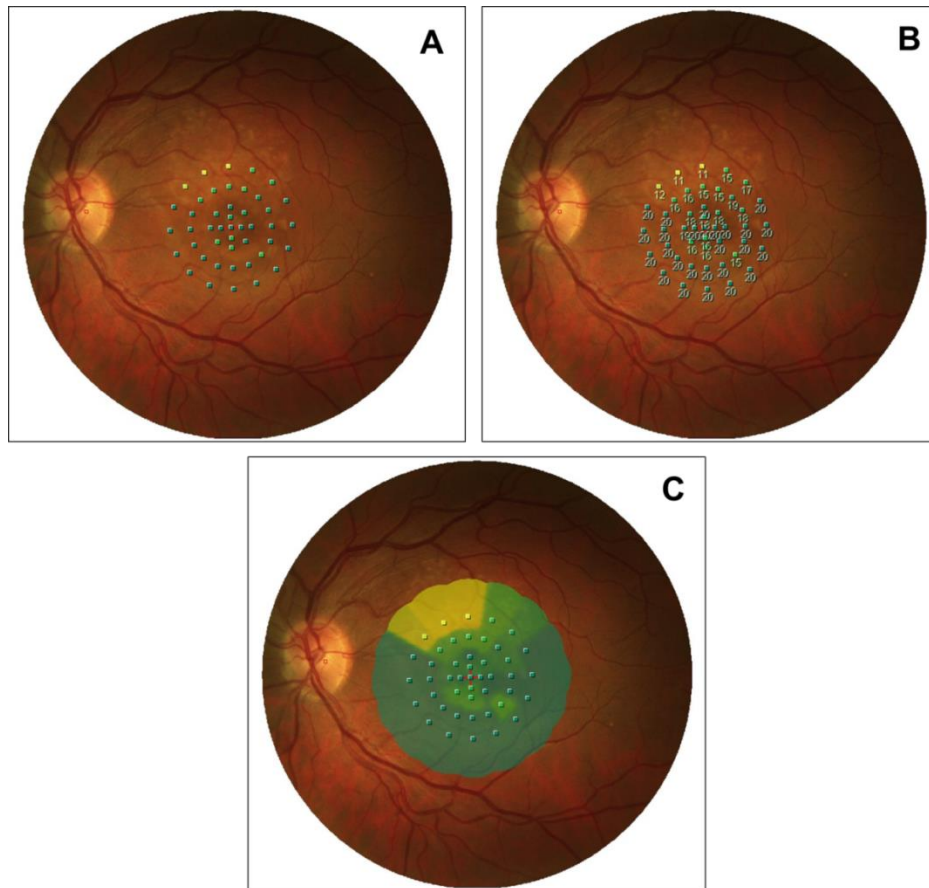


Figure 2.23: The display of microperimetry results from MP-1: symbolic (A), numeric (B) and interpolation (C) map

2.8 Diabetic retinopathy

Diabetic retinopathy (DR) refers to a group of long term microvascular complications as a result of diabetes mellitus which leads to retinal damage and, in some people, permanent visual loss. DR has been listed as one of the main eye diseases causing visual impairment by the World Health Organisation (WHO). Nearly all patients with type I diabetes and more than 77% of patients with type II diabetes will develop some form of DR, on average 15 years after the diabetes has been diagnosed.^{162, 163} In the USA, 86% and 40% of diabetic patients with type I

and type II diabetes respectively are estimated to have some form of DR.¹⁶⁴ In the UK, an annual incidence of any retinopathy and sight-threatening DR has been reported at 5.3% and 0.3% respectively in patients with type II diabetes.¹⁶⁵ As the number of people estimated to have diabetes mellitus and impaired glucose tolerance is predicted to reach 366 million and 472 million respectively by 2030, vision-threatening retinopathy is likely to increase¹⁶⁶ and thus requires more studies in order to be better understood.

When the central area of the retina (macula) is affected by exudation from the retinal microvasculature, the term diabetic maculopathy is used. When retinal thickening occurs the term diabetic macular oedema (DMO) is used: DMO can be clinical significant (CSMO). DMO can occur at any time during the course of DR but is most commonly found during the later stage of DR. DMO is more prevalent in type II diabetes and is the most common cause of visual impairment in diabetes

Based on a standard 7-field stereoscopic colour photographs, the Early Treatment of Diabetic Retinopathy Study (ETDRS) group¹⁶⁷ classified DR into 13 severity levels starting from level 10 (no sign of retinopathy) to level 85 (advanced proliferative diabetic retinopathy [PDR]).¹⁶⁸ Although the ETDRS scale has been intensively used by clinical trials and national/international research programs, it is considered to be too complex for clinical used. To overcome this complexity of ETDRS, the global diabetic retinopathy project group introduce an international severity scales aiming to simplify the DR and DMO classification system. The proposed DR severity scale comprises 5 levels starting from no apparent retinopathy, mild nonproliferative DR (mild NPDR), moderate NPDR, severe NPDR and PDR. For the DMO severity scale, a 2-tiered system was proposed. First, the scale aims to separate between the presence or absence of the retinal thickening and hard exudates at the posterior pole. If there is a presence of macular oedema, this should then be classified further as mild, moderate or severe DMO.¹⁶⁹

In the UK, the national screening committee (NSC) developed a classification applicable to screening for sight threatening diabetic retinopathy (STDR). The Diabetic Eye Screening Programme classification included four levels of DR (R), two levels of maculopathy (M), two levels of photocoagulation (P) and one unclassified level.¹⁷⁰ These grading criteria will be used to classify DR and DMO in diabetic patients recruited in my study.

The pathogenesis of DR is complex. The disruption of several factors and biochemical cascades in response to chronic hyperglycaemia have been shown to

be important in the pathogenesis of DR such as protein glycation, oxidative stress, protein kinase-C and advanced glycation end-products.¹⁶⁴ At the early stage of DR, thickening of capillary basement membrane, loss of pericytes and microaneurysms are the common vascular abnormalities of the retinal vessels.

The effect of long standing hyperglycaemia on the choroidal vasculature was first investigated by McLeod and Luty.¹⁷¹ In this study, post-mortem human choroidal tissue was stained with the alkaline phosphatase. According to their findings, extensive choriocapillaris dropout was clearly noted which they classified into diffuse and focal patterns. These dropouts were associated with BM-like basal laminar deposits.¹⁷² Similar results, showing the dropout or degeneration of the choriocapillaris in diabetic eyes was found by Gerl *et al*¹⁷³ using the compliment C5b-9 immunostaining method. Using tissue embedded alkaline phosphatase staining method, Fukushima *et al*¹⁷⁴ reported intra-choroidal microvascular abnormalities, observed outside the choriocapillaris suggesting a microaneurysm type formation of choroidal vessels.

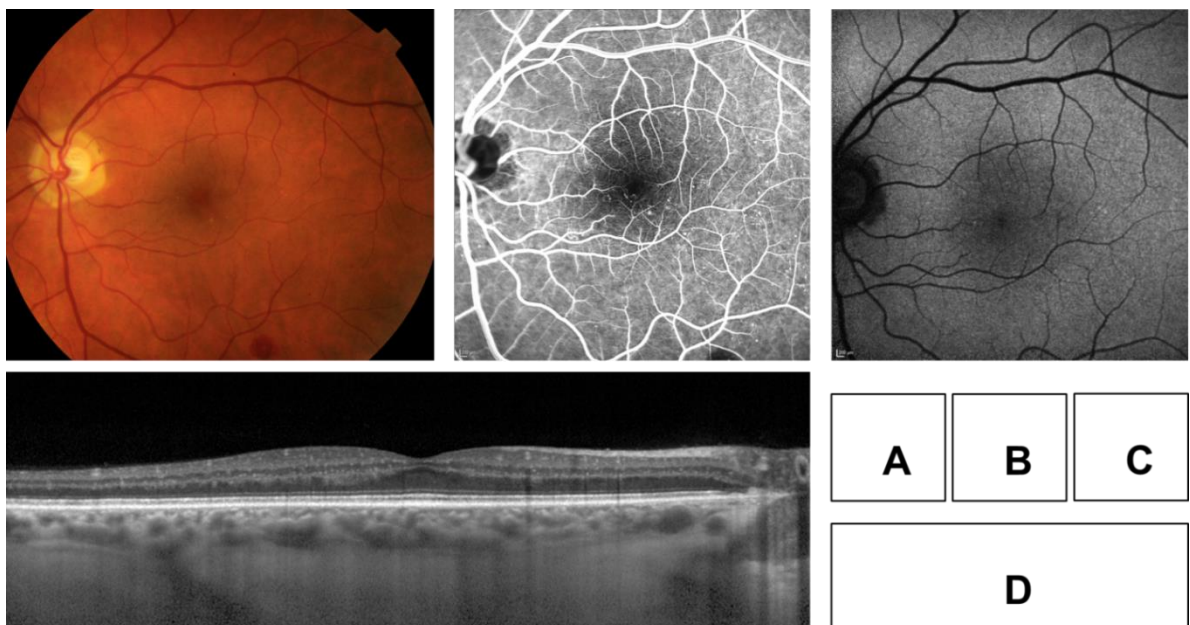


Figure 2.24: Fundus images of the left eye of a 55-year old patient with diabetic maculopathy without CSMO, colour fundus image (A), fundus fluorescein angiography image (B), blue wave autofluorescence image (C) and a cross sectional scan image (D)

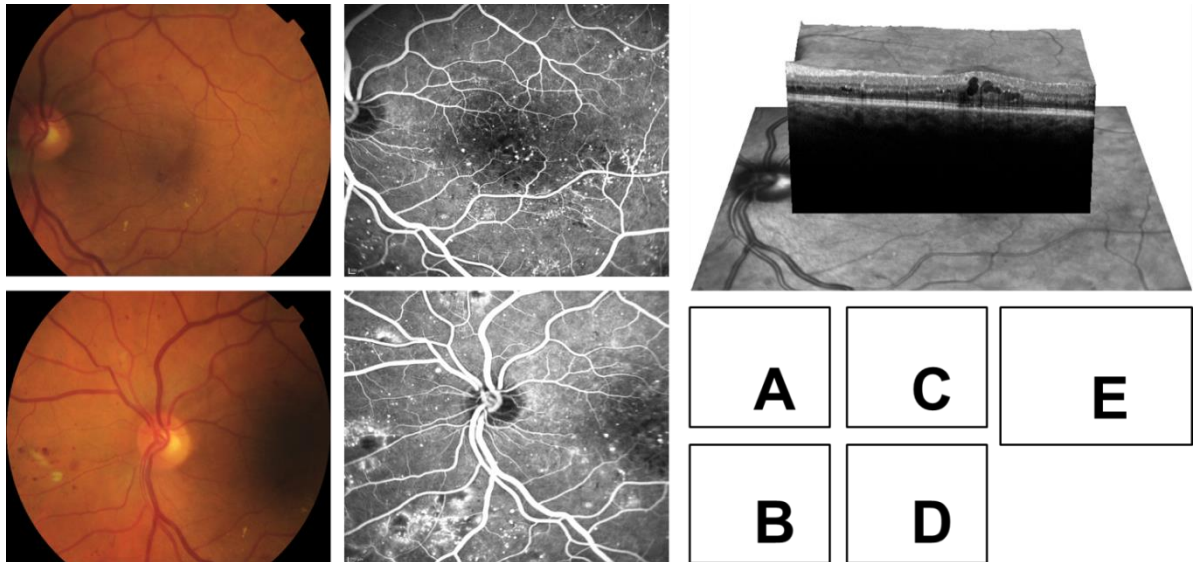


Figure 2.25: Fundus images of the left eye of a 51-year old patient with diabetic maculopathy with CSMO. Figure A and B show the colour fundus image of the macula and the optic disc, respectively. Figure C and D show the microaneurysms on fundus fluorescein angiography at the macula and the optic disc, respectively. Figure E shows an area of macular oedema within the retina on a 3D volume scan.

2.8.1 Study of choroidal structure using EDI OCT in diabetic retinopathy

Since EDI OCT was introduced by Spaide the question of choroidal structural changes has been raised by several ophthalmic groups for various types of chorioretinal diseases including DR. The evidence of choroidal thinning on OCT was reported by Rigatieri *et al*, Vujosevic *et al* and Querques *et al*. using different types of OCT modalities.¹⁷⁵⁻¹⁷⁷ Rigatieri *et al* investigated the ChT of 49 type 2 diabetic patients who had mild or moderate NPDR with or without DMO using Cirrus-HD OCT. In this study, the ChT of NPDR with DMO was significantly thinner than that of healthy subjects but not in NPDR without DMO. Rigatieri's study, however, did not mention whether AxL, time of imaging or the refraction were controlled during the analysis. Vujosevic *et al* observed a thinner choroid in NPDR and PDR eyes. They found no significant differences in ChT between no diabetic retinopathy eyes and healthy controls. A contradictory finding to Vujosevic's study was reported by Querques *et al*. Querques *et al* found thinner choroid in all patients with diabetes with or without DR than that of healthy eyes. Querques's results also differed from Rigatieri on the ChT of the NPDR without DMO eyes. These contradictory results may reflect the small number of DR patients included in each study.

Determination of choroidal structure changes in a larger sample size was conducted in China and Korea. No significant difference in mean ChT at the centre of the fovea was found in diabetic patients with and without DR compared to that of healthy eyes in a Chinese population based study.¹⁷⁸ The ChT of various DR stages from each research group is summarised in **Table 2.5**.

A considerable variability in the choroidal morphology in DR can be inferred from the results obtained from the above studies. In addition, none of the above studies have explored or reported the association between the structural changes that occur during the disease progression and blood flow of the choroid. One of the aims of the work presented in this thesis is to study the contribution of the choroid in the pathophysiology of DR. I will discuss this in detail in Chapter 6.

Table 2.5: Summary of previous research on choroidal thickness in various stages of DR

First author	DR classification					
	Controls	No DR	Mild to moderate NPDR	Severe NPDR	PDR	Treated PDR
Esmaeelpour et al	388±109	303±82*	291±64*			xx
Regatieri et al	232.3±15.2	xx	222.0±21.6 (no DMO)/169.5±14.7 (with DMO)*		xx	162.7±7.0*
Vujosevic et al	329.5±65.2	280.6±68.6	279.4±81.6*		230.5±25.8*	xx
Querques et al	309.8±75.1	238.4±47.9*	207.0±55.9 (no DMO)* / 190.8±48.4 (with DMO)*		xx	xx
Kim et al	276.0±58.1	262.3±68.4	244.6±77.0	291.1±107.7	363.6±74.9 †	239.8±57.4
Xu et al	261±103	266±108	249±86			xx

* *P* < 0.05 compared with controls

2.8.2 Study of ChBFlow using LDF in diabetic retinopathy

As mentioned above, LDF is the direct measurement of the blood flow in the choriocapillaris and has been used to determine the alteration of the sub-foveal choroidal blood circulation in diabetic patients. Schocket *et al.* measured the foveolar choroidal circulation in patients with PDR. Their results demonstrated a reduction of the ChBFlow in PDR patients by 27% compared to healthy volunteers. This reduction of ChBFlow was mainly caused by a decrease of ChBVolume. Additionally, they also showed a negative correlation between ChBVelocity and the duration of diabetes.¹⁷⁹ Similarly, Nagaoka *et al.* also demonstrated a reduction of ChBFlow in patients without DR (9.4 ± 2.5 au; $P < 0.05$) and NPDR without DMO (NPDR/-DMO) (10.8 ± 4.8 au; $P < 0.05$) compared to that of healthy controls (13.5 au).¹⁸⁰ The reduction was even greater in NPDR with DMO (NPDR/+DMO) (5.6 ± 2.0 ; $P < 0.01$) compared to healthy eyes. This hints at a possible relationship between reductions of ChBVelocity at the fovea and the severity of DR.¹⁸⁰ The regulation of the ChBFlow in diabetic patients was also investigated by Movaffaghy *et al.*¹⁸¹ using isometric exercise. Their results demonstrated a linear increase of ChBFlow in patients with DR when OPP increased by 50%, whereas, there were no changes of ChBFlow observed in patients with diabetes but no retinopathy and healthy controls.¹⁸¹

The results obtained from the above studies suggest an abnormality of ChBFlow in DR. However, none of the above studies have explored the association between the functional and the structural changes in DR. Thus, in Chapter 6, I will use LDF in conjunction with EDI OCT in order to further explore the association between the changes in choroidal function and the changes in choroidal structure in the DR pathophysiology.

2.9 Central serous chorioretinopathy

Central serous chorioretinopathy (CSCR) is a condition affecting the posterior segment of the eye. CSCR characteristically involves accumulation of serous fluid underneath the neurosensory retina with a predilection for the macula.¹⁸² CSCR was first described by Albrecht von Graefe in 1866¹⁸³ which he named as “relapsing central luetic retinitis”. Over 150 years since the first discovery of the condition, various terms have been employed to describe several aspects of CSCR including the chronicity of the disease, the tissue layers of primary involvement and various pathogenic concepts as shown in **Table 2.6**. The most common terms used for this

men compared to women.¹⁸⁷ An annual incidence of CSCR in Caucasian populations has been reported at 5.8 per 100,000 (9.9 in men and 1.7 in women).¹⁸⁶ In Asian populations, a database from Taiwan National Health Insurance Research estimated 4 times higher annual incidence of CSCR than in Caucasians.¹⁸⁵ The reason for lower incident rate in Caucasians compared to Asians may be due to the method used to diagnose CSCR. In reports from Caucasian populations, FA leakage was the main diagnostic criteria and over 30% of CSCR patients were excluded due to unavailable FA and 5% of CSCR patients were excluded due to spontaneously resolve.

Cassel *et al*¹⁸⁸ attempted to study the seasonal variation in CSCR based entirely on numbers of CSCR cases visiting their clinic throughout the year. Although Cassel failed to find any statistically significant association between the seasonal variation and CSCR, they observed a peak during March and April.

CSCR has been arbitrarily divided into acute, recurrent and chronic forms depending on symptom duration. Acute CSCR is often characterised by a shorter duration of symptoms, usually less than 3 months with self-limiting resolution of sub-retinal fluid (SRF);¹⁸⁹ some studies extend this period to 6 months.¹⁹⁰ CSCR is considered chronic when patient present with longer duration of symptoms. With advances in retinal imaging additional diagnostic features such as multifocal and widespread areas of RPE atrophy and OCT findings of retinal structural damage may help to ascertain the chronicity. Patients with chronic CSCR may have a worse prognosis with an increased likelihood of recurrence and involvement of both eyes. A long-term follow-up study of 150 CSCR patients reported around 30% CSCR patients had 1 or 2 episodes of recurrences during the follow-up period. Ficker *et al*¹⁹¹ and Fok *et al*¹⁹² found even higher recurrence rates at over 50% in their studies. Interestingly, Fok found an association risk of developing recurrent CSCR with patients with a history of psychiatric illness.¹⁹² The median time from diagnosis to recurrence was reported to be at 1.3 years.¹⁸⁶ The visual prognosis for patients with acute CSCR is relatively good following complete resolution of SRF.¹⁹⁰ Although a good recovery of vision is observed in CSCR patients, abnormalities of the macular function such as metamorphopsia and colour discrimination have been reported to persist in CSCR patients even after complete resolution of SRF.¹⁹³ The visual prognosis of chronic CSCR patients, on the other hand, is poorer than acute CSCR patients. The worsened visual prognosis in chronic CSCR patients is directly associated with persistent SRF and PED as well as a history of recurrent CSCR.¹⁹⁴

On the first episode of CSCR, approximately 75% of CSCR patients have unilateral involvement and 25% have bilateral involvement. Approximately 5% of patients with unilateral disease develop bilateral involvement.¹⁹⁵ This might indicate a subclinical involvement of asymptomatic fellow eyes in unilateral CSCR. In my study, EDI OCT and ICGA have been used in conjunction to clarify this subclinical involvement of the asymptomatic eyes and the results will be presented in Chapter 7.

Risk factors associated with the development of CSCR include stress, Type-A personality,¹⁸⁴ pregnancy,¹⁸⁷ increased level of endogenous steroid,¹⁹⁶ *Helicobacter Pylori* infection¹⁹⁷ and a history of using various types of corticosteroids¹⁹⁸ including steroid creams, steroid injections and steroid inhalers. Tillt *et al* investigated risks of developing CSCR associated with systemic factors in 230 patients compared with age-matched controls and found additional risks including psychopharmacological medications and hypertension.¹⁹⁹ Haimovici *et al* further identified antibiotic use, alcohol consumption and allergic respiratory disease as new additional risk factors associated with CSCR.²⁰⁰ Haimovici also identified untreated systemic hypertension as risk of CSCR confirming the result from Tillt's study. Recently, Rouvas *et al* reported higher number of patients with CSCR within the country that has financial crisis such as Greece. This is likely due to an increase of the socioeconomic strain during financial crisis period.²⁰¹

The pathophysiology of CSCR still remains incompletely understood as there are limited animal disease models available. Yoshioka *et al*²⁰² performed a series of experiments on animal models (Japanese monkey and Cynomolgus monkey) in which CSCR was induced by repeated adrenaline injections. Their results indicated an overlap between the areas of choriocapillaris endothelium damage and the overlying RPE damage. Extensive fibrin-platelet clots were also observed at the site of choriocapillaris damage. In human, ICGA has been used to assess the choroidal circulation. Prunte *et al*²⁰³ studied choroidal circulation of 32 patients with acute and chronic CSCR using ICG-videoangiography. They reported a localised delay arterial filling and a transient hyperpermeability of choroidal vessels in all of their CSCR patients. The results found in animal model as well as that found in human suggest the role of choroid in pathogenesis of CSCR.

With recent advances in ophthalmic imaging, choroidal dysfunction has been proposed as a primary site responsible for causing the leakage of water, electrolytes and proteins, inducing a localised RPE detachment, and subsequently inducing the

overlying retinal detachment. Although choroidal dysfunction is thought to be responsible for the pathogenesis, the cause for the dysfunction remains elusive. Abnormalities in choroidal autoregulation possibly contribute to the dysfunctional choroid. LDF and EDI OCT have been used in conjunction in the work presented in this thesis in order to investigate the autoregulatory ability of the choroid in CSCR.

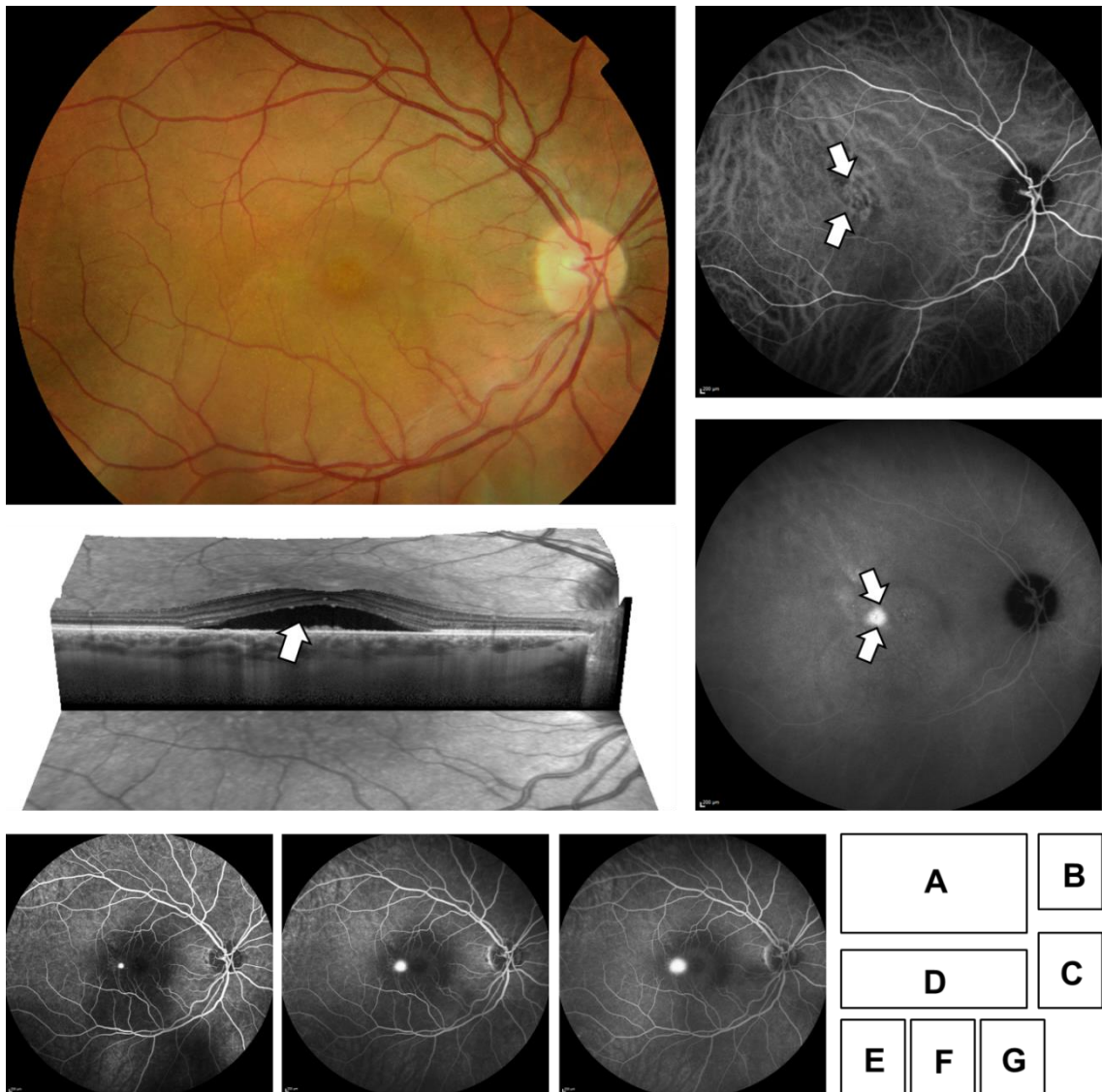


Figure 2.26: Fundus images of the right eye of a 40-year old male patient with acute CSCR: colour fundus photograph (A), indocyanine green angiography showing an area of choroidal vessel dilatation (arrows) at 30 seconds (B) and an area of choroidal vessel hyperpermeability (arrows) at 10 minutes (C), a cross-sectional EDI OCT (D) showing the fluid accumulation beneath the retina (arrow), and the fluorescein angiography showing leakage of the fluorescein dye at 30 seconds (E), 5 minutes (F) and 10 minutes (G) after the injection.

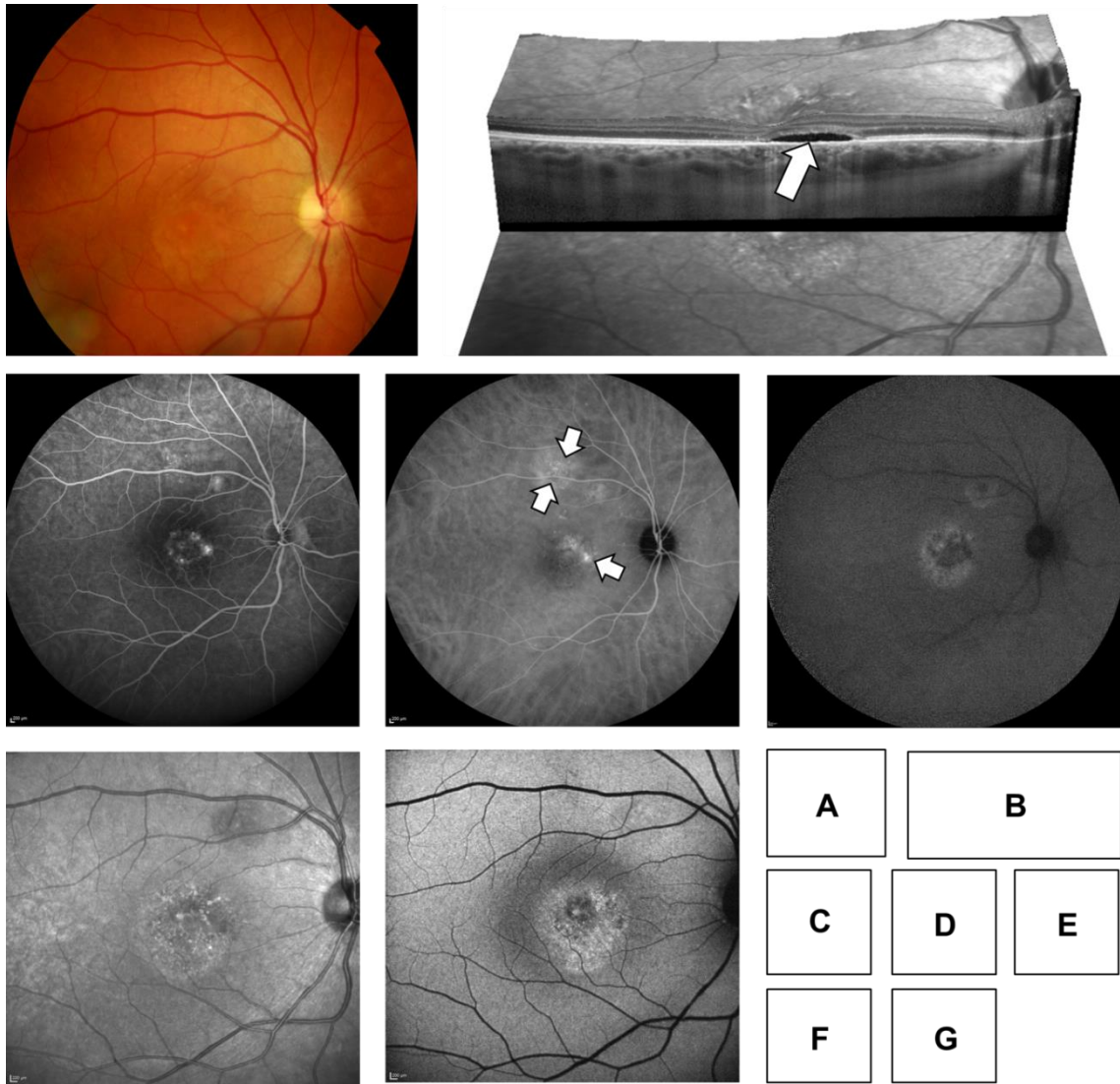


Figure 2.27: Fundus images of the right eye of a 46-year old male patient with chronic CSCR: colour fundus photograph (A), a cross-sectional EDI OCT (B) showing fluid accumulation beneath the retina (arrow), fluorescein angiography showing a leakage of the fluorescein dye at 5 minutes (C), indocyanine green angiography showing an area of choroidal vessel hyperpermeability (arrows) at 5 minutes (D), near-Infrared autofluorescence (E), infrared reflectance image (F) and blue wave autofluorescence (G).

2.9.1 Studies of choroidal structure using EDI OCT in central serous chorioretinopathy

With advanced ophthalmic imaging, investigators have observed several choroidal changes in patients with CSCR. Abnormalities identified on ICG include choroidal vascular hyperpermeability, delayed ICG filling, and vascular dilatation as I have described in the previous section.

The first EDI OCT study on CSCR was carried out retrospectively by Imamura *et al*²⁰⁴ on 28 eyes of 19 patients. The mean SfChT of CSCR patients was $505 \pm 124 \mu\text{m}$. This was $214 \mu\text{m}$ thicker than healthy eyes. The authors also observed no association between SfChT and age which is typically seen in healthy eyes. One of the main weaknesses of this study is that the authors did not report systemic disorders such as hypertension and diabetes. These underlying systemic disorders may also affect ChT and should be taken into account. Moreover, 6 fellow eyes without CSCR were included in their analysis. Thus, their results may not represent the changes in ChT that occur during the active stages of CSCR.

An increase in ChT has been reported previously not only in symptomatic eyes but also in asymptomatic fellow eyes. A retrospective study showed that the SfChT of asymptomatic fellow eyes of patients with unilateral CSCR (reported at $350 \pm 116 \mu\text{m}$, $n = 66$) was thicker compared to eyes of patients with no reported CSCR ($248 \pm 71 \mu\text{m}$, $n = 177$) ($P < 0.001$).²⁰⁵ This author also suggested an association between hyperpermeability and thickening of the ChT in asymptomatic eyes. Due to the nature of this retrospective study, however, unknown systemic diseases affecting the ChT may bias the results during patient selection and so results should be taken with some caution.

This thickening of the ChT in asymptomatic eyes has been confirmed by a recent prospective study by Kim *et al*.²⁰⁶ Kim prospectively studied the ChT on 30 patients with unilateral CSCR. The mean SfChT was $445.6 \pm 100.3 \mu\text{m}$, $378.4 \pm 117.4 \mu\text{m}$ and $266.8 \pm 55.5 \mu\text{m}$ for affected ($n = 30$), unaffected ($n = 30$) and normal eyes ($n = 30$), respectively. Compared to previous study by Maruko *et al*, Kim's study did not find any association between choroidal hyperpermeability and thickening of ChT in asymptomatic eyes. The discrepancy between these two studies may be due to the patient selection criteria used in these two studies. Kim included all unilateral CSCR without further identifying the chronicity of the disease. Hence, Kim's results may not represent the progression of CSCR.

The effects of therapeutic interventions of CSCR, such as laser photocoagulation (LP) and verteporfin photodynamic therapy (VPDT) on ChT have been evaluated by several research groups. Maruko *et al* analysed the changes of ChT from 12 eyes of 12 patients with LP treatment and 8 eyes of 8 patients with VPDT treatment. The ChT was found to remain at the similar level as the baseline at 4 weeks after treatment in LP group whereas the ChT increased significantly from a mean of 389 μm to 462 μm on day 2 after VPDT and decreased to 360 μm and 330 μm at week 3 and 4 respectively (all $P < 0.05$).²⁰⁷ This author also monitored the changes in ChT of CSCR patients after 1 year post-PDT. The ChT decreased by approximately 80% from baseline and hypofluorescence on ICG was observed in all eyes.²⁰⁸ In addition, the reduction of SfChT by approximately 10% was reported after absorption of SRF without any treatment interventions.²⁰⁹

The results obtained from the above studies have helped to further reinforce the role of the choroid in the pathogenesis of CSCR. However, these ChT measurements were mainly obtained at the subfoveal location and do not represent the 3D structure of the choroid. In addition, CSCR often extends beyond the fovea to the macula. Thus, in this thesis, the ChT and choroidal volume (ChVolume) will be used to describe the choroidal structure in CSCR. Using these two parameters, a better understanding of the choroidal structure in CSCR can be obtained.

2.9.2 Studies of ChBFlow using LDF in central serous chorioretinopathy

LDF has been used to study choroidal vascular function in CSCR. Kitaya *et al*²¹⁰ quantified ChBFlow in both eyes in 11 acute CSCR patients. A decrease in ChBFlow by approximately 45% in the affected eyes compared to their fellow eyes was reported in this study. Kitaya's study, however, cannot be used to directly represent the abnormal choroidal function due to various reasons: 1) as choroidal defects can occur in both eyes of CSCR patients, it would be incorrect to compare the ChBFlow between symptomatic eyes and fellow eyes. 2) A decrease in ChBFlow in CSCR does not entirely explain the function of the choroid or choroidal autoregulation as only a single time point of measurement was used.

More recently, Tittl *et al*²¹¹ determined the autoregulation capability of the choroidal vasculature in chronic inactive CSCR patients. In this study, a 6-minute isometric exercise was performed by 14 inactive CSCR patients and 14 age-matched healthy controls. The ChBFlow was recorded using a compact LDF device during exercise. Following exercise, an increase in OPP by approximately 85% was observed in both groups. At this level of OPP, Tittl observed an increase of ChBFlow

by approximately 20% in CSCR patients compared to an increase by approximately 10% in healthy controls. There are several weaknesses in Tittl's study: 1) the authors failed to mention the hyperpermeability of the choroidal vasculature. This would be required in order to confirm the persistence of CSCR disease. 2) Tittl's study used only patients with inactive CSCR, defined as having the last episode of SRF at least 6 months to 2 years prior to enrolment, their results may not be reproducible when CSCR is active.

To date, the information available on the autoregulation of choroidal blood flow in CSCR patients is very limited. Knowledge of the regulation of choroidal structure and function could help improve insight into the pathogenesis of CSCR.

2.10 Summary

Imaging techniques of the choroidal structures, especially EDI OCT have improved considerably over the past decade. EDI OCT is relatively easy to use and can be adapted from most commercially available SD OCT devices.

In order to study choroidal structure, previous studies have reported a single point ChT at the foveal centre on a single B-scan, however, there are several drawbacks to this approach: a single point ChT does not represent the 3D structure of the choroidal vasculature. In addition, there is a lack of a standardised protocol with a clear definition of the outer boundary of the choroid for the accurate measurement of the ChT. This leads to difficulties when comparing between studies.

ChT measurements have been previously reported in healthy and diseased eyes. However, to date, no clear links have been established between the changes that occur in the choroidal structure and the functional changes during the pathogenesis. This is due to a limited number of techniques that have been available to study choroidal function.

LDF has been previously used to directly measure the choroidal circulation in healthy and diseased eyes and is the only available method to study the choroidal autoregulation following physiological stimuli. Abnormalities in choroidal autoregulation have been shown to be associated with the pathogenesis of eye diseases and might be associated with visual outcomes of patients with chorioretinal diseases. In this thesis, I have used LDF and EDI OCT in conjunction to investigate the autoregulatory ability of the choroid in DR and CSCR in order to establish the relationship between the structural and functional changes of the choroid during the

pathogenesis of DR and CSCR. This novel approach will allow me to investigate the following research questions:

- What functional and/or structural changes in the choroid can be detected on EDI OCT and LDF in patients with DR and CSCR compared to healthy controls?
- Are these changes related to the chronicity of symptoms?
- Are these changes in any relationship with each other?
- Are there any functional and/or structural markers for the retinal changes and visual prognosis?

Chapter

3 Validation of EDI OCT and LDF

The choroid plays a major role in maintaining normal retina homeostasis as outlined in Chapters 1 and 2. Abnormalities of the choroidal integrity are associated with the pathogenesis of several chorioretinal diseases.

3.1 Background

Two novel techniques; enhanced depth imaging optical coherence tomography (EDI OCT) and laser Doppler flowmetry (LDF) have been used in this thesis as the key techniques for assessing the structure and function of the choroid, respectively. In this chapter, I will describe the validation of these techniques. First, I will describe a standardised protocol used to measure the choroidal thickness (ChT) on EDI OCT and report the inter- and intra-observer agreements of this protocol. Second, I will discuss the validation of LDF for choroidal blood flow (ChBFlow) measurements.

3.2 Standardisation of choroidal thickness measurements using EDI OCT

Histologically, the choroid consists of the BM, choriocapillaris, choroidal vessel layers and suprachoroid as I have described previously in Section 2.4.1.

The anterior boundary of the choroid is easily identifiable in normal OCT and EDI OCT images as the outer limit of the hyper-reflective band representing the RPE/BM complex. The outer boundary of the choroid, on the other hand, appears to vary depending on the image quality. Different research groups have defined the posterior boundary of the choroid as either the inner surface of the sclera or as the

area demarcated by the hyper-reflective margin between the end of large choroidal vessels and the sclera.^{47, 52, 212, 213} On EDI OCT images, the outer boundary of the choroid has been previously described by Spaide *et al*³² as the hypo-reflective space underneath the choroid or suprachoroidal space (SCS). Maul *et al*⁴⁴ described this layer as a well demarcated hyper-reflective band between the large choroidal vessels and the sclera or chorioidal-scleral interface (CSI). This lack of clarity in the definition of the outer boundary of the choroid in ChT measurements leads to difficulties when comparing between studies.

In this section, I will describe a standardised protocol developed to measure the ChT. This protocol has sub-classified the topographical appearance of the choroidal posterior boundary on EDI OCT in order to achieve accurate measurements for ChT. I validate the inter- and intra-observer agreements obtained using this technique for both topography and ChT measurements.

3.2.1 Subjects and methods

3.2.1.1 Subjects

Normal healthy volunteers with no known previous eye disease and patients with diabetes were recruited into this cross-sectional prospective observational study. For patients with diabetes, the inclusion criteria were men and women aged 18 or over with type 1 or 2 diabetes mellitus, with or without any stage of DR. The degrees of retinopathy and maculopathy were graded by trained graders using the Liverpool Diabetic Eye Study (LDES) grading protocol.²¹⁴ The exclusion criteria for patients with diabetes included pregnancy, previous macular or peripheral retinal laser treatment, contraindication to dilatation, history of intraocular injection or surgery and other significant eye diseases. The study was conducted in accordance with the Declaration of Helsinki. Informed consents were obtained from all subjects prior to their participation in the study.

All subjects underwent slit lamp biomicroscopy, best corrected visual acuity (BCVA) test using Early Treatment Diabetic Retinopathy Study (ETDRS) reading charts and EDI OCT scan. EDI OCT images were taken using the Spectralis SD OCT system (Heidelberg Engineering, Heidelberg, Germany). The EDI acquisition was performed using the protocol previously described by Margolis *et al*.⁴⁷ An Automatic Real Time-function (ART) of 100 was applied to each section using the built-in automatic averaging and real time eye-tracking features in order to obtain images of adequate quality for visualisation and to maximise signal-to-noise ratio. The images were exported at a 1:1 pixel ratio for analyses.

3.2.1.2 **Standardised protocol for defining choroidal margins**

Single 9 mm horizontal EDI OCT line scans passing through the centre of the fovea was used for analysis. For normal healthy volunteers, the foveal centre was defined as the point of maximum depression within an area of 500 μm in diameter.²¹⁵ In order to standardise the definition of the choroidal outer boundary, EDI OCT images were categorised based on the identification of SCS and CSI. When both the SCS and the CSI were identifiable in the image, the CSI was seen as a clear intermediate hyper-reflective band outer to the vascular-like structure of the choroid and the SCS was seen as a hypo-reflective band posterior to the CSI (**Figure 3.1**).

The images were classified into four sub-groups depending on the presence or the absence of the SCS and the CSI at the posterior boundary of the choroid (**Figure 3.2**).

- **Group A:** both structures (CSI and SCS) were identifiable and more than 80% of the CSI and SCS layers were identifiable across the length of the scan.
- **Group B:** 2 image categories were included within this group i) both structures (CSI and SCS) were observed in the scan; however, it was in less than 80% of the length of the scan. ii) only one of the structures were observed, either CSI or SCS.
- **Group C:** neither SCS nor CSI was observed in the scan, however, a distinct smooth line indicating the outer limit of the large choroidal vessels with the sclera was seen.
- **Ungradeable:** scans showed either no identifiable posterior boundary of the choroid or a portion of the choroidal structure was missing.

The anterior boundary of the choroid in each image was defined as the hyper-reflective band corresponding to the RPE-Bruch's membrane complex. The posterior boundary was defined and based on the classification as follows: for group A, the outer limit of the CSI was used; for group B, the outer limit of the CSI was used where both SCS and CSI were visible in the image. Where only one of the two was identifiable, the posterior boundary was drawn at either the outer limit of the CSI or the inner limit of the SCS. For group C, the smooth band signifying the outer limit of the large choroidal vessels was used.

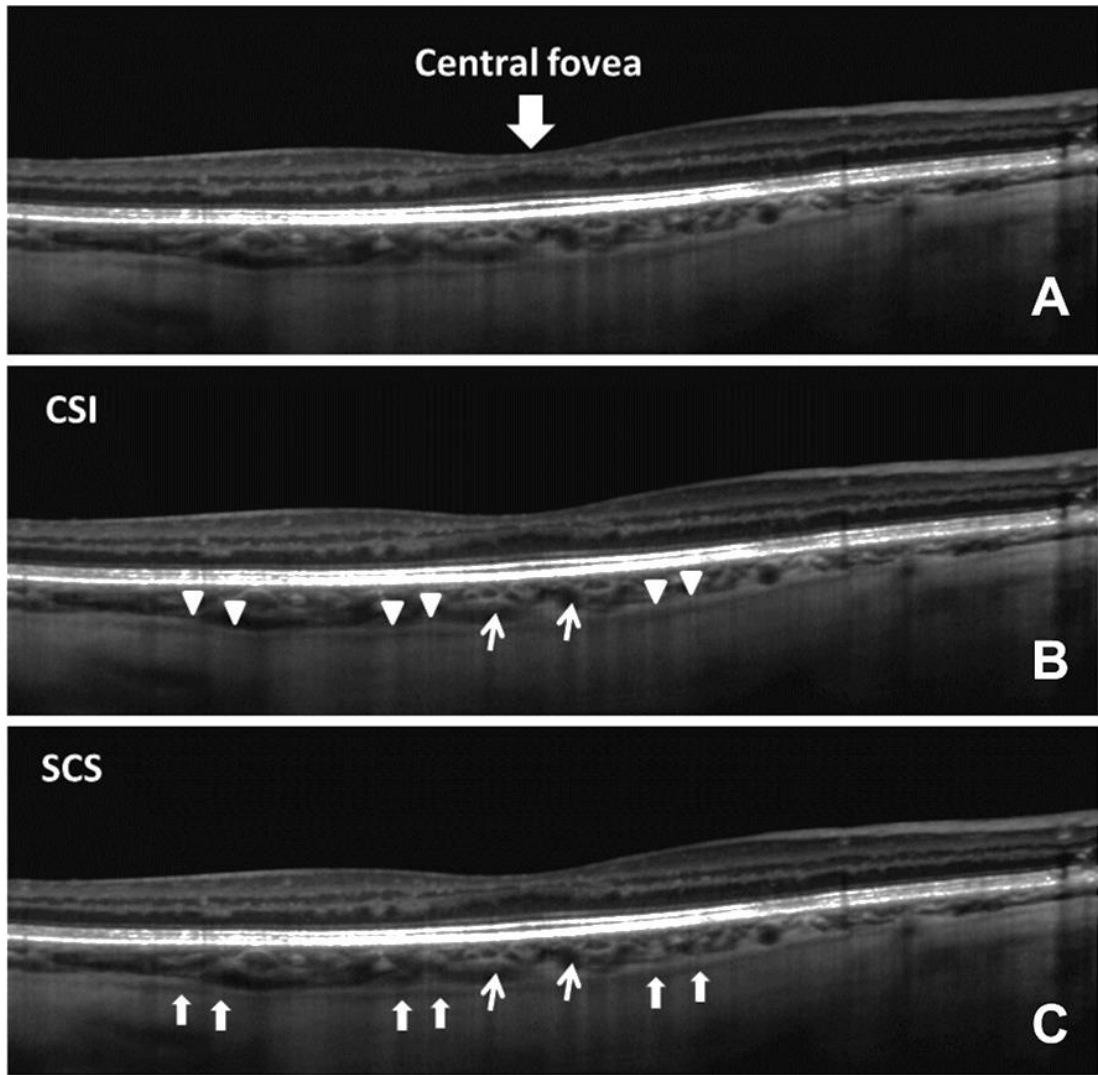


Figure 3.1: A single 9 mm horizontal line scan with enhanced depth imaging obtained from the right eye of a 55-year-old healthy male (A). The choroidal-scleral interface (CSI) (B) is indicated by a well demarcated hyper-reflective band (triangle heads) and the suprachoroidal space (SCS) (C) is indicated by the hypo-reflective band (arrows). The narrow arrows indicate the cross section of large choroidal vessels

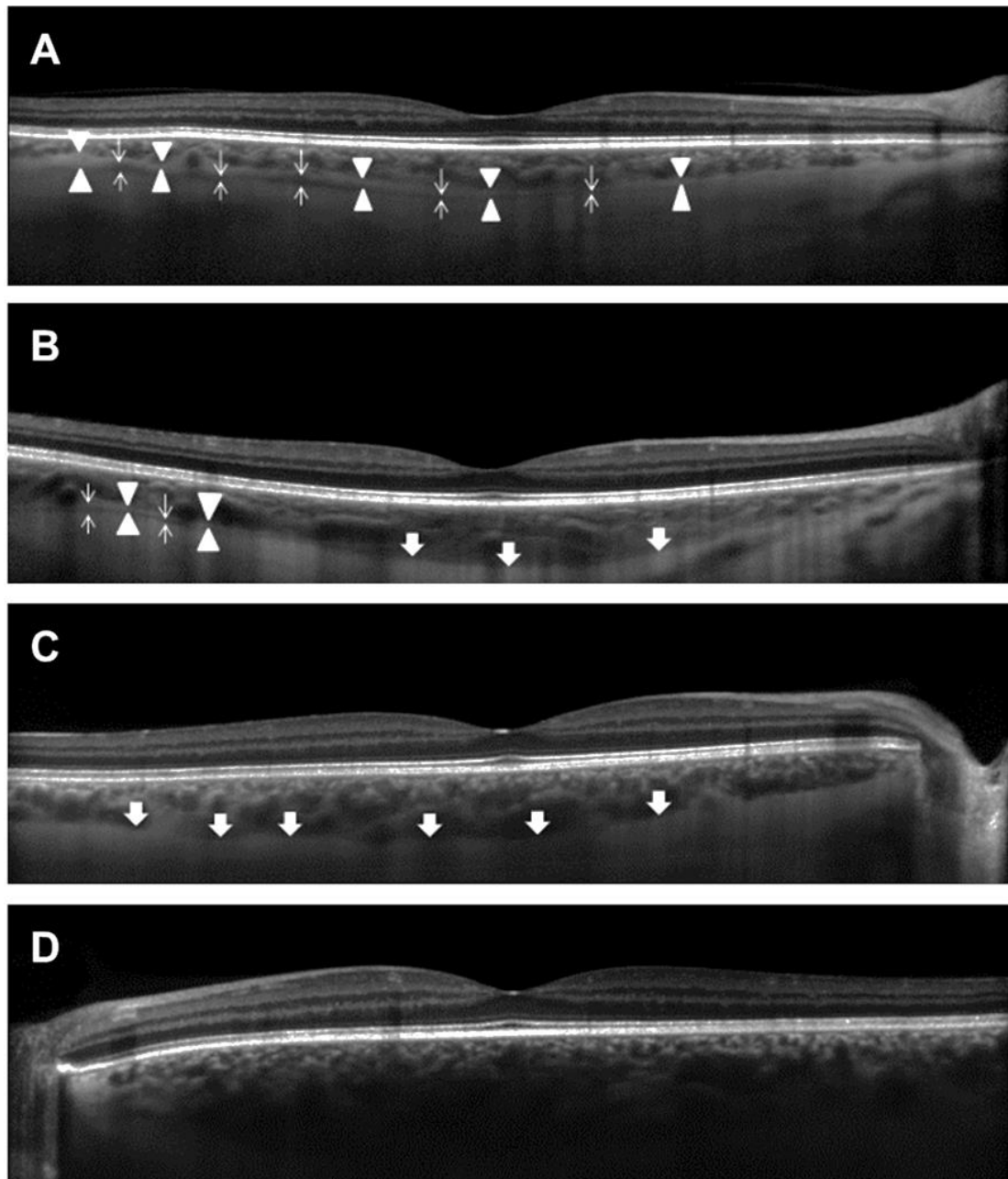


Figure 3.2: Example of EDI OCT image classifications categories. Group A (**A**), the choroidal outer boundary consists of more than 80% of the CSI (triangle heads) and the SCS (narrow arrows) across the length of the scan. Group B (**B**) consists of less than 80% of the CSI and the SCS across the length of the scan. Group C (**C**) consists of a smooth line between the outer limit of large choroidal vessels and the sclera (wide arrows) and ungradeable (**D**) when the outer choroidal boundary is not identifiable on the scan

3.2.1.3 *Measurement of choroidal thickness*

All EDI OCT images were classified and delineated using the proposed protocol by two masked expert observers (NB and ANS). In addition, observer NB repeated the classification and measurement tasks one week later, masked from the

previous measurements. The anterior and posterior boundaries of the choroid were manually delineated using ImageJ software version 1.45S (National Institutes of Health, USA). The ChT was then measured as the perpendicular distance between the anterior and posterior boundary at 500 µm intervals up to 3 mm nasal and 3 mm temporal from the foveal centre using a program developed in MATLAB R2012a (The Mathworks Inc., Natick, USA). The total ChT was calculated from the average ChT from the 13 locations measured. The SfChT was used to represent the ChT at the foveal centre.

Two evaluation iterations were performed. In the pilot study, the images from healthy volunteers were analysed to test if the standardisation methodology was valid. The second experiment was performed to evaluate whether the protocol was applicable for the management of disease represented by images from patients with diabetes.

To determine the inter-method variability, 10 images from each image classification category were randomly selected and used to determine the variability between 2 ChT measurement methods (Image J vs Heidelberg Eye Explorer software). For Heidelberg Eye Explorer software, the software version 1.9.10.0 was used to display the EDI OCT. The automatic line indicating the ILM was moved to the outer border of the hyper-reflective line indicating the RPE/Bruch's membrane complex. The automatic line detecting Bruch's membrane was moved to the posterior boundary of the choroid according to the specific group definition.

3.2.1.4 **Statistical analysis**

Statistical analyses were performed using the Statistical Package for Social Scientists (SPSS) program version 20 (SPSS Inc., IBM, USA).

In order to determine the level of agreement between observers on the evaluation of the choroidal topographical appearances on EDI OCT scans, the Cohen's kappa coefficient (K) was calculated (K less than 0.20 signifies poor agreement, K = 0.21 – 0.40 fair, K = 0.41 – 0.60 moderate, K = 0.61 – 0.80 substantial, K = 0.81 – 1.00 almost perfect agreement).²¹⁶

Inter- and intra-observer agreements for the thickness measurements were displayed using Bland and Altman plots.²¹⁷ The coefficient of repeatability (CR) was defined as 1.96 x standard deviation (SD) between two measurements. These analyses were done separately on 5 sets of images (i.e. group A, group B, group C, group agreed as ungradeable and non-agreed images) for the total ChT and the

SfChT. Intraclass correlation coefficient (ICC) was used to determine the reliability of the measurements. An ICC value below 0.40 represents poor agreement, 0.40 – 0.75 represents fair to good agreement and above 0.75 represents excellent agreement.²¹⁸ A 5% level of alpha was considered as significant.

3.2.2 Results

A total of 58 subjects (46 patients with diabetes and 12 healthy volunteers) were recruited in this study. The mean (\pm SD) age of the 12 healthy volunteers (5 males) was 43.3 (\pm 12) years (range 28 - 67). The mean age of the 46 subjects with diabetes (36 males) was 54.4 (\pm 15) years (range, 20-76). 82 EDI OCT images from both eyes of the 46 subjects were included in this study. In this group, EDI OCT scans could not be obtained from one of the eyes of 10 patients due to poor fixation. On clinical examination, 24 eyes were graded with M1 diabetic maculopathy and 1 eye had M0.5 maculopathy (M1 is described as any of: 1) exudate within 1 disc diameter (DD) of the centre of the fovea, 2) circinate or group of exudate $>$ 1 DD from the centre of the fovea but within the arcades and . 1 disc area (DA) in size, or 3) any microaneurysm or haemorrhage within 1DD of the centre of the fovea only if associated with a best visual acuity of 6/12; M0.5 is described as a circinate or group of exudates entirely within the arcade $<$ 1DA in size and more than 1DD from the centre of the fovea). 5 OCT scans passing through the fovea showed intraretinal fluid. There was no statistically significant difference in ChT measurements between the scans with maculopathy and without maculopathy ($P > 0.05$, data not shown). The log MAR visual acuity was -0.01 (± 0.11).

In the pilot study on 12 eyes of 12 healthy volunteers (one eye per subject), the inter- and intra-observer agreements on the choroidal posterior boundary classification were $K = 0.42$ and $K = 1$, respectively. The ICC for inter-observer agreement on the total ChT on the scans in which the image classification was agreed was 0.960 (95% confidence interval [CI], 0.684 – 0.994) and 0.992 (95% CI, 0.972 – 0.998) for intra-observer agreement.

3.2.2.1 *Inter-observer agreement*

This protocol was then applied to the 82 EDI OCT images of the 46 diabetic subjects. The inter-observer agreement on the image classifications was $K = 0.66$ (95% CI, 0.53 – 0.79; $P < 0.001$). Both observers agreed on the classification of 63 EDI OCT scans: 24 scans (38.1%) were classified as group A, 22 (34.9%) as group B, and 17 (27.0%) as group C.

There were excellent inter-observer agreements of ChT measurements in patients with diabetes on both the total ChT and SfChT, for scans that received the same classification from the observers. The inter-observer ICC values ranged from 0.963 to 0.985 with an overall ICC value of 0.972 (95% CI, 0.944 – 0.985) for the total ChT and from 0.916 to 0.986 with an overall ICC of 0.949 (95%CI, 0.900 – 0.972) for SfChT (**Table 3.1**).

The inter-observer CRs for the total ChT in EDI OCT scans classified as group A, B and C were 14.1µm, 40.7µm and 41.4µm respectively with an overall CR value of 33.1µm. The inter-observer CRs of the SfChT were approximately 2 times higher than those of the total ChT in each image classification.

Table 3.1: Summary of inter-observer agreements on the total and subfoveal choroidal thickness measurements

Inter-observer agreement	Total ChT			SfChT		
	ICC (95%CI)	Mean difference (95%CI) (µm)	CR (µm)	ICC (95%CI)	Mean difference (95%CI) (µm)	CR (µm)
Group A	0.985 (0.873 - 0.996)	7.1 (4.1 - 10.2)	14.1	0.986 (0.965 - 0.994)	4.4 (-0.4 - 9.2)	22.2
Group B	0.963 (0.913 - 0.984)	5.8 (-3.5 - 15.0)	40.7	0.916 (0.778 - 0.967)	18.5 (2.7 - 34.3)	69.8
Group C	0.971 (0.912 - 0.990)	10.7 (-0.2 - 21.6)	41.4	0.959 (0.880 - 0.985)	15.1 (-1.0 - 31.2)	61.4
Overall	0.972 (0.944 - 0.985)	7.6 (3.4 - 11.9)	33.1	0.949 (0.900 - 0.972)	12.2 (5.2 - 19.2)	54.4
Non-agreement	0.964 (0.878 - 0.988)	15.7 (3.4 - 28.0)	49.9	0.918 (0.747 - 0.971)	27.4 (5.5 - 49.3)	89.2

ICC: intraclass correlation coefficient; CI: confidence interval; CR: coefficient of repeatability, ChT: choroidal thickness

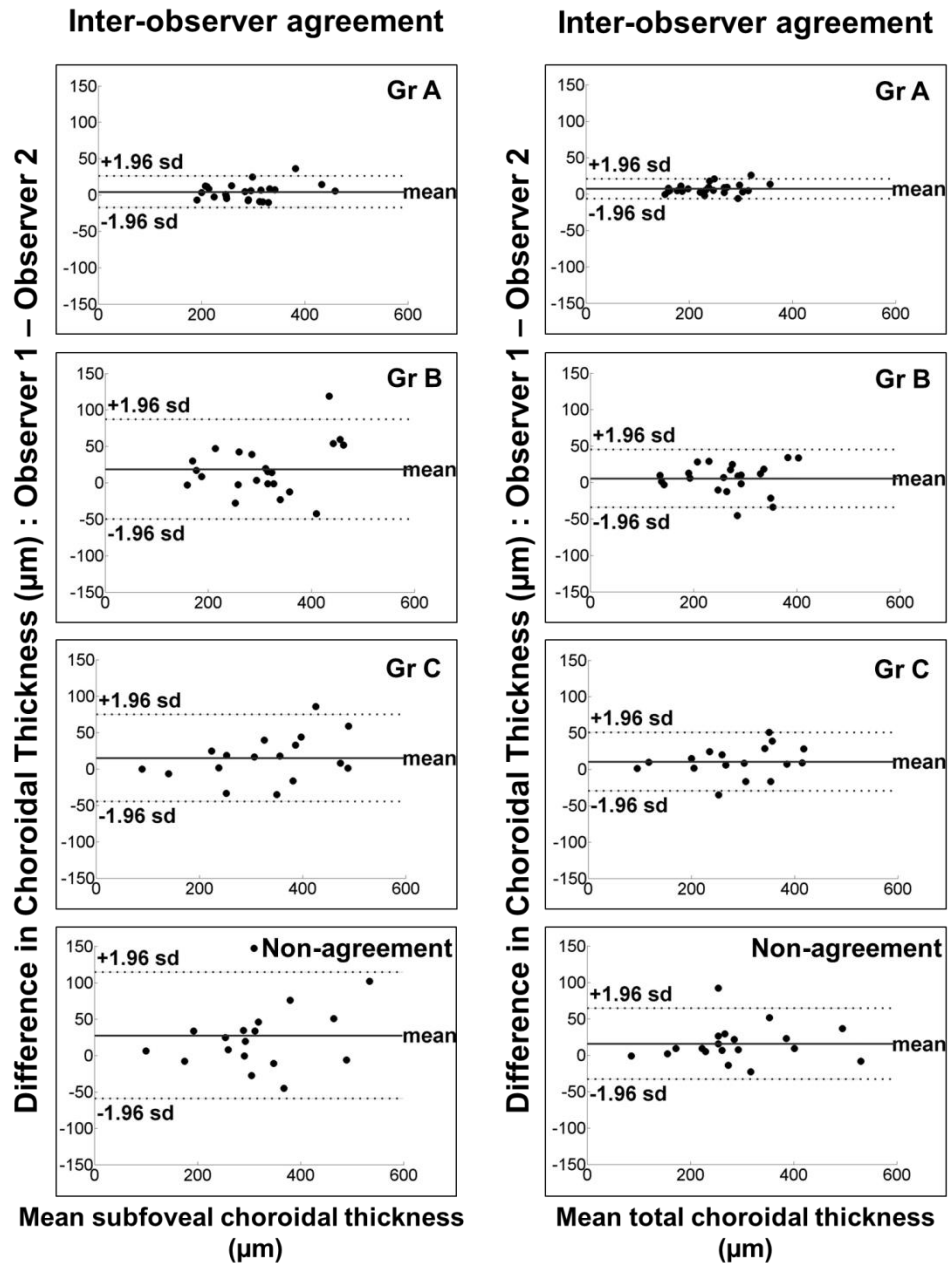


Figure 3.3: Bland-Altman plots showing inter-observer with mean difference (thick line) and 95% limits of agreement (dashed lines) for subfoveal choroidal thickness measurements (SfChT, left hand column) and total choroidal thickness measurements (ChT, right hand column) by classification: group A (A1 and A2), group B (B1 and B2), group C (C1 and C2), non-agreement (D1 and D2)

3.2.2.2 *Intra-observer agreement*

The intra-observer agreement on the image classification was $K = 0.86$ (95% CI, 0.76 – 0.95; $P < 0.001$) where 74 EDI OCT scans were given the same classification: 26 scans (35.1%) group A, 21 scans (28.4%) group B, 24 scans (32.4%) group C and 3 scans (4.1%) were ungradeable.

The ICC for intra-observer measurement agreement ranged from 0.989 to 0.996 with the overall ICC value of 0.995 (95%CI, 0.991 – 0.997) for the total ChT and 0.982 to 0.989 with the overall ICC of 0.985 (95%CI, 0.975 – 0.990) for subfoveal ChT (**Table 3.2**). The EDI OCT scans classified as group A showed greater reliability for both the total ChT and SfChT (as shown by the ICC value) than those EDI OCT scans containing less identifiable structures (group B and C).

The intra-observer CRs for the total ChT were 8.8 μ m, 22.1 μ m and 18.0 μ m for groups A, B and C respectively with an overall CR value of 17.5 μ m. The intra-observer CRs of the SfChT were approximately 2 times higher than those of the total ChT in each image classification.

Table 3.2: Summary of intra-observer agreements on the total and subfoveal choroidal thickness measurements

Intra-observer agreement	Total ChT			SfChT		
	ICC (95%CI)	Mean difference (95%CI) (μ m)	CR (μ m)	ICC (95%CI)	Mean difference (95%CI) (μ m)	CR (μ m)
Group A	0.996 (0.985 - 0.999)	2.9 (1.1 - 4.8)	8.8	0.989 (0.975 - 0.995)	2.0 (-2.4 - 6.4)	21.2
Group B	0.989 (0.973 - 0.996)	-4.2 (-9.3 - 1.0)	22.1	0.984 (0.961 - 0.993)	-4.5 (-13.0 - 4.1)	36.8
Group C	0.996 (0.991 - 0.998)	-0.5 (-4.4 - 3.4)	18.0	0.982 (0.958 - 0.992)	-0.6 (-10.7 - 9.5)	46.8
Overall	0.995 (0.991 - 0.997)	-0.3 (-2.4 - 1.8)	17.5	0.985 (0.975 - 0.990)	-0.8 (-5.1 - 3.6)	35.9
Non-agreement	0.981 (0.912 - 0.996)	6.3 (-4.9 - 17.4)	26.1	0.927 (0.686 - 0.985)	4.4 (- 21.3 - 30.0)	60.1

ICC: intraclass correlation coefficient; CI: confidence interval; CR: coefficient of repeatability, ChT: choroidal thickness

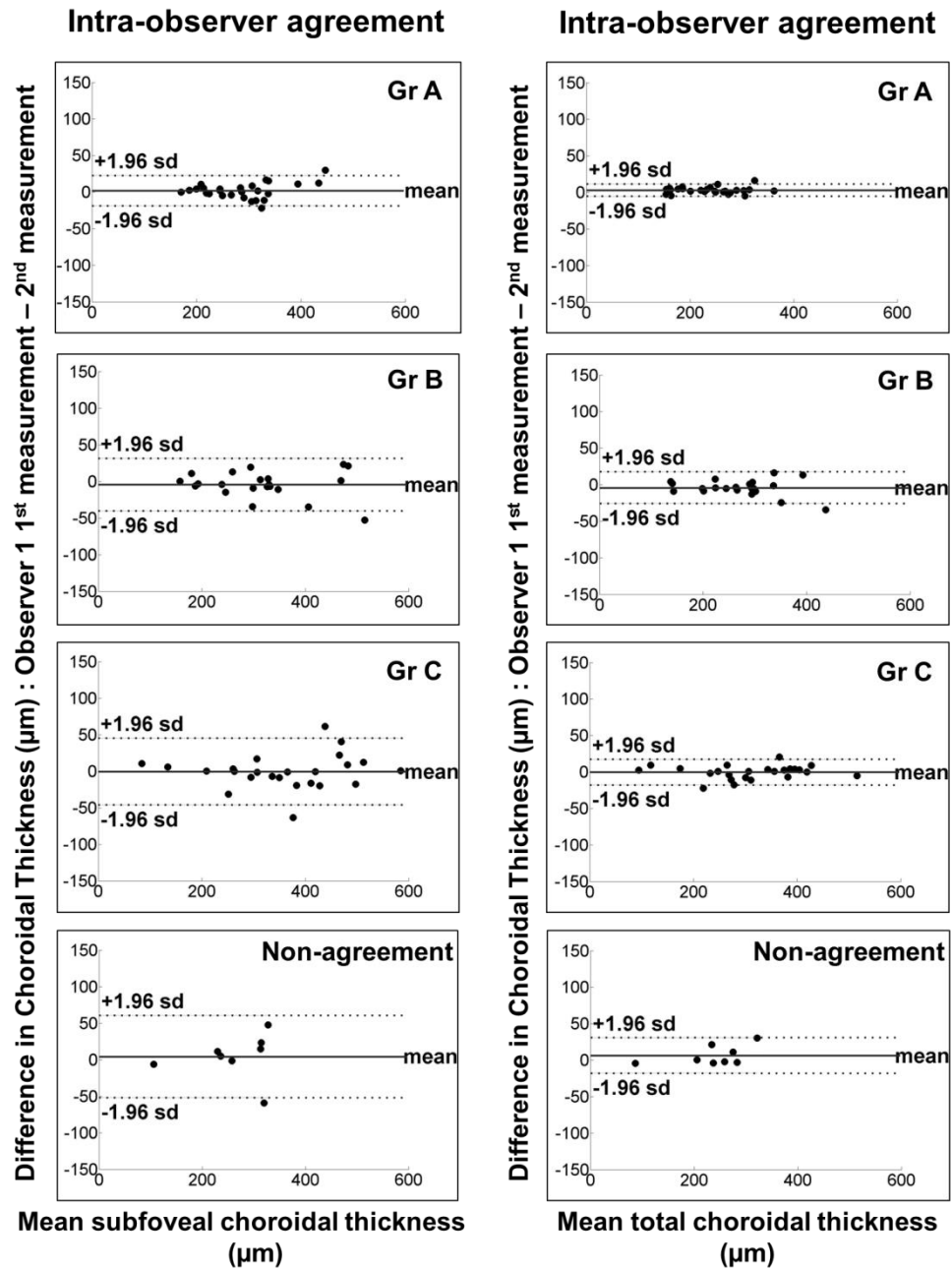


Figure 3.4: Bland-Altman plots showing intra-observer with mean difference (thick line) and 95% limits of agreement (dashed lines) for subfoveal choroidal thickness measurements (SfChT, left hand column) and the total choroidal thickness measurements (ChT, right hand column) by classification: group A (A1 and A2), group B (B1 and B2), group C (C1 and C2), non-agreement (D1 and D2)

3.2.2.3 *Inter-method agreement*

The ICC for intra-method measurement agreement ranged from 0.974 to 0.996 with the overall ICC value of 0.990 (95%CI, 0.979 – 0.995) for the total ChT and 0.934 to 0.985 with the overall ICC of 0.969 (95%CI, 0.936 – 0.985) for SfChT (**Table 3.3**). The EDI OCT scans classified as group A showed greater reliability for

both the total ChT and SfChT (as shown by the ICC value) than those EDI OCT scans containing less identifiable structures (group B and C).

The inter-method CRs for the total ChT were 9.9 μ m, 35.8 μ m and 21.5 μ m for groups A, B and C respectively with an overall CR value of 24.8 μ m. The inter-method CRs of the SfChT were approximately 2 times higher than those of the total ChT in each image classification.

Table 3.3: Summary of inter-method agreements on the total and subfoveal choroidal thickness measurements

Inter-method agreement	Total ChT			SfChT		
	ICC (95%CI)	Mean difference (95%CI) (μ m)	CR (μ m)	ICC (95%CI)	Mean difference (95%CI) (μ m)	CR (μ m)
Group A	0.996 (0.983 - 0.999)	-3.0 (-6.6 – 0.6)	9.9	0.969 (0.858 - 0.992)	-6.7 (-14.1 – 0.8)	19.0
Group B	0.974 (0.904 - 0.994)	-3.2 (-16.3 – 9.8)	35.8	0.934 (0.770 - 0.983)	-3.2 (-16.3 – 9.8)	49.6
Group C	0.995 (0.980 - 0.999)	3.8 (-4.0 – 11.7)	21.5	0.985 (0.945 - 0.996)	6.9 (-9.7 – 23.6)	45.6
Overall	0.990 (0.979 – 0.995)	-0.8 (-5.5 – 3.9)	24.8	0.969 (0.936 – 0.985)	-0.6 (-8.7 – 7.4)	40.8

ICC: intraclass correlation coefficient; CI: confidence interval; CR: coefficient of repeatability, ChT: choroidal thickness

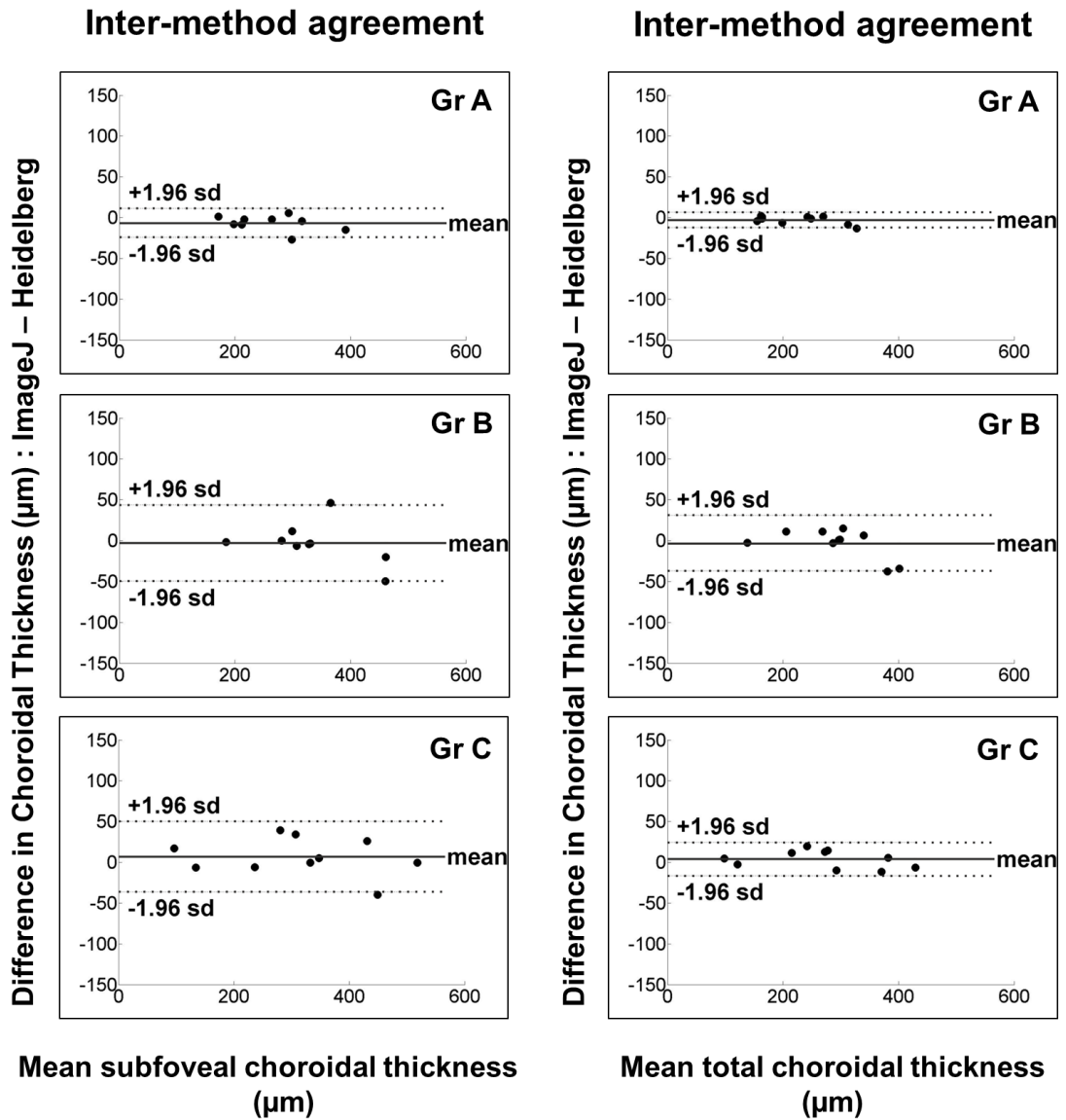


Figure 3.5: Bland-Altman plots showing inter-method agreements with mean difference (thick line) and 95% limits of agreement (dashed lines) for subfoveal choroidal thickness measurements (SfChT, left hand column) and the total choroidal thickness measurements (ChT, right hand column) by classification: group A (A1 and A2), group B (B1 and B2), group C (C1 and C2)

3.3 Validation of LDF measurements

In the studies I have conducted, I have used LDF to assess the choroidal circulation at the fovea as well as its autoregulation. Checking the LDF device for its hardware and software configurations was required before conducting my studies, and a precise operational protocol needed to be developed.

In this section, I will describe the initial situation of the LDF device as well as various experiments performed before using the device. These experiments were performed in 4 sub-studies: 1) to ensure the working condition of the LDF device, 2) to ensure the hardware and software configurations, 3) to ensure the validity of the LDF measurements, 4) to ensure the correct operational technique when using the LDF device. These experiments were done using a model flow simulator.

3.3.1 Subjects and methods

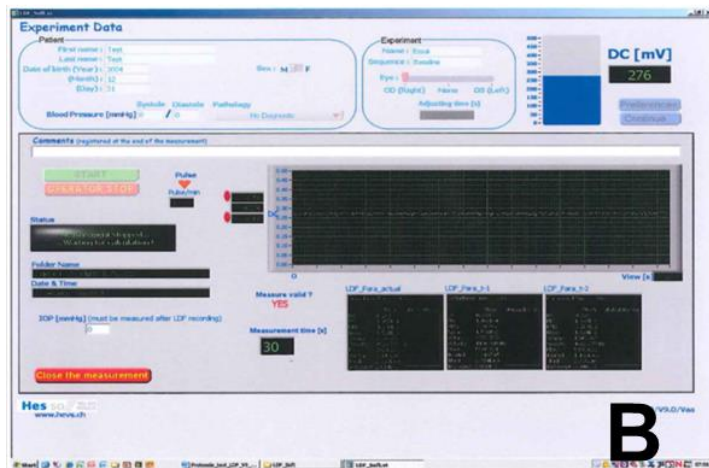
3.3.1.1 *The LDF system*

Initially, the LDF system at the Clinical Eye Research Centre (CERC) comprised of an Oculix system implemented on a mobile table. The system was custom designed/built and supplied by Professor Charles Riva and Dr Benno Petrig. A new LDF acquisition system, the Flom-S, was purchased from Professor Martial Geiser based at the Ophthalmology Research Institute in Sion, Switzerland in 2009.

The LDF system uses a diode laser beam with a wavelength of 670 nm. The laser beam is then delivered through the optical system of a fundus camera (Topcon). The intensity of the laser beam at the cornea is 50 μ W. The diameter of the laser beam is 150 μ m at the fovea. The system has 2 sets of photomultiplier tubes (PMTs) used to collect the light scattered back from the target. The diameter of these PMTs is approximately 150 μ m. When performing the LDF recording, the PMT is directly placed at the centre of the laser beam position. The sensitivity of the PMT can be adjusted from 0 to 100 depending on the signal strength. The signal from the PMT is then analysed automatically *via* either the Oculix or Flom-S device signal processors. Oculix LDF software version 2.1 (developed by Benno Petrig)²¹⁹ and LabVIEW version 4.5 (HES//SO Valais Wallis, Sion, Switzerland) are used to analyse the blood flow parameter derived from the Oculix and Flom-S systems, respectively. In this thesis, the Flom-S device is used. **Figure 3.6** shows the fundus camera based LDF device and the user interface of LabVIEW software used for the LDF signal analysis.



A



B

Figure 3.6: The LDF device (A) and the user interface of the LabVIEW software (B)

3.3.1.2 Artificial eye

The model flow simulator or “artificial eye” was developed by Professor Martial Geiser. It is a small device used to imitate the blood flow (Figure 3.7). The

device consists of an electrical input, an optical lens and a Teflon rotating wheel. The speed of the wheel is proportional to the voltage of the electrical supply to the motor. The lowest input is 2 volts and the highest input is 10 volts representing the lowest and the highest speed of the wheel respectively.

The laser beam from the LDF device is focused on the smooth surface of rotation wheel to create a test “flow” recording.

3.3.1.3 **Subjects**

Healthy subjects were recruited from PhD students within the Department of Eye and Vision Science. Subjects were fully dilated with 1% w/v tropicamide eye drops (Bausch and Lomb/Chauvin Pharmaceutical Ltd, Surrey, UK).

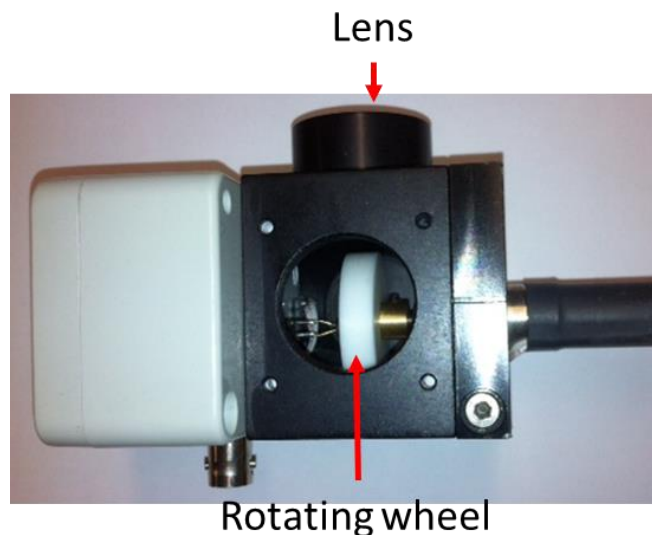


Figure 3.7: The artificial eye device

3.3.2 **Sub-study 1: To determine a working condition of the LDF device**

Blood flow parameters were recorded using the LDF device on three healthy subjects and on the artificial eye. For the artificial eye set at 8.6 volts was used. A recording of 30 seconds was done on both healthy eyes and the artificial eye. Because the device has two PMTs, blood flow parameters were also repeated using the two available PMTs. These LDF recordings from the two PMTs were used to determine the working condition of the PMT tubes. The Doppler shift power spectrums (DSPS) from all recordings were visualised.

3.3.2.1 Sub-study 1: Results

The results of LDF recording from healthy and artificial eye are shown in **Figure 3.8**. The mean velocity was 3908.88 Hz for a healthy eye and the mean velocity was 1667.21 Hz for the artificial eye. These values were higher and did not correspond to the mean Doppler shifted frequency observed on the DSPS. These miscalculations of the velocity from the DSPS were also observed when using both PMTs (**Figure 3.9**). In addition, the DSPS recordings derived from all LDF recordings were relatively low. These miscalculations of velocity and low DSPS suggested that there were problems related to the hardware and/or the system connection. In the next substudy I assessed the system configuration and its connection in order to determine the origin of these problems.

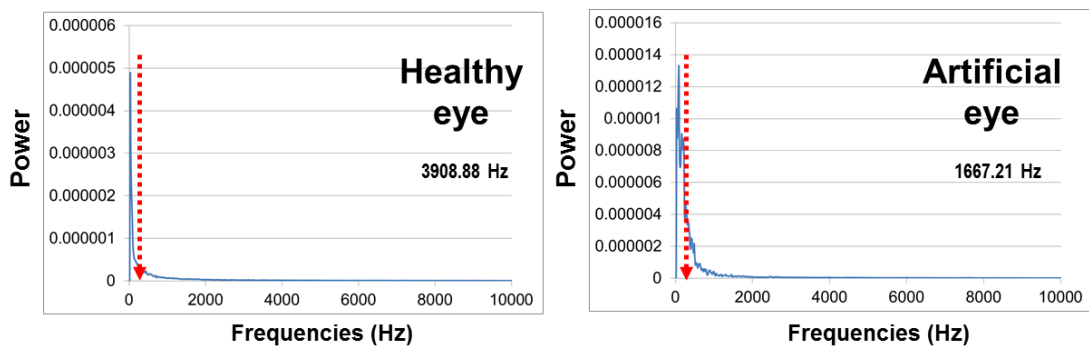


Figure 3.8: Examples of LDF recordings from a healthy eye and the artificial eye set at 8.6 volts. The red arrows indicate the mean Doppler shifted frequency (Hz) representing the expected velocity

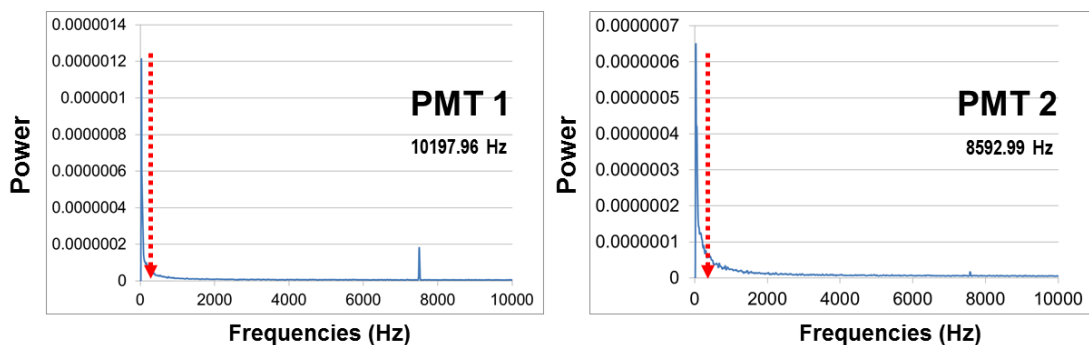


Figure 3.9: Examples of Doppler shift power spectrum (DSPS) from LDF recordings from 2 PMT of our fundus camera based LDF device. The red arrows indicate the mean Doppler shifted frequency (Hz) representing the expected velocity

3.3.3 Sub-study 2: LDF system configuration

To determine the LDF system configuration, the system was connected to the Flom-S signal processor using two different configurations: 1) the signal derived from the PMT fed to the Oculix and Flom-S signal processor; 2) the signal fed directly to the Flom-S signal processor. The LDF recordings for each system configuration were done on one healthy eye and the DSPS were analysed. **Figure 3.10** shows the different system connections.

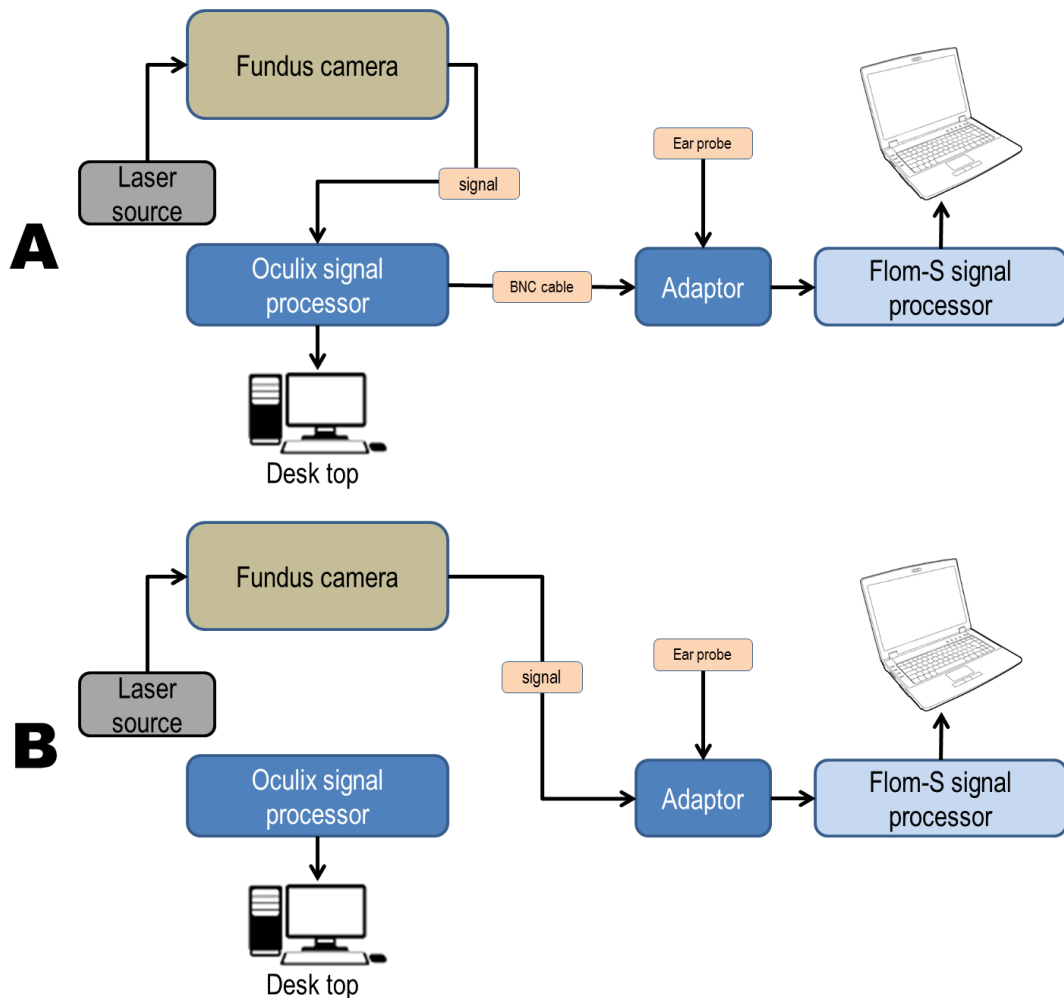


Figure 3.10: The LDF system connections: the signal derived from the PMT fed to the Oculix and Flom-S signal processor (A) and the signal fed directly to the Flom-S signal processor (B), BNC: Bayonet Neill–Concelman cable

3.3.3.1 Sub-study 2: Results

The DSPS from each of the system settings are shown in **Figure 3.11**. Abnormal peaks at 7500 Hz and 15000 Hz were clearly visible on both system

connections. These peaks were larger when the signal fed into the Oculix system. In addition, the DSPS was relatively low on both system connections.

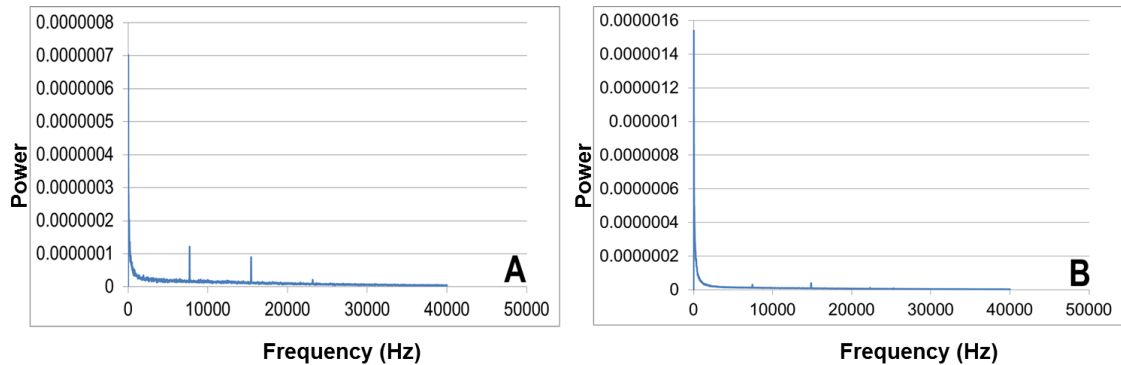


Figure 3.11: The DSPS from LDF recordings from 2 system connections, (A) the signal connected with the Oculix and Flom-S signal processor and (B) the signal fed directly to the Flom-S signal processor

3.3.3.2 *Substudies 1 and 2 summary*

From the observational results in substudies 1 and 2, the problems of the LDF device can be summarised as follow:

1. Adding an external signal processing device such as the Oculix signal processor to the Flom-S acquisition gives perturbation on the signal.
2. Low Doppler signal, this is mainly due to the optical arrangement of the system.
3. Wrong velocity calculation.

To solve these problems, the hardware of the Flom-S device signal processors system was modified and new LabVIEW LDF analysis software was updated.

Hardware modifications

1. To prevent the signal perturbation from the different ground connection, the Bayonet Neill–Concelman cable was reinstalled with a different mode. A new LDF and pulse signal acquisition card were installed. The data acquisition card with a signal differential between Dev1/ai2 - Dev1/ai8 was used.
2. A low pass filter at 20 KHz was used to filter out unwanted peaks. The schematic of this filter is shown in **Figure 3.12**.

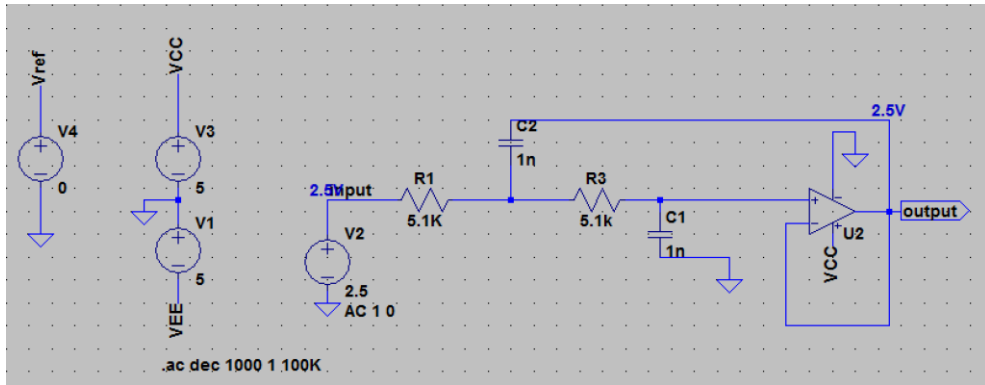


Figure 3.12: Schematic design of the low pass filter.

Software modifications and signal analysis parameters

1. The new LabVIEW software analyses the range of frequency with a bandwidth of 20 KHz.
2. The low cut-off frequency is at 30 Hz. The noise derived from the LDF recording begins at 15 KHz and end at 20 KHz.
3. The frequency at 50 Hz and 17000 Hz are used to assess the amplitude of the DSPS.
4. The length of the DSPS amplitude is 900 Hz and the DSPS amplitude validity factor is 10.

Figure 3.13 shows the schematic of the DSPS calculation from the new LabVIEW software.

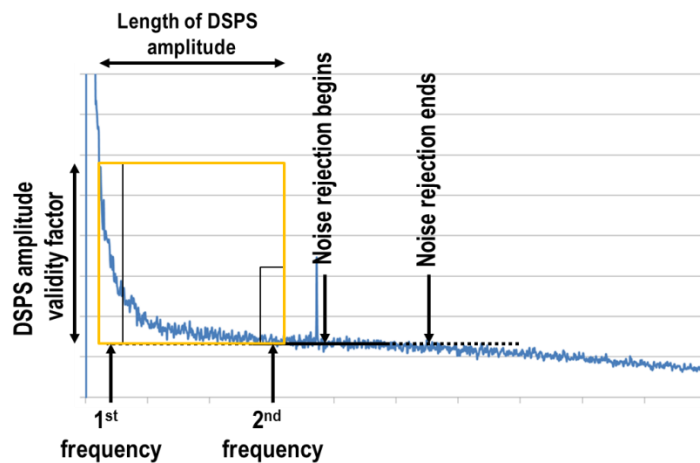


Figure 3.13: Schematic of parameters considered for noise calculation and amplitude of the DSPS calculation

3.3.3.3 LDF test after hardware and software modifications

The artificial eye set at 8.5 volts was used to compare the DSPS as well as the correct velocity calculation after the device and software modification. After the modification, ChBFlow parameters were recorded in a healthy eye and compared with before modification. **Figure 3.14** shows the comparison of DSPS before and after the modifications of the artificial eye and the healthy eye. The velocity was 1667 Hz and 2008 Hz for before and after modification, respectively for the artificial eye. The ChBVelocity was 5163 Hz and 1903 Hz for before and after modifications, respectively for the healthy eye. These results confirmed that after the modifications, good signal and correct velocity calculation were observed.

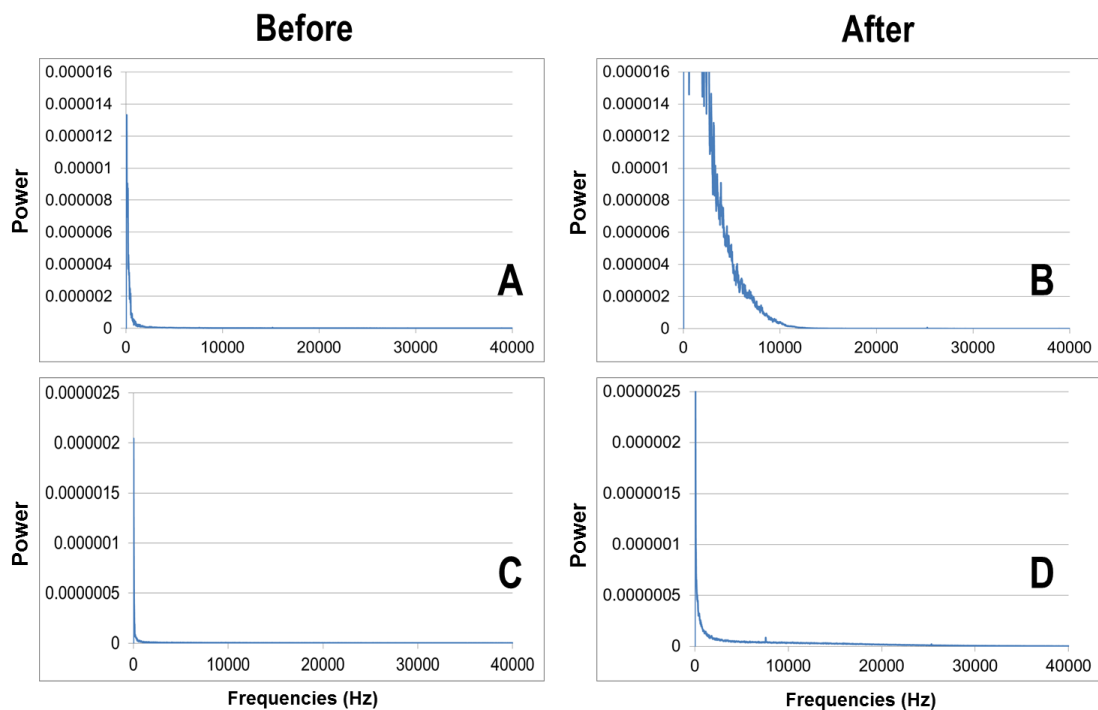


Figure 3.14: Comparison between the DSPS before and after the hardware modification. The DSPS derived from the artificial (A and B) and healthy (C and D) eyes before (A and C) and after (B and D) hardware modification.

3.3.4 Sub-study 3: validity of the LDF measurement

3.3.4.1 Experimental designs

Experiment 1: linearity of the measurements

The artificial eye was used to determine the linearity of the LDF measurement. The speed of artificial eye was adjusted by adjusting the electrical supply voltage from 1.5 volts to 10.5 volts. The laser beam was sharply focused on

the rotation wheel. A 30-second measurement was done for each of the rotating speed without adjusting the position of the laser beam. Accumulative blood flow parameters were calculated.

Experiment 2: The effect of the sensitivity of the photomultiplier tube

The artificial eye with the electrical supply set at 8.6 volts (auto-run mode) was used to assess the effect of the sensitivity of the PMT. The laser beam was sharply focused on the rotation wheel. The sensitivity of the PMT was adjusted from 50 to 80 without adjusting the position of the laser beam.

Experiment 3: The effect of returning light

Filter films with the density of 0.3D, 0.6D, 0.9D and 1.2D were used to determine the effect of lights at the photodetector. The laser beam was sharply focused on the rotation wheel of the artificial eye (auto-run mode). A 20-second measurement was done for each of film density without adjusting the position of the laser beam.

3.3.4.2 Sub-study 3: Results

Linearity of the measurements

The direct photocurrent (DC) level (corresponding to the amount of light scattered back from the tissues) from all rotation speeds remained within 3.03% of the baseline. As expected, an increase in the rotation speed of the artificial eye caused the velocity to increase linearly ($R^2 = 1.00$, $p < 0.01$). An increase in the rotation speed did not affect the volume ($R^2 = 0.380$, $p = 0.28$). The flow was increased linearly from the slowest speed to the higher speed similar to that of velocity as expected. **Figure 3.15** shows the linearity of all LDF parameters.

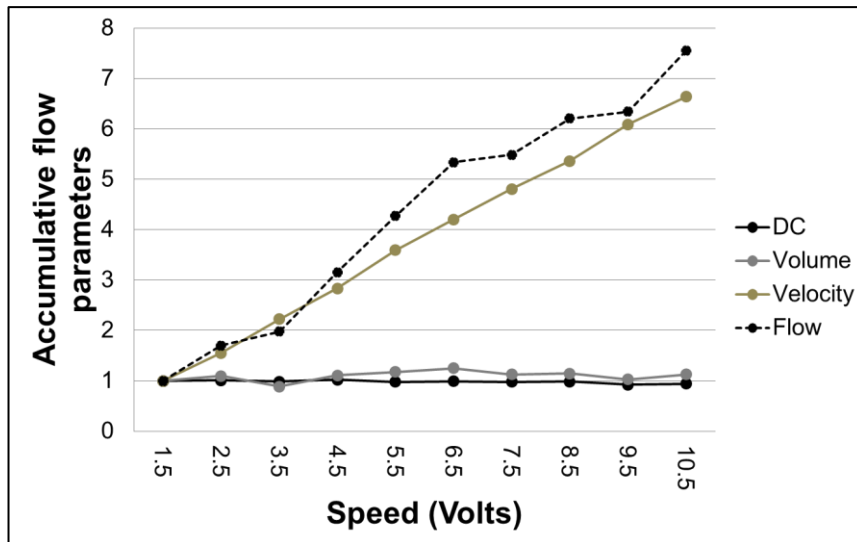


Figure 3.15: Linearity of the blood flow parameters

The effect of the sensitivity of the photomultiplier tube

The effect of PMT sensitivity is shown in **Figure 3.16**. As expected, the level of DC increased linearly following the adjustment of PMT sensitivity from 50 to 80. An increase in PMT sensitivity did not affect the level of volume, velocity and flow. The volume, velocity and flow remained constant up to 50% increasing of the sensitivity level from baseline. The constant flow parameters showed some degree of fluctuation after a 60% increase in PMT sensitivity.

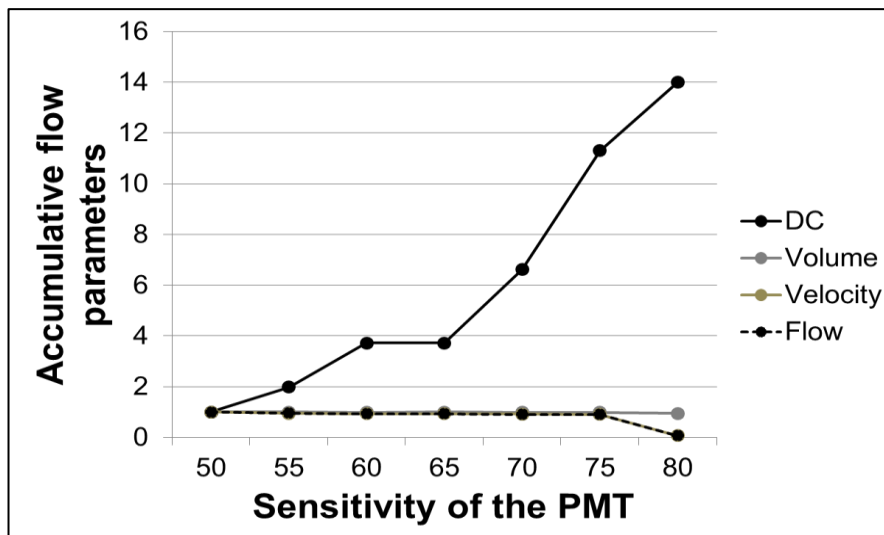


Figure 3.16: The effect of PMT sensitivity

The effect of light

As expected, the DC level decreased dramatically as higher film densities were applied. The decreased level of DC reached 90% lower than baseline when the light was filtered out by 1.2D film. The volume, velocity and flow did not change significantly from baseline (5.4%, 4.5% and 4.8% respectively). **Figure 3.17** shows the different level of flow parameters from different filter densities.

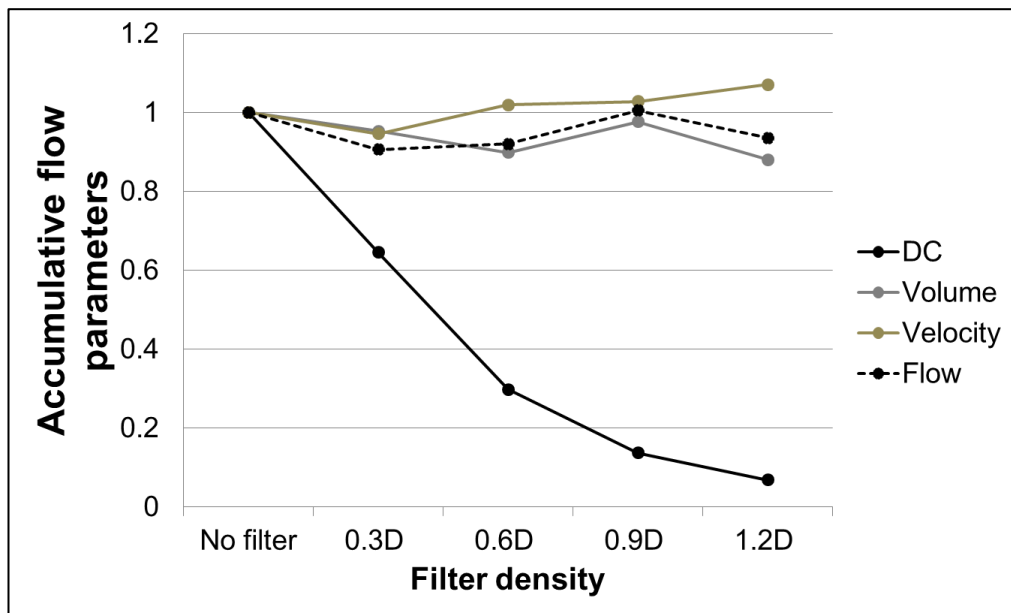


Figure 3.17: The blood flow parameters at different filter density

3.3.4.3 *Sub-study 3 summary*

From the results obtained from these experiments, it can be summarised as follow:

1. The DC level and volume are independent of the speed of the artificial eye whereas the velocity and flow are dependent.
2. These results obtained from the section provide reassurance of the working condition of the LDF device and PMTs.
3. Adjusting the sensitivity of the PMT affects the DC level but does not have any effect on flow parameters.
4. The level of DC is directly dependent on the amount of light return back from the detected light. The different DC levels, however, do not affect the flow parameters when the same location is measured.

3.3.5 Sub-study 4: The operational technique of using the LDF device

3.3.5.1 Experimental designs

The effect of the focus of the laser beam

To determine the effect of the laser beam focus LDF measurements were performed on 3 healthy volunteers. Prior to the LDF measurements, the focal point of the laser beam was adjusted on the fovea as shown in the figure below either in focus (**Figure 3.18A**) or out of focus (**Figure 3.18B**). Flow parameters were measured for 10 seconds at the fovea.

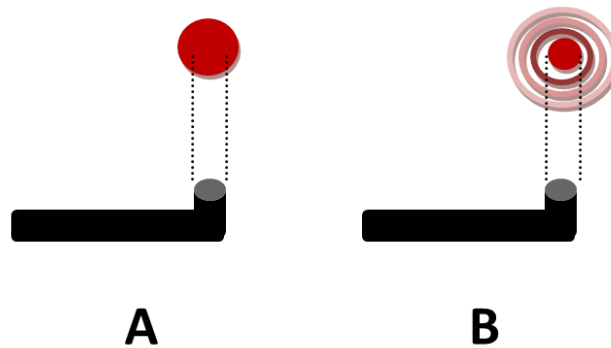


Figure 3.18: The different patterns of laser beam on the fovea: focus (A) and out of focus (B)

The effect of the photomultiplier tube position

To determine the effect of the position of the PMT on the blood flow parameters detected by the LDF, the laser beam was sharply focused on the rotation wheel of the artificial eye. The position of the PMT was moved as in **Figure 3.19**, horizontally and vertically to the laser point without the adjustment of the laser beam. A voltmeter was used to measure the signal input from each PMT position.



Figure 3.19: The position of the PMT (blue circle) and the laser beam (red circle)

3.3.5.2 Part 4: Results

The focus of the laser beam on the fovea

The DC level from 2 of the 3 subjects was higher but not significant ($p > 0.05$) when the laser beam was focused on the fovea compared to the unfocused laser beam. Although there were no statistically significant differences detected, the mean volume, velocity and flow were greater when the laser was sharply focused on the fovea compared to those with the unfocused laser beam. **Figure 3.20** shows effect of focus of the laser beam on LDF measurements on 3 healthy volunteers.

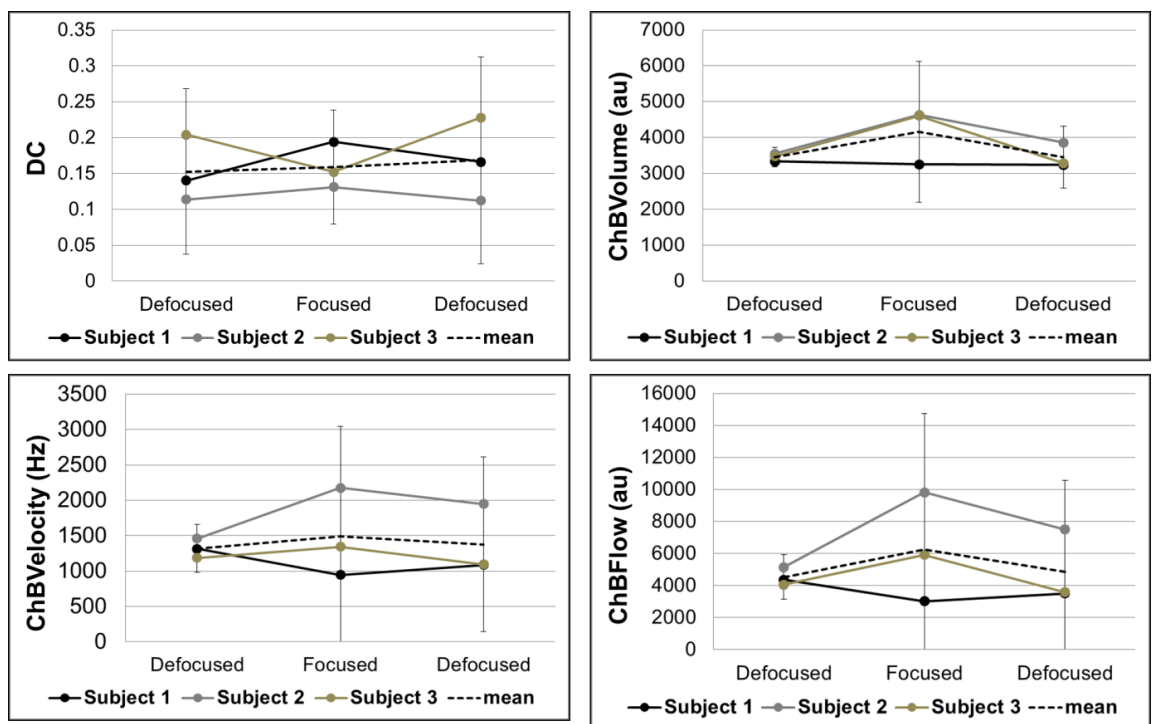


Figure 3.20: The effect of focus of the laser beam

The effect of the photomultiplier tube position

Figure 3.21 shows the variations of the DC levels representing different amounts of light returning back to the PMT. The highest signal was found when the PMT was carefully aligned over the laser spot. The signal became weaker when the PMT was moved away from the laser spot.

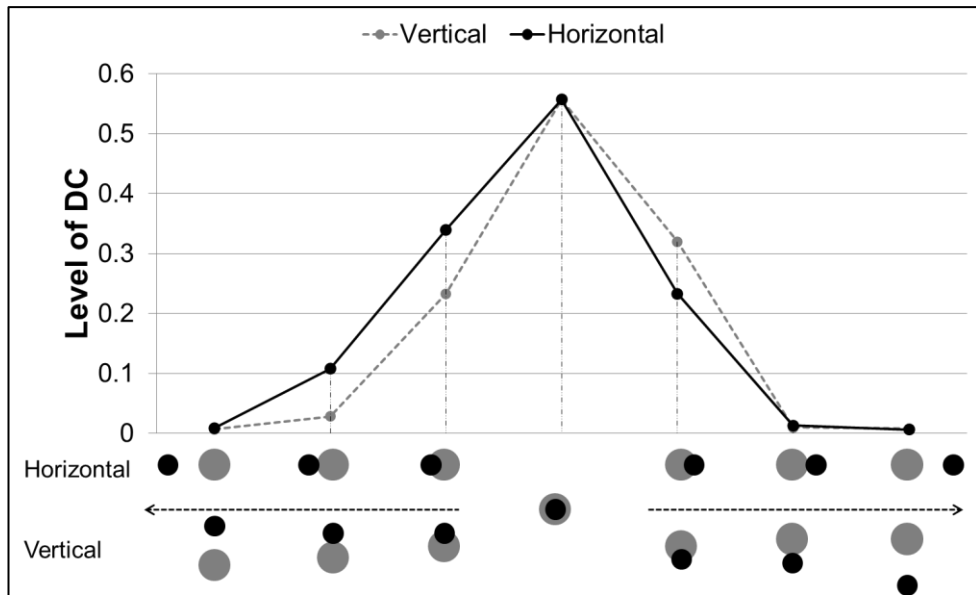


Figure 3.21: The DC levels (the amount of detected light on PMT) due to different PMT positions

3.3.5.3 *Sub-study 4 summary*

From the results obtained from these experiments, it can be summarised as follow:

1. A relationship between changes in ChBFlow parameters was clearly observed as the level of focus of the laser beam moved from defocused to focused. A higher LDF signal was observed when the laser beam was in focused.
2. The positioning of the detector probe over the laser beam had a direct effect on the DC level which fell as the alignment between them was lost.
3. Great care needs to be taken during ChBFlow measurements with the current LDF system. However, good results can be obtained with careful attention to detail and appropriate technical support.

3.4 Summary

In this chapter, I have validated the EDI OCT and LDF techniques which are core to the two clinical studies that I will be presenting in Chapters 5 to 7.

I have developed a protocol to standardise ChT measurements on EDI OCT which is able to handle the presence or absence of the SCS and the CSI seen on the images as hypo-reflective and hyper-reflective bands respectively. Using these criteria, I classified the images into 4 groups: A, B, C and ungradeable. A good

agreement in grading the images and excellent inter- and intra-observer agreements was achieved by using this protocol. This protocol will also be used in analysing volumetric scans to construct the thickness and volume map of the choroid in Chapter 7.

I have validated the hardware and software of the LDF system and standardised operational techniques for the LDF device. The LDF technique provides a direct measurement of choroidal circulations including ChBVolume, ChBVelocity and ChBFlow. Since these parameters are all derived from the DSFS, confirmation of normal spectrum is required frequently, preferably at the beginning of the experiment session.

Using LDF to measure choroidal circulation can be challenging. In order to obtain reliable LDF results, several aspects need to be considered. First, the laser beam needs to be in precise focus on the patient's fovea. Second, the operator needs to maintain accurate alignment of the recording PMT over the focal point of the laser beam. Third, the operator needs to ensure that the exact same location or close to the same location is maintained in order to achieve a high reproducibility of the results. This is very important, particularly, when LDF is used to test the effect of external physiological stimuli. However with attention to detail and sufficient training good results can be obtained.

Chapter

4 Patients and Methods

In my thesis, I will study the choroidal structure and function in patients with diabetes and patients with central serous chorioretinopathy (CSCR) utilising data from two controlled observational non-interventional studies, the Diabetic Retinopathy Functional and Structural Study (DREFUS study) and the Liverpool CSCR study. In this chapter, I present the details of the methodology, patient recruitment, inclusion and exclusion criteria, investigation techniques and image acquisition and analysis protocols used in both studies.

4.1 Background

When I started my experiments for my PhD in 2012 there were fewer than 100 publications on choroidal thickness (ChT) measurement using enhanced depth imaging optical coherence tomography (EDI OCT) and approximately 200 on choroidal blood flow measurement. There were none that incorporated the techniques of EDI OCT and laser Doppler flowmetry (LDF) to study choroidal structure and function.

My research presented in this thesis was conducted in St Paul's Eye Unit, Royal Liverpool University Hospital. Patients were screened prospectively using the protocol specific to each study before their participation. Healthy participants with no known eye diseases (control groups) for each study were recruited through University of Liverpool announcements, patients' relatives and St Paul's Eye Unit staff. A written informed consent was obtained from all participants before enrolment. Studies were undertaken in accordance with the tenets of the Helsinki

Declaration. The two observational studies were designed as single-centre, cross-sectional case-control studies and took place in the Clinical Eye Research Centre (CERC) of St Paul's Eye Unit.

4.2 Diabetic Retinopathy: Functional and Structural Study (DREFUS study)

This study commenced in 2010. The protocol was developed by Mr Claudio Campa. The first patient was recruited in to the study in October 2010. I contributed to the study since January 2012 when I started my PhD.

4.2.1 Patient recruitment criteria

Patients with type 1 or type 2 diabetes mellitus aged over 18 attending St. Paul's Eye Unit, Royal Liverpool University Hospital were recruited into this cohort. Patients were excluded if unable to fully understand informed consent and/or unable to comply with study procedures. Additional exclusion criteria for patients with diabetic retinopathy (DR) included any other ocular diseases that may affect the blood-retina barrier (i.e. vascular occlusion) or any retinochoroidal abnormalities other than DR. Patients with a previous history of any intraocular procedure within the past 3 months including macular laser photocoagulation (in the study eye), peripheral scatter retinal laser photocoagulation in the study eye in the last 6 months were also excluded from the study. Patients with diabetes were the sub-divided into 4 groups as shown in **Table 4.1**.

Table 4.1: Patient and healthy control inclusion and exclusion criteria in the DREFUS study

Group	Inclusion	Exclusion
Group A	<ol style="list-style-type: none"> 1. Patients with established type 1 or type 2 diabetes mellitus; 2. Diabetic maculopathy (diffuse exudative or focal) without CSMO 3. BCVA \geq 35 ETDRS letters 	<ol style="list-style-type: none"> 1. Presence of CSMO 2. Presence of ischaemic maculopathy 3. Opacities of the ocular media, limitations of pupillary dilation or any other problems sufficient to preclude good quality stereo fundus photographs 4. Fixation unstable on MP1 (fixation points < 75% within 4°)
Group B	<ol style="list-style-type: none"> 1. Patients with established type 1 or type 2 diabetes mellitus 2. Diabetic maculopathy (diffuse exudative or focal) with CSMO 3. BCVA \geq 35 ETDRS letters 	<ol style="list-style-type: none"> 1. Presence of significant ischaemic maculopathy 2. Opacities of the ocular media, limitations of pupillary dilation or any other problems sufficient to preclude good quality stereo fundus photographs 3. Fixation unstable on MP1 (fixation points < 75% within 4°)
Group C	<ol style="list-style-type: none"> 1. Patients with established type 1 or type 2 diabetes mellitus 2. Significant ischaemic maculopathy 3. BCVA \geq 35 ETDRS letters 	<ol style="list-style-type: none"> 1. Any other ocular disease that may affect blood-retina barrier 2. Opacities of the ocular media, limitations of pupillary dilation or any other problems sufficient to preclude good quality stereo fundus photographs 3. Fixation unstable on MP1 (fixation points < 75% within 4°)
Group D	<ol style="list-style-type: none"> 1. Patients with established type 1 or type 2 diabetes mellitus 2. No features of diabetic retinopathy 3. BCVA \geq 35 ETDRS letters 	<ol style="list-style-type: none"> 1. Opacities of the ocular media, limitations of pupillary dilation or any other problems sufficient to preclude good quality stereo fundus photographs 2. Fixation unstable on MP1 (fixation points < 75% within 4°)
Controls	<ol style="list-style-type: none"> 1. Healthy subjects with HbA1c value 4-6.5% 	<ol style="list-style-type: none"> 1. Ocular disease that may affect blood-retina barrier (i.e. vascular occlusion) 2. Opacities of the ocular media, limitations of pupillary dilation or any other problems sufficient to preclude good quality stereo fundus photographs 3. Fixation unstable on MP1 (fixation points < 75% within 4°)

CSMO = clinically significant macular oedema; significant ischaemic maculopathy is defined either 1) foveal avascular zone (FAZ) greatest linear diameter \geq 1000 μ m or 2) \geq 50% of the original capillary outline nonperfused in the presence of otherwise unexplained reduction of VA.

4.2.2 Sample size estimation

The sample size was calculated based on 4 primary outcomes; retinal microperimetry sensitivity (dB), central ring implicit time of multifocal electroretinography (mfERG), oscillatory potential (OP) amplitude and LDF choroidal blood flow (ChBFlow) at the fovea. A statistical power of 90% was used in the sample size calculation based on the analysis of variance (ANOVA) and a paired t-test. For ChBFlow, a mean difference of 4 arbitrary unit (AU) with SD of 5 AU was judged clinically relevant.¹⁸⁰ Based on this calculation, the sample size required for the study was 30 participants for each group.

4.2.3 Investigation procedures of DREFUS study

All participants included in the study underwent the investigations as shown in **Figure 4.1** at the baseline visit. Each examination procedure is described in the following section.

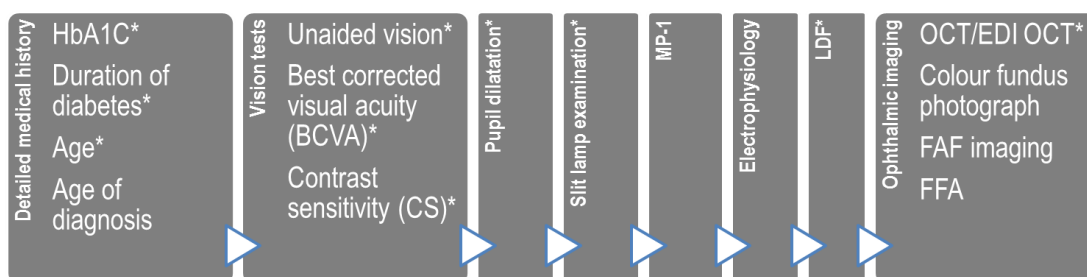


Figure 4.1: Investigation procedures of DREFUS study, * represents the procedures included in the analyses for this thesis

4.2.4 Detailed medical history

The medical history including duration of diabetes, age, smoking status, ethnicity, age of first diagnosis with diabetes and systemic diseases of patients and healthy controls were assessed by a qualified researcher or medical staff. A blood sample was collected from all participants for cholesterol and HbA1c level tests.

4.2.5 Vision tests

4.2.5.1 Best corrected visual acuity

The best corrected visual acuity (BCVA) was measured by accredited opticians using the Early Treatment Diabetic Retinopathy Study (ETDRS) reading charts (Precision Vision, Illinois, USA). One set of ETDRS charts consists of 3 charts, Chart R for refraction, Chart 1 for right eyes, and Chart 2 for left eye (**Figure**

4.2). Each chart contains 14 rows with 5 letters for each row. A 62.9 x 65.4 x 17.8 cm illuminator (Precision vision, NY, USA) with a 2 x 20 W standard fluorescent lamps (Sylvania standard daylight F20W/54-765/RS) was used to back illuminate the chart. Bulbs were changed on a 3 monthly basis.

The procedure was performed according to the ETDRS protocol in a darkened room. Briefly, the participant was seated at a distance of 4 metres from the ETDRS chart. Correct refraction was established using Chart R. The right eye was tested first followed by the left eye. The participant started to read from the upper left corner and proceeded towards the lower right corner according to their ability to recognise the letters correctly. Any correctly identified letters were counted and recorded on the specific form. This number of letters was then converted to a logarithmic equivalence of BCVA and used to represent individual vision.

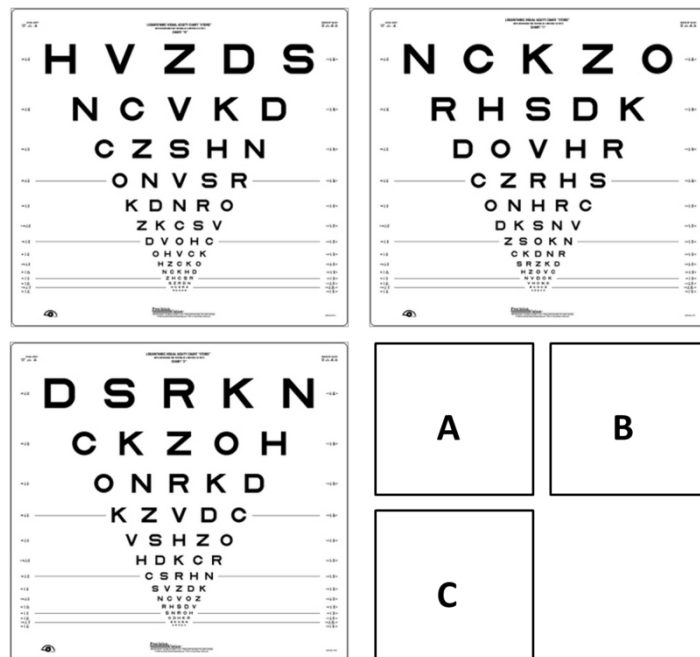


Figure 4.2: Visual assessment charts. ETDRS chart “R” (A), ETDRS chart “1” (B) and ETDRS chart “2” (C).

4.2.5.2 Contrast sensitivity (CS)

Contrast sensitivity (CS) was measured with a set of Pelli-Robson contrast sensitivity charts (HAAG-Streit, Essex, UK). One set of charts consists of 2 charts (Chart 1 for the right eye and Chart 2 for the left eye, **Figure 4.3**). Each chart contains 48 letters (6 letters per line). The letters on each line are arranged in a group of 3 letters with the same contrast level starting from high (black) to low (white).

The chart was illuminated with 100-foot candle light and the distance used for the CS test was at 1 metre. The participant started the test reading from the highest contrast (VRS for right eye and HSZ for left eye) until they were unable to read two or three letters in a single group. The total number of letters seen and the contrast score of the last group were recorded and reported as a logarithmic equivalence of CS.

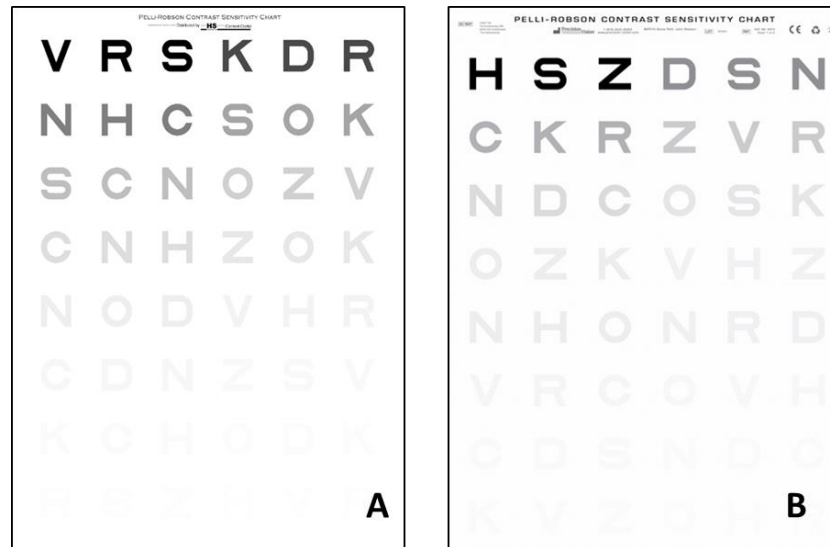


Figure 4.3: Pelli-Robson contrast sensitivity charts. One set of chart consists of 2 charts: chart 1 (A) for right eye and chart 2 (B) for left eye.

4.2.6 Pupil dilatation and blood pressure measurement

The pupil was dilated using 1% w/v tropicamide and 2.5% w/v phenylephrine hydrochloride eye drops (Bausch and Lomb/Chauvin Pharmaceutical Ltd, Surrey, UK). After the instillation of the eye drops, the pupil was allowed to dilate for approximately 20 minutes.

Blood pressure (BP) was measured at the upper arm with a digital automatic device (Welch Allyn vital signs devices, Welch Allyn Inc, NY, USA). An appropriate-sized cuff was used for each participant. The participant was in a sitting position for a minimum of 5 minutes before the BP measurement. The mean arterial pressure (MAP) was calculated according to the following formula:¹²²

$$MAP = BP_{diast} + \frac{1}{3} (BP_{syst} - BP_{diast})$$

Equation 4.1: MAP = mean arterial pressure; BP_{diast} = diastolic blood pressure;
 BP_{syst} = systolic blood pressure

4.2.7 Slit lamp examination

Each participant underwent complete ocular examination including a slit lamp anterior chamber evaluation and dilated binocular indirect high-magnification ophthalmoscopy.

4.2.8 Choroidal blood flow parameters measurement and isometric exercise

The sequence for the ChBFflow measurement using LDF for each participant is shown in **Figure 4.4**.

LDF procedures were explained to the participants and baseline BP was recorded. The relative ChBFflow parameters including ChBVelocity, ChBVolume and ChBFlow at the fovea were obtained using the Topcon based LDF system as described in Chapter 3. During the LDF recording, the participant was asked to fixate directly at the probing laser beam. The detector was placed at the centre of the illuminated site. The light scattered back by the moving red blood cells and the surrounding tissues were detected via the optical fibre aperture with a diameter of 150 μ m. For each participant, 3 consecutive measurements of 30 seconds were obtained at baseline.

After baseline measurements, participants performed the isometric exercise (weight lifting) for a minimum of 2 minutes. One ChBFlow measurement was taken while the participant continued lifting a weight (1 kilo). A repeated BP measurement was done during the last ChBFlow measurement. In order to achieve a similar DC level, proper fixation was monitored and the foveal location was confirmed by direct observation through the fundus camera for each LDF recording.

The signal from the optical fibre was then analysed automatically via the Flom-S device and the LDF software (LabVIEW) version 4.5 (HES//SO Valais Wallis, Sion, Switzerland). The portion of the stable measurement within 20% fluctuation was used in the signal analysis in order to prevent the effect of minor movements and blink.

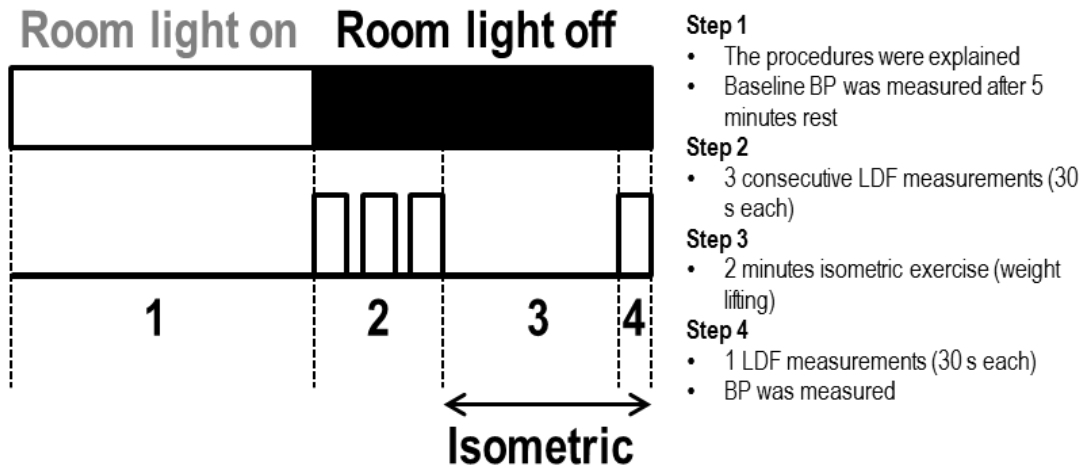


Figure 4.4: The sequence of choroidal blood flow measurement with isometric exercise for DREFUS study

4.2.9 EDI OCT

A single horizontal line EDI OCT scan of 9 mm centred on the fovea was performed on the Spectralis SD OCT system (Heidelberg Engineering, Heidelberg, Germany). The EDI acquisition was performed using either the protocol previously described by Margolis *et al*⁴⁷ or the build-in EDI modality. In the Margolis manoeuvre, the device was moved closer to the participant's eye to obtain an inverted image. On both EDI OCT image acquisitions, an Automatic Real Time-function (ART) of 100 was applied using the built-in automatic averaging and real time eye-tracking features in order to obtain images with adequate quality for visualisation and to maximise the signal-to-noise ratio. Measurement of ChT was done as described previously in Chapter 3 by moving the automatic corresponding reference lines of the retinal segmentation to the relevant choroidal structures.

ChT was measured as the perpendicular distance between the anterior and posterior choroidal boundaries at 500 μ m intervals up to 3 mm nasal and 3 mm temporal from the foveal centre. The total ChT over a 6 mm length of a B-scan was defined as the average ChT of the measurements at the aforementioned 13 locations.

4.3 Liverpool Central Serous Chorioretinopathy Study (Liverpool CSCR Study)

I undertook all aspects of the study including design, protocol development, ethical approvals, patient recruitment and protocol for each investigation. I also performed most of the tests.

4.3.1 Patient recruitment criteria

Treatment naïve patients with CSCR attending St Paul's Eye Unit with visual symptoms and SRF seen at the fovea on OCT were recruited. Patients were excluded if unable to fully understand the informed consent and/or unable to comply with study procedures. Additional exclusion criteria for patients with CSCR included pregnancy, high myopia or hyperopia (greater than ± 6 D), any chorioretinal abnormalities other than CSCR, previous history of any intraocular procedures including laser vision correction, any forms of treatments, such as photodynamic therapy or intravitreal injections and other ocular disease that may affect blood-retina barrier (i.e. vascular occlusion).

4.3.2 Sample size estimation

The sample size was calculated based on the two primary outcomes; ChT on EDI OCT and ChBFlow at the fovea. A statistical power of 90% was used for the sample size calculation based on a paired t-test and the significant level of 0.05. A mean change in EDI OCT and LDF of 90 μm and 4 units, respectively, were judged clinically relevant.^{220,210} Based on this calculation, sample sizes required for comparisons between groups were 27 for EDI OCT and 24 for LDF. The sample size was adjusted to 10 % larger than the actual calculation in order to cover potential drop-outs during the process of the study. Thus, a sample size of 30 participants was set for each group.

4.3.3 Investigational procedures for Liverpool CSCR study

All participants included in the study underwent investigations as shown in **Figure 4.5**. Each examination procedure is described in the following section.

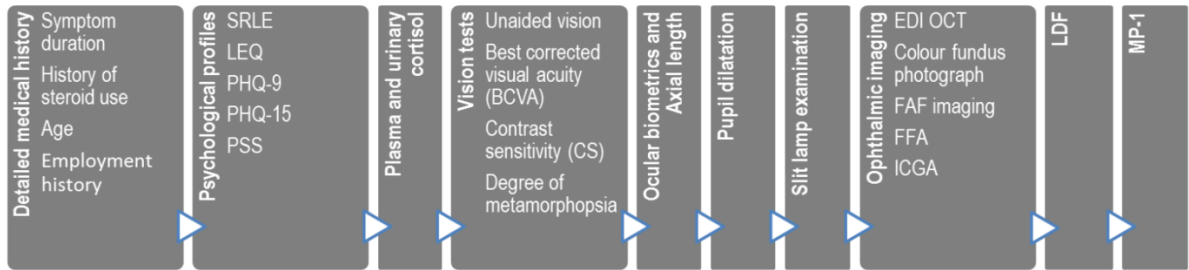


Figure 4.5: Investigation procedures of Liverpool CSCR study

4.3.4 Detailed medical history

History of ocular diseases, age, smoking status, ethnicity, occupation and other medical histories of CSCR patients and healthy controls were assessed by a qualified researcher or medical staffs. Additionally, CSCR patients were also asked about the visual symptoms of CSCR, duration of visual symptoms and history of steroid use.

4.3.4.1 *Socio-economic classification*

The social class of CSCR patients was defined through their occupation converted to the categorical score using the occupation code search tool, available at:

http://www.neighbourhood.statistics.gov.uk/HTMLDocs/dev3/ONS_SOC_occupation_coding_tool.html. This coding matches the patient's occupation to the National

Statistics Socio-economic classification (NS-SEC) score. The simplified NS-SEC analytical class was selected to represent patients' social class and used for the analyses (**Table 4.2**).

Table 4.2: NS-SEC analytic classes

NS-SEC level	Social class	Example of occupation
1	Higher managerial, administrative and professional occupations	N/A
1.1	Large employers and higher managerial and administrative occupations	Army officer
1.2	Higher professional occupations	GP
2	Lower managerial, administrative and professional occupations	Nurse
3	Intermediate occupations	Teaching Assistant
4	Small employers and own account workers	Antiques dealer
5	Lower supervisory and technical occupations	Watchmaker
6	Semi-routine occupations	Security
7	Routine occupations	Sale
8	Never worked and long-term unemployed	N/A
	Not classified	Student

4.3.5 Quality of life impact and psychological profile questionnaires

An established questionnaire for international research and clinical practice was used to determine the patients' quality of life and the psychological stress components. This questionnaire consists of 5 items as follows:

1. The survey of recent life experience (SRLE): SRLE consists of 51 items with scoring from 1 to 4.²²¹
2. The life events questionnaire (LEQ): LEQ consists of 12 items used for assessing chronic stresses.²²²
3. The patient health questionnaire 9 (PHQ-9): PHQ-9 consists of 9 items.²²³
4. The patient health questionnaire 15 (PHQ-15): PHQ-15 consists of 15 items.²²³
5. The perceived stress scale (PSS): PSS consists of 14 items.²²⁴

4.3.6 Plasma and urine cortisol

The blood and urine samples were collected (before 12.00 AM) from all the participants for determining the level of urine and plasma cortisol.

4.3.7 Vision tests

Vision testing (BCVA and CS) was carried out in the Liverpool CSCR study using the same protocol as in the DREFUS study.

The degree of metamorphopsia was determined using the M-chart (Inami & Co., Ltd., Tokyo, Japan). The M-chart consists of 19 dotted lines with the dot interval

ranging from 0.2 – 2.0° visual angle. The type II chart with two dotted lines was used in this study (**Figure 4.6**). The chart was read at a distance of 30 cm starting with the vertical straight line (0° visual angle). The patient was guided to concentrate on the fixation point at the centre of the two dotted lines. The next dot interval was displayed to patients until patients recognised a straight line. The score in which each participant recognised a straight line was recorded for the vertical score. The chart was then rotated 90° to assess the horizontal degree of metamorphopsia.

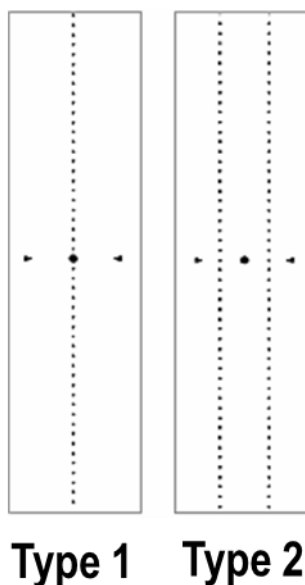


Figure 4.6: Type 1 and Type 2 M-chart.

4.3.8 Ocular biometric and axial length

The ocular biometrics including corneal curvature, cylinder, anterior chamber depth and the axial length (AxL) were automatically measured with the IOL master® (Carl Zeiss Ltd, Cambridge, UK).

4.3.9 Intra ocular pressure measurement

The IOP was measured using a handheld tonometer (Tono-Pen AVIA, Reichert technologies, NY, USA) after local anaesthesia with 0.05% proxymetacaine eye drops (Bausch and Lomb/Chauvin Pharmaceutical Ltd, Surrey, UK).

4.3.10 Ophthalmic imaging

4.3.10.1 EDI OCT volume scan

The EDI OCT volume scan was acquired using the EDI modality on the Spectralis SD OCT system (Heidelberg Engineering, Heidelberg, Germany). The

EDI OCT volume scanning protocol consisted of 25 B-scans covering an area of 30x20 degrees of the macula, centred at the fovea. The distance between consecutive B-scans was 240 µm. A minimum ART setting of 60 was applied using the built-in averaging and eye-tracking features.

4.3.10.2 *Single raster EDI OCT with isometric exercise*

The arrangement for the EDI OCT scan acquisition for each participant is shown in **Figure 4.7**.

The procedures were explained. After 5 minutes rest, BP was measured at the upper arm with a digital automatic device in a sitting position. Single horizontal and vertical line EDI OCT scans of 9 mm centred at the fovea were performed as described above in Section 4.2.9. The horizontal EDI OCT scan was set as the reference scan.

Participants then performed isometric exercise (squatting) for a minimum of 2 minutes and 30 seconds. At the end of squatting, one horizontal EDI OCT scan was acquired using the built-in follow-up setting while the participant remained in the squatting position. During the follow-up EDI OCT acquisition, a repeated BP measurement was done.

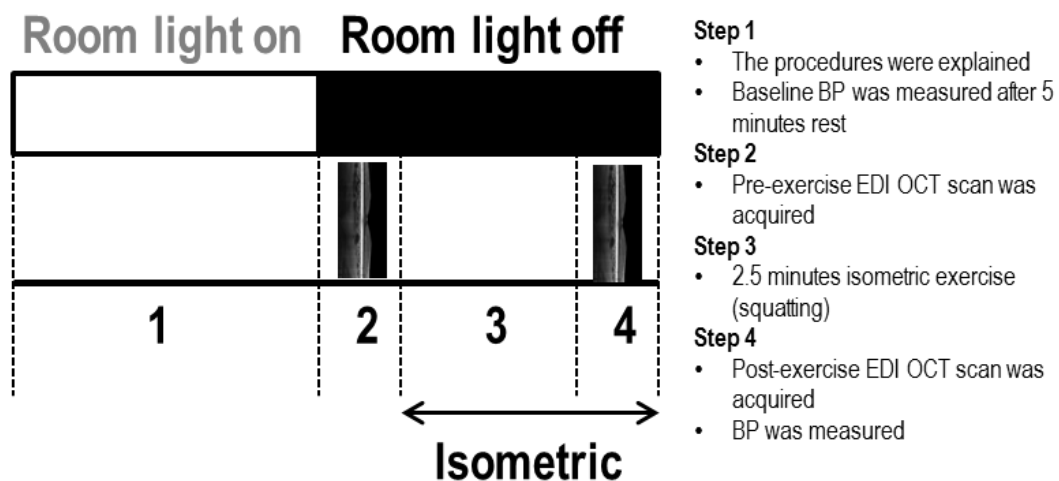


Figure 4.7: The sequence of EDI OCT image acquisition with isometric exercise

4.3.10.3 *Choroidal thickness measurements*

The EDI images on both volumetric and horizontal scans were viewed using Heidelberg Eye Explorer Version 1.9.10.0. For volumetric scans, ChT data maps

were manually created by moving the automatic corresponding reference lines of the retinal segmentation to the relevant choroidal layer for each B-scan as described in Chapter 3. A software-standardised ETDRS grid with diameters of 1, 3 and 6 mm was used to create topographical 3-dimensional ChT and choroidal volume (ChVolume) maps. The centre point SfChT and the ChT value of each of the 9 ETDRS subfields were also recorded. The mean macular ChT (MChT) of all ETDRS subfields were calculated using **Equation 4.2**. The volumetric scan was also used to create a 6 × 6 mm ChT map using a program developed in MATLAB R2012a (The Mathworks Inc., Natick, USA).

For the EDI OCT with isometric exercise, ChT measurements were done first on the follow-up scans in order to reduce the bias of the measurement. The reference scans were measured one week later and masked from the follow-up scan. ChT was measured as the perpendicular distance between the anterior and posterior boundary at 500 µm intervals up to 3 mm nasal and 3 mm temporal from the foveal centre.

$$MChT = \frac{\sum_1^9 ETDRS \text{ subfield}}{9}$$

Equation 4.2: Mean macular ChT (MChT) calculation

4.3.10.4 *Colour fundus photography*

Fundus images were captured on a TopCon 50-Dx camera (Topcon Medical systems, Inc., New Jersey, USA). Each image was focused on the macula centred on the fovea with a field of view of 50°.

4.3.10.5 *Fundus fluorescein angiography (FFA) and indocyanine green angiography (ICGA)*

Fluorescein and indocyanine green injections were performed by a qualified nurse. The procedure, risks and benefits of FFA and ICGA were explained to participants prior to the injection. 5 ml of 20% (w/v) of sodium fluorescein (Martindale Pharmaceuticals, Essex, UK) and 5 ml of 5 mg/ml of ICG solution (ICG-pulsion®, Pulsion Medical Systems, Uxbridge, UK) were used respectively. The ICG dye was first injected into the antecubital vein while a qualified imaging technician captured a video and several retinal images from time 0 up to 10 minutes. The

fluorescein dye was injected at 1 minute and 30 seconds after the ICG dye injection. FFA Images were also taken from 0 minute up to 10 minutes. The ICGA and FFA image acquisitions were performed on HRA 2 (Heidelberg Engineering, Heidelberg, Germany) with 50° field of view.

Choroidal vascular hyperpermeability was defined as an area of focal hyperfluorescence on ICGA as described by previous studies.^{210, 225} Briefly, choroidal vascular hyperpermeability on ICGA can be seen as a focal or multifocal areas of hyperfluorescence with unclear boundaries within the choroid. The area of choroidal vascular hyperpermeability was marked using a late ICGA frame (5 minutes after the ICG administration onwards) and exported for further analysis.

4.3.10.6 *Other fundus imaging*

Infrared reflectance (IR) image, NIR AF image, FAF image and blue reflectance image (RED free) were captured on HRA 2 (Heidelberg Engineering, Heidelberg, Germany). For each image, a 50° macular shot (centred at the fovea) was captured using the high resolution mode. In order to obtain adequate quality images, an ART setting of 50 was applied during each image acquisition. The wavelength specification for each imaging technique is shown in **Table 4.3**.

For FAF images, 20 seconds of retinal bleaching was done before image acquisition. This was done by exposing the retina with 488 nm light (FAF mode) for 20 seconds. During this time, the image focus was adjusted. After 20 seconds, the ART setting was activated. The FAF image was then captured after the ART reached the maximum value.

Table 4.3: Fundus imaging modality

Type of image	Acquisition mode	Excitation	Filter
Infrared reflectance (IR)	Indocyanine green mode	820 nm	No filter
Near infrared autofluorescence (NIR AF)	Indocyanine green mode	790 nm	830 nm
Fundus autofluorescence (FAF)	Fluorescein mode	488 nm	500 nm*
Blue reflectance image (RED free)	Fluorescein mode	488 nm	No filter

**20 seconds of bleaching required before the image acquisition*

4.3.10.7 *Relative grey value measurement*

The FAF and NIR AF images were exported with the overlaid EDTRS grid. A rectangular area was inserted onto each EDTRS subfield and the optic disc as shown in **Figure 4.8** using Image-J software version 1.48 (National Institutes of Health, USA). The same rectangular dimension was used on every FAF and NIR AF images. The mean grey value of each area was automatically calculated using a histogram function within the image-J software. The mean grey value from each of the outer EDTRS subfield was use as a reference for each of the corresponding inner EDTRS subfield. The average of all outer EDTRS subfields was used as a reference for the central EDTRS subfield. The relative FAF and NIR AF were calculated using the following equation:

$$\text{Relative AF} = \frac{\text{mean AF within area of interest} - \text{mean AF of ONH}}{\text{mean AF within reference area} - \text{mean AF of ONH}}$$

Equation 4.3: Equation describing the relative AF (both FAF and NIR AF) calculation

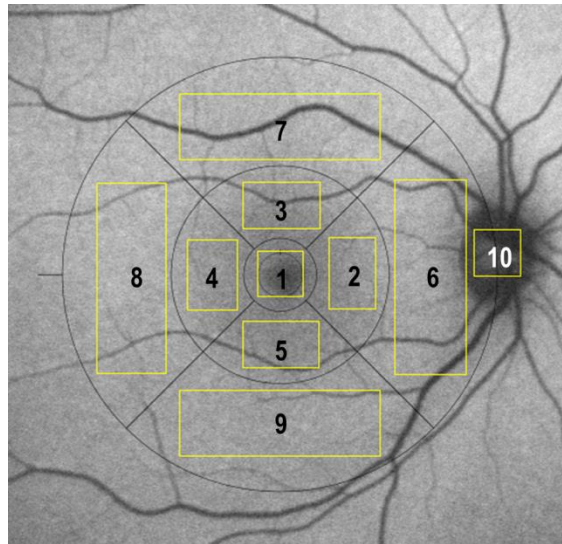


Figure 4.8: Example of the area for measuring the mean grey values. The area marked as 1, 2, 3, 4 and 5 were assigned as the area of interest. The area marked as 6, 7, 8 and 9 were assigned as the reference area for each of the corresponding area (6 for 2, 7 for 3, 8 for 4 and 9 for 5). The average of the mean grey value from all reference area ($\frac{6+7+8+9}{4}$) was used as the reference for the central subfield (1).

The area marked as 10 represents the mean grey value of optic disc.

4.3.11 Choroidal blood flow parameter measurement with isometric exercise

The sequence for the ChBFlow measurement using LDF for each participant is shown in **Figure 4.9**. The procedure was similar to that of DREFUS study. The main difference was that in Liverpool CSCR study, participants performed 2.5 minutes of squatting instead of weight lifting.

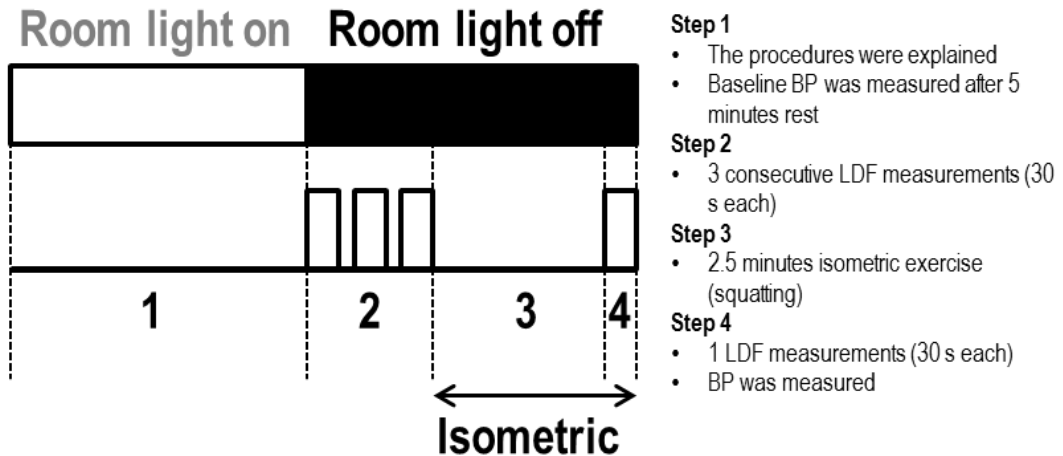


Figure 4.9: The sequence of investigation of choroidal blood flow measurement with isometric exercise for the Liverpool CSCR study

The ocular perfusion pressure (OPP) at baseline and at the end of isometric exercise were calculated using the equation below

$$OPP = \frac{2}{3}MAP - IOP$$

Equation 4.4: The ocular perfusion pressure formulation, MAP is calculated using Equation 4.1

The change in choroidal vascular resistance (Rm) after isometric exercise was calculated using the equation below.

$$\text{Change in } Rm = \text{Change in } OPP / \text{Change in } ChBFlow.$$

Equation 4.5: Choroidal vascular resistance change formulation

4.3.12 Microperimetry

The retinal sensitivity at the macula was measured using a MP1 microperimeter (Nidek Technologies, Vigonza, Italy). Each participant performed 2 separate examinations: 1) fixation and 2) microperimetry examination.

4.3.12.1 Fixation examination

The participant's fundus was carefully aligned with the instrument. Once the fundus was aligned and focused, one retinal image was captured and used to locate reference points for an automatic eye tracking system. The participant was asked to fixate at the fixation target while the operator started the fixation examination. Fixation was recorded for 20 seconds for each participant.

Three bicurve ellipse area (BCEA) values provided by the MP1 microperimeter were used to represent the fixation ability. These BCEA values represent the standard deviation (SD) of horizontal and vertical eye movements based on plotting each fixation point on Cartesian axes. Each of the BCEA value represents each of 3 ellipses on which the eye fixates on the target for 68.2%, 95.4% and 99.6% of time corresponding to 1, 2 and 3 (SDs), respectively. The BCEA values obtained during the fixation test were used to estimate the static fixation and the BCEA values obtained during the microperimetry examination (section 4.3.12.2) were used to represent the dynamic fixation for each participant.

4.3.12.2 Microperimetry examination

Microperimetry procedures were first explained to each participant. The microperimetry was performed automatically with an automatic eye tracking system. The examination was performed in the dark. A colour photograph was captured after the completion of the microperimetry test. For the purpose of this study, the following parameters were used:

Table 4.4: Microperimetry parameters

Parameter	Description
Size of stimulus	Goldman III
Fixation target	a bright red cross of 2 degrees
Background	white
Threshold strategy	4-2-1
Number of stimulus points	45
Area	12 degree in diameter
Starting light attenuation	10 dB
Projection time	200 ms

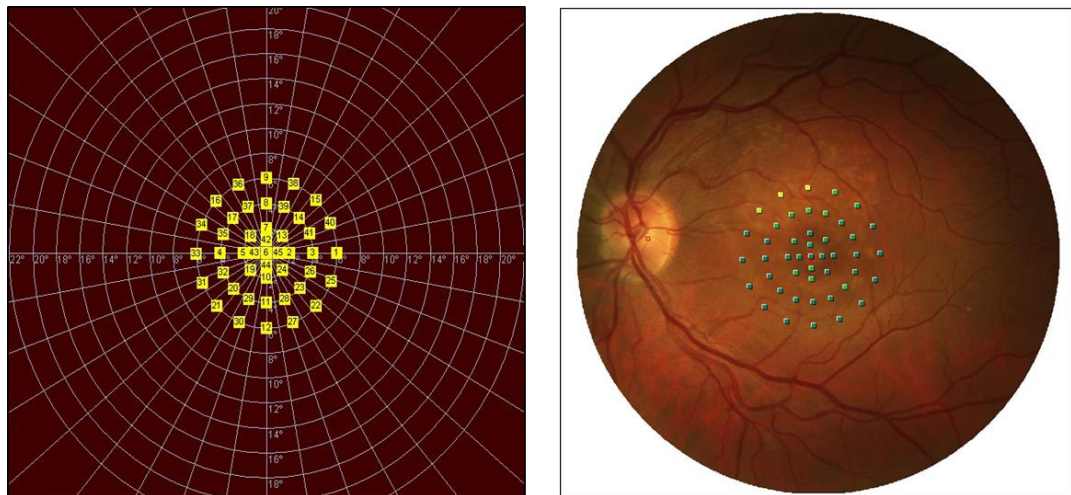


Figure 4.10: The pattern of microperimetry examination used in the Liverpool CSCR study

4.4 Statistical analyses

All statistical analyses in this thesis were performed by using the SPSS program version 20 (SPSS Inc., IBM, USA). The group comparison of categorical data was assessed using the Chi-square test. For continuous data, the collected data were first tested for normal distribution using the Kolmogorov-Smirnov test. If the data fitted a normal distribution, the t-test (independent or paired) was used for two group comparison and the ANOVA with appropriate group-wise comparison was used for more than two group comparison. If data showed a non-normal distribution, an appropriate non-parametric test was used. A 5% level of significance was considered to be statistically significant.

4.5 Summary

In this section, I have described the patient groups, procedures, investigations and analytical techniques used to investigate structure and function of the choroid in diabetic retinopathy and CSCR.

Chapter 5 Healthy choroid

The thickness of the choroid has previously been histologically determined at approximately 200 μm . As the choroid mainly consists of blood vessels, the histological determination of the choroidal structure may not be accurate due to a considerable amount of volume loss during tissue specimen preparation and fixation. The technique of EDI OCT allows the assessment of the choroidal structure in real time. In order to study the pathological changes of the choroid in diabetic retinopathy (DR) and central serous chorioretinopathy (CSCR), I performed a study of the choroidal structure in a cohort of healthy volunteers using EDI OCT.

5.1 Background

Spaide *et al* studied 34 eyes of 17 healthy participants and reported the mean subfoveal choroidal thickness (SfChT) of 318 μm and 335 μm for right and left eyes respectively.³² Since this first report, many have investigated the variability of the choroidal structure and its thickness has been reported ranging from 272 μm to 347 μm in Caucasian, 253 μm to 354 μm in Asian and 315 μm in Arabic eyes as previously described in Chapter 2.

In the healthy UK population, Rahman reported the mean (\pm SD) SfChT of 332 \pm 90 μm for right eyes and 332 \pm 91 μm for left eyes.⁵⁹ However, there is a lack of other aspects such as the relationship between the ChT and age as well as ocular factors influencing the thickness of the choroid. A more recent study of the ChT by Bafiq *et al*²²⁶ have also shown a similar SfChT to that reported by Rahman at 346 \pm

54.1 μm , $321 \pm 55.2 \mu\text{m}$ and $340 \pm 44.6 \mu\text{m}$ for healthy subjects with white, black and Asian decent living in the UK.

The centre point under the fovea is the most common location to measure the ChT that has been used to represent the choroidal structure by most of the published articles. This single point measurement on a single B-scan may not be suitable to represent the 3 dimensional vascularised structure of the choroid. In order to obtain more information of normal choroidal structure, I analysed data derived from a single horizontal line EDI OCT scan of 9 mm and an EDI OCT volume scan covering an area of 30×20 degrees of the macula for each eye. Both scan protocols were described in Chapter 4. The EDI OCT scan acquisitions were performed on Spectralis SD OCT system (Heidelberg Engineering, Heidelberg, Germany). The key research questions of this chapter are as follow:

- To determine the ChT profile on 2-dimensional (2-D) cross-sectional scan and 3-D scan of normal healthy eyes
- What is the relationship between the choroidal structure and other ophthalmic factors?
- Are there any differences in topographic variation in retinal and choroidal thickness at the macula?

These normative analyses of the choroidal structure will be used for comparisons with choroidal structure data obtained from patients with DR in Chapter 6 and patients with CSCR in Chapter 7.

5.2 Choroidal horizontal thickness

Forty-five healthy participants (23 from the DREFUS study and 22 from the Liverpool CSCR study) were included in this analysis. Four participants were then excluded due to high myopia (refractive error $> \pm 3$ dioptres; $N = 2$) and previous laser vision correction ($N = 2$). Hence, the analyses included 41 horizontal EDI OCT line scans of 9 mm centred on the fovea from 41 healthy participants without ophthalmic diseases. Index eye was randomly selected for each participant.

The mean age of healthy participants was 45 years (range: 29 – 67). The mean refractive error was 0 dioptres (range: -2.75 – 2.60) and the mean logMAR vision was 0 (range: -0.26 – 0.06). The mean systolic BP (BP_{syst}) was 118.6 mmHg (95% confidence interval (CI): 113.8 – 123.4) and the mean diastolic BP (BP_{diast}) was 76.2 mmHg (95% CI: 73.7 – 78.7).

The ChT was measured as the perpendicular distance between the anterior and posterior choroidal boundary at 500 μm intervals up to 3 mm nasal and 3 mm temporal from the foveal centre. The thickest point was observed at the subfoveal location with the ChT of 351 μm (95% CI: 321 – 381). The ChT became thinner nasally and temporally to the fovea. The ChT of the nasal side was thinner than that of the temporal side (**Figure 5.1**). There were significant differences between other measured locations compared to at the foveal centre except for the 500 μm nasal location as shown in **Table 5.1**.

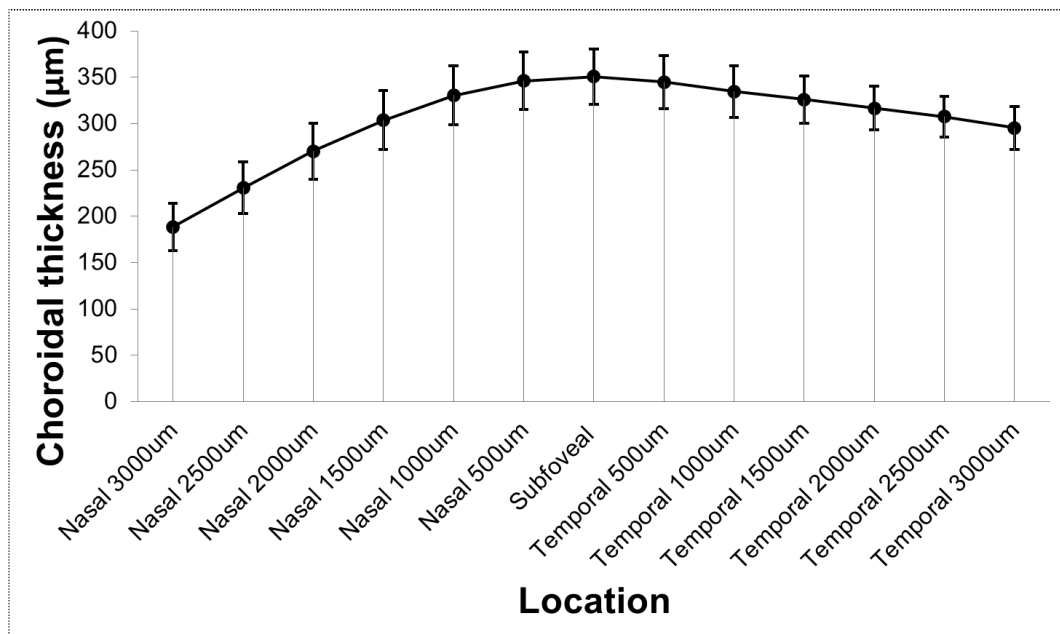


Figure 5.1: Mean EDI OCT choroidal thickness at each location 500 μm apart across a 6 mm horizontal line scan centred on the foveal centre of 41 eyes of 41 healthy participants (error bars = 95% confidence interval, age: as continuous variable not shown)

Table 5.1: Mean ChT (95% confidence interval; CI) at each location 500 μm apart across a 6 mm horizontal line scan (P = paired sample comparison to the SfChT)

Location	Mean (95%CI) (μm)	Mean difference from the fovea (95%CI) (μm)	P
Subfoveal	351 (321 - 381)	N/A	N/A
Total ChT	304 (278 - 330)	N/A	N/A
Nasal 500 μm	346 (315 - 377)	-5 (-9 - 0)	0.068
Nasal 1000 μm	330 (298 - 362)	-20 (-29 - -12)	< 0.001
Nasal 1500 μm	304 (272 - 336)	-47 (-58 - -36)	< 0.001
Nasal 2000 μm	270 (240 - 301)	-80 (-93 - -68)	< 0.001
Nasal 2500 μm	231 (203 - 258)	-120 (-135 - -105)	< 0.001
Nasal 3000 μm	188 (163 - 214)	-163 (-183 - -143)	< 0.001
Temporal 500 μm	345 (316 - 374)	-6 (-1 - -11)	0.029
Temporal 1000 μm	335 (307 - 362)	-16 (-7 - -25)	0.001
Temporal 1500 μm	326 (300 - 352)	-25 (-13 - -37)	< 0.001
Temporal 2000 μm	317 (293 - 340)	-34 (-20 - -49)	< 0.001
Temporal 2500 μm	307 (286 - 329)	-43 (-26 - -61)	< 0.001
Temporal 3000 μm	295 (272 - 319)	-56 (-35 - -77)	< 0.001

5.2.1 Difference of the choroidal thickness between right and left eyes

The ChT of both left and right eyes demonstrated a similar pattern as previously described. The thickest location of the choroid was found at the foveal centre in both eyes as shown in **Figure 5.2**. The mean SfChT and total ChT were 363.4 μm (95% CI: 334.8 – 392.0) and 313.3 μm (95% CI: 287.4 - 339.2), respectively for right eye. The mean SfChT and total ChT were 339.1 μm (95% CI: 308.2 – 367.0) and 291.6 μm (95% CI: 265.0 - 318.2), respectively for left eye. The ChT of right eye was consistently thicker than that of left eye at all the locations measured. The magnitudes of differences in ChT were 13.16 to 23.56 μm for the nasal region, 5.90 to 14.58 μm for the temporal region and 18.85 μm at the foveal location (**Table 5.2**). These differences were clearly demonstrated on the nasal region of the eye whereas the differences of the ChT for the temporal region did not reach the significance level.

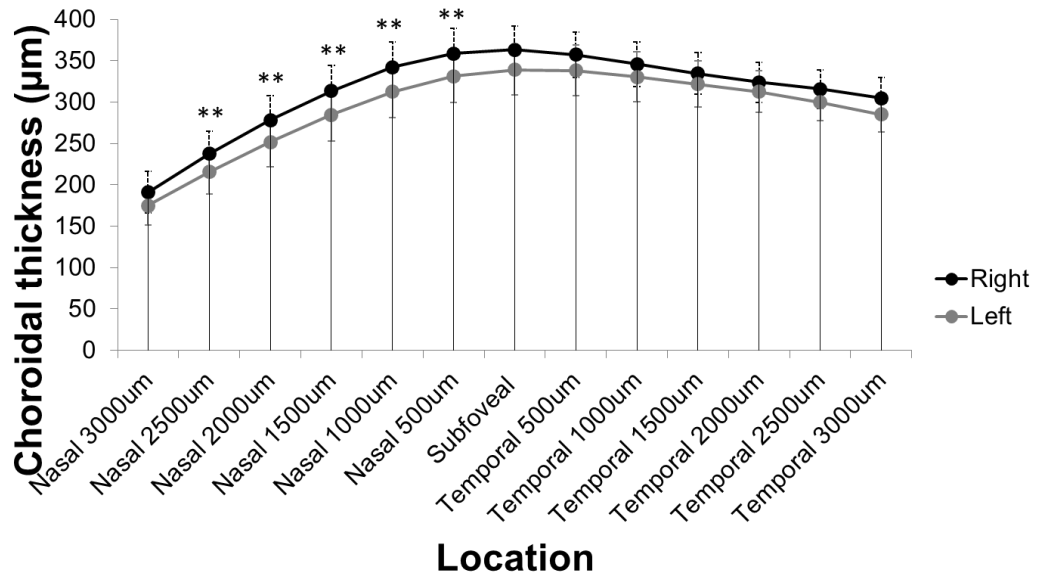


Figure 5.2: The mean (95% confidence interval; error bars) horizontal choroidal thickness at different locations between right (black) and left (grey) eyes

Table 5.2: Mean difference in ChT (95% confidence interval; CI) between right and left eyes at each location 500 μm apart across a 6 mm horizontal line scan (P = paired sample comparison)

Location	Mean difference (μm)	95% CI (μm)	P
Subfoveal	18.85	-0.23 - 37.92	0.05
Total ChT	17.09	1.72 - 32.45	0.03
Nasal 500 μm	21.97	3.40 - 40.55	0.02
Nasal 1000 μm	23.56	6.10 - 41.03	0.01
Nasal 1500 μm	23.15	6.99 - 39.32	0.01
Nasal 2000 μm	20.85	4.54 - 37.15	0.01
Nasal 2500 μm	16.41	0.79 - 32.03	0.04
Nasal 3000 μm	13.16	-1.52 - 27.84	0.08
Temporal 500 μm	13.72	-6.26 - 33.69	0.17
Temporal 1000 μm	10.38	-10.78 - 31.55	0.33
Temporal 1500 μm	7.79	-13.60 - 29.19	0.47
Temporal 2000 μm	5.90	-14.41 - 26.20	0.56
Temporal 2500 μm	10.74	-8.10 - 29.59	0.26
Temporal 3000 μm	14.58	-4.24 - 33.40	0.13

5.2.2 Difference of the choroidal thickness between male and female

Twenty-six of 41 eyes were from male participants: mean ages were 46.2 years (95% CI: 42.3 – 50.1) for male and 44.1 years (95% CI: 37.4 – 50.9) for females. There were no statistically significant differences in age, refraction and logMAR vision between male and female participants. The mean SfChT and total ChT were 346.7 μm (95% CI: 308.7 - 384.6) and 305.0 μm (95% CI: 271.5 - 338.5), respectively for male participants and 357.9 μm (95% CI: 303.5 - 412.2) and 302.2 μm (95% CI: 257.2 - 347.1) respectively, for female participants. There were no differences on ChT at any of the measured locations between genders as shown in **Figure 5.3**.

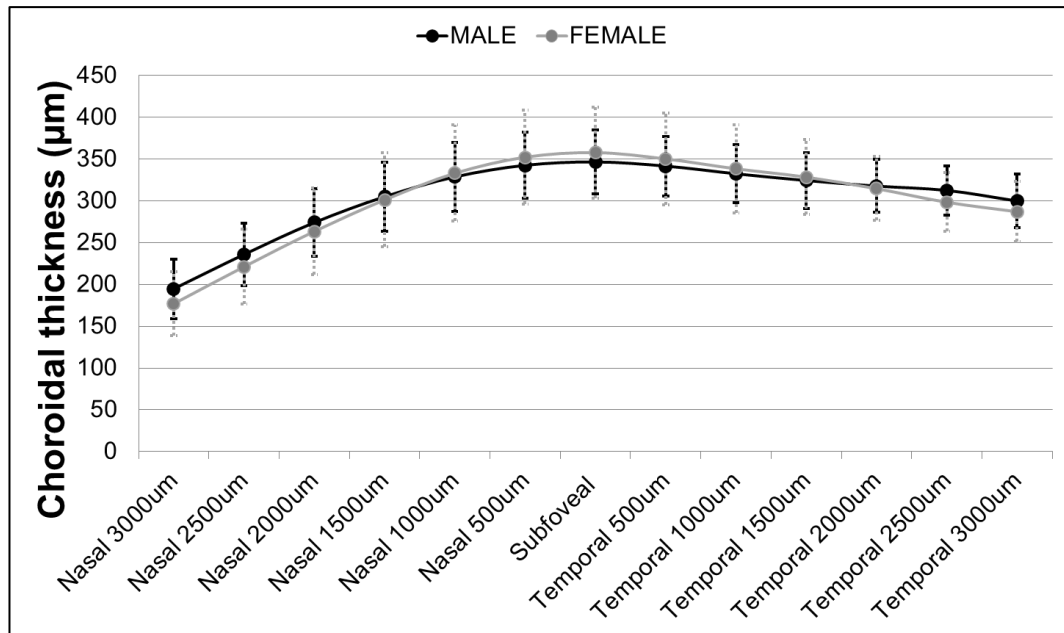


Figure 5.3: The mean (95% confidence interval, error bars) of the choroidal thickness at different locations between males (black) and females (grey)

5.2.3 Choroidal thickness and ageing

The association between age, refractive errors and ChT at each location were examined. The results from the correlation analyses are shown in **Table 5.3**. There was a significant negative correlation between ChT and age. This association was stronger at the locations farther from the fovea. The correlation coefficient was higher on the temporal side than the nasal side.

In order to determine the effect of ageing, the participants were divided into 3 age groups to cover the age distribution of our healthy cohort (range 29 to 67): 1) < 41 years old (N = 16), 2) 41 – 50 years old (N = 14) and 3) over 50 years old (N = 11). The mean SfChT and total ChT were 374.1 (95% CI: 324.8 - 423.4) and 318.3 (95% CI: 280.3 - 356.2) for group 1; 368.5 (95% CI: 311.8 - 425.2) and 327.7 (95% CI: 275.6 - 379.8) for group 2 and 294.2 (95% CI: 244.8 - 343.6) and 253.0 (95% CI: 209.1 - 296.9) for group 3. There were no statistical significant differences in ChT between Group 1 and 2 at any of the measured locations. The ChT reduced starting from the foveal centre in group 3 compared to group 1 ($P = 0.073$) and continued to decrease on the temporal side but not on the nasal side. A similar reduction in ChT was also presented when comparing the ChT between group 2 and 3 as shown in **Figure 5.4**.

When age was used as a main predictor for the ChT, the linear regression has shown that age accounted approximately 36.58% of the reduction of ChT in normal aging process. The models to predict the SfChT and total ChT according to age are shown in **Equation 5.1A** and **Equation 5.1B**.

$$\text{Subfoveal ChT} = 511.61\mu\text{m} - (3.54 \times \text{Age}(\text{years}))\dots\dots\dots\mathbf{A}$$

$$\text{Total ChT} = 433.94 - (2.86 \times \text{Age}(\text{years}))\dots\dots\dots\mathbf{B}$$

Equation 5.1: The model predicting the ChT using age as a main predictor for the ChT at the centre of the fovea (A) and the total ChT (B)

Table 5.3: The relationship between horizontal ChT, age and refraction

Location	Age	P	Refraction	P
Subfoveal	-0.398	0.01	-0.051	0.75
Total ChT	-0.373	0.02	-0.084	0.60
Nasal 500µm	-0.355	0.02	-0.079	0.62
Nasal 1000µm	-0.314	0.05	-0.081	0.61
Nasal 1500µm	-0.286	0.07	-0.046	0.78
Nasal 2000µm	-0.270	0.09	-0.032	0.84
Nasal 2500µm	-0.245	0.12	-0.048	0.77
Nasal 3000µm	-0.261	0.11	-0.108	0.51
Temporal 500µm	-0.430	0.01	-0.041	0.80
Temporal 1000µm	-0.446	0.00	-0.076	0.64
Temporal 1500µm	-0.442	0.00	-0.113	0.48
Temporal 2000µm	-0.453	0.00	-0.149	0.35
Temporal 2500µm	-0.437	0.00	-0.178	0.27
Temporal 3000µm	-0.408	0.01	-0.199	0.22

P: Pearson correlation

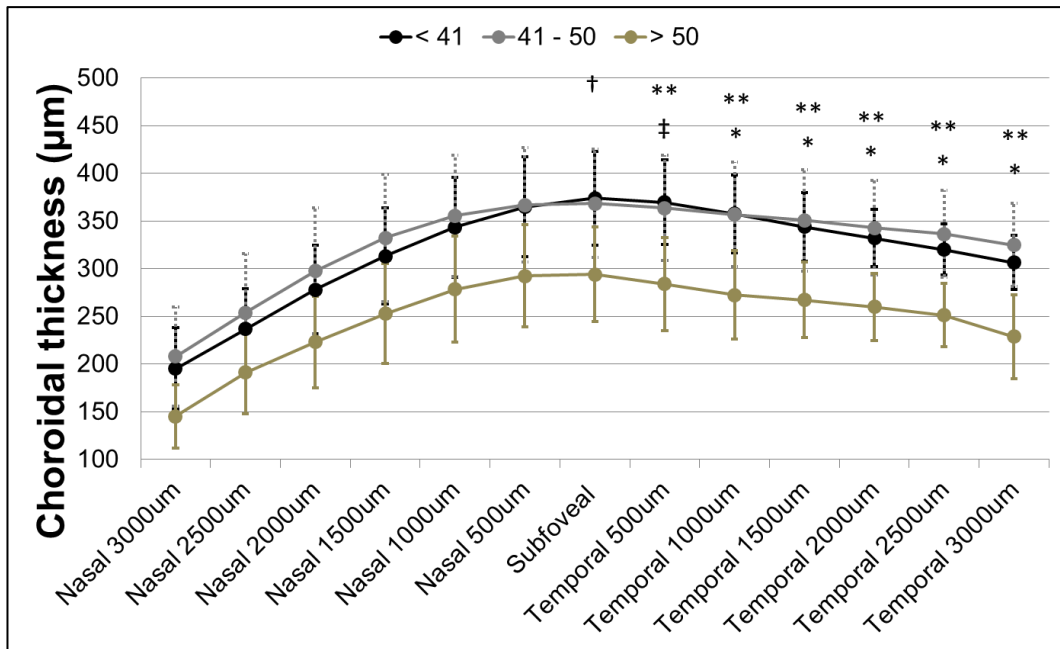


Figure 5.4: The mean (95% confidence interval; error bars) choroidal thickness at different locations of each age group; < 40 years old (black), 41 – 50 years old (grey) and > 50 years old (gold). † represents $p = 0.073$ (< 41 vs > 50), ‡ represents $p = 0.066$ (41 – 50 vs > 50), ** represents $p < 0.05$ (< 41 vs > 50) and * represents $p < 0.05$ (41 – 50 vs > 50)

Table 5.4: The percentage of age accounted for the choroidal thickness at each location and regression coefficients between the ChT and age.

Location	R (%)	b₀	b₁	P
Subfoveal	39.8	511.61	-3.54	0.01
Total ChT	37.3	433.94	-2.86	0.02
Nasal 500µm	35.5	496.34	-3.30	0.02
Nasal 1000µm	31.4	466.52	-3.00	0.05
Nasal 1500µm	28.6	427.58	-2.73	0.07
Nasal 2000µm	27.0	381.49	-2.45	0.09
Nasal 2500µm	24.5	323.08	-2.04	0.12
Nasal 3000µm	26.1	277.21	-1.95	0.11
Temporal 500µm	43.0	512.67	-3.69	0.01
Temporal 1000µm	44.6	502.60	-3.70	0.00
Temporal 1500µm	44.2	480.06	-3.39	0.00
Temporal 2000µm	45.3	460.53	-3.17	0.00
Temporal 2500µm	43.7	437.00	-2.85	0.00
Temporal 3000µm	40.8	421.01	-2.77	0.01

b₀: intercept, b₁: slope

5.3 Choroidal thickness and volume under the macula

In the previous section, I have described the variation of ChT on a 2-D single B-scan. However, this single scan passing through the fovea does not give sufficient information about the 3-D structure of the choroid. In order to evaluate the choroid of the entire macula, the topographical 3-dimensional ChT and choroidal volume (ChVolume) maps were created using the EDI OCT volume scanning protocol described in Chapter 4. In brief, the scan consisted of 25 B-scans covering an area of 30 × 20 degree of the macula, centred at the fovea. A software-standardised ETDRS grid was used to create topographical 3-dimensional maps. This grid divides the macula into 3 concentric areas *via* 3 concentric rings: 1) The centre ring measures central area within 1 mm diameter, 2) the inner ring measures an area between 1 to 3 mm and 3) the outer ring measures an area between 3 to 6 mm. The grid also divides the area of inner and outer rings equally into 4 sectors: superior, inferior, temporal and nasal. The SfChT, the ChT and ChVolume value of each of the 9 ETDRS subfields were recorded.

Data from 43 eyes of 22 healthy participants from the Liverpool CSCR project (5 participants were female and 17 participants were male) were included in the ChT and ChVolume map analyses (the DREFUS data were excluded due to the lack of axial length and the anterior chamber depth data). One eye was excluded due to poor scan quality. Mean age of the participants in this group was 42.5 years (95%CI: 39.1 – 45.8).

5.3.1 Differences of choroidal volume between two eyes

The mean of 4m refractive error was 0.11 (95% CI, -0.18 – 0.39) and 0.10 (95% CI, -0.36 – 0.56) for right and left eye, respectively. The axial length and the anterior chamber depth between right and left eyes were similar as shown in **Table 5.5**.

The mean macular ChT (MChT) and ChVolume over the macula were 362 (95%CI, 324.70 – 399.10) μm and 9.86 (8.87 – 10.85) mm^3 , respectively for the right eye. The left eye demonstrated thinner choroid compared to the right eye with the mean MChT and ChVolume over the macula of 328 (95%CI, 287.91 – 367.29) μm and 8.94 (95%CI, 7.91 – 9.98) mm^3 , respectively. The mean ChT and ChVolume of the right and the left eyes as well as the mean difference between right and left eyes of the 9-EDTRS subfields at the macula are shown in **Table 5.6** and **Figure 5.5**.

There were significant differences between right eyes and left eyes in all the EDTRS subfields at the macula (All $P < 0.05$). The mean ChT and mean ChVolume

were significantly greater by approximately 8% in right eyes compared to left eyes whereas no statistically significant difference was detected between the mean retinal thickness of right and left eyes.

Table 5.5: The demographical characteristics of healthy right and left eyes

Parameter	Right eye	Left eye	Mean difference	P
Vision				
4 meter refraction (diopters)	0.11 (-0.18 – 0.39)	0.10 (-0.36 – 0.56)	0.01 (-0.36 – 0.37)	0.97
logMAR	-0.12 (-0.15 - -0.09)	-0.13 (-0.16 - -0.11)	0.01 (-0.01 – 0.04)	0.30
Ocular biometrics				
Axial length (mm)	23.53 (23.24 – 23.82)	23.53 (23.16 – 23.89)	0.00 (-0.15 – 0.16)	0.95
Anterior chamber depth (mm)	3.31 (3.15 – 3.48)	3.34 (3.17 – 3.51)	-0.03 (-0.21 – 0.19)	0.12

Table 5.6: The choroidal thickness and choroidal volume distribution over the 9 ETDRS subfields of right and left eyes of 22 healthy participants

ETDRS	Choroidal thickness (μm)				Choroidal volume (mm^3)			
	Right eye	Left eye	Mean difference	<i>P</i>	Right eye	Left eye	Mean difference	<i>P</i>
Central	392 (348.86 – 434.69)	351 (302.92 – 399.84)	33.10 (9.47 – 56.72)	<0.05	0.31 (0.27 – 0.34)	0.28 (0.24 – 0.31)	0.02 (0.01 – 0.04)	<0.05
Inner nasal	369 (324.05 – 413.13)	331 (282.37 – 379.25)	30.7619 (9.35 – 52.18)	<0.05	0.58 (0.51 – 0.65)	0.52 (0.44 – 0.60)	0.05 (0.01 – 0.08)	<0.05
Inner superior	392 (352.15 – 431.76)	356 (314.61 – 398.05)	29.33 (5.71 – 52.95)	<0.05	0.62 (0.55 – 0.68)	0.56 (0.49 – 0.63)	0.05 (0.01 – 0.08)	<0.05
Inner temporal	377 (336.99 – 416.01)	340 (298.02 – 382.94)	28.76 (6.49 – 51.03)	<0.05	0.59 (0.53 – 0.65)	0.53 (0.47 – 0.60)	0.05 (0.01 – 0.08)	<0.05
Inner inferior	373 (329.52 – 416.75)	340 (294.00 – 385.14)	25.62 (6.01 – 45.23)	<0.05	0.59 (0.52 – 0.66)	0.53 (0.46 – 0.61)	0.04 (0.01 – 0.07)	<0.05
Outer nasal	294 (254.70 – 334.11)	268 (225.29 – 310.05)	21.24 (0.50 – 41.98)	<0.05	1.56 (1.35 – 1.77)	1.42 (1.19 – 1.64)	0.11 (0.00 – 0.22)	<0.05
Outer superior	373 (336.18 – 409.73)	341 (304.93 – 378.03)	26.29 (4.49 – 48.08)	<0.05	1.98 (1.78 – 2.17)	1.81 (1.62 – 2.00)	0.14 (0.03 – 0.24)	<0.05
Outer temporal	345 (311.42 – 378.95)	312 (280.04 – 343.20)	26.19 (6.45 – 45.93)	<0.05	1.83 (1.65 – 2.01)	1.65 (1.49 – 1.82)	0.14 (0.02 – 0.25)	<0.05
Outer inferior	343 (304.62 – 380.56)	309 (271.59 – 346.51)	25.81 (6.42 – 45.19)	<0.05	1.82 (1.61 – 2.02)	1.64 (1.44 – 1.84)	0.14 (0.03 – 0.24)	<0.05
Total	362 (324.70 – 399.10)	328 (287.91 – 367.29)	27.46 (8.92 – 45.99)	<0.05	9.86 (8.87 – 10.85)	8.94 (7.91 – 9.98)	0.73 (0.24 – 1.22)	<0.05

P 2-tailed paired sample *T*-test

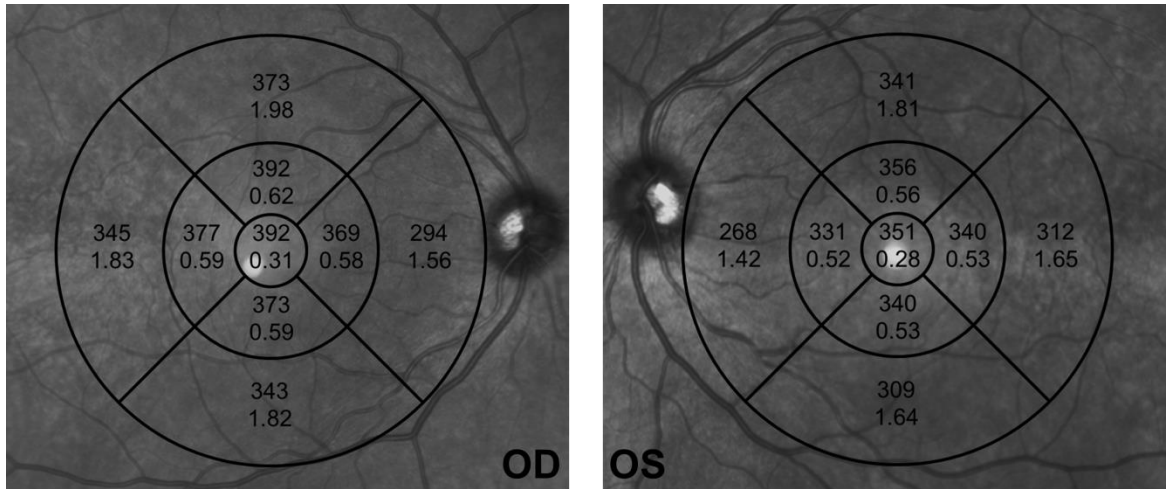


Figure 5.5: Representative image of the mean ChT (top row) and ChVolume (bottom row) in each of the ETDRS subfield of right and left eyes

5.3.2 The pattern of thickness and volume of the choroid and the retina at the macula

The relationship between the retina and the choroid may be useful to determine the choroidal functional unit in correlation with the retinal topographical distribution. Thus, in this section, the topographical variation of the ChT, ChVolume, the retinal thickness and retinal volume at the macula were created compared with that of the retina.

For the choroid, the thickest mean ChT was observed at the central subfield (right eye: 392.0 µm [95% CI: 348.9 – 434.7] and left eye: 351.4 µm [95% CI: 302.9 - 399.8]). The ChT was thinner in the inner and outer ETDRS subfields (range from 330.8 – 392.0 µm for inner subfields and 267.7 – 373.3 µm for outer subfields). Among the inner and outer ETDRS subfields, superior subfields were the thickest and the nasal subfields were the thinnest. The ChT of the outer nasal subfield was the thinnest of all the ETDRS subfields.

The topographical distribution of the retina, on the other hand, showed the central subfield to be thinnest compared to the inner and outer EDTRS subfields (central subfield: right eye: 283.4 µm [95% CI: 276.5 - 290.2] and 282.9 µm [95% CI: 276.5 - 289.2]). The inner ETDRS subfields were generally thicker than the outer EDTRS subfields and the nasal ETDRS subfields were the thickest. **Figure 5.6** shows the distinctive pattern of the thickness distribution of the choroid and the retina on right and left eyes.

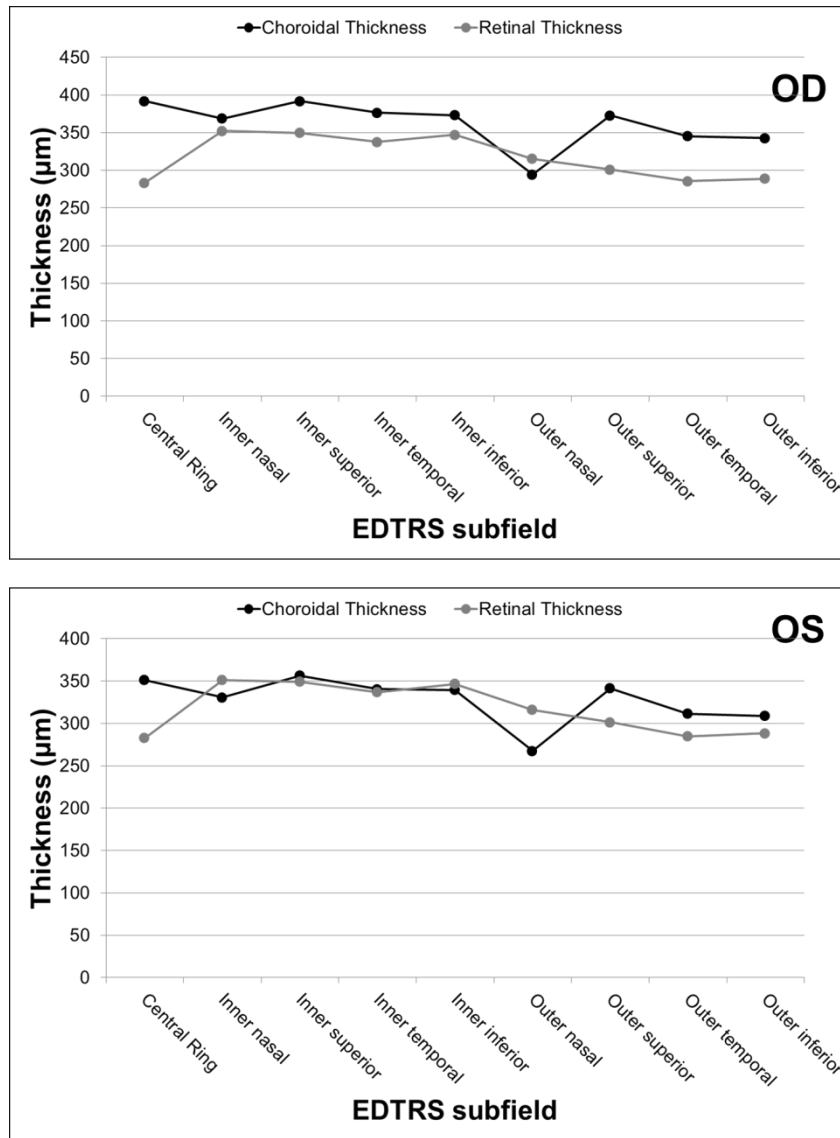


Figure 5.6: The mean choroidal thickness and retinal thickness in each of the EDTRS subfield of right (OD) and left (OS) eyes

The topographic distribution of the mean volume of the choroid and retina were comparable between right and the left eyes. For the choroid, the highest mean ChVolume was observed in the superior subfields, followed by the temporal, inferior and nasal subfields on both the inner and outer EDTRS rings, respectively. In contrast to the ChVolume distribution, the highest retinal volume was observed at the nasal subfield, followed by the superior, inferior and temporal on both the inner and outer EDTRS rings. **Figure 5.7** shows the pattern of the ChVolume and retinal volume distribution over the macula on right and left eyes.

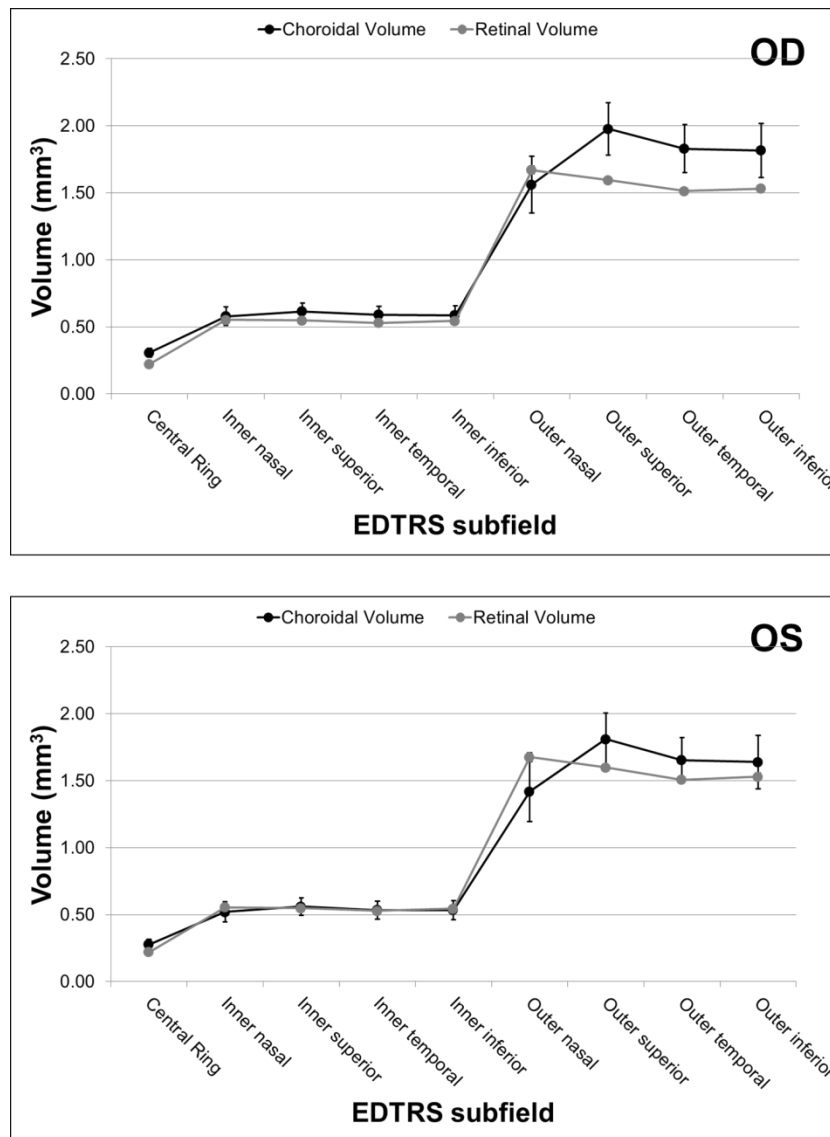


Figure 5.7: The mean choroidal volume and retinal volume in each of the ETDRS subfield of right (OD) and left (OS) eyes

5.4 Summary

In this chapter I have studied the ChT based on single horizontal and volumetric scans in a cohort of healthy population with no history of ocular diseases. At the centre of the fovea, the mean ChT was 351 μm in healthy volunteers with an age range of 29 – 67 years old. This was the thickest point of the horizontal line scan. The SfChT from our population was comparable to the previous mean SfChT from a study with similar age and race distribution.²¹² The ChT decreased further away from the foveal centre, notably in nasal to the fovea. The thinning of the choroid by approximately 46% was observed at the 3000 μm nasal to the foveal centre and by approximately 16% was observed at the 3000 μm temporal to the

foveal centre. No significant differences in the mean ChT were observed between male and female healthy participants. No significant differences in mean ChT at the foveal centre towards the temporal side between right and left eyes, however, at the nasal side, ChT of the right eyes was significantly thicker than the left eye.

Age was the main factor that affected the ChT in my cohort. When categorised by decade, no significant differences were found between healthy choroid from individual < 41 years old and those between 41 – 50 years of age. But in those ≥ 50 years old, the ChT was reduced temporal to the fovea compared to the nasal side. This was clearly demonstrated by our linear correlation and the regression analyses, age accounted for the thinning of the choroid by approximately 40 – 45% in the temporal side and about 26 – 35% in the nasal side. The models to predict the SfChT and total ChT according to age were derived. From these models, the choroidal thinning is calculated to be 35.4 μm for SfChT and 28.6 μm for the total ChT per decade.

As the choroid is a 3D structure, the point measurement of the ChT may not be suitable to represent the choroidal structure. Hence, I have further determined the thickness and volume of the choroid across the macula using the ETDRS grid. The mean MChT and total ChVolume were 362 μm and 9.86 mm^3 , respectively, for the right eye and 328 μm and 8.94 mm^3 , respectively for the left eye. There were significant differences in the ChT between two eyes. Right eyes had thicker ChT and greater ChVolume than left eyes. This asymmetrical thickness and volume was not present for the intraretinal layers in the same scan.

Lastly, the pattern of the topographic variation of choroidal structure over the macula was particularly unique with the nasal subfield being the thinnest and central subfield being the thickness, followed by the superior subfields. This pattern was reversed of that of the retina which was thinnest at the central subfield and the thickest found at the nasal subfield. The thinnest choroid was observed at the outer nasal subfield where the retina was the thickest.

In summary, my data have demonstrated a topographic variation of the choroid and confirmed findings seen in histological specimens. This will help the reader to fully appreciate a normal choroidal structure and understand the structural changes of the choroid in Chapters 6 and 7 where this normative data will be used to compare with the data derived from patients with diabetic retinopathy (DR) and central serous chorioretinopathy (CSCR). I will discuss the results of my findings in Chapter 8.

Chapter
6 Choroidal structure and
function in DR

Diabetic retinopathy (DR) is a microvascular complication of a prolonged elevation of blood sugar in diabetes mellitus (DM).

According to the World Health Organisation (accessed 08/2015), 9% of adults over 18 will have diabetes and diabetes will account for the 7th leading cause of death worldwide.²²⁷ In the UK, recent estimates for 2015 indicate 3,333,069 people are diagnosed with diabetes. This figure increased by nearly 60% over the past decade and it has been projected to reach 5 million over the coming decade.²²⁸ Nearly all patients diagnosed with type 1 and around two thirds with type 2 will have some forms of DR. Moreover, the prevalence of DR has been estimated around 30% of people with DM worldwide.²²⁹

A chronic long standing raised blood sugar is known to affect several aspects of the normal retinal environment. The pathogenesis of DR is complex and involves several mechanisms. These include the vasoconstriction of retinal vessels,²³⁰ loss of retinal pericytes and endothelial cells, elevation of O₂ metabolism by-products²³¹ and inflammation of the retina²³⁰ causing vascular leakage and micro-aneurysms. In order to gain better understanding of the role of choroid in the pathogenesis of diabetes, I investigated its structure and function in patients with DM and DR compared with healthy individuals.

6.1 Background

DR is a microvasculopathy of the eye in patients with prolonged hyperglycaemia which are best described in the retina. The first significant evidence of choroidal involvement in DR was from the histological study of the choroid by

McLeod and Luty in 1994 in which they described a significant dropout of choriocapillaris in DM and termed it as diabetic choroidopathy.¹⁷¹ They also reported zones of tortuous and constricted choriocapillaris, and intra- and extrachoroidal neovascularisation (**Figure 6.1**).²³²

Figure 6.1: The outline of blood vessels stained with alkaline phosphatase (APase) showing the tortuosity of the choriocapillaris (A), area of diffuse (B) and complete loss (C) of choriocapillaris in diabetic patients. The cytochemical staining with nonspecific esterase (NSE) and the APase staining show the loss of capillary networks in a diabetic patient (E) compared to a healthy eye (F) (Source: ²³²)

Over the past two decades since McLeod and Luty published their findings, interest in the role of the choroid in the pathogenesis of diabetes has been limited primarily due to the difficulties of structural visualisation and functional analysis. The recent advent of OCT technologies with improved resolution such as EDI OCT and swept-source OCT (SS OCT) has given new impetus. Six studies by 6 different groups have reported variable and inconsistent ChT results in patients with different degrees of DR as discussed in Chapter 2 (**Table 2.5**). The exact choroidal structural changes in DR remain poorly established.

Choroidal blood flow (ChBFlow) at the fovea of patients with DR has been studied previously using LDF as I have described in Chapter 2. The ChBFlow has been estimated by LDF to reduce by 27% in Schocket's study¹⁷⁹ and 25% in Nagaoka's study.¹⁸⁰ These studies directly compared ChBflow between DR classifications. This might not be appropriate as changes in retinal structure often occur during the course of DR. The structural changes of the retina found in DR (especially diabetic macular oedema) may alter the scattering property of the monochromatic laser beam used in LDF. Information on the autoregulation of ChBFlow in DR patients is limited. Movaffaghy *et al* studied the choroidal autoregulation using LDF and suggested that choroidal regulatory ability is impaired in DR patients but not in DM.¹⁸¹ As there is a lack of detail on how the ChBFlow was measured as well as patient selection criteria, the exact choroidal autoregulation ability in DR patients, yet again, remains poorly understood.

I aimed to study the role of the choroid in the pathogenesis of DR and to investigate the structural characteristics at the macula using EDI OCT. The autoregulation ability of the choroid in patients with DR was assessed using LDF. The study was performed to answer the following research questions:

- What functional and/or structural changes in the choroid can be detected on EDI OCT and LDF in patients with DR compared to healthy controls?
- Are these changes related to the severity of diabetic maculopathy?

6.2 Patient characteristics

This was a prospective study of the choroidal structure and function in DR patients. The DM patients with or without DR were recruited as a part of the Diabetic Retinopathy: Functional and Structural (DREFUS) study at the Clinical Eye Research Centre, St. Paul's Eye Unit, Royal Liverpool University Hospital as previously described in Chapter 4. Data were obtained from patients attending their baseline visit between October 2010 and December 2015. Normative data were obtained by combining the DREFUS study control group and Liverpool CSCR study control group. Only 1 eye per participant was selected.

Seventy-nine patients with DM, 25 healthy controls from the DREFUS study and 20 healthy controls from the Liverpool CSCR study were included. Among 79 DM patients, 24 were classified as group A (having focal or diffuse exudative diabetic maculopathy without CSMO), 40 as group B/C (focal or diffuse exudative diabetic maculopathy with CSMO and/or any signs of significant ischaemia) and 15

as group D (diabetic controls). Patients and controls characteristics are shown in **Table 6.1**.

The mean (\pm SD) age was 61.5 ± 10.8 years, 55.8 ± 12.9 years and 53.9 ± 12.4 years for diabetic controls (group D), DR patients group A and group B/C respectively. There was no significant difference in age amongst DM patients, however, the patients in each of the DM groups were significantly older than healthy controls (46.2 ± 11.2 years, $P < 0.05$). Because there was a significant difference in mean age of healthy controls compared to patients with diabetes, data were adjusted for age.

The gender distribution was similar between the groups. The duration of DM and the level of glycosylated haemoglobin (HbA1c) were significantly higher in diabetic patients that developed retinopathy compared to those without signs of retinopathy. As expected, the vision was significantly worse in patients with DR (mean of 0.00 [95% confidence interval (CI); -0.05 - 0.06] for group A and 0.08 [95% CI; 0.02 - 0.14] for group B/C) compared to diabetic controls (-0.03 [95% CI; -0.10 - 0.05]) and healthy controls (-0.13 [95% CI; -0.15 - -0.11]). Patients in group B/C had the lowest CS score with the mean of 6.3 letters lower than that of controls and 4.2 letter lower than that of diabetic controls.

Table 6.1: Characteristics of 124 participants including healthy controls and DM patients categorised as diabetic controls and patients with diabetic maculopathy with and without CSMO. Eye specific data is provided for the study eye.

	Controls	Patient with diabetes mellitus		
		Group D (Diabetic/-DR)	Group A (DM/-CSMO)	Group B/C (DM/+CSMO/Is chaemic)
N (eyes)	45	15	24	40
Male	28	9	14	23
Female	17	6	10	17
Ratio[†]	1.65	1.50	1.40	1.35
Age (years)	46.2 (42.8 - 49.5)	61.5 (55.6 - 67.5)*	55.8 (50.4 - 61.2)*	53.9 (49.9 - 57.9)*
Duration of diabetes (years)	N/A	6.8 (2.9 - 10.6)	16.3 (12.3 - 20.3)**	15.3 (12.9 - 17.7)**
HbA1c (mmol/mol)	N/A	7.1 (6.4 - 7.8)	8.7 (8.0 - 9.4)**	8.6 (8.0 - 9.2)**
4-meter refraction (dioptries)	-0.1 (-0.5 - 0.3)	-0.5 (-2.3 - 1.4)	0.6 (0.1 - 1.1)	-0.3 (-0.9 - 0.4)
logMAR	-0.13 (-0.15 - -0.11)	-0.03 (-0.10 - 0.05)	0.00 (-0.05 - 0.06)*	0.08 (0.02 - 0.14)*
Contrast sensitivity	41.2 (40.9 - 41.5)	39.1 (37.6 - 40.6)	38.0 (36.5 - 39.5)*	34.9 (33.3 - 36.5)*.**
Systolic BP (mmHg)	119.2 (114.8 - 123.7)	131.1 (122.3 - 139.8)*	133.7 (126.3 - 141.1)*	133.7 (129.2 - 138.2)*
Diastolic BP (mmHg)	76.8 (74.3 - 79.3)	75.4 (71.5 - 79.3)	77.3 (73.8 - 80.9)	76.2 (73.1 - 79.3)
% of hypertension	4%	47%	71%	60%

* $P < 0.05$ compared to healthy controls, ** $P < 0.05$ compared to diabetic controls, [†] $P = 0.975$ (Chi-square)

6.3 Structure of the choroid in DR

In order to determine the changes of choroidal structure, a single 9 mm horizontal EDI OCT line scan passing through the centre of the fovea was used for each eye. ChTs were measured as the perpendicular distance between the anterior and posterior boundary (see Chapter 3 for the definitions of these boundaries) at 500 μm intervals up to 3 mm nasal and 3 mm temporal from the foveal centre.

Of 124 total eyes shown in **Table 6.1**, 8 eyes were excluded, leaving 116 (94%) for the analyses. Reasons for exclusion from the analyses were: 1 eye (group A), 2 eyes (group B/C) and 1 eye (group D) for missing choroidal outer boundary, 1 eye (group D) for other ophthalmic disease that might affect the ChT, 1 eye (group D) for high myopia (refraction > -6D) and 2 eyes of healthy controls for previous laser vision correction (Lasik).

6.3.1 Choroidal thickness in diabetic patients without any signs of retinopathy

The ChTs of each location along the horizontal line scan of 43 control eyes were compared with 12 eyes of diabetic controls (Group D). The mean SfChT was 327.2 μm (95% CI; 301.5 - 360.4) for controls and 300.5 μm (95% CI; 238.2 - 362.8) for diabetic patients without any signs of retinopathy following adjustment of age to an individual of age 49.3 years ($P = 0.46$). The mean total ChT was 286.8 μm (95% CI; 261.6 - 312.0) and 255.7 μm (95% CI; 202.3 - 309.1) for controls and diabetic controls, respectively ($P = 0.32$). Although, the mean ChT of each measured location was not significantly different between healthy controls and diabetic controls, on average the diabetic controls were 31.1 μm (range from 20.7 to 40.1) thinner along the scan as shown in **Figure 6.2**.

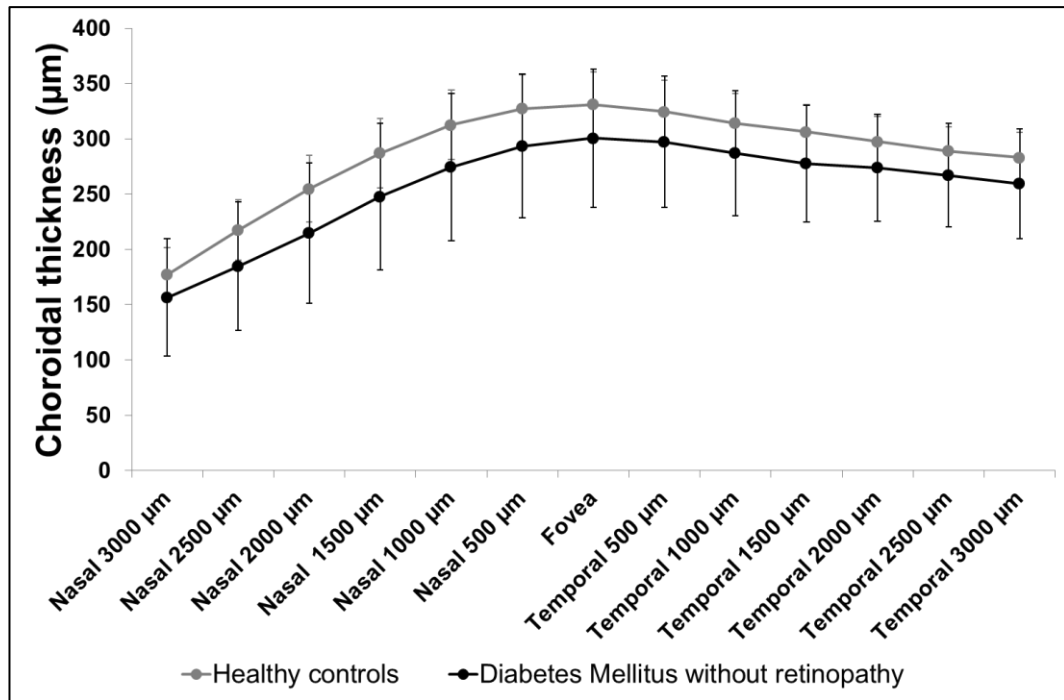


Figure 6.2: Mean choroidal thickness at each location 500 µm apart across 9 mm horizontal EDI OCT scans through the fovea of healthy and diabetic eyes. Error bars represent 95% confidence interval

6.3.2 Choroidal thickness in diabetic patients with retinopathy

Next, the thickness of the choroid of patients with DR was assessed and compared with that of healthy and diabetic control eyes (DM with DR = 61, controls = 43, diabetic controls = 12). The overall choroidal morphology of DM patients with DR was almost identical to the choroidal morphology of healthy controls (see **Chapter 5** for further details). In all groups (DM patients with DR, diabetic controls and healthy controls), the thickest ChT was observed at the foveal location and the ChT became thinner nasally and temporally.

After adjusting for the effect of age (the adjustment of age to an individual of age 52.2 years), mean SfChTs were 317.5 µm (95% CI; 290.0 - 345.0), 299.9 µm (95% CI; 248.7 - 351.2) and 303.8 µm (95% CI; 281.8 - 325.8) for healthy eyes, diabetic eyes without DR and those with retinopathy, respectively. Healthy eyes remained the thickest for the overall ChT with a total ChT of 276.2 µm (95% CI; 252.7 - 299.8) followed by DM with DR with a total ChT of 262.9 µm (95% CI; 244.7 - 281.8). The diabetic eyes without retinopathy were the thinnest with a total ChT of 253.9 µm (95% CI; 210.0 - 297.8). Although this pattern of ChT was found to be uniform in all the measured locations as shown in **Figure 6.3**, no statistically

significant differences were observed between healthy eyes, diabetic eyes without DR and those with retinopathy ($P > 0.05$).

The ChT changes in relation to the severity of diabetic maculopathy were determined. **Figure 6.4** shows the mean ChT of each location along the horizontal axis of each of the studied groups. Eyes with focal or diffuse exudative diabetic maculopathy without CSMO (group A) had a slightly thicker mean SfChT (323.8 μm [95% CI; 288.2 - 359.3] vs 317.2 μm [95% CI; 289.9 - 344.6]) and mean total ChT (279.7 μm [95% CI: 249.3 - 310.2] vs 276.0 μm [95% CI; 252.5 - 299.4]) compared with healthy controls. The thickness of the choroid of DR eyes without CSMO also increased in all the measured locations compared to those of diabetic controls. Eyes with CSMO and/or signs of significant ischaemia (group B/C) had a slightly thinner SfChT (291.8 μm [95% CI; 264.3 - 319.4] vs 317.2 μm [95% CI; 289.9 - 344.6]) and mean total ChT 252.9 μm [95% CI; 229.3 - 276.5] vs 276.0 μm [95% CI; 252.5 - 299.4]) compared to healthy eyes. No significant differences in the ChT were observed between groups A, B/C, healthy controls and diabetic controls at any measured location ($P > 0.05$).

Intra-retinal (IRF) and sub-retinal fluid (SRF) were presented on EDI OCT in 11 eyes of DR patients without CSMO (group A) and 36 eyes of DR patients with CSMO and/or signs of significant ischaemia (Group B/C). ChTs decreased in eyes with IRF and SRF by approximately 28 μm (95%CI; -42.9 - 99.5) for group A and 26.9 μm (95% CI; -91.0 - 144.7) for group B/C compared to those eyes without the morphological changes seen on OCT ($P > 0.05$ for both groups).

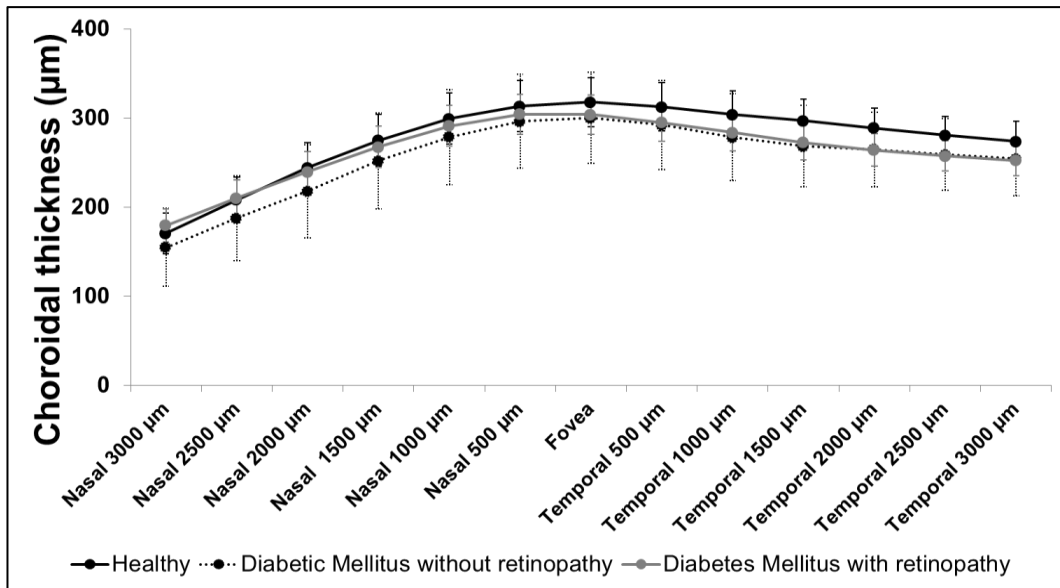


Figure 6.3: Mean choroidal thickness at each location 500 µm apart across 9mm horizontal EDI OCT scans through the fovea of healthy, diabetic with and without retinopathy. Error bars represent 95% confidence interval

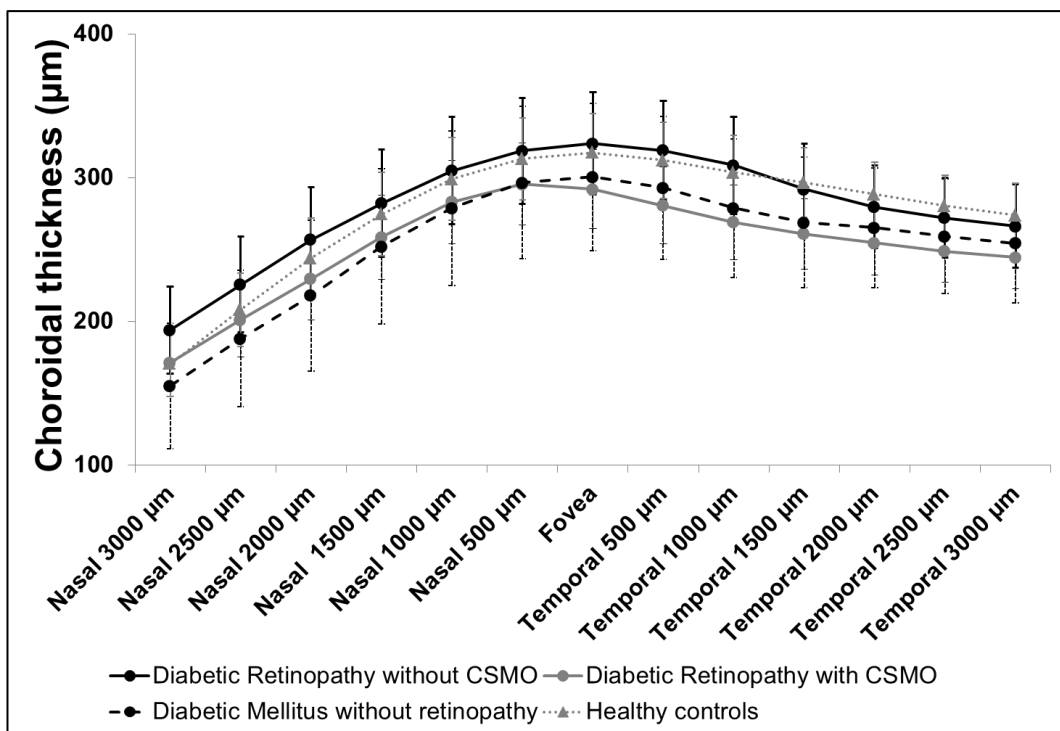


Figure 6.4: Mean choroidal thickness at each location 500 µm apart across 9mm horizontal EDI OCT scans through the fovea of healthy, diabetic with and without retinopathy. DR eyes are categorised as no CSMO and with CSMO and/or signs of significant ischaemic. Error bars represent 95% confidence interval

6.3.3 The relationship between choroidal thickness and degree of retinopathy and maculopathy

The relationship between ChT and systemic factors such as age, duration of diabetes, HbA1c, systolic and diastolic BP in diabetes is shown in **Table 6.2**. Age was negatively correlated with ChT at all locations. Neither HbA1c, systolic BP, diastolic BP nor duration of diabetes showed any association with ChT.

Table 6.2: The relationship between the horizontal ChT and systemic factors in diabetic patients (Pearson's r)

Location	Systemic factors				
	Age	Duration of DM	HbA1c	Systolic BP	Diastolic BP
Subfoveal	-.51**	0.11	0.15	-0.22	0.07
Total ChT	-.51**	0.12	0.19	-0.19	0.11
Nasal 500µm	-.51**	0.11	0.15	-0.21	0.07
Nasal 1000µm	-.49**	0.12	0.18	-0.21	0.07
Nasal 1500µm	-.46**	0.13	0.20	-0.22	0.06
Nasal 2000µm	-.43**	0.14	0.20	-0.19	0.07
Nasal 2500µm	-.41**	0.15	0.21	-0.16	0.04
Nasal 3000µm	-.37**	0.14	0.25*	-0.15	0.01
Temporal 500µm	-.50**	0.10	0.15	-0.20	0.10
Temporal 1000µm	-.48**	0.10	0.16	-0.17	0.15
Temporal 1500µm	-.48**	0.11	0.16	-0.14	0.18
Temporal 2000µm	-.50**	0.11	0.16	-0.13	0.18
Temporal 2500µm	-.50**	0.11	0.14	-0.13	0.16
Temporal 3000µm	-.48**	0.07	0.15	-0.13	0.12

* $P < 0.05$, ** $P < 0.01$

The degree of retinopathy (R) and maculopathy (M) were graded according to National Diabetic Eye Screening Programme (NDESP) criteria with the modification used in the Liverpool Diabetic Eye Screening Programme (LDESP) with addition of R1.5 and M0.5. Twelves, thirty, nine and twenty-two patients were graded at the retinopathy level of R0, R1, R1.5 and R2, respectively. Of the 73 diabetic patients, 12, 14 and 47 patients were graded as M0, M0.5 and M1, respectively. No significant differences in ChT were found between any of the retinopathy or maculopathy grade groups. The ChT was found to be positively

associated with the retinopathy grades as shown in **Figure 6.5** but not the maculopathy grades. This association, however, was no longer significant after adjusting for the effect of age.

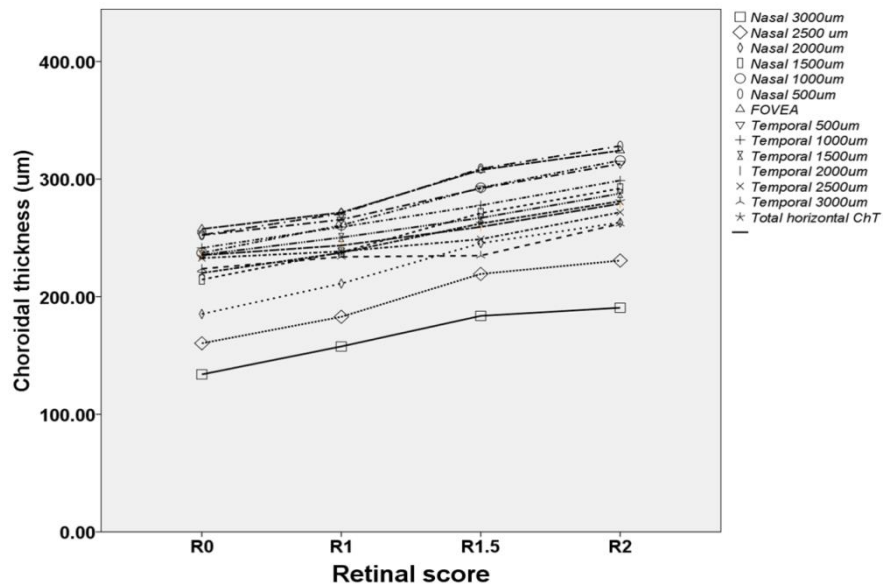


Figure 6.5: The association between ChT at each measured location and the grade of retinopathy

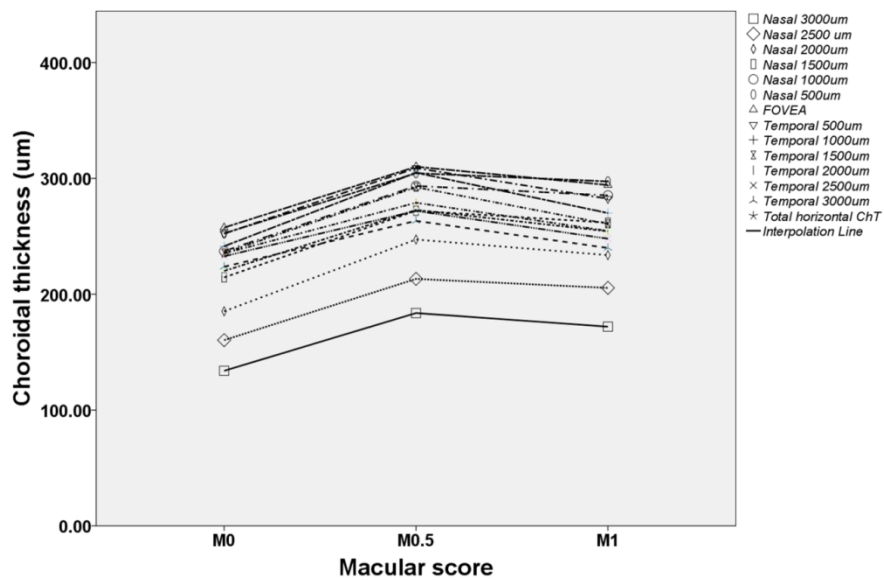


Figure 6.6: The association between ChT at each measured location and the grade of maculopathy

6.4 Autoregulation ability of choroidal function in DR

The ability of the choroid to autoregulate its flow was assessed using the LDF technique as described in Chapter 2, Section 2.6. Of the 124 eyes recruited for the DREFUS study, LDF data were available from 70. There was no significant difference in systolic BP, diastolic BP or MAP between groups at baseline as shown in **Table 6.3**. Following isometric exercise, the systolic BP increased significantly by 24% in controls, 22% in diabetic controls, 16% in DR patients group A and 20% in DR patients group B/C. The diastolic BP also increased significantly from the baseline level by 21%, 10%, 11% and 17% in controls, diabetic controls, DR patients group A and B/C, respectively. The MAP increased by 22%, 15%, 13% and 18% in controls, diabetic controls, DR group A and DR group B/C, respectively. No significant differences in the changes in MAP were observed between groups A, B/C, healthy controls and diabetic controls following the isometric exercise ($P > 0.05$).

Table 6.3: Systemic characteristics of healthy subjects, patients with diabetes and patients with DR (with 95% confidence interval) at baseline and after isometric exercise

	Controls	Patients with diabetes			P
		Group D (Diabetic/-DR)	Group A (DM/-CSMO)	Group B/C (DM/+CSMO/is chaemic)	
Number of subjects	20	8	14	28	N/A
Before exercise					
Age	50.3 (44.2 - 56.3)	61.3 (52.2 - 70.3)	58.0 (48.9 - 67.1)	52.2 (47.1 - 57.3)	>0.05
Systolic BP	121.7 (113.6 - 129.7)	131.1 (117.0 - 145.2)	134.5 (124.9 - 144.1)	124.7 (119.7 - 129.7)	>0.05 [†]
Diastolic BP	77.8 (74.2 - 81.4)	77.4 (71.2 - 83.5)	78.7 (74.6 - 82.8)	76.2 (73.8 - 78.6)	>0.05
MAP	92.4 (88.1 - 96.7)	95.3 (87.5 - 103.1)	97.3 (92.5 - 102.2)	92.4 (89.6 - 95.2)	>0.05
After exercise					
Systolic BP	149.1 (141.1 - 157.1)	159.4 (142.0 - 176.8)	155.6 (143.2 - 168.1)	149.2 (141.8 - 156.6)	>0.05 [†]
Diastolic BP	94.3 (88.7 - 99.8)	84.9 (75.0 - 94.7)	86.9 (81.0 - 92.8)	89.0 (85.7 - 92.2)	>0.05
MAP	112.5 (106.4 - 118.6)	109.7 (99.9 - 119.5)	109.8 (103.5 - 116.2)	109.0 (104.8 - 113.3)	>0.05
Change in MAP	1.22 (1.16 - 1.29)	1.15 (1.08 - 1.22)	1.13 (1.07 - 1.20)	1.18 (1.14 - 1.22)	>0.05 [†]

[†], Mann-Whitney U test

Mean differences of all the choroidal blood flow parameters between baseline and at the end of isometric exercise are listed in **Table 6.4**. No statistically significant fluctuation of the DC level before and at the end of the isometric exercise on any of the 4-groups was noted.

At the end of isometric exercise, no statistically significant changes in ChBFlow or ChBVolume were found in any of the groups except for ChBVelocity of DR in group B/C. The ChBVelocity of DR group B/C increased by approximately 8% at the end of exercise compared to baseline ($P = 0.007$). **Figure 6.7** shows the mean DC, ChBVolume, ChBVelocity and ChBFlow of 4 groups at baseline and at the end of exercise.

When the mean changes of ChBFlow parameters from baseline were compared between groups, no statistically significant differences were found between controls (-8% for ChBVolume, 4% for ChBVelocity and -5% for ChBFlow), diabetic controls (-7% for ChBVolume, -4% for ChBVelocity and -11% in ChBFlow), DR group A (2% for ChBVolume, 5% for ChBVelocity and 6% for ChBFlow) and DR group B/C (1% for ChBVolume, 8% for ChBVelocity and 11% for ChBFlow) as shown in **Table 6.5** and **Figure 6.8**.

To investigate the relationship between choroidal structure and function, a linear correlation was used. **Table 6.6** lists the correlation coefficients between the changes in ChBFlow parameters and the mean ChT at the foveal centre and the total ChT. No correlation was found between the changes of ChBFlow parameters and the structure of the choroid in any of the 4 groups.

Table 6.4: Mean differences in DC, ChBVolume, ChBVelocity and ChBFlow with 95% CI of healthy subjects, patients with diabetes and patients with DR

Choroidal blood flow parameters	Controls	Patients with diabetes		
		Group D (Diabetic/-DR)	Group A (DM/-CSMO)	Group B/C (DM/+CSMO/ischaemia)
DC	0.01 (-0.01 - 0.02)	0.01 (0.00 - 0.01)	0.00 (-0.01 - 0.01)	0.01 (0.00 - 0.02)
ChBVolume (AU)	8.57 (-5.76 - 22.90)	3.14 (-4.77 - 11.04)	0.50 (-2.06 - 3.06)	1.18 (-0.66 - 3.02)
ChBVelocity (Hz)	-12.22 (-38.89 - 14.45)	16.03 (-30.60 - 62.66)	-16.11 (-76.54 - 44.31)	-32.87* (-55.99 - -9.75)
ChBFlow (AU)	638.76 (-724.98 - 2002.51)	1973.17 (-2038.25 - 5984.59)	-304.39 (-1945.77 - 1336.99)	13.73 (-963.63 - 991.08)

* , paired sample *t*-test with $P < 0.05$

Table 6.5: Comparison of DC, ChBVolume, ChBVelocity and ChBFlow changes from baseline between DR patients and controls. Results are shown as a fraction of 1.

Choroidal blood flow parameters	Controls	Patients with diabetes			P
		Group D (Diabetic/-DR)	Group A (DM/-CSMO)	Group B/C (DM/+CSMO/ischaemia)	
Change in DC	0.98 (0.94 - 1.02)	0.98 (0.96 - 1.00)	1.00 (0.96 - 1.05)	0.96 (0.93 - 1.00)	>0.05
Change in ChBVolume	0.92 (0.77 - 1.06)	0.93 (0.55 - 1.32)	1.02 (0.73 - 1.31)	1.01 (0.83 - 1.19)	>0.05 [†]
Change in ChBVelocity	1.04 (0.98 - 1.09)	0.96 (0.86 - 1.06)	1.05 (0.92 - 1.17)	1.08 (1.02 - 1.13)	>0.05
Change in ChBFlow	0.95 (0.79 - 1.11)	0.89 (0.51 - 1.26)	1.06 (0.74 - 1.39)	1.11 (0.87 - 1.36)	>0.05 [†]

[†] , Mann-Whitney *U* test,

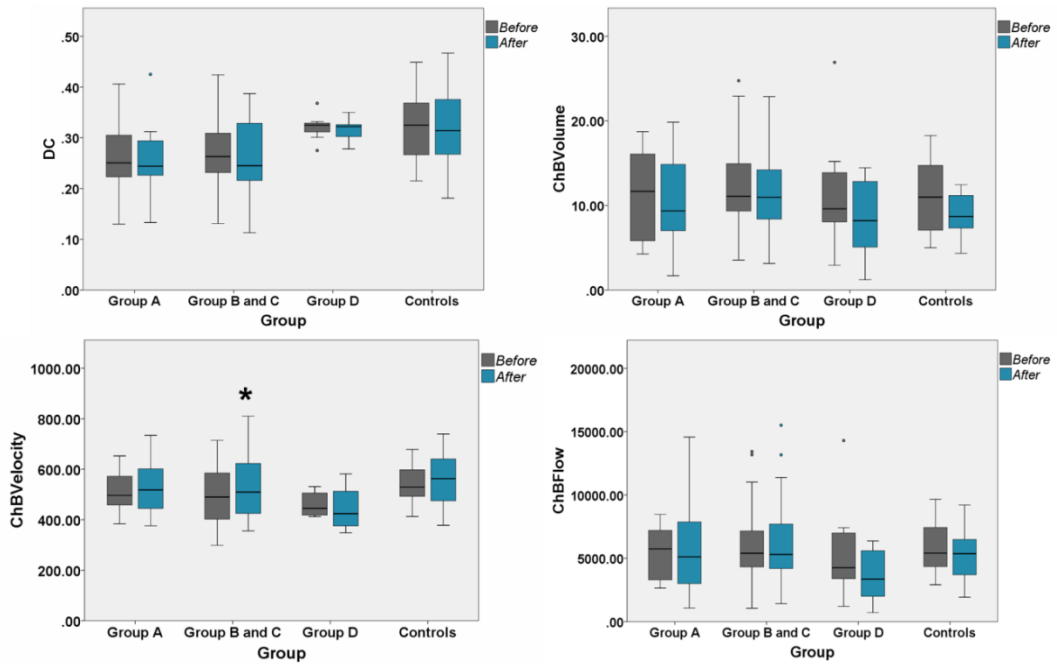


Figure 6.7: The mean DC, ChBVolume, ChBVelocity and ChBFlow at baseline and at the end of isometric exercise in diabetic patients without DR (group D), DR without CSMO (group A), DR with CSMO/ischaemia (group B/C) and healthy controls

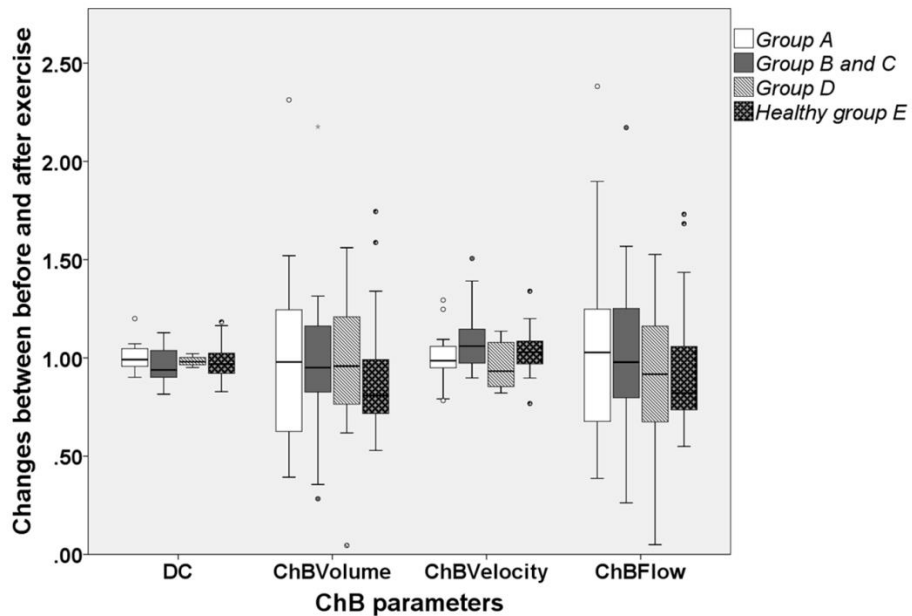


Figure 6.8: Changes in DC, ChBVolume, ChBVelocity and ChBFlow from baseline in diabetic patients without DR (group D), DR without CSMO (group A), DR with CSMO/ischaemia (group B/C) and healthy controls

Table 6.6: Pearson's correlation coefficients between choroidal thickness and changes in choroidal blood flow parameters from baseline following isometric exercise.

		Changes in choroidal blood flow parameters from baseline			
		DC	ChBVolume	ChBVelocity	ChBFlow
Choroidal thickness (μm)	Controls				
	SfChT	0.38	0.16	0.01	0.17
	Total ChT	0.40	0.16	-0.05	0.16
	Group D (Diabetic/-DR)				
	SfChT	0.27	-0.23	0.71	-0.03
	Total ChT	0.26	-0.10	0.74	0.10
	Group A (DM/-CSMO)				
	SfChT	-0.30	-0.06	-0.18	-0.12
	Total ChT	-0.27	-0.07	-0.23	-0.14
	Group B+C (DM/+CSMO/Ischaemic)				
	SfChT	-0.24	-0.25	0.14	-0.16
	Total ChT	-0.16	-0.18	0.13	-0.10

6.5 Summary

In this chapter, the ChT and ChBFlow parameters of patients with DM and DR were studied using EDI OCT and LDF respectively and compared to healthy eyes. Age was the main factor affecting the ChT in healthy controls and DM patients with and without DR. Since the healthy controls were significantly younger than DM and DR patients, age was used as a covariate in all analyses.

The ChT was measured at different 13 locations along the horizontal line scan through the foveal centre. The mean SfChT and total ChT were found to be independent of the level of retinopathy and maculopathy. The mean ChT was approximately 10 to 20% less in diabetic eyes compared to healthy eyes. These reductions in ChT, however, did not differ significantly from the healthy eyes.

The mean ChT in DR patients without CSMO was greater than healthy and diabetic eyes without retinopathy. The ChT of DR patients with CSMO/ischaemia, on the other hand, was slightly thinner than healthy and diabetic eyes without retinopathy. No significant differences in the ChT were observed between groups A, B/C, healthy controls and diabetic controls at any measured locations.

There was no correlation between duration of diabetes, retinopathy score or maculopathy score and the choroidal thickness. Age was associated with the

thickness of the choroid in diabetic patients similar to that found in healthy eyes as shown in Chapter 5.

LDF was used to determine the changes in choroidal blood flow parameters following an acute increase of MAP. Following the isometric exercise, the MAP was increased by approximately 20% in healthy controls and 13 -18 % in diabetic patients. No statistical significances in ChBFlow and ChBVolume were observed in healthy, diabetic controls, and DR patients with and without CSMO between baseline and at the end of the exercise. A statistically significant increase in ChBVelocity by 8% was observed following an increase of MAP by 18% in DR patients with CSMO/ischaemia. When the mean change of choroidal blood flow parameters from baseline was compared between groups, no significant differences in the changes in LDF parameters were observed.

In summary, I have studied the choroidal structure and function of the choroid within the context of diabetes compared to that of healthy eyes. I will discuss the implication of my findings in Chapter 8.

Chapter

7 Choroidal structure and function in CSCR

Central serous chorioretinopathy (CSCR) is a type of macular degeneration resulting from the accumulation of fluid underneath the neurosensory retina at the macula (subretinal fluid; SRF).²³³

CSCR is a relatively uncommon but frequently highly symptomatic condition of the posterior pole of the eye. It is the second most common cause of reduced central vision in the working age population, after diabetic retinopathy and the fourth most common retinopathy across any age group. CSCR has also been suggested to rank second after age-related macular degeneration (AMD) as the presumed cause of subretinal neovascularisation (CNV).¹⁹⁰ With a mean age of onset usually between 41 and 45 years,^{200, 234, 235} it mostly affects young adults in the working age population.

Several studies have demonstrated the range of abnormalities of the choroid involved in the pathogenesis of CSCR including choroidal ischaemia,²³⁶ delayed filling,²³⁷ dilatation of choroidal veins²³⁸ and focal choroidal hyperpermeability.^{239,240} To further elucidate the effect of these known abnormalities and their contribution to the development of CSCR, with support from colleagues I designed the Liverpool CSCR study to investigate the pathophysiology of CSCR using enhanced depth imaging optical coherence tomography (EDI OCT) and laser Doppler flowmetry (LDF).

7.1 Background

CSCR is characterised by fluid accumulation and the detachment of the neurosensory retina. The pathophysiology of why the SRF accumulation of CSCR

remains incompletely understood. The abnormality of choroidal function has been proposed for causing the leakage of water, electrolytes and proteins inducing the RPE detachment, and subsequently inducing localised retinal detachment. This evidence is based on indocyanine green angiography (ICGA) alteration of choroidal vasculature.²⁴¹ Choroidal thickness (ChT) has been shown to be increased in EDI OCT studies²⁰⁴⁻²⁰⁶ along with reports of reduced choroidal blood flow.²¹⁰

The corticosteroid pathway, a pathway which plays an important role in maintaining blood pressure and electrolyte homeostasis, has been proposed to be involved in the pathogenesis of CSCR. Corticosteroids or adrenal steroids originate from the cholesterol synthesis within the adrenal cortex. These adrenal steroids are classified as glucocorticoid (cortisol) and mineralocorticoid (aldosterone) hormones. Glucocorticoids have affinity towards the glucocorticoid receptor (GR) and the mineralocorticoid receptor (MR) while mineralocorticoids have affinity towards the MR.²⁴² In aldosterone-sensitive tissue including the neuroretina, MR is prevented from binding to the cortisol by an enzyme called 11 β -hydroxysteroid dehydrogenase type II (HSD2). The 11 β -HSD2 enzyme protects MR from binding to the cortisol by converting cortisol to an inactive form with less affinity called cortisone.^{242, 243} Under normal physiological conditions, the activations of GR and MR are maintained at a balanced level in order to control the hydrostatic gradients. Hence, excessive MR activation may result in impaired vascular reactivity and inhibits the vascular relaxation and may be involved in the pathogenesis of CSCR.

In order to explore this pathway of CSCR, animal experiments were carried out by Zhao *et al.*²⁴⁴ In their study, Zhao injected rat eyes with a high dose of aldosterone and found thickening, vessel dilatation and leakage in the choroid within 24 hours but not in the retina. These events were not observed when aldosterone was injected with an MR antagonist. The authors suggested that MR activation by excess endogenous and exogenous glucocorticoids may be the underlying cause of CSCR. In addition, they also reported improvement in vision and SRF resolution of 2 CSCR patients with the MR antagonist eplerenone. However, this therapy has not yet been studied in a randomised controlled trial and its application is yet to be established.

Figure 7.1: Mineralocorticoid receptor pathway (Adapted from ²⁴³)

This corticosteroid theory, however, contradicted with Han *et al*²⁴⁵ who studied ChT in patients on high dose corticosteroid therapy and found no obvious signs of CSCR.

To date, the autoregulation of the choroid in CSCR patients has not been studied. This is because there are a very limited number of methods that can be used to directly assess choroidal circulation.

In this study, I aimed to generate data on choroidal function and structure using LDF and EDI OCT in conjunction. The main hypothesis of this Chapter is

“Failure of choroidal autoregulation is responsible for the retinal changes seen in CSCR”.

The study intends to answer the following research questions to arrive at the above answer:

- What changes in the choroid can be detected on EDI OCT and LDF in patients with CSCR compared to age-matched controls?
- Are these changes related to the chronicity of symptoms?
- Do these changes bear any relationship with each other?
- Are there any functional and/or structural markers of prognosis?

In addition, the structure and function of the retina and the RPE and the association of presumed risk factors (such as age, duration of symptoms, ethnicity, smoking, exercise, BP, cortisol levels, personality traits) in CSCR will also be explored.

7.2 Patient recruitment for the Liverpool CSCR study

Patient recruitment was undertaken between August 2013 and December 2014. All patients were seen at the outpatient unit of St Paul's Eye Unit, Royal Liverpool University Hospital. I reviewed patients list of the medical retina clinics on a weekly basis in advance and pre-screened case notes and ophthalmic images for a possible diagnosis of CSCR. The breakdown of participants is shown in the consort chart.

CSCR was diagnosed if patients had serous detachment of neurosensory retina involving the macula confirmed by OCT. One hundred and nine patients of 667 pre-screened were documented as having CSCR (**Figure 7.2**). CSCR patients were then screened using the Liverpool CSCR study specific inclusion and exclusion criteria. Patients were excluded if they had high myopia or hyperopia (greater than ± 3 diopters), any retinochoroidal abnormalities other than CSCR, previous history of any intraocular procedures including laser vision correction, any forms of treatments such as photodynamic therapy or intravitreal injections, fixation unstable and presence of ocular media opacities. After exclusion of 42 of the 109 people with documentation of a diagnosis of CSCR, 67 remained and were invited to attend a dedicated research clinic. 3 declined participation leaving 64 who were consented and included in the study and underwent observational non-invasive investigations as listed in Chapter 3.

For healthy controls, 50 potential participants contacted me after and were pre-screened. The inclusion criteria for healthy controls included best corrected visual acuity (BCVA) over 35 EDTRS letters. The exclusion criteria for healthy controls included any retinochoroidal abnormalities, high myopia or hyperopia (greater than ± 3 diopters), fixation unstable and presence of ocular media opacities.

29 participants met the entry criteria and were screened. 4 declined participation leaving 25 who were consented and included in the observational study.

All participants were considered for inclusion in the studies of choroidal response to isometric exercise. After exclusions as shown in **Figure 7.2**, 10 CSCR and 22 controls underwent the choroidal autoregulation study. The main reason for excluding CSCR patients from the choroidal autoregulation study was due to high BP at baseline (>140/90).

Consort flow diagram of Liverpool CSCR study

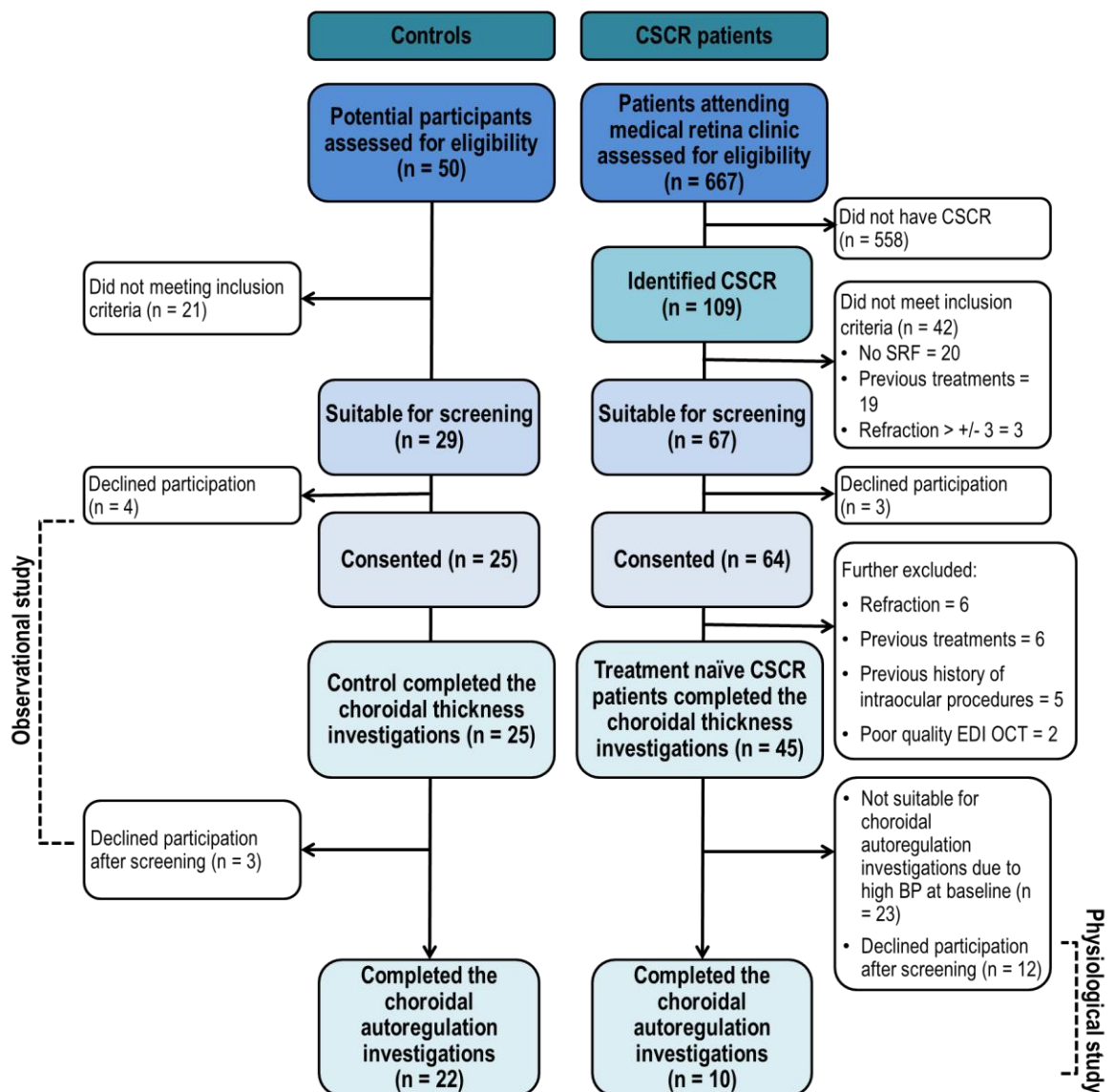


Figure 7.2: The patient recruitment consort chart of the Liverpool CSCR study

The numbers of CSCR patients and controls used for different parts of the study are summarised in **Table 7.1**.

Table 7.1: Number of participants available for analyses

Main part (number of participants)	Study	Corresponding section
Observational study (CSCR = 64, controls = 25)	• Demographic	7.3.1
	• Symptoms	7.3.1
	• Risk analysis	7.3.1.1
	• Socio-economic classification	7.3.1.2
	• Fluorescein angiography	7.4.4.1
	• Indocyanine green angiography	7.4.4.2
	• Fundus autofluorescence	7.4.4.4
Structure of the choroid in CSCR study (CSCR = 45, controls = 25)	• Choroidal thickness (ChT) and choroidal volume (ChVolume) on EDI OCT	7.4
	• EDI OCT and ICGA	7.4.4.3
Interventional study (CSCR = 13, controls = 22)	• Quality of life impact and psychological profile	7.3.1.3
	• Cortisol level	7.3.1.4
	• Vision, ocular biometry and the degree of metamorphopsia	7.3.2
	• Fixation and retinal sensitivity on MP-1	7.6
Physiological study CSCR = 10, controls = 22	• Choroidal autoregulation investigations	7.5

7.3 Observational case controlled study

7.3.1 CSCR patient characteristics

64 CSCR patients and 25 controls were included. Demographic features are shown in **Table 7.2**.

51 (79.7%) and 13 (20.3%) of CSCR patients were male and female, respectively (male to female ratio = 3.9). 20 (80%) of controls were male. There was no significant difference in the ratio between male and female in both groups.

Among 64 CSCR patients, 49 (76.6%) were diagnosed with unilateral CSCR and 15 (23.4%) were diagnosed with bilateral CSCR. The duration of symptom of 3 months was used as a cutoff for acute and chronic CSCCR. By using this cutoff, 25 (39.1%) had the acute form of CSCR with mean duration of disease of 63.3 days (95% confidence interval (CI): 39.0 – 87.5) while 39 (60.9%) had the chronic form

with a mean duration of disease of 951.8 days (95% CI: 393.5 – 1510.2). Among 64 CSCR patients, 49 (76.5%) were classified as having active (due to the presence of SRF at study entry) and 15 (23.4%) were inactive. 9 (14.1%) CSCR patients were current smokers with an average of 15 cigarettes per day, while 24 (34.5%) and 25 (39.1%) were ex-smokers or had never smoked, respectively.

Thirty-three percent of CSCR patients had been diagnosed with hypertension and 5% diabetes mellitus. During the patient interview as part of the screening process, 9% patients reported having problems with the urinary tract system while 16% had problems with the gastrointestinal tract and 6% had heart problems.

The main symptom associated with CSCR was blurred and reduced vision (77%) followed by central scotoma (66%), metamorphopsia (64%) and dyschromatopsia (28%) (**Figure 7.3**). Central scotoma was described by the patients as a transient experience of seeing a dark spot or a grey patch in the central vision. Thirty percent of CSCR patients also reported ocular pain and discomfort in the affected eye with few cases reporting migraine following the occurrence of CSCR.

Table 7.2: Characteristics of CSCR patients and healthy controls screened for the Liverpool CSCR study

	CSCR patients	Controls	P
<i>Male</i>	51 (80%)	20 (80%)	<i>n/a</i>
<i>Female</i>	13 (20%)	5 (20%)	<i>n/a</i>
<i>Ratio</i>	3.9	4	0.97
<i>Age (years)</i>	48.6 (45.6 – 51.5)	42.2 (39.2 – 45.2)	<0.05
<i>Duration of CSCR (days)</i>	613 (256.4 – 970.3)	N/A	N/A

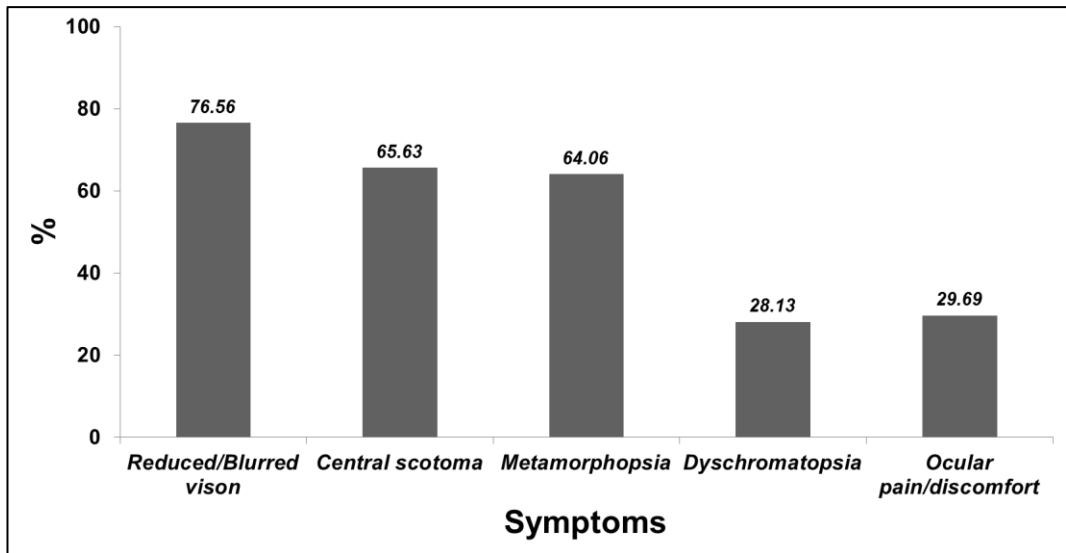


Figure 7.3: Symptoms associated with CSCR

7.3.1.1 *The risks of developing CSCR*

Data available for risk factor analysis: 64 CSCR patients and 25 healthy controls and are shown in **Table 7.3**.

The risk of developing CSCR was determined from the patient's history comparing with that of healthy controls. Risk factors for developing CSCR included history of steroid usage, smoking status, systemic disorders and hypertension. Steroids were used by 35 (55%) CSCR patients compared to 7 (28%) by healthy controls. The most common type of steroids was intra-articular injection (16 patients [25.1%]) and steroid inhalers (15 patients [23.4%]). Among those who had used steroids, 20 (31%) used only 1 type of steroid while 10 (16%) and 5 (8%) a combination of 2 and 3 types. There was a strong association between overall steroid use and CSCR (odds ratio [OR], 3.1 [95% CI: 1.1 – 8.5]; $P = 0.02$) but this association was not found for type of steroid or number of steroid types.

Smoking was reported in 33 (51.6%) CSCR patients compared to 14 (56%) healthy controls. 24 (37.5%) CSCR patients and 8 (32.0%) healthy controls were ex-smokers. Hypertension was the leading systemic disorder in CSCR patients, followed by gastrointestinal tract and urinary tract problems. No significant association with CSCR was identified for smoking or any systemic disorders in my cohort.

Table 7.3: Risk factor (at any time point prior to the CSCR)

	CSCR	Controls	OR (95% CI)	P
History of steroid usage				
<i>Never used steroid</i>	29 (45%)	18 (72%)	N/A	N/A
<i>Had used steroid</i>	35 (55%)	7 (28%)	3.1 (1.1 – 8.5)	0.02
<i>1 type of steroid</i>	20 (31%)	3 (12%)	3.3 (0.9 – 12.4)	0.06
<i>2 types of steroid</i>	10 (16%)	3 (12%)	1.4 (0.3 – 5.4)	0.66
<i>3 types of steroids</i>	5 (8%)	1 (4%)	2.0 (0.2 – 18.3)	0.52
Type of steroid usage				
<i>Steroid tablets</i>	13 (20.3%)	2 (8.0%)	2.9 (0.6 – 14.1)	0.16
<i>Steroid injection</i>	16 (25.0%)	4 (16.0%)	1.8 (0.5 – 5.9)	0.36
<i>Steroid inhalers (mouth/nasal sprays)</i>	15 (23.4%)	2 (8.0%)	3.5 (0.3 – 3.8)	0.10
<i>Topical steroids (lotions, creams or gel)</i>	11 (17.2%)	4 (16.0%)	1.1 (0.3 – 3.8)	0.89
<i>Steroid eye drops</i>	0 (0%)	0 (0%)	n/a	n/a
<i>Only systemic</i>	10	2	0.5 (0.1 – 2.3)	0.50
<i>Only topical</i>	10	1	0.2 (0.0 – 1.9)	0.17
<i>Both systemic and topical</i>	15	4	0.6 (0.2 – 2.1)	0.57
Systemic disorders				
<i>Hypertension</i>	21 (33%)	0 (0%)	n/a	n/a
<i>Diabetic mellitus</i>	3 (5%)	0 (0%)	n/a	n/a
<i>Urinary tract problems</i>	6 (9%)	1 (4%)	2.5 (0.3 – 21.7)	0.40
<i>Gastrointestinal problems</i>	10 (16%)	2 (8%)	2.1 (0.4 – 10.5)	0.34
<i>Heart problems</i>	4 (6%)	1 (4%)	1.6 (0.2 – 15.1)	0.70
<i>Past surgery</i>	22 (34%)	13 (52%)	0.5 (0.2 – 1.2)	0.13

OR = odds ratio; P = Fisher's Exact test significant level

7.3.1.2 **Socio-economic classification of CSCR patients in Liverpool and Merseyside**

Occupation data were available from 58 CSCR patients. Patient occupation was converted to the National Statistics Socio-Economic Classification (NS-SEC) as described in Section 4.3.4.1 of Chapter 4. Briefly, NS-SEC is a tool used to classify adult socio-economic status based on occupation. NS-SEC has eight classes ranging from highest (higher managerial, administrative and professional occupations) to lowest (never worked and long-term unemployed).

The NS-SEC survey in 2011 ²⁴⁶ reported class frequencies in England as NS-SEC level 2 (20.9%) followed by NS-SEC level 6 (14.0%) and NS-SEC level 3 (12.8%). The lowest proportion was NS-SEC level 1 (2.4%). This socio-economic structure was similar in the population within Merseyside.

The socio-economic class distribution of CSCR patients in the Liverpool CSCR study is shown in **Figure 7.4**. The majority of CSCR patients participating in my study were in the NS-SEC level 2 (24.1%). This was similar to the socio-economic class distribution of population within the Merseyside and the England as a whole. Interestingly, the socio-economic class of CSCR patients in the NS-SEC level 4 (19.0%) was approximately 2-times higher than that of Merseyside ($P = 0.002$) and England ($P = 0.021$). This NS-SEC level represents population classed as having small numbers of employees and own account workers. Examples of occupations in the NS-SEC level 4 are restaurant owner, antique dealer, gardener and self-employed. **Figure 7.5** shows the comparison of NS-SEC level of CSCR patients with the population within the Merseyside and England.

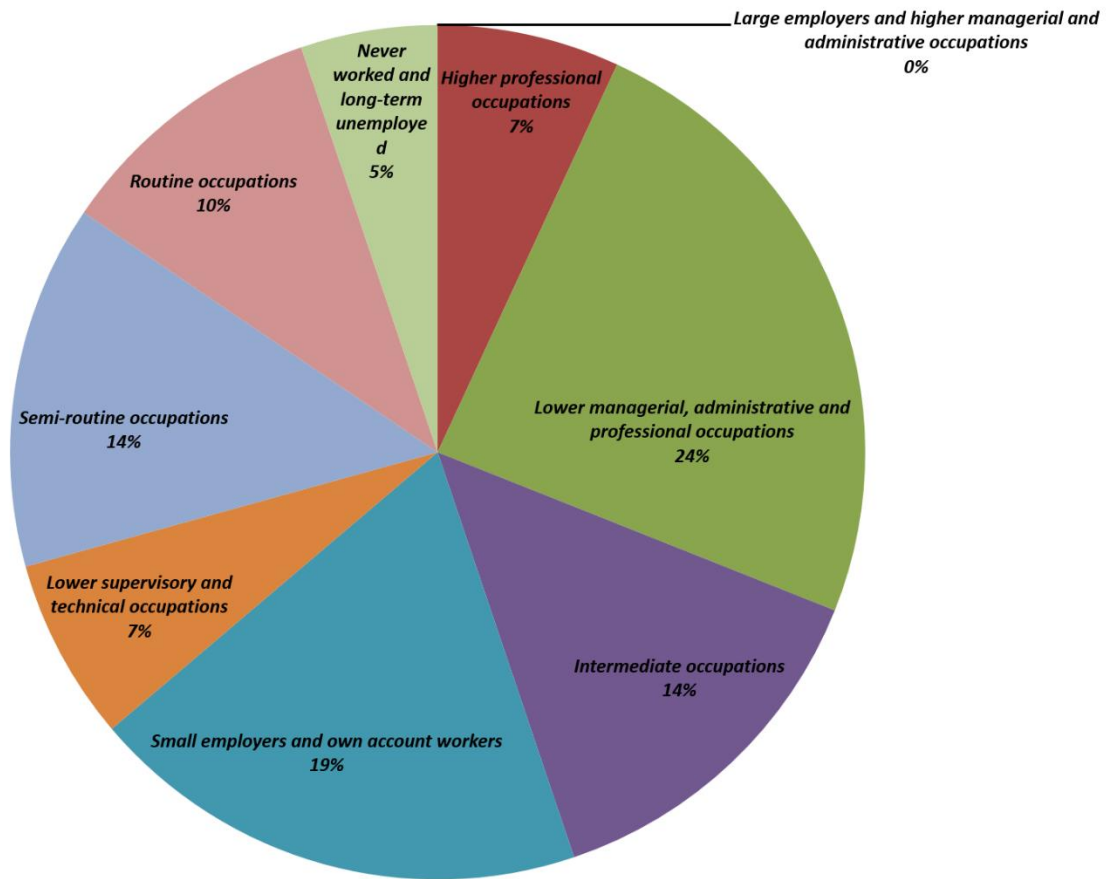


Figure 7.4: The Socio-economic classification of CSCR patients attending St Paul's Eye Unit and recruited into the Liverpool CSCR study

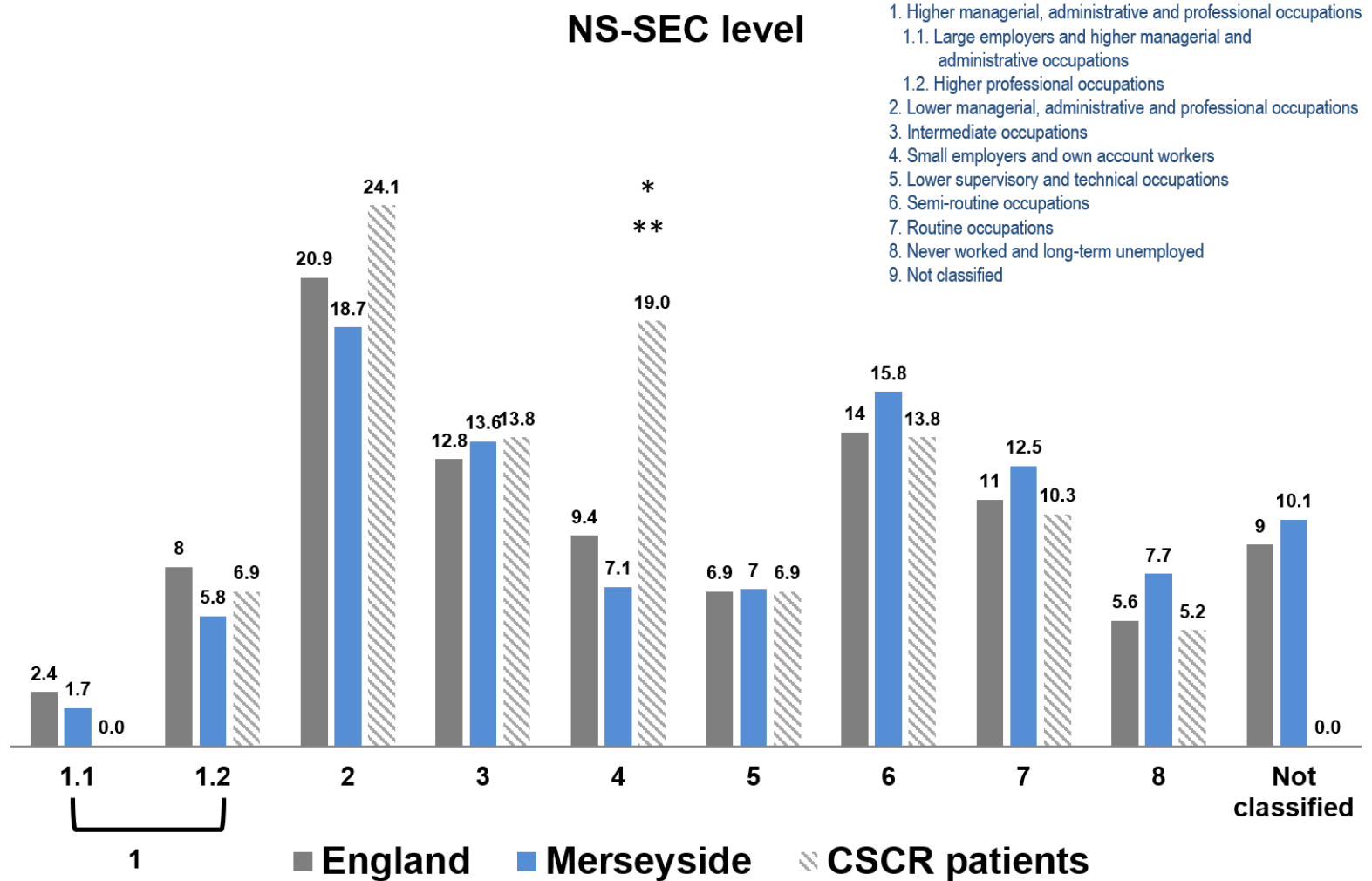


Figure 7.5: The socio-economic classification of CSCR patients attending St Paul’s Eye Unit compared with Merseyside and the general population in England(* represents $P = 0.03$ and ** represents $P = 0.002$)

7.3.1.3 *Quality of life impact and psychological profile questionnaires*

Data available for analysis: 13 CSCR patients and 22 healthy controls.

To determine the stress profile in patients with CSCR, 5 established questionnaires for international research and clinical practice were used. The Survey of Recent Life Experience (SRLE) was used to determine the incidence of acute stressors. This interaction between the patient's behaviour and acute stressors include social/cultural difficulties, work, time pressure, finances, social acceptability and social victimisation. The Life Events Questionnaire (LEQ) was used to assess chronic stress over the previous 6 months. The degree of depression and somatic symptoms were assessed via the Patient Health Questionnaire (PHQ)-9 and PHQ-15, respectively. Finally, the Perceived Stress Scale (PSS) was used to determine the perception of stress.

Twenty two healthy controls and 13 CSCR patients completed this set of quality of life questionnaires. The mean overall SRLE was 80.1 for healthy controls and 75.5 for CSCR patients. The SRLE cultural, social, finance and work related aspects profiles of CSCR patients and healthy controls showed no significant difference. The mean LEQ, PHQ-9, PHQ-15 and PSS were 1.1, 6.1, 5.8 and 22.4, respectively for CSCR patients. These scores were greater than those of healthy controls (LEQ: 0.9, PHQ-9: 4.0; PHQ-15:3.7 and PSS: 19.0; **Figure 7.6**) but did not reach significance. Due to a relatively small sample size used for these analyses, a larger number of CSCR patients is required in order to confirm the results obtained from this section.

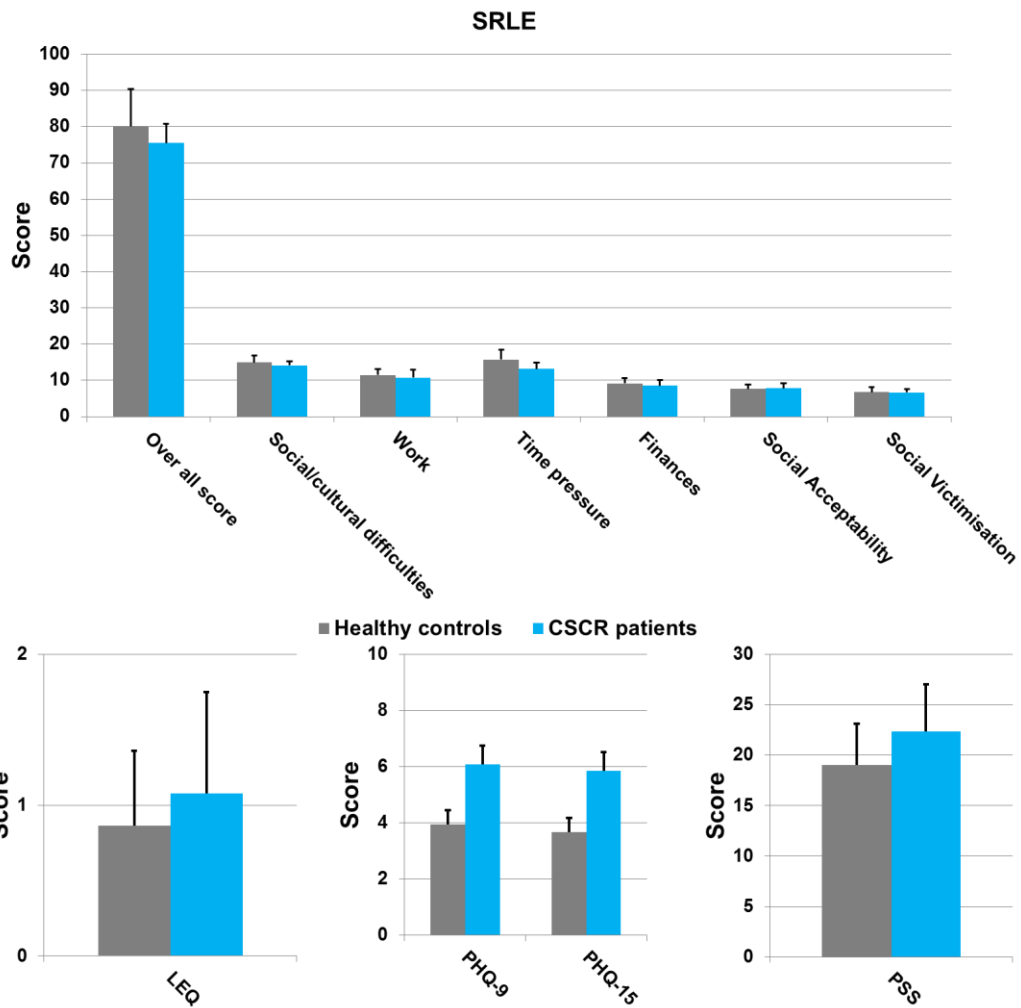


Figure 7.6: Quality of life and psychological profile of CSCR patients (N = 13) and healthy controls (N = 22)

7.3.1.4 *Cortisol level in CSCR*

Data available for cortisol level analysis: 12 CSCR patients and 22 healthy controls.

Endogenous cortisol levels in plasma and urine were assessed. All blood samples were collected before 12.00 PM and the first urine was collected immediately after the subject woke up.

The mean urine cortisol level was 54.2 nmol/L (95% CI: 21.2 – 87.2) for CSCR patients and 76.0 nmol/L (95% CI: 53.2 – 98.8) for healthy controls. There was no significant difference between the urine cortisol levels in both groups (**Figure 7.7**). The plasma cortisol was elevated slightly in CSCR patients (350.5 nmol/L [95%

CI, 238.1 – 463.0]) compared with healthy controls (319.1 nmol/L [95% CI: 260.4 – 377.9]) but the difference was not statistically significant.

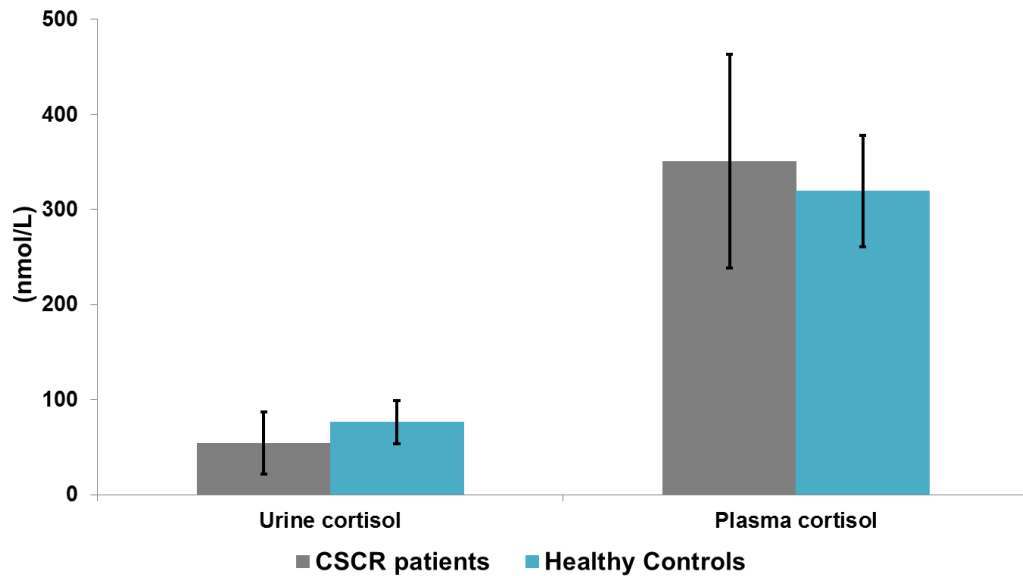


Figure 7.7: The cortisol level in urine and plasma of CSCR patients and healthy controls

7.3.2 Vision and ocular biometry

The vision, ocular biometrics and degree of metamorphopsia (M-score) were determined on 10 CSCR patients and compared with data obtained from 22 controls as shown in **Table 7.4**.

The mean BCVA of CSCR patients was 76.9 letters (95% CI: 69.3 - 84.5) (0.2 logMAR units [95% CI: 0.0 - 0.3]) and was significantly worse than that of controls (91.3 letters [95% CI: 89.7 - 92.8]; -0.1 logMAR units [95% CI: -0.2 - 0.1]; $P < 0.05$). There was approximately 6 letters difference in contrast sensitivity between CSCR patients (35.5 letters [95% CI: 31.0 - 40.0]) and controls (41.1 letters [95% CI: 40.7 - 41.6]) and the difference was statistically significant ($P < 0.05$). The mean M-horizontal (1.1° [95% CI: 0.5 - 1.6]) and M-vertical (0.5° [95% CI: 0.1 - 0.9]) of CSCR eyes were significantly higher than those of controls (mean M-horizontal 0.0° [95% CI: 0.0 - 0.0] and M-vertical 0.0° [95% CI: 0.0 - 0.1], both $P < 0.05$). It is worth noting that 2 and 4 controls subjects had a slight distortion of vision during the M-horizontal and M-vertical tests, respectively.

On A-scan biometry, CSCR eyes had shorter axial length (AxL; 23.1 mm [95% CI: 22.7 - 23.5]) and shallower anterior chamber depth (ACD; 3.2 mm (95% CI:

3.0 - 3.4)) compared to controls (AxL; 23.6 mm [95% CI: 23.3 - 23.9] and ACD = 3.2 mm [95% CI: 3.0 - 3.4]). These differences, however, did not reach a significant level. Similarly, no statistical differences were found in 4-metre refraction and cylinder between CSCR and healthy eyes.

Table 7.4: Vision and ocular biometric characteristics of controls and CSCR patients

	Controls	CSCR	P
BCVA (letters)	91.3 (89.7 - 92.8)	76.9 (69.3 - 84.5)	<0.05*
logMAR vision	-0.1 (-0.2 - -0.1)	0.2 (0.0 - 0.3)	<0.05*
Contrast sensitivity (letters)	41.1 (40.7 - 41.6)	35.5 (31.0 - 40.0)	<0.05 [†]
M-horizontal (°visual angle)	0.0 (0.0 - 0.0)	1.1 (0.5 - 1.6)	<0.05 [†]
M-vertical (°visual angle)	0.0 (0.0 - 0.1)	0.5 (0.1 - 0.9)	<0.05 [†]
4-meter refraction (dioptries)	0.1 (-0.2 - 0.4)	0.6 (-0.2 - 1.4)	0.61 [†]
Axial length (mm)	23.6 (23.3 - 23.9)	23.1 (22.7 - 23.5)	0.09 [†]
Cylinder (mm)	0.7 (0.5 - 0.9)	0.8 (0.5 - 1.0)	0.87*
Anterior chamber depth (mm)	3.3 (3.2 - 3.5)	3.2 (3.0 - 3.4)	0.31*

* Independent Samples Test, [†] Mann-Whitney Test

7.4 Structure of the choroid in CSCR

Data available for choroidal thickness (ChT) and choroidal volume (ChVolume) analysis include: 45 CSCR eyes of 45 CSCR patients (out of a total 64 patients) and 25 eyes of 25 healthy controls. Note, 19 CSCR patients were excluded from this analysis due to various reasons including high myopia or hyperopia (greater than ± 6 dioptres, $N = 6$), previous history of any intraocular procedures including laser vision correction ($N = 5$), treatment after recruitment into the study (such as photodynamic therapy or intravitreal injections ($N = 6$) and poor quality of EDI OCT ($N = 2$).

The demographic characteristics of healthy controls and CSCR patients included in the study are summarised in **Table 7.5**. There were no significant differences in age and gender ratio between CSCR patients and controls. CSCR patients had significantly lower vision than healthy controls ($P < 0.05$). Systolic and diastolic BP, MAP and OPP in CSCR patients were significantly higher than in healthy controls ($P < 0.05$). There were no significant differences in IOP and heart rate between the two groups.

Table 7.5: Clinical characteristics of healthy subjects and CSCR patients (with 95% confidence interval)

	Healthy controls	CSCR patients	P
No. of eyes	25	45	N/A
Age (years)	42.2 (39.2 – 45.2)	47.1 (43.5 – 50.8)	0.07*
Sex; female : male	5 : 20	7 : 38	0.64**
IOP (mmHg)	16.5 (15.4 – 17.7)	16.5 (15.7 – 17.4)	0.97*
logMAR vision	-0.1 (-0.1 – 0.0)	0.2 (0.1 – 0.3)	<0.05 [†]
Systolic BP (mmHg)	118.8 (115.1 – 122.5)	136.6 (129.9 – 143.3)	<0.05 [†]
Diastolic BP (mmHg)	75.1 (72.0 – 78.2)	83.8 (80.2 – 87.4)	<0.05*
Heart rate	68.6 (64.7 – 72.4)	70.5 (66.3 – 74.7)	0.52*
Mean arterial blood pressure (MAP) (mmHg)	89.7 (86.6 – 92.8)	101.4 (97.1 – 105.7)	<0.05*
OPP (mmHg)	43.3 (41.1 – 45.5)	51.4 (48.3 – 54.6)	<0.05*

* Independent Samples Test, ** Chi-Square Tests, [†] Mann-Whitney Test

7.4.1 Choroidal thickness and volume in patients with CSCR

The mean subfoveal ChT (SfChT) and mean macular ChT (MChT) (95% confidence interval: CI) of CSCR eyes were 468.5 μm (95% CI: 437.1 – 499.9) and 428.9 μm (95% CI: 399.4 – 458.4), respectively and were significantly thicker than those of controls (SfChT: 361.4 μm [95% CI: 319.8 – 402.2] and MChT: 337.0 μm [95%CI: 299.9 – 374.1]; both $P < 0.05$).

The mean difference of the MChT was 91.9 μm (95% CI; 44.4 - 139.3) with the greatest difference at the centre of the fovea (107.2 μm [95%CI: 55.8 - 158.5]).

Figure 7.8 demonstrates the ChT and ChVolume over the macula of healthy eyes and CSCR eyes. The ChTs in all EDTRS subfields in CSCR patients were significantly thicker than those of the control group (all $P < 0.05$).

The mean ChVolume (11.7 mm^3 [95% CI: 10.9 – 12.5]) in CSCR patients were significantly higher than that of healthy controls (9.2 mm^3 [95% CI: 8.2 – 10.2], $P < 0.05$). In particular, the greatest difference in ChVolume was observed at the

outer ETDRS subfield nasal to the fovea: the ChVolume increased from 20.7% in the temporal subfield to 32.5% in the nasal subfield.

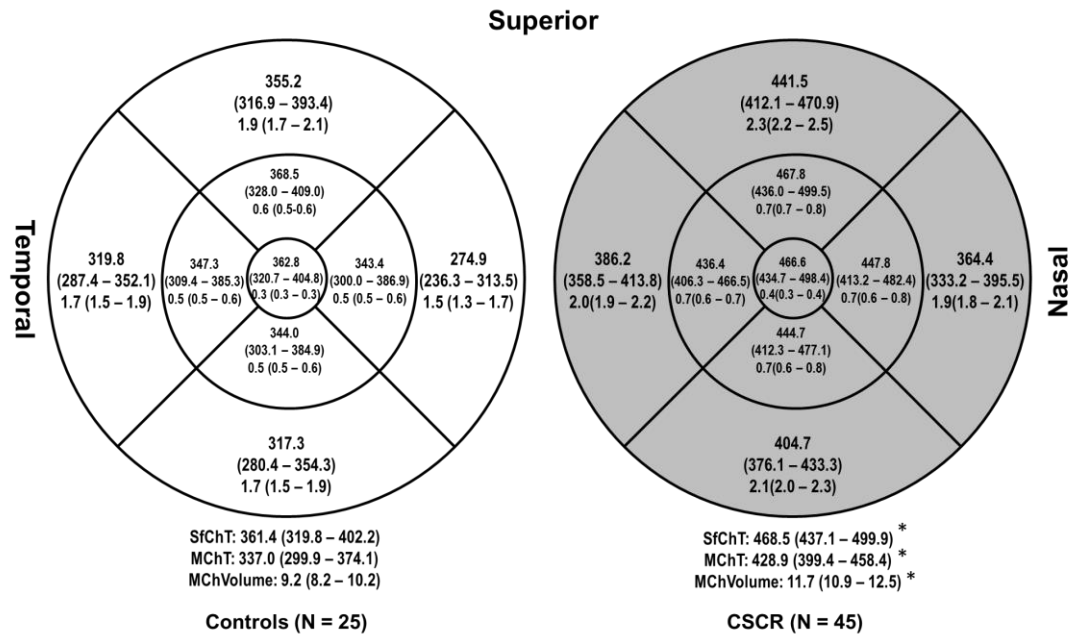


Figure 7.8: EDTRS maps of choroidal thickness (ChT) and volume of healthy controls and CSCR patients (all in microns). SfChT represents the subfoveal ChT. MChT and MChVolume represent the average of mean ChT and ChVolume of the 9-ETDRS subfields, respectively. (* and grey filled subfields denote subfields significantly different to those of healthy controls $P < 0.05$)

7.4.2 Choroidal thickness and volume based on activity and duration of CSCR

7.4.2.1 *Active and inactive CSCR*

Data available for ChT and ChVolume analysis included 9 inactive CSCR eyes and 36 active CSCR eyes. The activity of CSCR was determined by presence and absence of SRF on OCT at the visit.

Figure 7.9 shows the mean ChT and mean ChVolume of patients with active and inactive CSCR. The mean SfChT and MChT of eyes with active CSCR were 476.1 μm (95% CI: 438.6 – 513.1) and 437.1 μm (95% CI: 402.6 – 471.7), respectively. The mean of ChT of 9 ETDRS subfields ranged from 372.2 μm to 475.4 μm with the thickest at the central ETDRS subfield.

The mean SfChT of inactive CSCR was 438.3 μm (95% CI: 382.6 – 494.0) and the mean MChT was 395.9 μm (95% CI: 337.7 – 454.1). The MChT of inactive CSCR was lower by approximately 10% compared with that of active CSCR, but not significantly different. There were no statistically significant differences in ChT between active and inactive CSCR in any of the ETDRS subfields.

There was no significant difference between the mean MChVolume of eyes with active CSCR (11.9 mm^3 [95% CI: 10.9 – 12.8]) and that of eyes with inactive CSCR (10.7 mm^3 [95% CI: 9.1 – 12.3]). The ChVolume of inactive CSCR was lower by approximately 10% for each ETDRS subfield compared to active CSCR, but did not reach significant level.

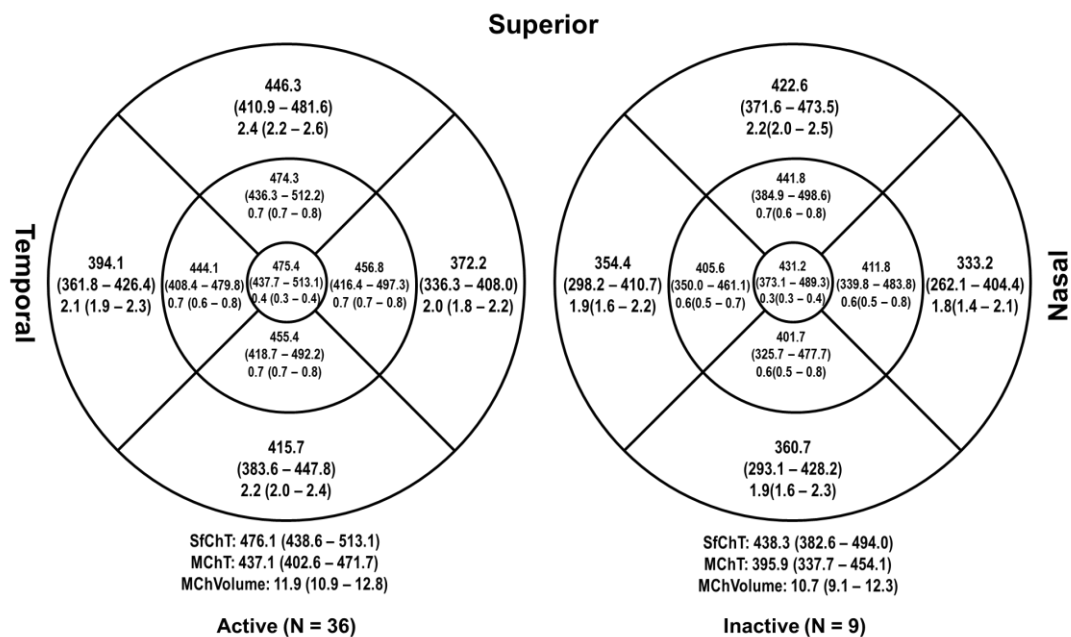


Figure 7.9: EDTRS maps of choroidal thickness (ChT, all in microns) and volume (mm³) of patients with active and inactive CSCR. SfChT represents the subfoveal ChT. MChT and MChVolume represent the average of mean ChT and ChVolume of the 9 ETDRS subfields, respectively

7.4.2.2 Acute and chronic CSCR

Data available for ChT and ChVolume analysis included 15 acute CSCR eyes and 30 chronic CSCR eyes.

Figure 7.10 shows the mean ChT and mean ChVolume in 9 ETDRS subfields of patients with acute and chronic CSCR. In acute CSCR, the mean SfChT was 481.7 µm (95% CI: 423.4 – 540.0) and the mean MChT was 438.1 µm (95% CI: 381.6 – 494.6). In chronic CSCR, the mean SfChT was 461.9 µm (95% CI: 422.6 – 501.3) and the mean MChT was 424.3 µm (95% CI: 387.9 – 460.7). Although the SfChT and MChT in eyes of chronic CSCR were slightly lower than those of eyes with acute CSCR, these differences did not reach significant level.

The MChVolume was 11.9 mm³ (95% CI: 10.3 – 13.4) and 11.5 mm³ (95% CI: 10.6 – 12.5) for acute and chronic CSCR, respectively, and the difference between them was not significant. Although the ChVolumes in eyes of chronic CSCR was slightly lower than those of eyes of acute CSCR, there were no statistically significant differences.

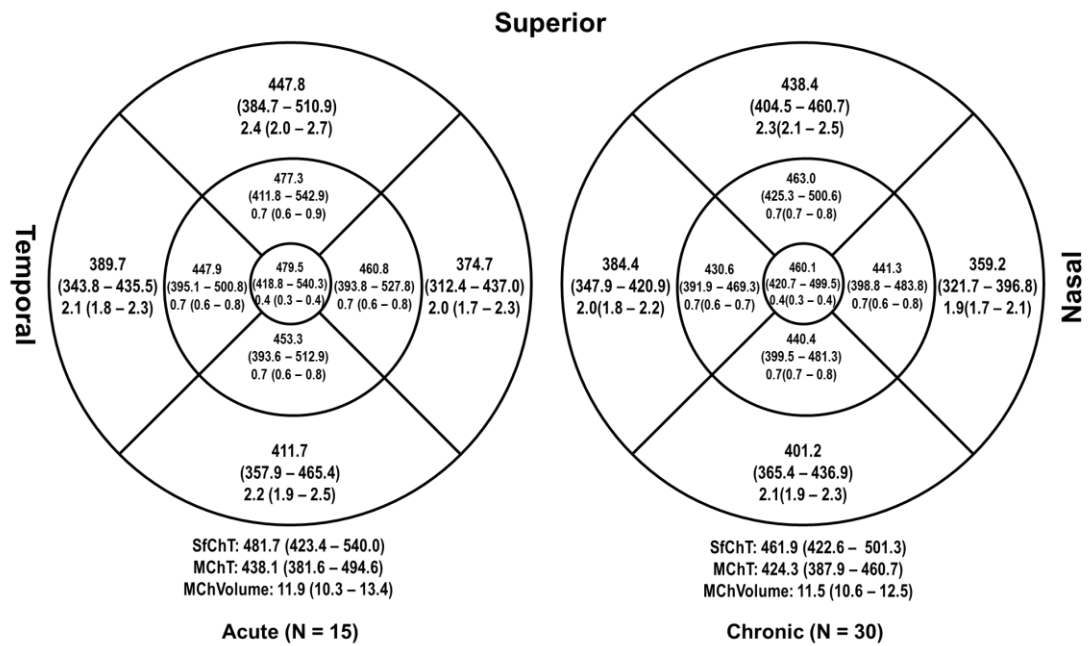


Figure 7.10: EDTRS maps of choroidal thickness (ChT, all in microns) and volume (mm³) of patients with acute and chronic CSCR. SfChT represents the subfoveal ChT. MChT and MChVolume represent the average of mean ChT and ChVolume of the 9-ETDRS subfields, respectively

7.4.2.3 **Choroidal thickness and volume in unilateral and bilateral CSCR**

Data available for ChT and ChVolume analysis in this subsection included 35 unilateral CSCR and 10 bilateral CSCR, and 25 healthy controls.

In this subsection, 4 comparisons were performed: 1) ChT and ChVolume of symptomatic eyes between unilateral, bilateral CSCR and healthy controls, 2) ChT and ChVolume between both eyes of unilateral and bilateral CSCR, 3) ChT and ChVolume between asymptomatic eyes of unilateral CSCR and healthy controls and 4) ChT and ChVolume between asymptomatic eyes with and without choroidal vascular hyperpermeability as defined by ICG as described in Section 4.3.10.6 in Chapter 4.

The mean age of patients with unilateral CSCR was 45.6 years (95% CI: 41.7 – 49.5) and 52.6 years (95% CI: 43.0 – 62.2) for bilateral CSCR. As patients with bilateral CSCR were significantly older than healthy controls ($P = 0.026$), age was considered as a covariate during the analysis.

After controlling for the effect of age, the mean SfChT was 465.6 μm (95% CI: 431.2 – 500.0) for unilateral CSCR and 496.5 μm (95% CI: 429.9 – 563.1) for bilateral CSCR. The mean MChT were 424.1 μm (95% CI: 392.3 – 456.0) and 460.3 μm (95% CI: 398.7 – 522.0) for unilateral CSCR and bilateral CSCR, respectively. The mean ChT of the 9 ETDRS subfields of each CSCR group are shown in **Figure 7.11**. The age corrected mean ChTs of bilateral CSCR were not significantly higher than those of unilateral CSCR, however, the mean ChTs of unilateral and bilateral CSCR were significantly higher than those of healthy eyes respectively (both $P < 0.05$).

The ChVolume values in both the CSCR groups were significantly larger than those of healthy controls while eyes of bilateral CSCR had the largest ChVolume.

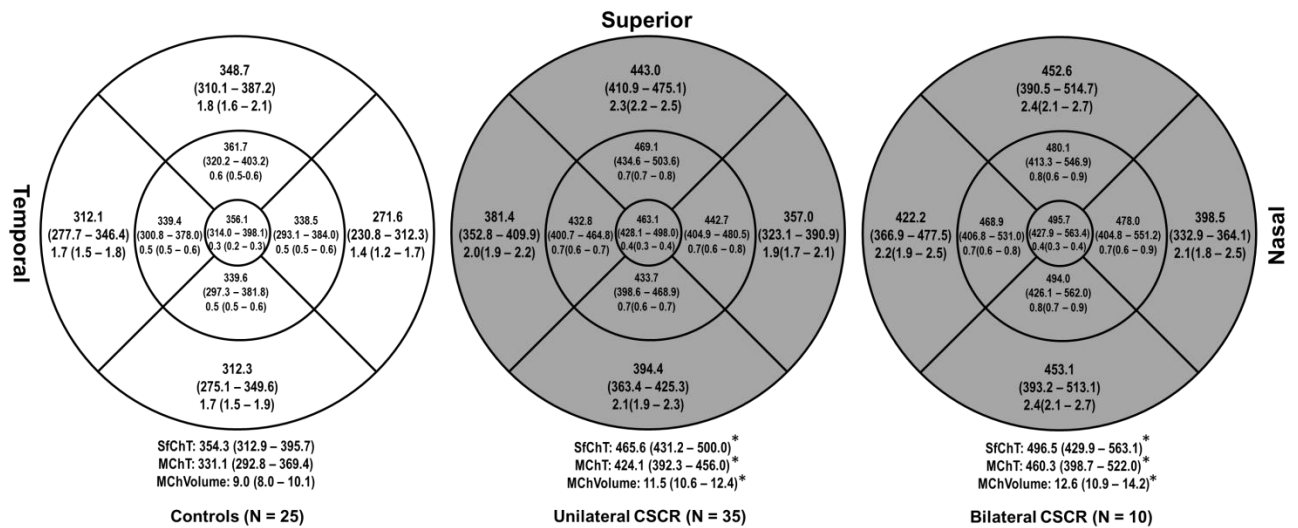


Figure 7.11: Age-adjusted subfoveal ChT (SfChT), mean macular ChT (MChT), the ChT value 9 ETDRS subfields (all in microns), mean macular ChVolume (MChVolume) and ChVolume of 9 ETDRS subfields (all in mm³) of healthy controls (Left) and CSCR patients categorised as unilateral (middle) or bilateral (right) (* and grey filled subfields denote subfields significantly different to those of healthy controls $P < 0.05$, adjusted age = 45.4 years)

In the second comparison, I compared the ChT and ChVolume in both eyes of unilateral and bilateral CSCR respectively. The differences in mean ChT and ChVolume between symptomatic eyes and fellow eyes of unilateral and bilateral CSCR over the 9 ETDRS subfields are shown in **Figure 7.12**.

In patients with unilateral CSCR, the mean SfChT, MChT and MChVolume of the symptomatic eyes were 463.1 μm (95% CI: 427.6 – 498.6), 423.8 μm (95% CI: 390.8 - 456.9) and 11.5 mm^3 (95% CI: 10.6 - 12.4), respectively. These were significantly higher than those of the asymptomatic fellow eyes (mean SfChT: 392.8 μm [95% CI: 358.0 - 427.7], MChT: 362.7 μm [95% CI: 331.5 - 394.0] and MChVolume: 9.9 mm^3 [95% CI: 9.1 - 10.8]. The mean ChTs and ChVolumes of all the 9 ETDRS subfields of the symptomatic eyes were significantly higher than the fellow eyes (all $P < 0.01$). The differences of 2 eyes of unilateral CSCR ranged from 45.8 μm to 71.7 μm (mean difference of MChT of 61.1 μm [95% CI: 46.3 – 75.9]) (**Figure 7.12 right**).

For patients with bilateral CSCR, the mean SfChT, MChT and MChVolume of the chosen index eyes were 476.6 μm (95% CI: 419.2 - 534.1), 443.3 μm (95% CI: 394.0 - 492.6) and 12.1 mm^3 (95% CI: 10.7 - 13.4), respectively. The mean SfChT, MChT and MChVolume of the fellow eye were 470.5 μm (95% CI: 392.9 - 548.2), 429.3 μm (95% CI: 367.8 - 490.8) and 11.7 mm^3 (95% CI: 10.0 - 13.3), respectively. There were no significant differences found between the two eyes of patients with bilateral CSCR (**Figure 7.12 left**).

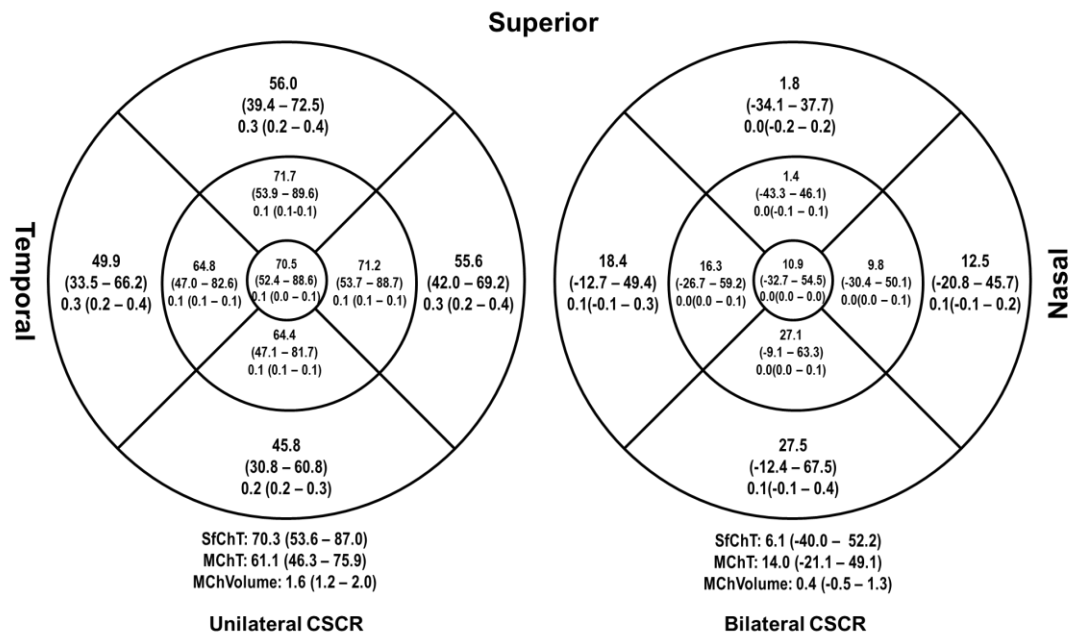


Figure 7.12: EDTRS maps of the differences of choroidal thickness (ChT, all in microns) and volume (mm^3) between the symptomatic eyes and the fellow eyes of patients with unilateral and bilateral CSCR. SfChT represents the subfoveal ChT. MChT and MChVolume represent the average of mean ChT and ChVolume of the 9-ETDRS subfields, respectively

In the third comparison, I compared the ChT and ChVolume of 35 asymptomatic fellow eyes of unilateral CSCR to healthy controls. The mean SfChT, MChT and MChVolume of the asymptomatic fellow eyes of unilateral CSCR were $393.3 \mu\text{m}$ (95% CI: 356.3 – 430.3), $365.2 \mu\text{m}$ (95%CI: 331.6 – 398.8) and 10.0mm^3 (95% CI: 9.1 – 10.9), respectively. These values were 8% higher than those of healthy eyes in all the ETDRS subfields, but did not reach a significant level (all $P > 0.05$) (**Figure 7.13**).

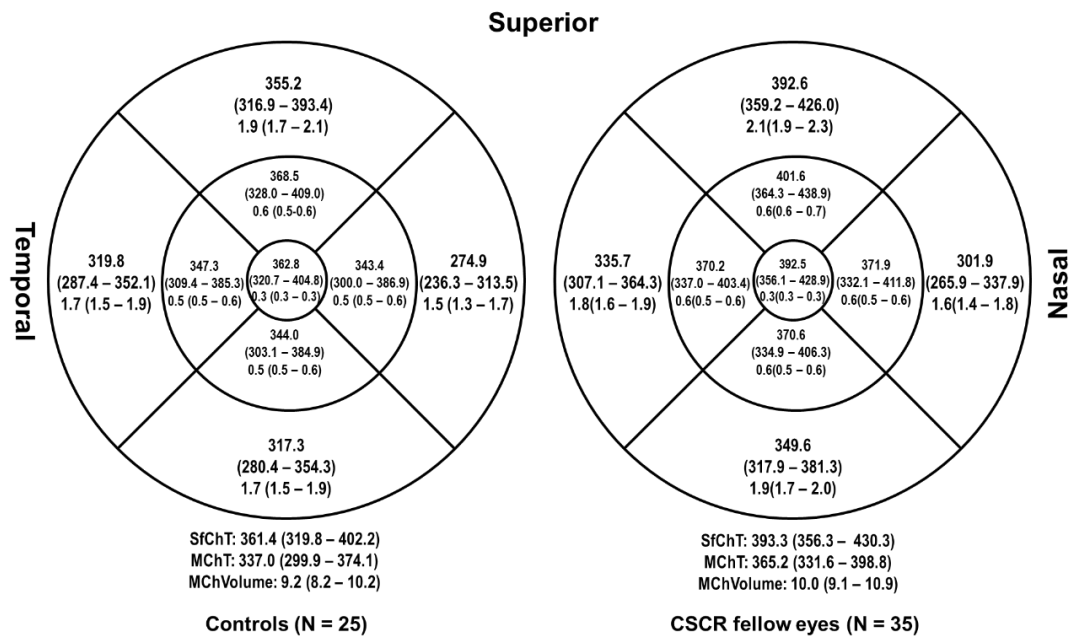


Figure 7.13: EDTRS maps of choroidal thickness (ChT, all in microns) and volume (mm^3) of healthy controls and asymptomatic fellow eyes of unilateral CSCR patients. SfChT represents the subfoveal ChT. MChT and MChVolume represent the average of mean ChT and ChVolume of the 9-ETDRS subfields, respectively

In the fourth comparison, I compared the ChT and ChVolume of asymptomatic fellow eyes of unilateral CSCR with and without choroidal vascular hyperpermeability.

ICGA data was available for 20 fellow eyes of 35 patients with unilateral CSCR. 12 (60%) fellow eyes had ICG hyperfluorescence signifying choroidal vascular hyperpermeability. The mean ChT and ChVolume in all ETDRS subfields of the fellow eyes with choroidal vascular hyperpermeability were approximately 3% higher than those of the fellow eyes without choroidal vascular hyperpermeability, but the differences did not reach significant level (all $P > 0.05$) (**Figure 7.14**).

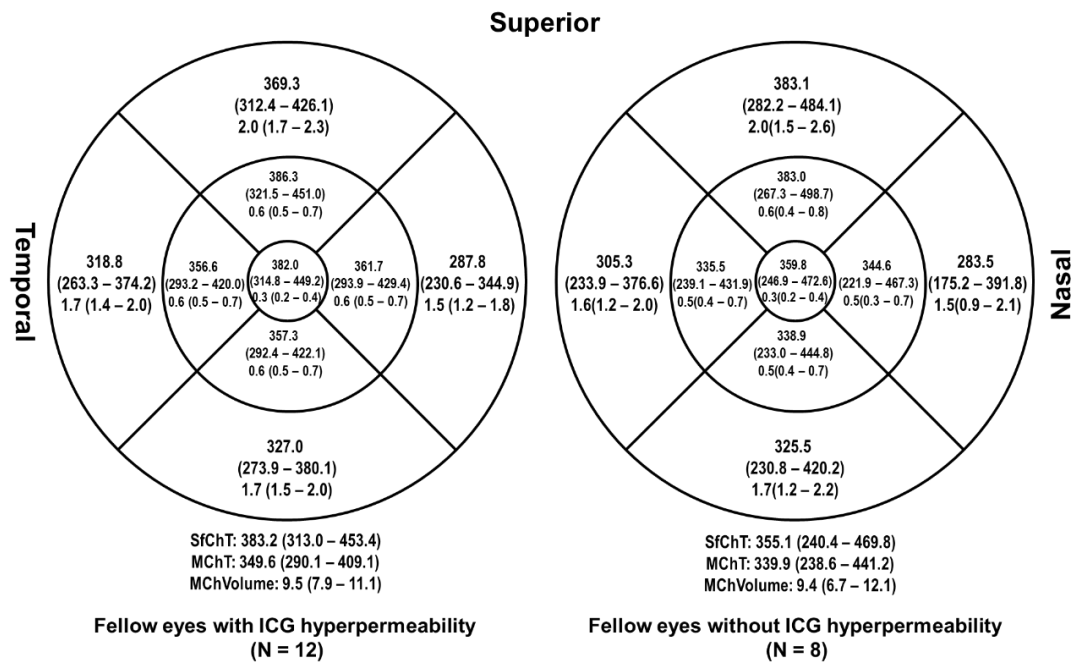


Figure 7.14: EDTRS maps of choroidal thickness (ChT, all in microns) and volume (mm³) of fellow eyes of unilateral CSCR patients with and without choroidal vascular hyperpermeability. SfChT represents the subfoveal ChT. MChT and MChVolume represent the average of mean ChT and ChVolume of the 9-ETDRS subfields, respectively

7.4.3 The relationship between choroidal structure and risks associated with CSCR

In the previous section I presented the possible role of endogenous and exogenous steroids and hypertension as a causative factor for CSCR. In this section, I have investigated if there is a correlation between increased ChT seen on EDI OCT and these presumed risk factors. Data available for this analysis included 45 CSCR and 25 healthy controls.

7.4.3.1 *Impact of steroid usage on choroidal structure*

Among 45 CSCR patients included in the choroidal structure analyses, 24 patients used steroids (53.3%): 8 patients had used systemic steroids only, 6 had used topical steroids only and 10 had used both systemic and topical steroids. The mean SfChT, MChT and MChVolume of CSCR patients who had a history of steroid usage were 468.5 μm (95% CI: 427.8 - 509.2), 425.4 μm (95% CI: 389.7 - 461.0) and 11.6 mm^3 (95% CI: 10.6 - 12.5), respectively. These values were not significantly different from those of CSCR patients without history of steroid usage (SfChT; 468.5 μm [95% CI: 415.8 - 521.2], MChT; 432.9 μm [95% CI: 381.1 - 484.7] and MChVolume: 11.8 mm^3 [95% CI: 10.3 - 13.2], *all P > 0.05*). The differences in ChT and ChVolume over the 9 ETDRS subfields between these two groups are shown in **Figure 7.15**. It can be observed from **Figure 7.15** that the magnitude of difference in ChT was highest at the inner superior subfield and lowest at the outer nasal subfield.

Among 25 healthy controls, 7 had used steroids. The mean ChTs and ChVolumes of these 7 participants who had a history of steroid usage did not significantly differ from those of the other 18 participants (*all P > 0.05*).

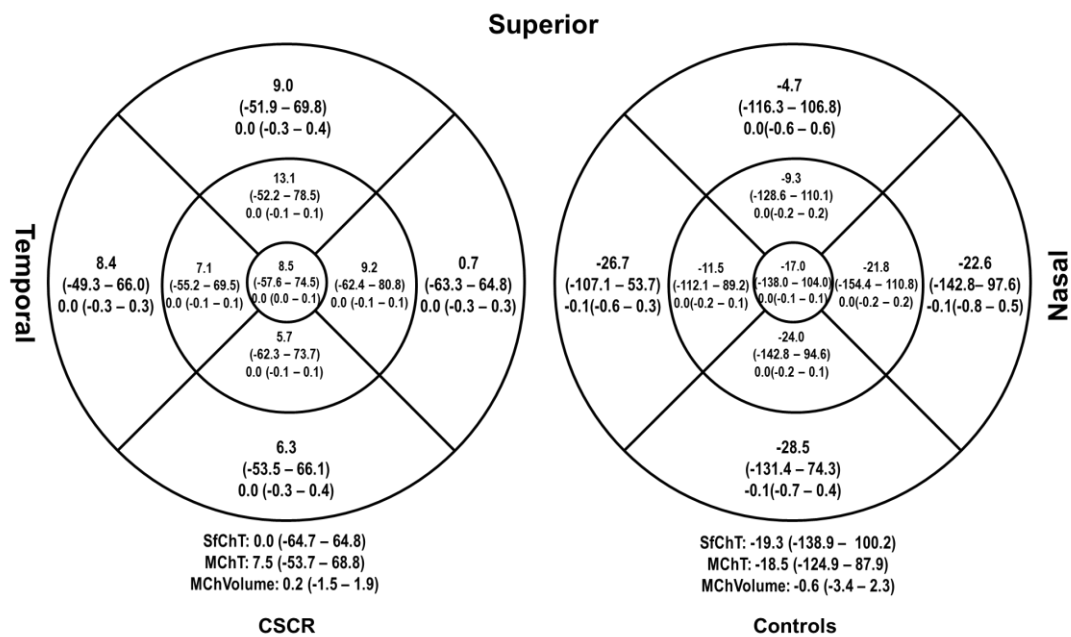


Figure 7.15: EDTRS maps of the differences in choroidal thickness (ChT, all in microns) and volume (mm^3) of CSCR patients and healthy controls with and without history of steroid usage. SfChT represents the subfoveal ChT. MChT and MChVolume represent the average of mean ChT and ChVolume of the 9 ETDRS subfields, respectively

7.4.3.2 Impact of hypertension on choroidal structure

Patients with CSCR were classified as: normotension (BP < 140/90 mmHg without medication) or hypertension (any of: antihypertensive medication, systolic BP \geq 140 mmHg or diastolic BP \geq 90 mmHg).

Among 45 CSCR patients, 22 (48.9%) had normotension and 23 (51.1%) had hypertension, as per our definition. The mean MChT of healthy controls, CSCR patients with normotension and CSCR patients with hypertension was 353.3 μm (95% CI: 311.8 – 394.7), 439.9 μm (95% CI: 395.0 – 484.8) and 502.4 μm (95% CI: 455.5 – 549.4), respectively. The SfChT and the ChT of all the ETDRS subfields of CSCR patients with hypertension were significantly higher than those of healthy controls after controlling for the effect of age (all $P < 0.001$). The SfChT of 8 out of 9 ETDRS subfields of CSCR patients with normotension were also significantly higher than those of healthy controls ($P < 0.05$) (except for the outer nasal subfield [$P = 0.07$]). Although the mean SfChT, MChT and ChTs of all the ETDRS subfields of CSCR with hypertension were thicker than those of CSCR with normotension, the differences were not statistically significant (**Figure 7.16**).

I further investigated the relationship between ChT and hypertension by comparing ChT parameters of CSCR patients with SRF present at study entry (18 CSCR patients with normotension and 18 CSCR patients with hypertension were available for this sub-analysis). The mean MChT was 399.5 μm (95% CI: 349.4 – 449.7) and 474.7 μm (95% CI: 424.5 – 524.9) for CSCR patients with normotension and hypertension respectively ($P < 0.05$). When SRF was present, the SfChT and 3 out of 9 ChT ETDRS subfields of CSCR with hypertension were significantly higher than those of CSCR with normotension (**Figure 7.17**).

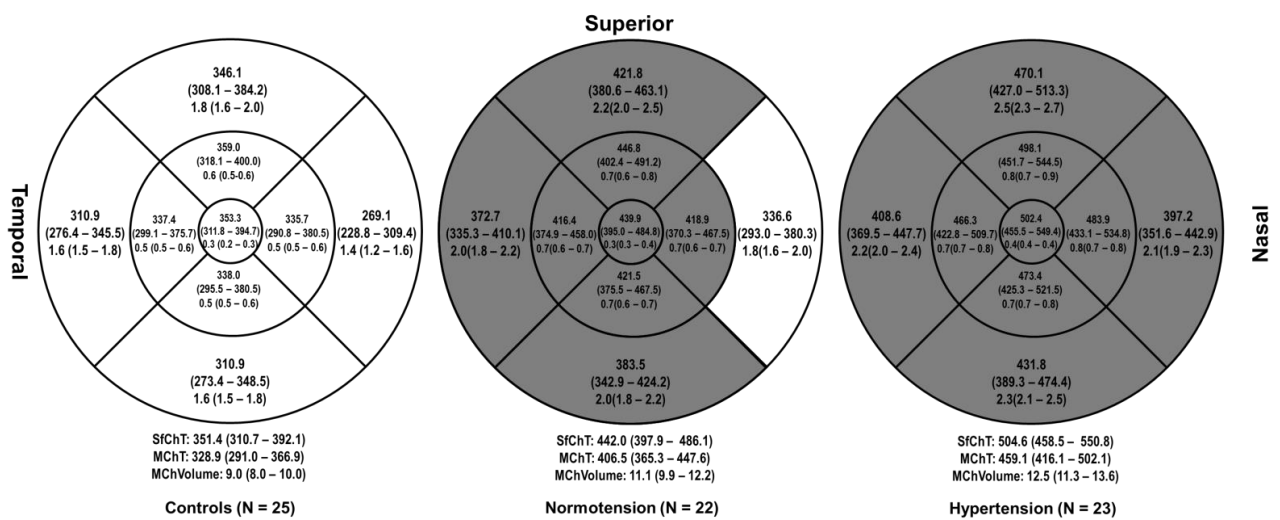


Figure 7.16: Age-adjusted subfoveal ChT (SfChT), mean macular ChT (MChT), the ChT value 9 ETDRS subfields (all in microns), mean macular ChVolume (MChVolume) and ChVolume of 9 ETDRS subfields (all in mm^3) of healthy controls (left) and CSCR patients categorized as normotension (middle) or hypertension (right) (* and grey filled subfields denote subfields significantly different to those of healthy controls $P < 0.05$, adjusted age = 45.4 years)

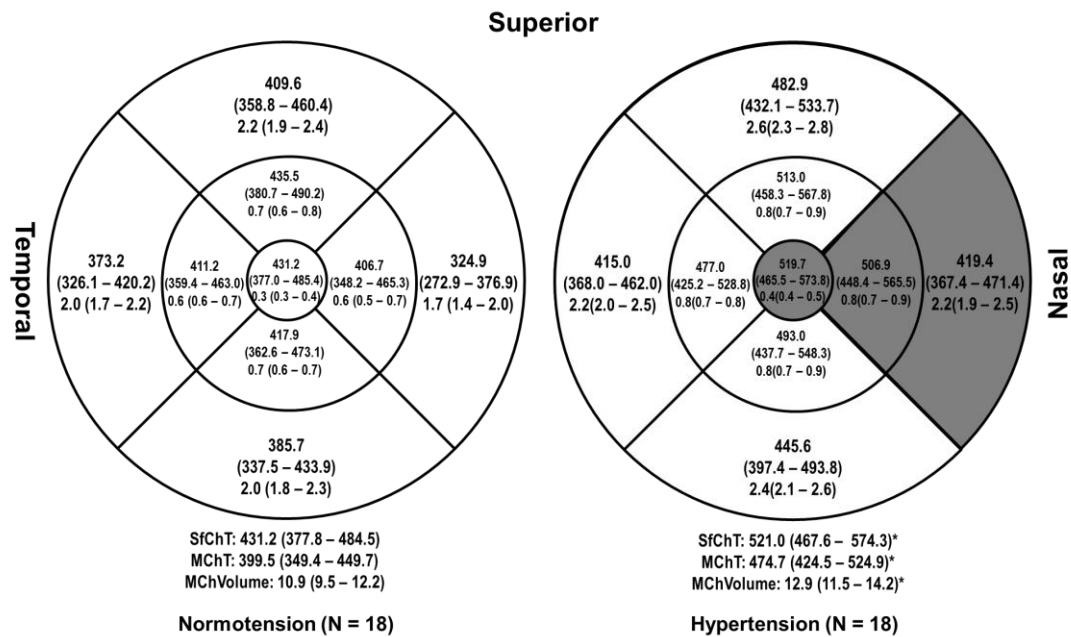


Figure 7.17: Age-adjusted subfoveal ChT (SfChT), mean macular ChT (MChT), the ChT value 9 ETDRS subfields (all in microns), mean macular ChVolume (MChVolume) and ChVolume of 9 ETDRS subfields (all in mm³) of CSCR patients categorised as normotension (left) or hypertension (right) who had SRF at the study entry (* and grey filled subfields denote subfields significantly different to those of normotension $P < 0.05$, adjusted age = 48.3 years)

7.4.3.3 The interaction of steroid use and hypertension in CSCR

Further analysis of covariance of the interaction between hypertension and history of using steroid was performed. Twelve CSCR patients with hypertension (out of 23) and 12 CSCR patients with normotension (out of 22) had a history of steroid usage.

The results from this analysis model are presented in **Table 7.6** and **Figure 7.18**. In brief, the use of steroids caused an average increase of choroidal thickness ranging from 7.9 to 29.5 μm in the selected fields, however, these increases were not significant ($P > 0.05$). Furthermore, there was no apparent interaction between steroid usage and hypertension ($P > 0.05$) across the studied metrics. On the other hand, hypertension on its own was shown to have significant associations with ChTs and ChVolumes.

Following the adjustment of the age and steroid usage effects on the ChT, the mean SfChT, MChT and all 9 ETDRS subfields of CSCR patients with hypertension remained significantly thicker than those of healthy eyes, and not significantly thicker than those of CSCR patient with normotension. Additionally, the

mean SfChT, MChT and ChT of 4 out of 9 ETDRS subfields of CSCR patients with normotension were significantly thicker than those of healthy controls (**Figure 7.19**).

Table 7.6: The age-adjusted subfoveal ChT (SfChT), mean macular ChT (MChT) and the ChT value of each of the 9 ETDRS subfield (all in microns) of healthy controls and CSCR patients who had a history of steroid usage. CSCR patients were also categorised as normotension and hypertension (adjusted age = 45.4 years).

	Controls		CSCR with normotension		CSCR with hypertension	
	No	Yes	No	Yes	No	Yes
SfChT	345.1 (296.4 - 393.8)	366.6 (289.4 - 443.8)	436.6 (369.4 - 503.8)	445.7 (386.8 - 504.7)	491.5 (427.5 - 555.5)	518.2 (455.2 - 581.1)
MChT	323.0 (277.6 - 368.4)	343.2 (271.4 - 415.1)	403.5 (340.9 - 466.1)	408.2 (353.3 - 463.1)	443.3 (383.7 - 502.9)	474.8 (416.2 - 533.4)
Central	347.7 (298.1 - 397.3)	366.7 (288.3 - 445.2)	438.6 (370.2 - 507.0)	440.4 (380.4 - 500.4)	486.2 (421.1 - 551.3)	518.4 (454.4 - 582.4)
Inner nasal	328.9 (275.0 - 382.8)	352.4 (267.1 - 437.7)	415.7 (341.4 - 490.1)	421.1 (355.9 - 486.3)	479.4 (408.7 - 550.2)	488.9 (419.3 - 558.5)
Inner temporal	333.3 (287.9 - 378.6)	346.9 (275.1 - 418.7)	416.0 (353.4 - 478.6)	416.0 (361.1 - 470.8)	437.3 (377.7 - 496.8)	494.3 (435.7 - 552.9)
Inner superior	355.6 (306.6 - 404.6)	366.9 (289.3 - 444.5)	445.0 (377.3 - 512.6)	447.7 (388.4 - 507.0)	480.1 (415.8 - 544.5)	515.7 (452.4 - 579.0)
Inner inferior	330.6 (279.7 - 381.4)	355.9 (275.4 - 436.4)	415.4 (345.3 - 485.6)	425.7 (364.2 - 487.2)	461.1 (394.4 - 527.9)	486.2 (420.5 - 551.8)
Outer nasal	262.3 (213.9 - 310.6)	286.1 (209.5 - 362.7)	331.8 (265.1 - 398.5)	340.3 (281.8 - 398.8)	402.0 (338.5 - 465.5)	393.5 (331.0 - 455.9)
Outer temporal	302.5 (262.0 - 343.1)	331.2 (266.9 - 395.4)	370.0 (314.0 - 425.9)	374.0 (324.9 - 423.1)	380.3 (327.1 - 433.6)	436.3 (383.9 - 488.7)
Outer superior	344.0 (298.6 - 389.5)	350.7 (278.7 - 422.7)	419.2 (356.5 - 481.9)	423.3 (368.3 - 478.3)	450.8 (391.1 - 510.5)	489.2 (430.4 - 547.9)
Outer inferior	302.2 (257.6 - 346.9)	332.1 (261.5 - 402.8)	379.8 (318.2 - 441.4)	385.8 (331.8 - 439.8)	412.5 (353.8 - 471.1)	451.2 (393.5 - 508.8)

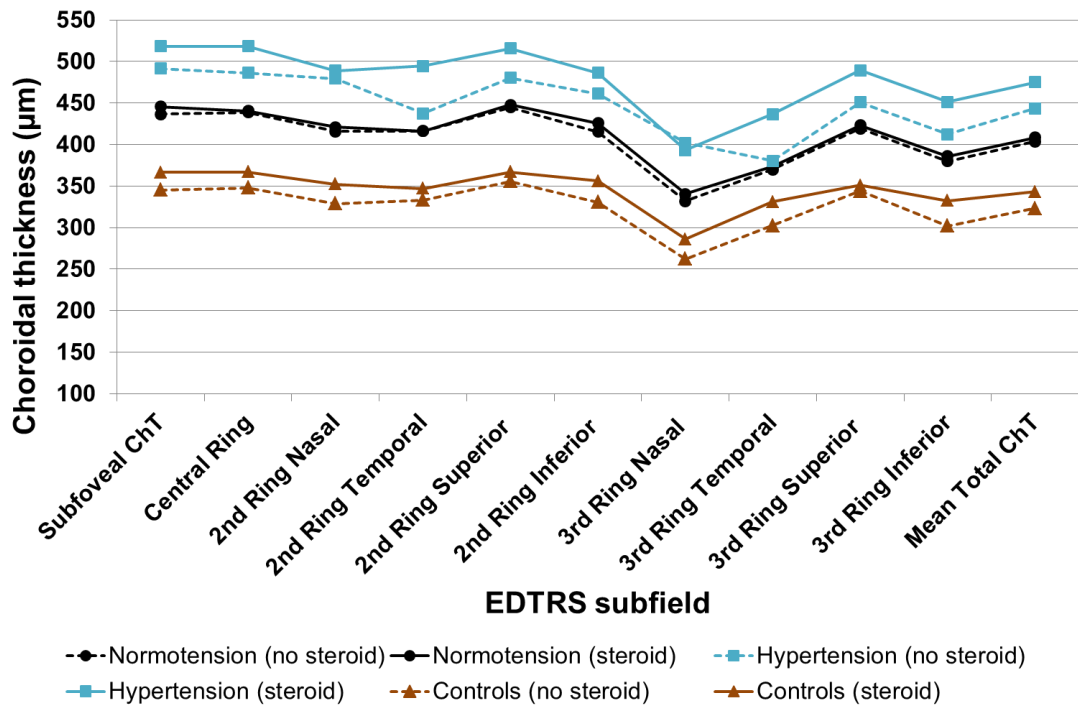


Figure 7.18: The age-adjusted subfoveal ChT (SfChT), mean macular ChT (MChT) and the ChT value of each of the 9 ETDRS subfield (all in microns) of healthy controls and CSCR patients who have had history of steroid usage (adjusted age = 45.4 years)

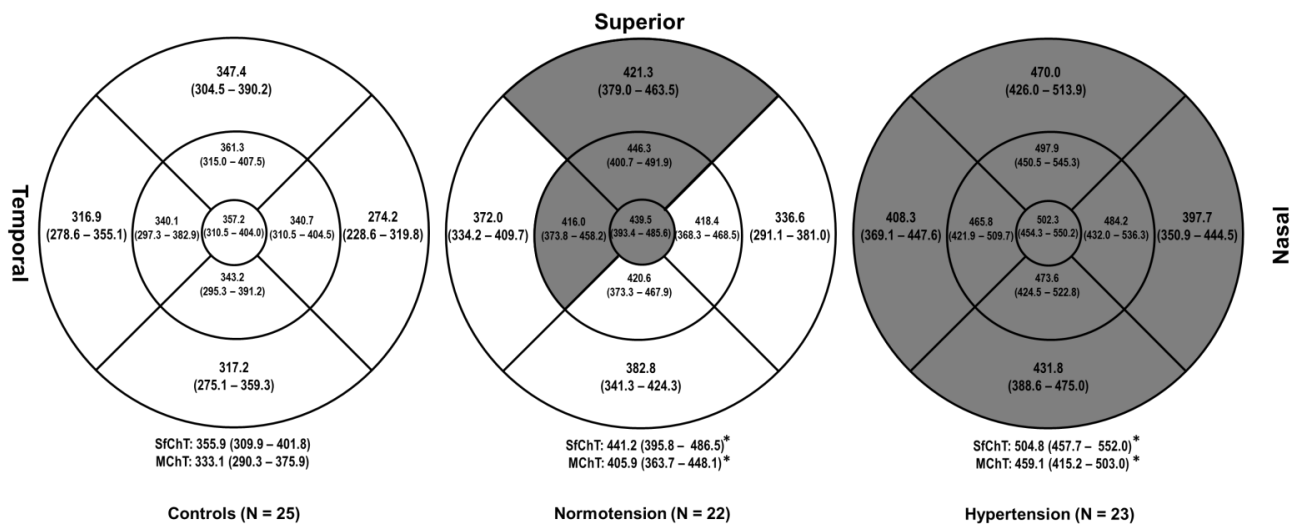


Figure 7.19: Age- and steroid usage-adjusted subfoveal ChT (SfChT), mean macular ChT (MChT) and the ChT value of each of the 9 ETDRS subfield (all in microns) of healthy controls (left) and CSCR patients categorized as normotension (middle) or hypertension (right) (* and grey filled subfields denote subfields significantly different to those of healthy controls $P < 0.05$; adjusted age = 45.4 years)

7.4.4 The association between choroidal thickness and other imaging techniques

In this section, I will summarise the findings on FA, ICGA and autofluorescent imaging. **Table 7.7** summarises the data available for analyses within this section.

Table 7.7: Data available for fundus imaging analyses

Fundus imaging techniques	Number of CSCR patients	Number of healthy controls	Comments
Fluorescein angiography (FA)	36	N/A	N/A
Indocyanine green angiography (ICGA)	34	N/A	20 ICG images (only those captured with 50° view mode) from 20 CSCR patients were used for subanalysis with ChT
Fundus autofluorescence (FAF)	62	25	2 CSCR patients were excluded due to poor image quality
Near infrared autofluorescence (NIR-AF)	58	25	6 CSCR patients were excluded due to poor image quality

N/A: not available for analysis

7.4.4.1 Fluorescein angiography appearance in CSCR

Patterns of FA were determined and classified into 4 categories: pinpoint, ink blot, smoke stack and patchy hyperfluorescence, as shown in **Figure 7.20**. Of the 36 CSCR eyes with FA available, 1 eye had no leakage, 5 had a hyperfluorescent spot defined as pinpoint hyperfluorescence, 9 had hyperfluorescence defined as ink blot pattern, 1 had hyperfluorescence defined as smoke stack, 15 had patchy pattern of hyperfluorescence and 5 had mixed hyperfluorescence patterns. CSCR patients with mixed FA pattern had the longest duration of symptom (1082 days [95% CI: -89.7 – 2253]), followed by those with patchy FA pattern (459.8 days [95% CI: 153 – 765.9]), ink blot (181.3 days [95% CI: 92.0 – 270.5]) and pin point (107.8 days [84.1 – 131.4]). The mean logMAR vision of those eyes with patchy and mixed patterns of FA was worse than that of eyes with pinpoint and ink blot patterns.

When the CSCR eyes were subcategorised as acute or chronic according to symptom duration, there were no obvious FA patterns associated with acute CSCR while patchy FA pattern was found in the majority of eyes with chronic CSCR.

Table 7.8: FA pattern (in %) seen in acute and chronic CSCR

Type of CSCR	FA patterns					
	<i>No leakage</i>	<i>Pinpoint</i>	<i>Ink blot</i>	<i>Smoke stack</i>	<i>Patchy</i>	<i>Mix</i>
Acute	1 (11.1%)	2 (22.2%)	2 (22.2%)	1 (11.1%)	3 (33.3%)	0 (0%)
Chronic	0 (0%)	3 (11.1%)	7 (25.9%)	0 (0%)	12 (41.7%)	5 (13.9%)
Total	1 (2.8%)	5 (13.9%)	9 (25.0%)	1 (2.8%)	15 (41.7%)	5 (13.9%)

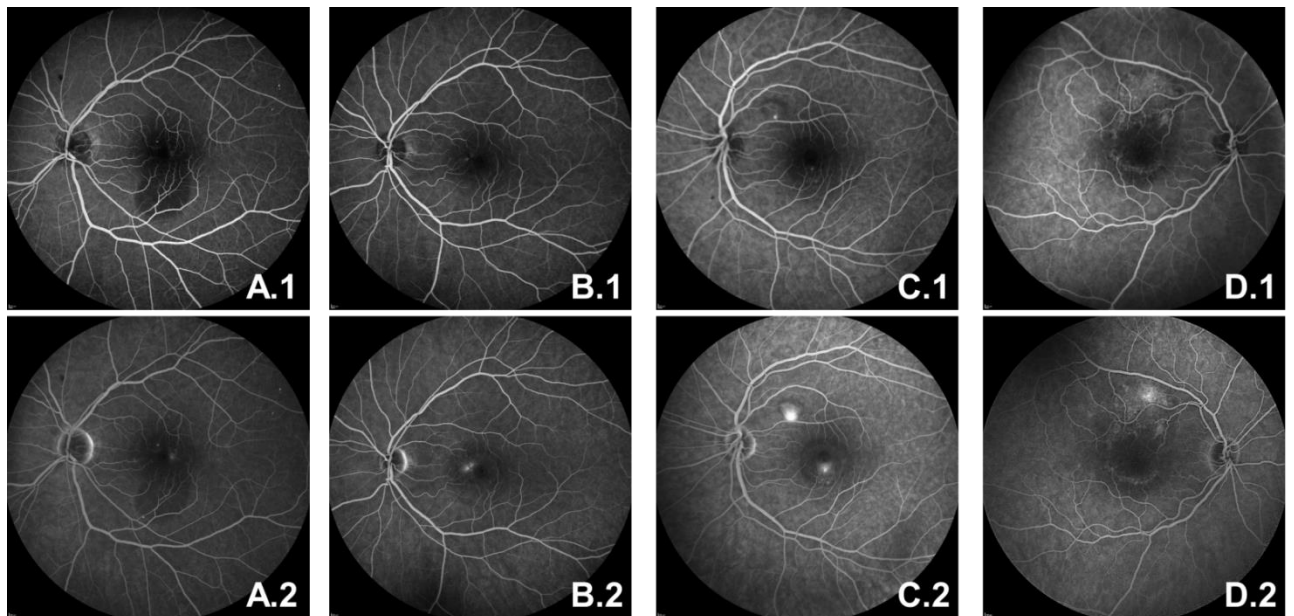


Figure 7.20: FA patterns of CSCR eyes: A1-2 an early and late of pinpoint FA pattern; B1-2 early and late of ink blot FA pattern; C1-2 early and late of smoke stack FA pattern; D1-2 early and late of patchy FA pattern

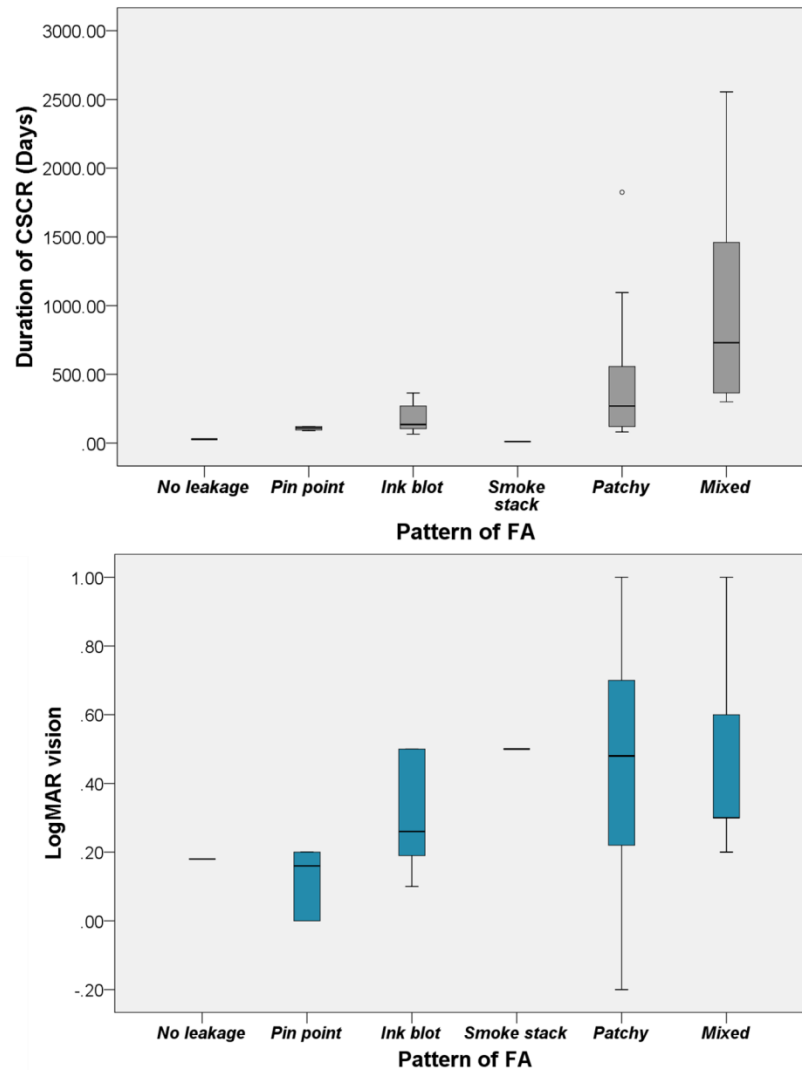


Figure 7.21: Box plots of logMAR vision and duration of symptom of each FA pattern. The tinted box represents the inter quartile range and the whiskers represent lowest and the highest scores

7.4.4.2 *Indocyanine green angiography appearance in CSCR*

The available ICGA data were from 11 bilateral CSCR and 23 unilateral CSCR. For the index eye, choroidal vascular hyperpermeability shown on ICGA (**Figure 7.22**) was found in all the 34 CSCR eyes regardless of whether patient had unilateral or bilateral CSCR. 100% of bilateral CSCR patients also had choroidal vascular hyperpermeability in their fellow eyes. In the patients with unilateral CSCR, choroidal vascular hyperpermeability was found in 13 (56.5%) fellow eyes.

In unilateral cases, the mean duration of choroidal vascular hyperpermeability appearing following the ICGA injection was 1.2 minutes (95% CI: 0.7 – 1.7) for the symptomatic eyes and 3.6 minutes (95% CI: 2.1 – 5.1) for asymptomatic fellow eye

($P < 0.05$) which was significantly longer than that of the asymptomatic fellow eye. In bilateral CSCR cases, there was no significant difference detected in the mean duration of choroidal vascular hyperpermeability appearance between the index eyes (1.0 minutes [95% CI: 0.0 – 2.2]) and the fellow eyes (1.5 minutes [95% CI: 0.3 – 2.8]).

There was no significant difference in the mean duration of choroidal vascular hyperpermeability appearance of the index eye between acute and chronic CSCR cases (1.3 minutes vs 1.1 minutes; $P = 0.8$).



Figure 7.22: The choroidal vascular hyperpermeability as seen on the ICGA of patients with unilateral CSCR (A) and bilateral CSCR (B)

7.4.4.3 *The association between choroidal structure and choroidal vascular hyperpermeability seen on ICGA*

In order to assess the relationship between the choroidal vascular hyperpermeability detected on ICGA and ChT, 20 CSCR patients with available ICGA data captured with 50° view mode were selected. Among 20 CSCR patients, 17 patients were unilateral CSCR and 3 patients were bilateral. Among 17 unilateral CSCR patients, 5 patients also had choroidal vascular hyperpermeability detected on ICGA in their asymptomatic fellow eyes.

The ChT and the percentage of choroidal vascular hyperpermeability were calculated for every 1 mm² of the 6 × 6 mm macular map, centred at the fovea. The choroidal vascular hyperpermeability $\geq 50\%$ of the area within 1 mm² square was considered as hyperpermeability area otherwise considered as non-

hyperpermeability area as shown in **Figure 7.23**. The 6 × 6 mm ChT and the percentage of choroidal vascular hyperpermeability maps were created for 23 affected eyes (17 eyes from 17 unilateral CSCR and 6 eyes from 3 bilateral CSCR).

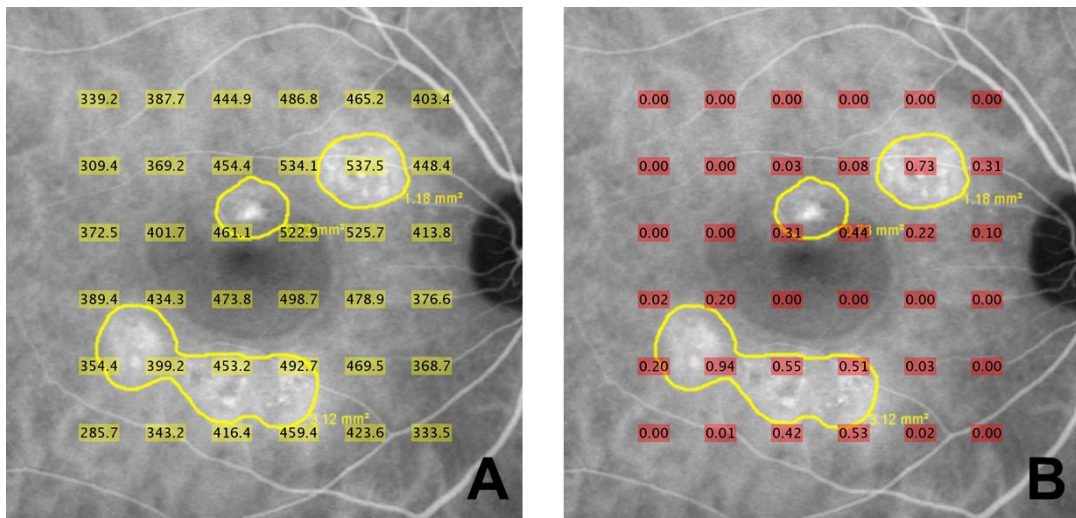


Figure 7.23: The representative 6 × 6 mm map of choroidal thickness (A) and choroidal vascular hyperpermeability (B)

The mean ChT at the hyperpermeability area of the 23 affected eyes was 422.4 µm (95% CI: 381.7 - 463.0) which was significantly thicker compared with 383.6 µm (95% CI: 346.1 - 421.1) of the area without choroidal vascular hyperpermeability ($P < 0.05$). In bilateral CSCR, 2 fellow eyes had thinner choroid within the area of hyperpermeability while 1 fellow eye had similar thickness in both areas as shown in **Table 7.9** (with yellow background).

Table 7.9: Mean ChT at the hyperpermeability area and non-hyperpermeability area of CSCR eyes

Subject	Type of CSCR	Eye	ChT of hyperpermeability area (μm)	ChT of non-hyperpermeability area (μm)
No. 1	Bilateral	OD	341.7	385.4
		OS	437.9	402.5
No. 2	Unilateral	OD	389.6	305.1
No. 3	Unilateral	OS	264.1	254.8
No. 4	Unilateral	OD	448.8	409.0
No. 5	Unilateral	OD	468.4	418.9
No. 6	Unilateral	OD	361.7	319.0
No. 7	Unilateral	OD	351.3	333.0
No. 8	Unilateral	OD	578.4	527.3
No. 9	Unilateral	OD	506.0	454.1
No. 10	Unilateral	OS	705.2	627.0
No. 11	Bilateral	OD	471.4	442.7
		OS	398.6	409.5
No. 12	Bilateral	OD	442.0	392.0
		OS	428.7	429.0
No. 13	Unilateral	OS	445.8	380.3
No. 14	Unilateral	OS	384.9	262.8
No. 15	Unilateral	OD	381.6	359.2
No. 16	Unilateral	OS	311.0	285.0
No. 17	Unilateral	OS	468.5	408.0
No. 18	Unilateral	OS	411.9	368.1
No. 19	Unilateral	OS	291.1	254.9
No. 20	Unilateral	OD	425.3	395.0
Total	N/A	N/A	422.4	383.6

* The yellow background represents the fellow eyes of patients with bilateral CSCR

In 5 unilateral CSCR patients, choroidal vascular hyperpermeability was present in asymptomatic fellow eyes. A significantly thicker choroid was found at the hyperpermeability area seen on ICGA ($P < 0.05$) with the mean ChT of 328.0 μm (95% CI: 201.5 - 454.5) compared to 291.5 μm (95% CI: 193.2 - 389.8) at the non-hyperpermeability area.

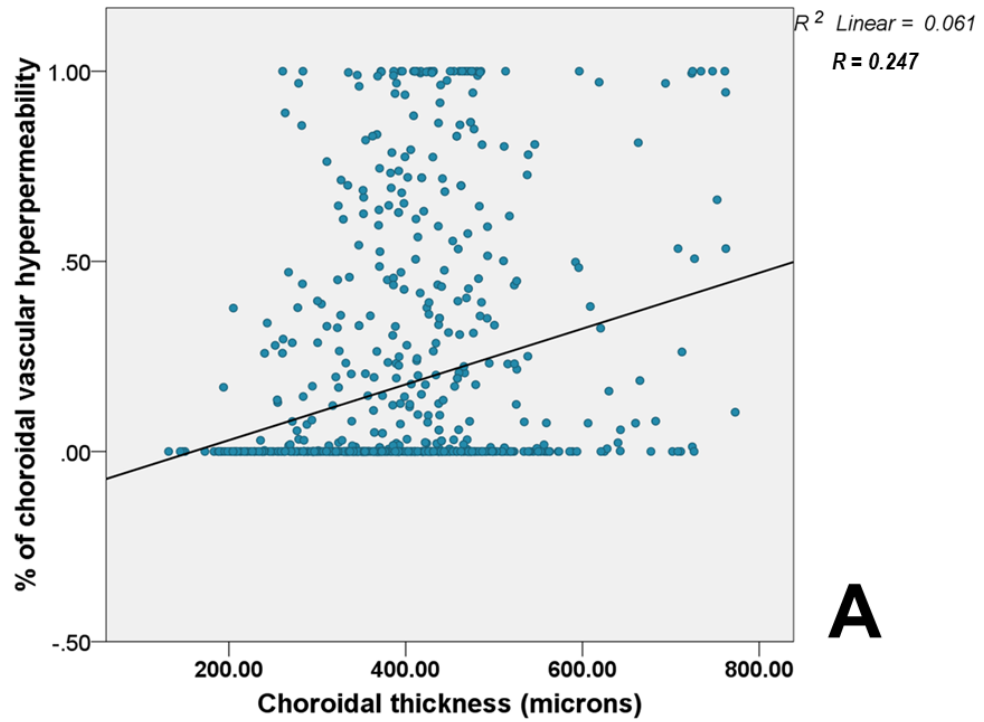
The ChT of 12 asymptomatic fellow eyes of 12 unilateral CSCR without choroidal vascular hyperpermeability was compared with the ChT of non-hyperpermeability area of the CSCR eyes (index eyes). The mean ChT of non-hyperpermeability area in the index eyes was significantly thicker than that of asymptomatic fellow eyes (394.9 μm (95% CI: 327.7 - 462.0) vs 334.3 μm (95% CI: 278.6 - 390.1); $P < 0.05$).

In each of the 1 mm² area, there was a statistically significant positive relationship between the percentage of choroidal vascular hyperpermeability and ChT for both affected ($r = 0.247$, $P < 0.05$) and un-affected fellow eyes ($r = 0.101$, $P = 0.012$) (**Figure 7.24**). Additionally, the changes in ChT associated with the choroidal vascular hyperpermeability detected on ICGA could be predicted using the **Equation 7.1A** for the symptomatic eyes and **Equation 7.1B** for asymptomatic fellow eyes.

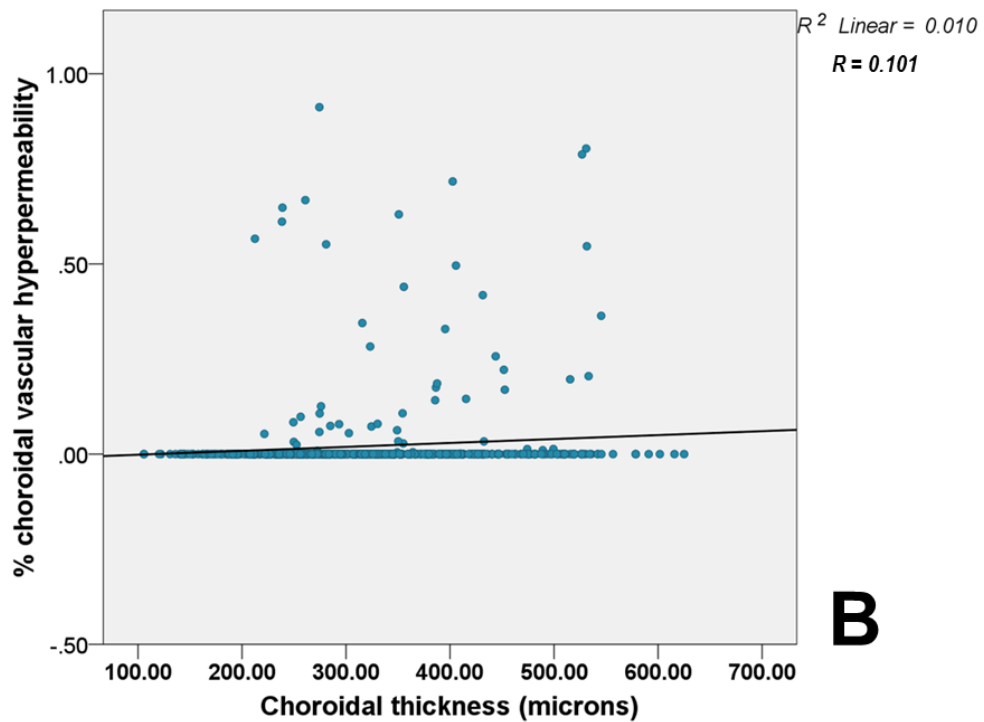
$$\text{Choroidal thickness } (\mu\text{m}) = 378.99 + (83.5 \times \% \text{ of the hyperpermeability}) \quad \mathbf{A}$$

$$\text{Choroidal thickness } (\mu\text{m}) = 320.37 + (98.9 \times \% \text{ of the hyperpermeability}) \quad \mathbf{B}$$

Equation 7.1: The model for predicting the choroidal thickness (ChT) using the choroidal vascular hyperpermeability detected on ICGA (% of choroidal vascular hyperpermeability) as a main predictor for the symptomatic eyes (A) and the asymptomatic fellow eyes (B)



A



B

Figure 7.24: The relationship between the percentage of choroidal vascular hyperpermeability and ChT within each 1 mm² sector for the symptomatic eyes (A) and the asymptomatic fellow eyes (B)

7.4.4.4 Fundus autofluorescence imaging and its association with choroidal changes in CSCR

Another commonly used imaging modality in the diagnosis of CSCR is fundus autofluorescence (FAF) imaging. Higher level of relative FAF represents an increased or abnormal area of autofluorescence which can be seen as an area of higher intensity compared to surrounding area and a lower level of relative FAF represents a decreased or abnormal area of autofluorescence which can be seen as an area of lower intensity compared to surrounding area. The analysis was done on 62 FAF images of 62 CSCR eyes and 25 FAF images of 25 control eyes. FAF images of 2 CSCR patients were excluded due to poor image quality. I have calculated the relative FAF level from the grey level of the area of interest as shown in **Figure 7.25**.

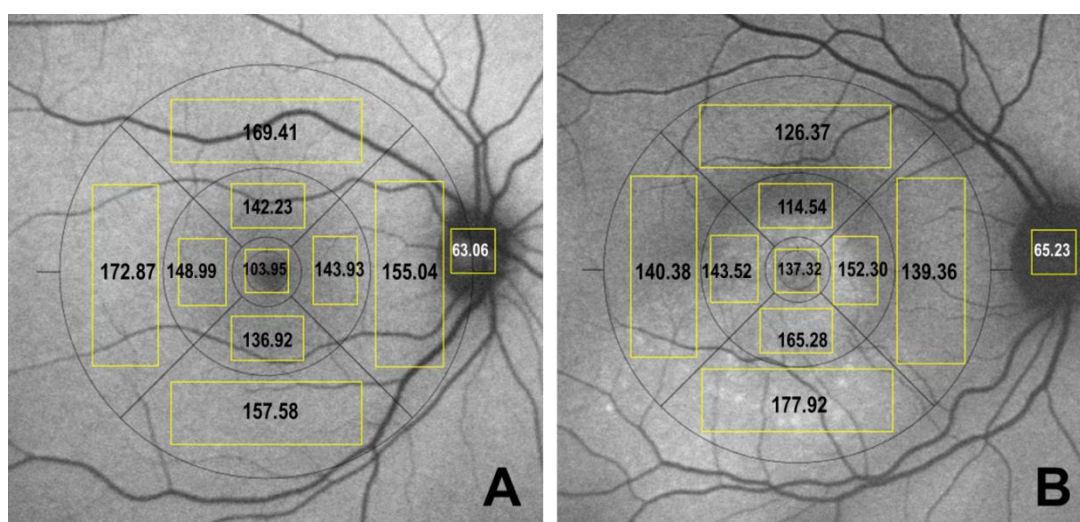


Figure 7.25: Examples of the mean grey scale values obtained from the FAF histogram of each location over the macula of the right eye of a healthy control (A) and the right eye of a CSCR patient (B)

In normal healthy eyes, the relative FAF level was lower at the central area (0.35 [95% CI: 0.30 – 0.40]) compared to the area surrounding (**Table 7.10**). There were no significant differences found in FAF levels between the two eyes in controls.

In affected eyes of CSCR patients, a similar FAF distribution to that of healthy controls was found. However, the level of relative FAF was significantly higher than healthy controls in each subfield (all $P < 0.05$; **Figure 7.26**). The relative FAF levels of the affected eyes are shown in **Table 7.10**. The relative FAF levels in

each subfield in the CSCR eyes were significantly higher than those of unaffected fellow eyes in the unilateral CSCR cases.

Table 7.10: Relative FAF level of controls and CSCR patients

ETDRS subfields					
Group	Central	Nasal	Temporal	Superior	Inferior
Controls	0.35 (0.30 – 0.40)	0.77* (0.72 – 0.83)	0.74* (0.70 – 0.78)	0.65* (0.61 – 0.69)	0.79* (0.75 – 0.84)
CSCR patients	0.56 (0.50 – 0.62)	0.93* (0.85 – 1.01)	0.88* (0.81 – 0.95)	0.83* (0.75 – 0.91)	0.98* (0.88 – 1.07)
P	0.00	0.01	0.04	0.01	0.03

* $P < 0.05$ compared to the central subfield within the group

When CSCR patients were subdivided into acute and chronic, acute CSCR eyes showed significantly higher levels of relative FAF only at the central subfield compared to control eyes ($P < 0.05$). CSCR patients with chronic, on the other hand, showed significant higher relative FAF levels in all subfields compared to that of healthy eyes (all $P < 0.05$) and higher than acute CSCR in temporal and inferior subfields ($P < 0.05$; **Figure 7.27**).

A linear correlation revealed that the relative FAF level did not correlate with either ChT or ChVolume in both healthy and CSCR eyes but was related to the retinal thickness on each corresponding subfield. Negative correlations between the level of relative FAF and retinal thickness were found at the temporal ($r = -0.28$; $P < 0.05$), superior ($r = -0.48$; $P < 0.05$) and inferior ($r = -0.27$; $P < 0.05$) subfields in CSCR patients. Interestingly, these negative correlations between the level of relative FAF and retinal thickness were also presented in controls' eyes at temporal ($r = -0.56$; $P < 0.05$) and inferior ($r = -0.50$; $P < 0.05$) subfields. Moreover, higher relative FAF level was strongly associated with poorer logMAR vision ($r = 0.28$; $P = 0.03$) in CSCR whereas this relationship did not exist for healthy controls. No association between the relative FAF level and age was observed in either controls or CSCR patients.

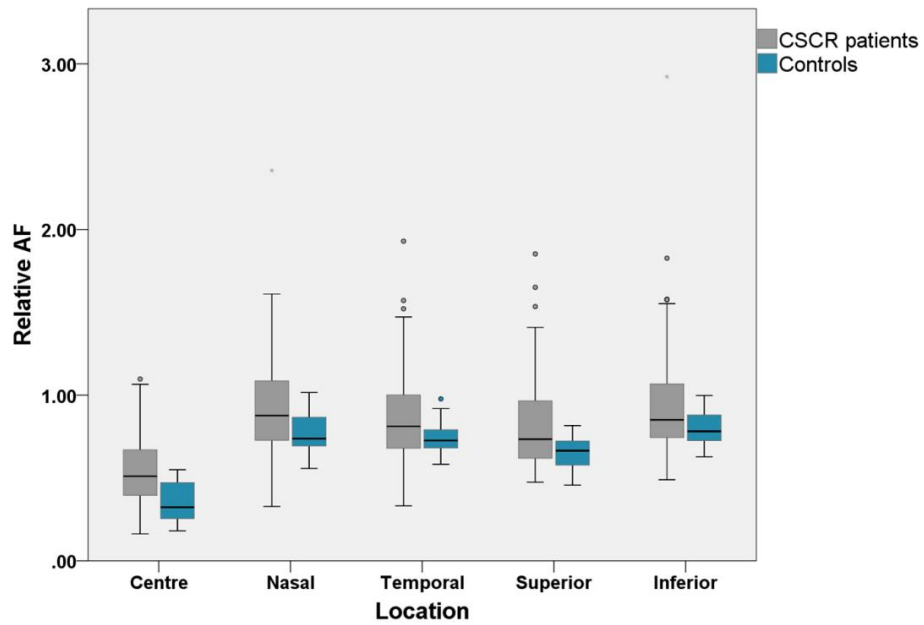


Figure 7.26: Relative FAF levels of the affected eyes of CSCR and the control eyes. The tinted box represents the inter quartile range and the whiskers represent the lowest and the highest scores

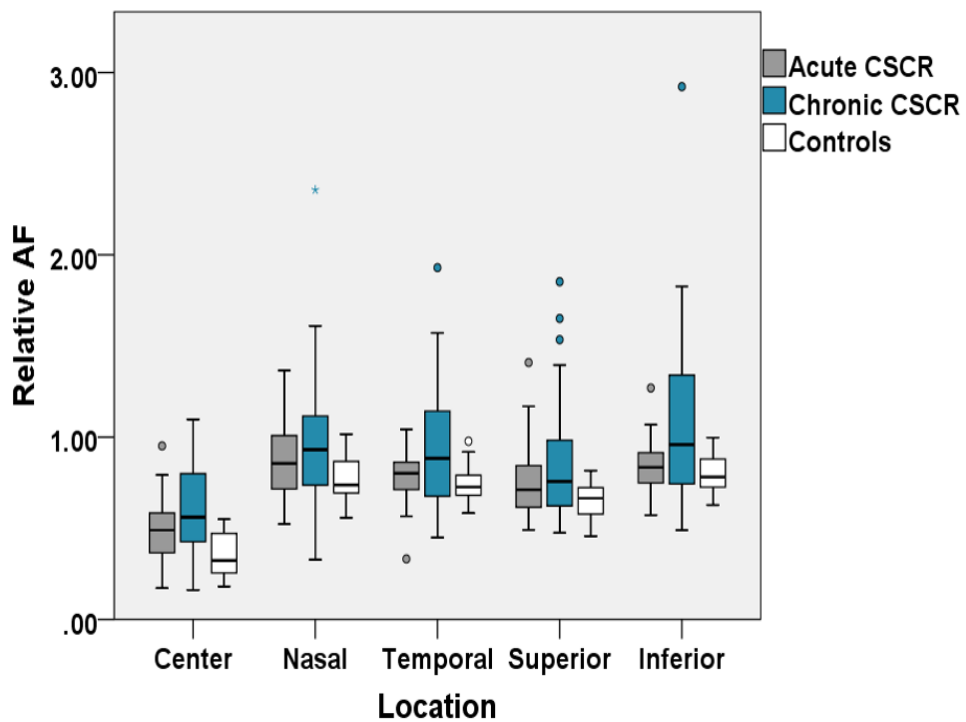


Figure 7.27: Relative FAF levels of the affected eyes of CSCR (categorised as acute and chronic) and the control eyes. The tinted box represents the inter quartile range and the whiskers represent the lowest and the highest scores

7.4.4.5 Fundus near-infrared autofluorescence imaging and its association with choroidal changes in CSCR

Similar to the analysis on FAF images, the relative near infrared autofluorescence (NIR-AF) of normal healthy eyes and CSCR eyes were calculated. Among 83 NIR-AF images, 58 were from CSCR eyes (6 CSCR patients were excluded due to poor image quality) and 25 NIR-AF images were from healthy eyes. **Figure 7.28** Error! Reference source not found. shows the examples of mean grey scale values obtained from the histogram of each location of NIR-AF image.

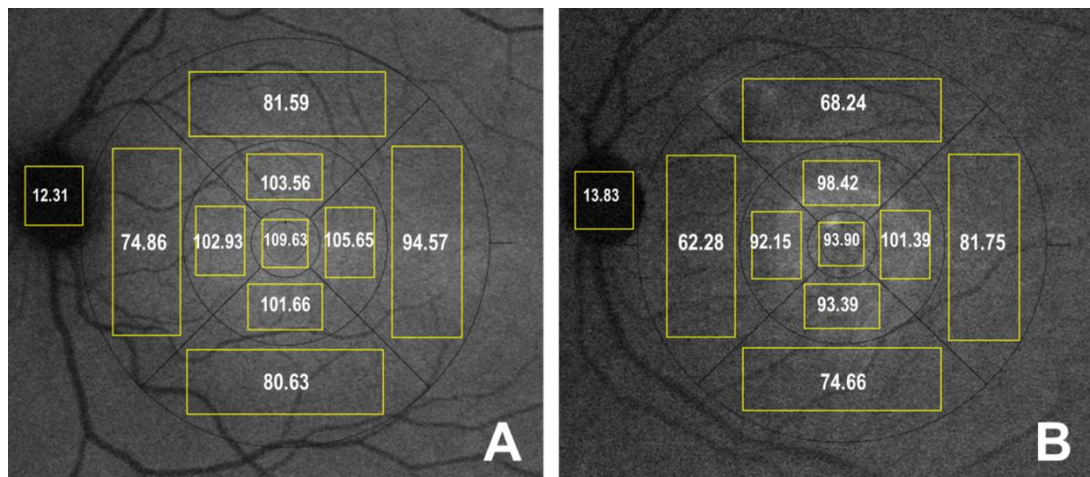


Figure 7.28: Examples of the mean grey scale values obtained from the NIR-AF histogram of each location over the macula of the left eye of a healthy control (A) and the left eye of a CSCR patient (B)

In healthy eyes, the relative NIR-AF level was the highest at the central area (1.62 [95% CI: 1.53 – 1.71]) compared to the surrounding area (**Table 7.11**; all $P < 0.05$). There was no significant difference in NIR-AF levels between the two eyes in controls. The relative NIR-AF levels of the CSCR affected eyes are shown in **Table 7.11**. A slight decrease of the NIR-AF level at the central area but a small increase in the NIR-AF levels on the surrounding areas were found when compared to healthy eyes, as shown in **Figure 7.29**. These differences, however, did not reach a significant level.

Table 7.11: Relative NIR-AF level of controls and CSCR patients

ETDRS subfields					
Group	Central	Nasal	Temporal	Superior	Inferior
Controls	1.62 (1.53 – 1.71)	1.36* (1.31 – 1.41)	1.20* (1.15 – 1.25)	1.30* (1.22 – 1.37)	1.36* (1.26 – 1.45)
CSCR patients	1.40 (1.26 – 1.54)	1.39 (1.27 – 1.52)	1.30* (1.20 – 1.40)	1.46 (1.31 – 1.61)	1.41 (1.31 – 1.51)
P	0.17	0.41	0.10	0.11	0.19

* $P < 0.05$ compared to the central subfield within the group

The group comparison of NIR-AF levels between controls, acute and chronic CSCR demonstrated a lower but insignificant NIR-AF level at the centre area of CSCR eyes when compared to controls ($P > 0.05$; **Figure 7.30**). In addition, patients with chronic CSCR showed higher NIR-AF levels at the nasal, temporal, superior and inferior areas when compared to those patients with acute CSCR, however, the differences did not reach significant level.

In normal healthy eyes, the central NIR-AF level was significantly negatively associated only with age ($r = -0.41$, $P = 0.04$). This association did not present in CSCR eyes ($r = -0.22$, $P = 0.10$). In CSCR eyes, the NIR-AF level was negatively associated with the duration of symptom ($r = -0.28$, $P = 0.04$), logMAR vision ($r = -0.36$, $P < 0.05$) and the thickness of the retina ($r = -0.30$, $P = 0.02$). The relative NIR-AF level did not show any correlations with either ChT or ChVolume in either healthy or CSCR eyes.

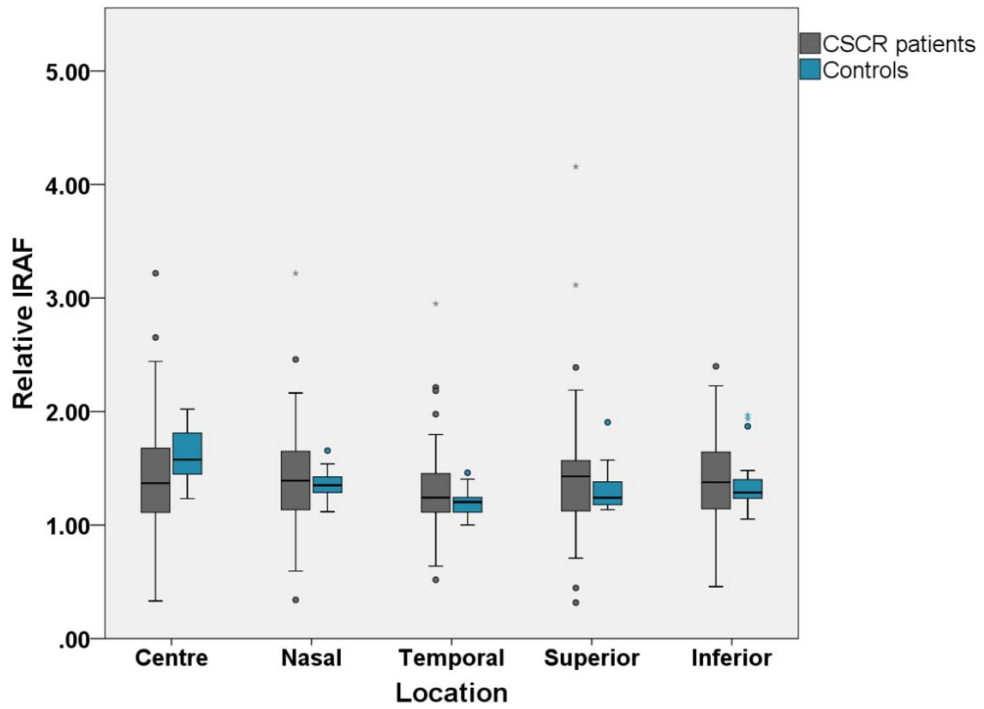


Figure 7.29: Relative NIR-AF levels of CSCR and control eyes. The tinted box represents the inter quartile range and the whiskers represent lowest and the highest scores

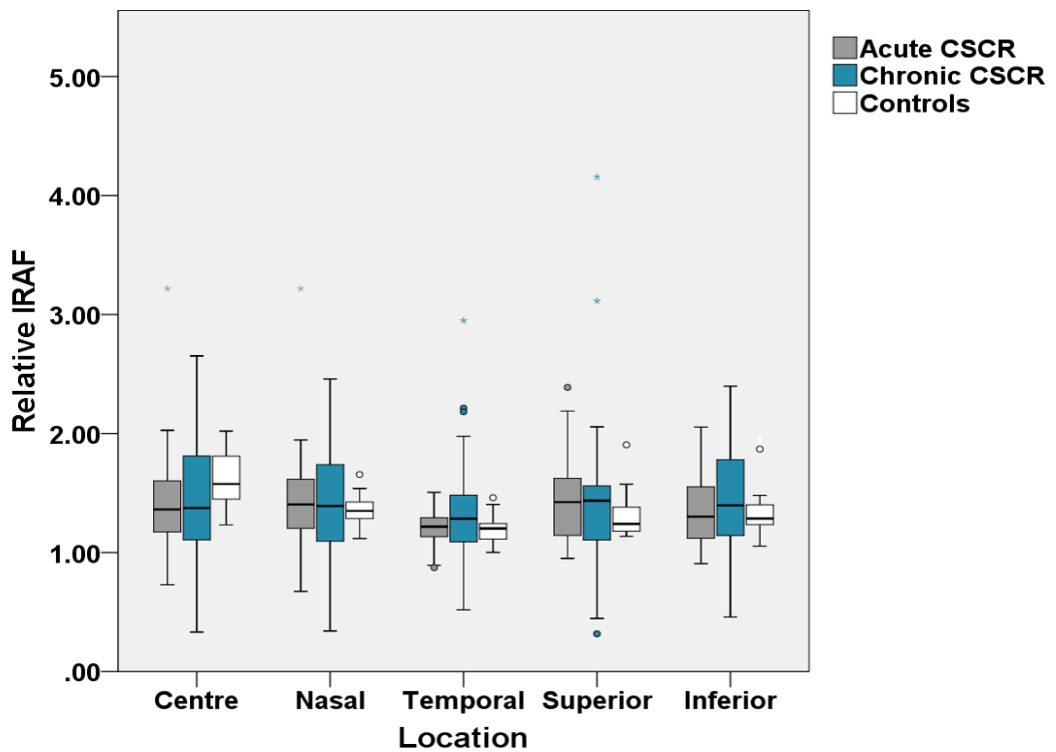


Figure 7.30: Relative NIR-AF levels of the affected CSCR eyes (categorised as acute and chronic) and the control eyes. The tinted box represents the inter quartile range and the whiskers represent the lowest and the highest scores

7.5 Choroidal autoregulation in CSCR

Autoregulation is the ability of a vascular bed to maintain blood flow and vascular structure despite changes in perfusion pressure. To determine this ability of the choroidal vasculature, I used the EDI OCT and LDF in conjunction with isometric exercise in order to assess the choroidal ability to maintain its structure and function, respectively.

Data available for choroidal autoregulation analysis: 10 CSCR (3 bilateral CSCR and 7 unilateral CSCR) and 23 healthy controls.

7.5.1 Autoregulatory ability of choroidal structure

2 CSCR patients and 5 controls were female. The mean age of CSCR patients was 46.7 years (95% CI: 41.0 – 52.4) and 42.3 years (95% CI: 38.9 – 45.7) for controls ($P = 0.14$). The mean IOP was 15.8 mmHg (95% CI: 14.4 – 17.2) for CSCR patients and 16.2 mmHg (95% CI: 14.8 – 17.6) for controls. At the baseline (before isometric exercise), the mean systolic BP of 122.2 mmHg (95% CI: 115.8 - 128.6) and diastolic BP of 76.6 mmHg (95% CI: 69.6 - 83.6) of CSCR patients were slightly but not significantly higher than those of controls (systolic BP: 115.2 mmHg [95% CI: 110.7 - 119.6] and diastolic BP: 74.9 mmHg [95% CI: 72.3 - 77.5]). Following isometric exercise, the mean systolic BP of CSCR patients increased by 39% compared to 43% in control group. The diastolic BP also increased in both groups; however, the level of increase was lower than that of systolic BP (22% for CSCR patients and 20% for controls). This increase in systolic and diastolic BPs corresponded to a 30% increase in MAP and a 40% increase in OPP in both CSCR and control groups, respectively, as shown in **Table 7.12**. There were no significant differences in the changes in MAP and OPP between baseline and at the end of the isometric exercise in both CSCR patients and controls groups.

Table 7.12: Systemic characteristics of controls and CSCR patients (with 95% confidence interval) at baseline and at the end of isometric exercise

	Controls	CSCR patients	P
Number of subjects	22	10	
Age	42.3 (38.9 - 45.7)	46.7 (41.0 - 52.4)	0.14
Male:Female	17:5	8:2	0.86*
IOP	16.2 (14.8 - 17.6)	15.8 (14.4 - 17.2)	0.95 [†]
Before exercise			
Systolic BP	115.2 (110.7 - 119.6)	122.2 (115.8 - 128.6)	0.07
Diastolic BP	74.9 (72.3 - 77.5)	76.6 (69.6 - 83.6)	0.61
MAP	88.3 (85.3 - 91.2)	91.8 (85.4 - 98.2)	0.22
OPP	42.8 (41.0 - 44.6)	45.3 (40.5 - 50.1)	0.19 [†]
After exercise			
Systolic BP	164.0 (156.0 - 172.1)	170.3 (157.9 - 182.7)	0.37
Diastolic BP	89.5 (84.2 - 94.8)	93.1 (84.3 - 101.9)	0.17 [†]
MAP	114.3 (108.8 - 119.8)	118.8 (109.3 - 128.3)	0.19 [†]
OPP	60.1 (56.3 - 63.9)	63.5 (56.6 - 70.4)	0.13 [†]
Change in MAP	1.30 (1.23 - 1.37)	1.29 (1.23 - 1.36)	0.93
Change in OPP	1.41 (1.32 - 1.51)	1.40 (1.32 - 1.48)	0.83

*, Pearson Chi-Square; [†], Mann-Whitney U test

The ChT and retinal thickness were measured at the foveal centre and intervals of 500 µm nasally and temporally to the foveal centre. **Figure 7.31** shows an example of the differences in retinal thickness (**Figure 7.31A**) and ChT (**Figure 7.31B**) after isometric exercise in the right eye of a 46-year old CSCR patient. One healthy control was excluded from the analysis as the scan after isometric exercise failed to be aligned to the baseline reference scan. No significant differences were found between the retinal thickness before and after squatting at any of the measured locations in both control and CSCR groups as shown in **Figure 7.32**.

In the healthy controls, the mean SfChT and total ChT were 376.6 µm (95% CI: 326.0 – 427.1) and 326.5 µm (95% CI: 285.5 – 367.4), respectively at baseline compared to 384.0 µm (95% CI: 329.9 – 438.1) and 331.9 µm (95% CI: 288.8 – 374.9) after squatting. The mean difference in the mean ChT at all locations between baseline and after squatting ranged from 2.76 to 11.86 µm, but not reach statistical significance (**Figure 7.33A**).

In 13 CSCR affected eyes, the mean SfChT and total ChT were 435.3 μm (95% CI: 378.2 - 492.4) and 375.5 μm (95% CI: 327.9 - 423.1), respectively at the baseline compared to 446.3 μm (95% CI: 393.4 - 499.2) and 387.0 μm (95% CI: 341.4 - 432.7) at the end of the squatting ($P < 0.05$). There was significant increase in the ChT at the end of exercise compared to the baseline in all the locations except for the location of 3000 μm and 500 μm temporal to the fovea, as shown in **Figure 7.33B**.

The autoregulatory ability of choroidal structure in unaffected fellow eyes of 7 unilateral CSCR patients was also assessed. There were significant differences in ChT between baseline and at the end of squatting of the unaffected fellow eyes at 1500 μm , 2000 μm , 2500 μm and 3000 μm locations temporal to the fovea whereas difference was not found in other measured locations, as shown in **Figure 7.34**.

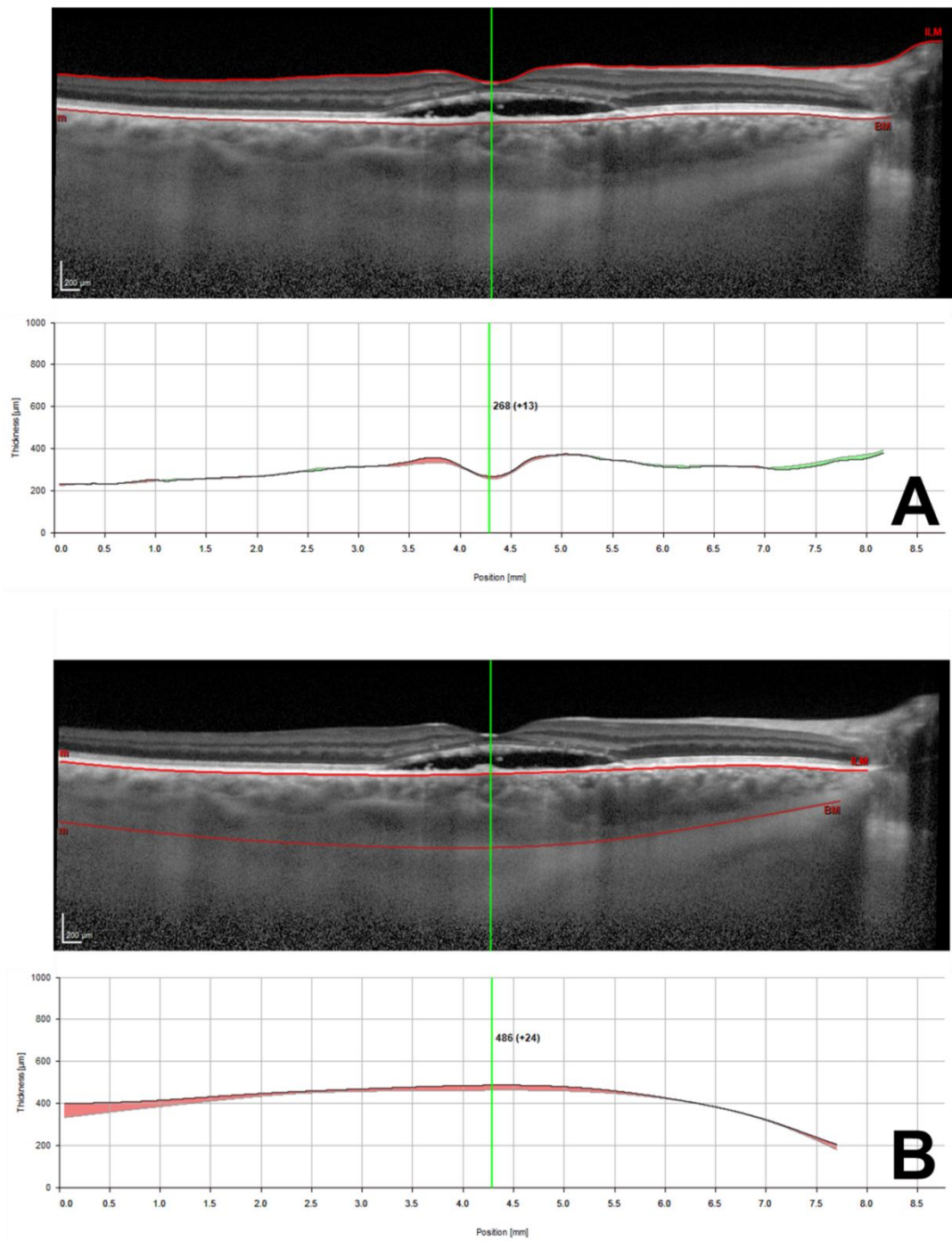


Figure 7.31: Example of differences in the retinal thickness (A) and choroidal thickness (B) measurements of the left eye of a CSCR patient between baseline and at the end of squatting

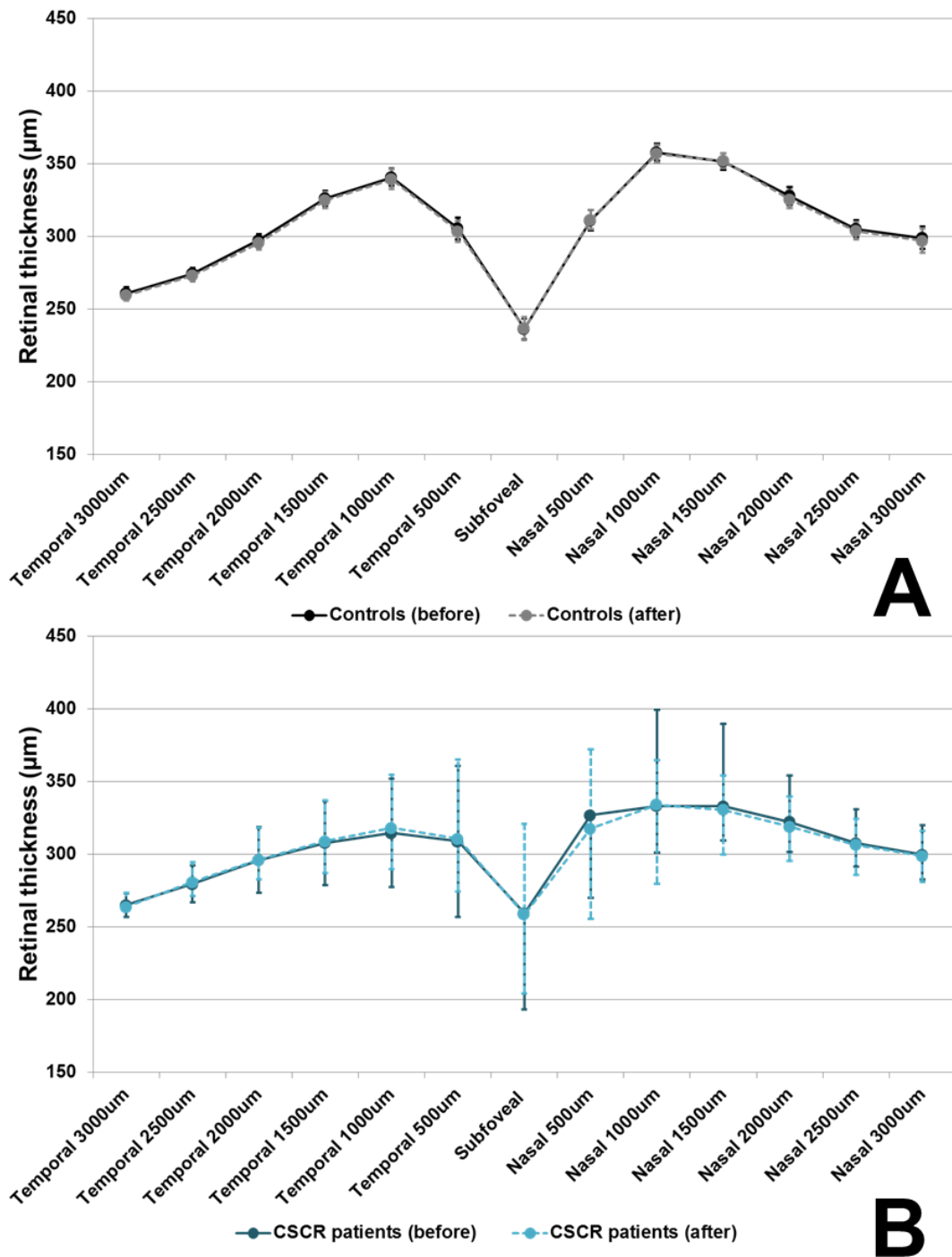


Figure 7.32: The mean (95% confidence interval; error bars) retinal thickness (RT) measured along the horizontal axis of the index eyes at baseline (marked as before) and at the end of squatting (marked as after) in controls (A) and CSCR patients (B)

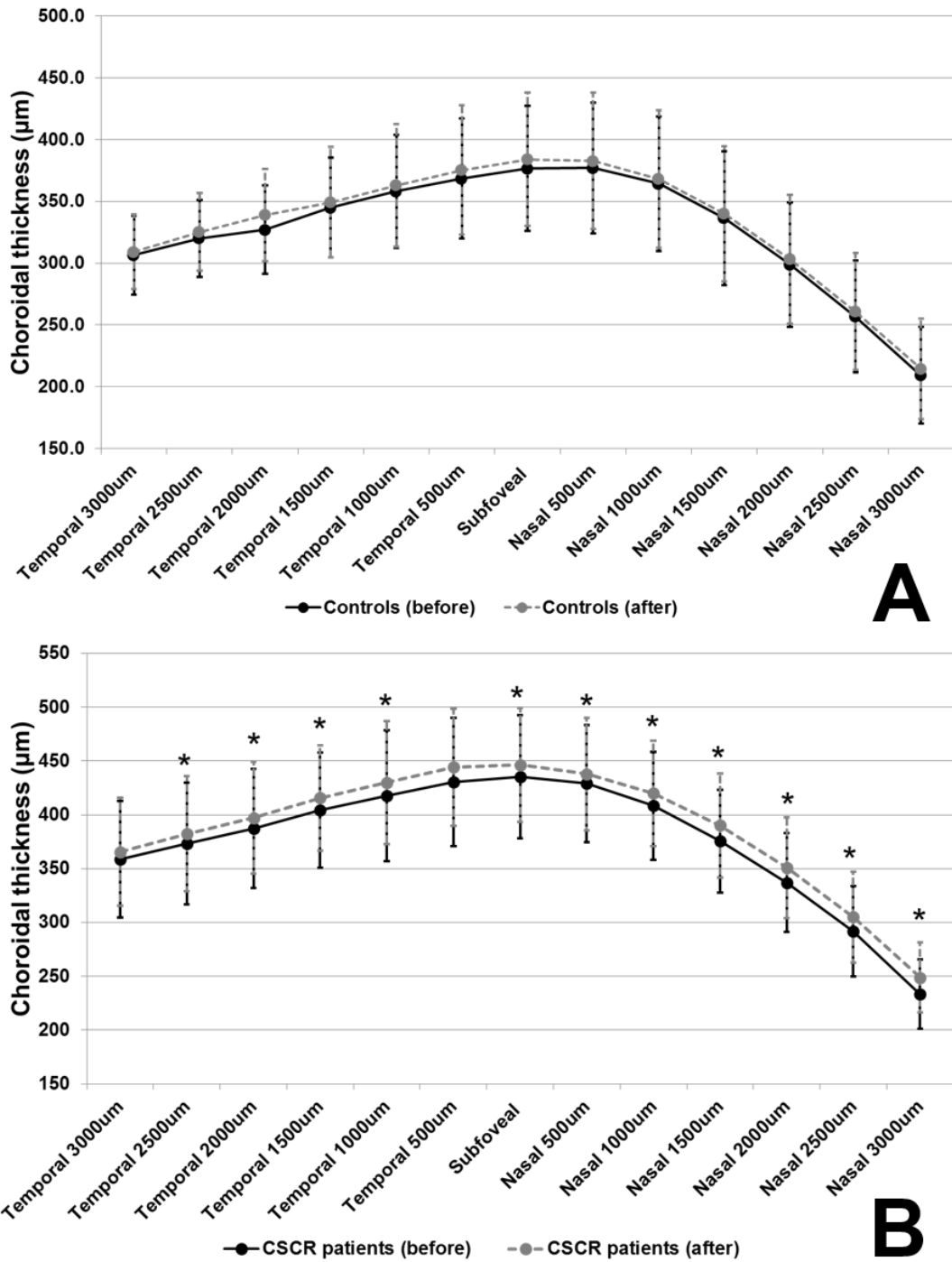


Figure 7.33: The mean (95% confidence interval; error bars) choroidal thickness (ChT) measured along the horizontal axis of the index eyes at baseline (marked as before) and at the end of squatting (marked as after) in controls (A) and CSCR patients (B) (* represents $P < 0.05$)

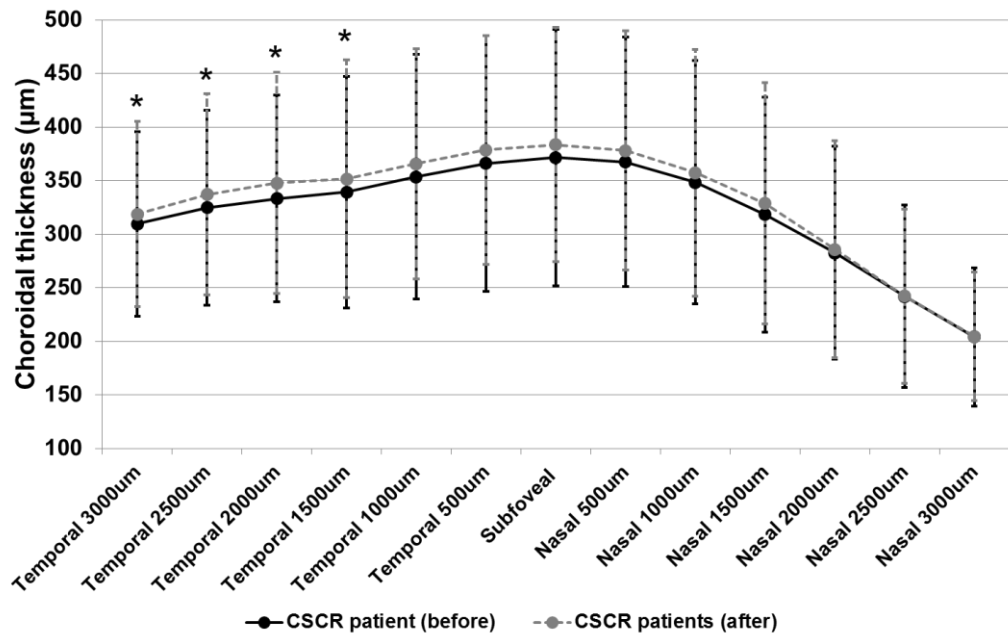


Figure 7.34: The mean (95% confidence interval; error bars) choroidal thickness (ChT) measured along the horizontal axis of the asymptomatic fellow eyes of patients with unilateral CSCR at baseline (marked as before) and at the end of squatting (marked as after) (* represents $P < 0.05$)

7.5.2 Autoregulation ability of choroidal function

Data of 10 patients with CSCR and 22 healthy controls were included in this analysis. Two healthy controls were excluded due to change in the LDF recording program. The mean age of CSCR patients was 46.7 years (95% CI: 41.0 – 52.4) and 43.4 years (95% CI: 40.11 - 46.69) for controls ($P = 0.26$). The mean IOP was 15.8 mmHg (95% CI: 14.4 – 17.2) for CSCR patients and 16.0 mmHg (95% CI: 14.6 - 17.4) for healthy controls. At the baseline (before isometric exercise), the mean systolic BP and diastolic BP were 122.4 mmHg (95% CI: 114.6 - 130.2) and 76.4 mmHg (95% CI: 70.1 - 82.7), respectively for CSCR patients. The mean systolic BP was significantly higher than that of controls (111.7 mmHg [95% CI: 107.2 - 116.2]) but not mean diastolic BP (healthy controls diastolic BP: 72.3 mmHg [95% CI: 69.2 - 75.4]). This higher systolic BP reflected on higher MAP and OPP at the resting stage in CSCR patients when compared to that of healthy controls as shown in **Table 7.13**. After isometric exercise, the mean systolic BP of CSCR patients increased by 36% compared to 40% in control group while diastolic BP increased by 18% for controls and 12% for CSCR patients. These increases in systolic and diastolic BP corresponded to approximately 28% and 23% increase in MAP and 40% and 31% for OPP in controls and CSCR patients, respectively, as shown in **Table 7.13**. There were no significant differences in the increase in mean MAP and OPP after isometric exercise in both CSCR patients and controls groups.

Table 7.13: Systemic characteristics of healthy subjects and CSCR patients (with 95% confidence interval) at baseline and after isometric exercise

	Controls	CSCR patients	P
Number of subjects	20	10	
Age	43.4 (40.1 - 46.7)	46.7 (41.0 - 52.4)	0.26
IOP	16.0 (14.6 - 17.4)	15.8 (14.4 - 17.2)	0.88 [†]
Before exercise			
Systolic BP	111.7 (107.2 - 116.2)	122.4 (114.6 - 130.2)	0.01
Diastolic BP	72.3 (69.2 - 75.4)	76.4 (70.1 - 82.7)	0.16
MAP	85.4 (82.1 - 88.8)	91.7 (85.1 - 98.3)	0.05
OPP	41.0 (38.8 - 43.1)	45.4 (40.5 - 50.2)	0.04
After exercise			
Systolic BP	156.2 (149.3 - 163.1)	167.0 (148.0 - 186.0)	0.58 [†]
Diastolic BP	85.9 (81.7 - 90.0)	85.7 (77.2 - 94.2)	0.97
MAP	109.3 (104.6 - 114.0)	112.8 (102.3 - 123.3)	0.45
OPP	56.9 (53.8 - 60.0)	59.4 (51.8 - 67.0)	0.43
Change in MAP	1.28 (1.23 - 1.33)	1.23 (1.17 - 1.29)	0.18
Change in OPP	1.40 (1.32 - 1.47)	1.31 (1.23 - 1.38)	0.13

[†], Mann-Whitney U test

The mean differences of DC, ChBVolume, ChBVelocity and ChBFlow between baseline and at the end of isometric exercise are represented in **Table 7.14**. No significant difference in choroidal blood flow parameters at baseline and at the end of squatting was noted in either healthy controls or CSCR patients. **Figure 7.35** shows the mean DC, ChBVolume, ChBVelocity and ChBFlow at baseline and at the end of squatting in controls and CSCR patients respectively.

When the mean changes in choroidal blood flow parameters from baseline were compared between groups, the change in ChBVolume was significantly larger in CSCR patients (-2%) compared to that of healthy controls (1%) ($P = 0.03$). No significant difference was observed in the change in ChBVelocity (-1% for CSCR and 2% for controls) while the change in ChBFlow (-3% for CSCR and 3% for controls) was at a borderline significance ($P = 0.07$), as represented in **Table 7.15**. **Figure 7.36** shows the changes in DC, ChBVolume, ChBVelocity and ChBFlow at the end of isometric exercise of controls and CSCR patients. There was no significant difference in the change in Rm between controls and CSCR patients.

Table 7.14: The mean differences in DC, ChBVolume, ChBVelocity and ChBFlow between baseline and at the end of isometric exercise (with 95% confidence interval) of controls and CSCR patients

Choroidal blood flow parameters	Controls	P	CSCR	P
DC	0.001 (-0.005 - 0.008)	0.73	-0.009 (-0.021 - 0.003)	0.11
ChBVolume (AU)	-38.13 (-85.36 - 9.11)	0.11	77.15 (-37.73 - 192.03)	0.16
ChBVelocity (Hz)	-24.29 (-64.37 - 15.79)	0.22	46.09 (-39.28 - 131.46)	0.25
ChBFlow (AU)	-155.23 (-335.28 - 24.82)	0.09	371.36 (-175.60 - 918.32)	0.16

Table 7.15: Comparison of DC, ChBVolume, ChBVelocity and ChBFlow changes from baseline between DR patients and controls. Results are shown as a fraction of 1

Choroidal blood flow parameters	Controls	CSCR	P
Change in DC	0.99 (0.97 - 1.02)	1.04 (0.99 - 1.09)	0.25 [†]
Change in ChBVolume	1.00 (1.00 - 1.02)	0.98 (0.95 - 1.01)	0.03
Change in ChBVelocity	1.02 (0.99 - 1.04)	0.99 (0.96 - 1.02)	0.25 [†]
Change in ChBFlow	1.03 (1.00 - 1.06)	0.97 (0.93 - 1.02)	0.07 [†]
Change in Rm	1.36 (1.29 - 1.44)	1.35 (1.26 - 1.43)	0.60 [†]

[†], Mann-Whitney U test

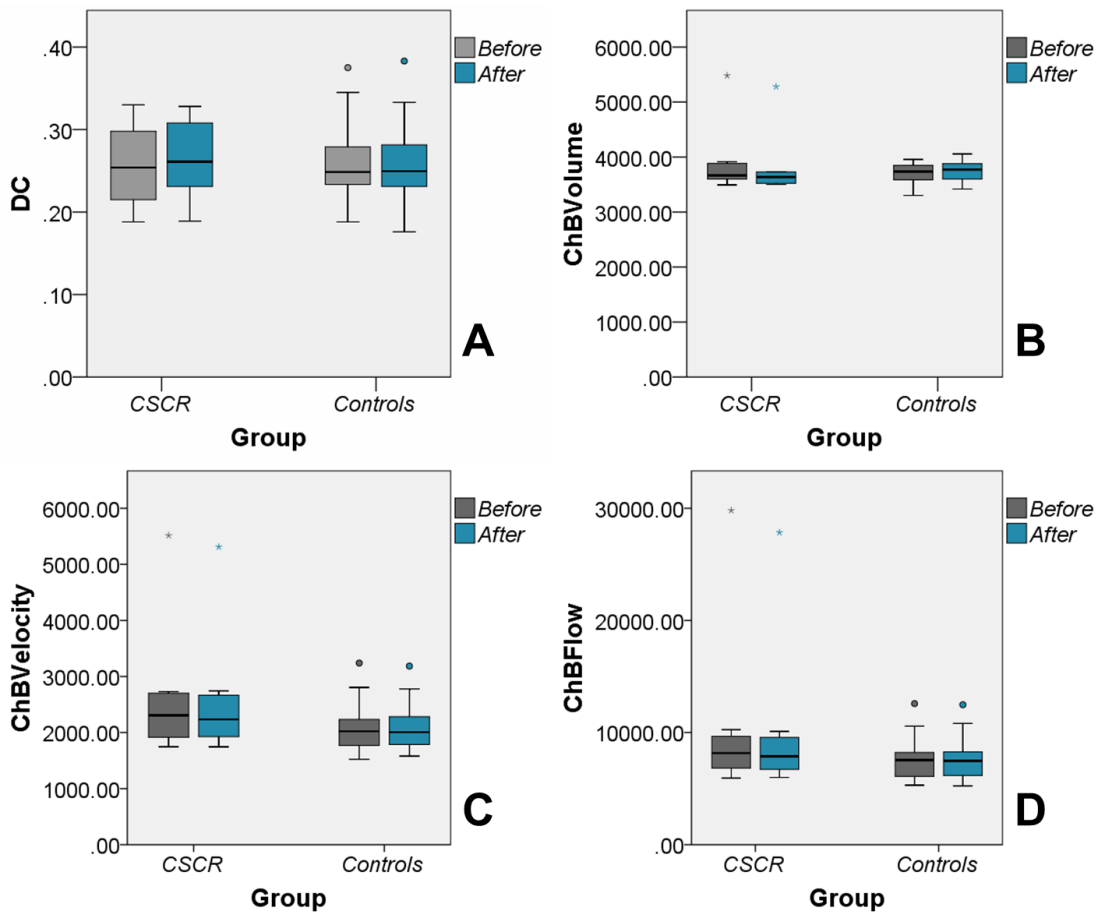


Figure 7.35: The mean DC (A), ChBVolume (B), ChBVelocity (C) and ChBFlow (D) at baseline (before isometric exercise) and after isometric exercise of CSCR patients and healthy controls. The tinted box represents the inter quartile range and the whiskers represent the lowest and the highest scores

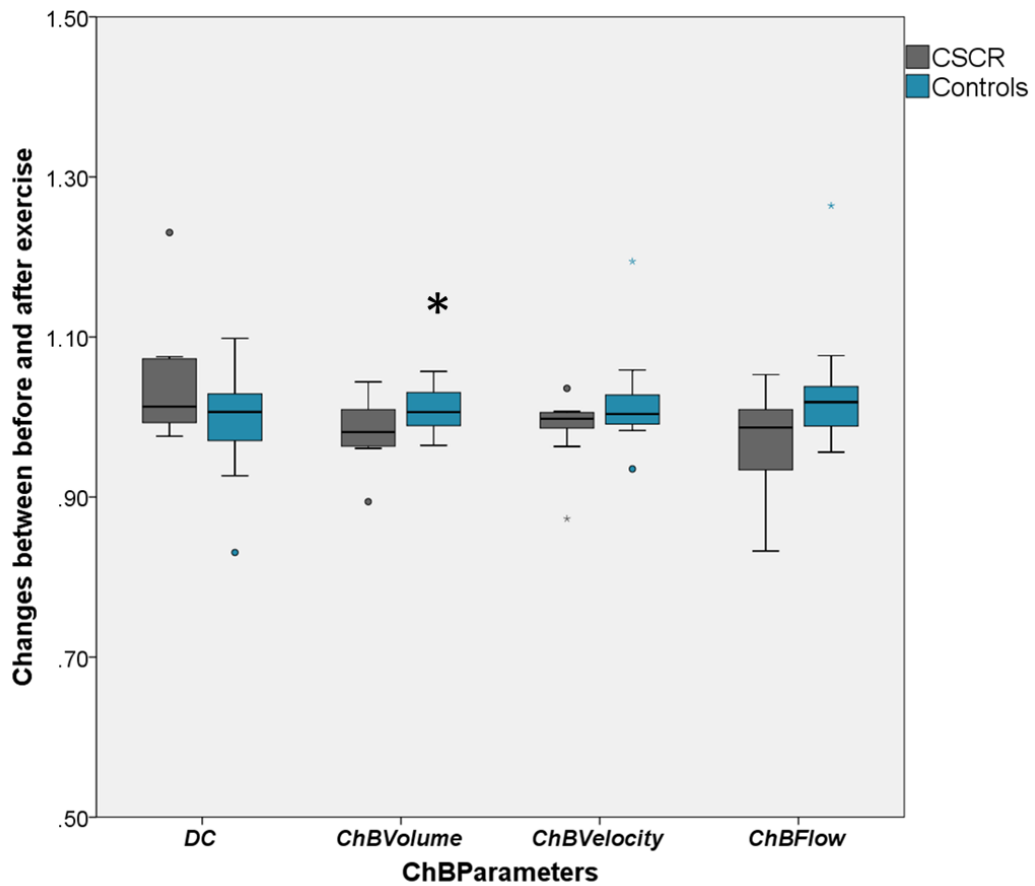


Figure 7.36: Changes in DC, ChBVolume, ChBVelocity and ChBFlow in CSCR patients and healthy controls following the isometric exercise. The tinted box represents the inter quartile range and the whiskers represent the lowest and the highest scores

7.5.3 The relationship between choroidal structure and function

Linear correlation was used to determine the relationship between changes of ChBFlow parameters, systemic parameters, choroidal vascular resistance (R_m ; calculated using the equation 4.5

$[Change\ in\ R_m = Change\ in\ OPP / Change\ in\ ChBFlow]$), and the thickness of the choroid and retina following isometric exercise.

In healthy controls, there was a positive correlation between the changes in DC level to the total retinal thickness and a negative correlation between changes in ChBVelocity and total retinal thickness. These relationships, however, were not observed in CSCR patients. There were no relationships found between the changes in choroidal function parameters and changes in ChT after an increase of OPP.

In CSCR patients, on the other hand, no significant relationship was observed between changes in choroidal blood flow parameters to the change in the ChT. Interestingly, the change in ChBVolume was significantly negatively correlated with the change in Rm (**Figure 7.37**) and was found exclusively in CSCR patients. **Table 7.16** summarises the relationship between changes in choroidal function and choroidal and retinal structure after increase of OPP.

Table 7.16: Pearson's correlation coefficients between changes in choroidal function and structure following isometric exercise

		Change in choroidal function			
		DC	ChBVolume	ChBVelocity	ChBFlow
Change in choroidal and retinal structure	<i>Controls</i>				
	SfChT	-0.16	-0.30	0.30	0.15
	Total ChT	-0.08	-0.31	0.14	0.04
	SfRT	0.28	0.22	-0.38	-0.32
	Total RT	0.46*	0.10	-0.46**	-0.45
	Rm	0.39	0.02	-0.32	-0.30
	<i>CSCR</i>				
	SfChT	-0.32	0.14	0.40	0.37
	Total ChT	-0.40	0.11	0.46	0.41
	SfRT	-0.40	0.32	0.41	0.47
	Total RT	0.18	0.18	-0.16	-0.02
Rm	0.46	-0.83***	-0.16	-0.51	

* $P = 0.047$, ** $P = 0.046$ and *** $P = 0.003$; SfChT = subfoveal choroidal thickness, SfRT = subfoveal retinal thickness, Rm = choroidal vascular resistance

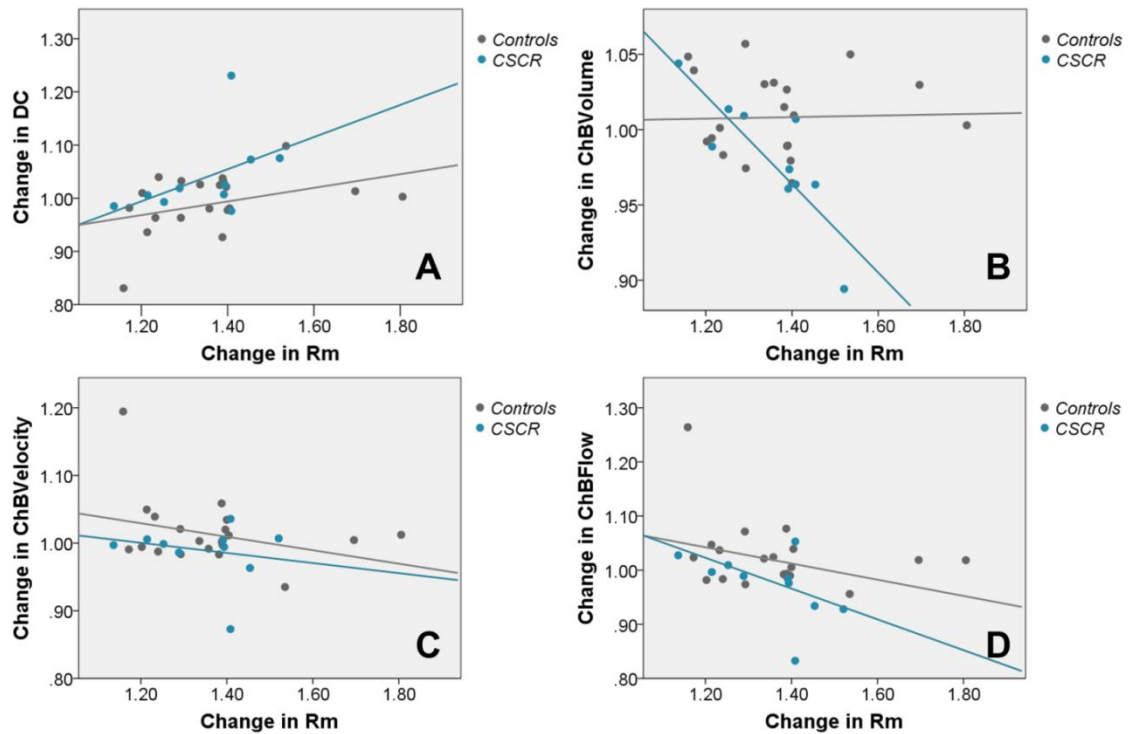


Figure 7.37: The scatter plot of changes in choroidal vascular resistance (Rm) after isometric exercise with changes in DC, ChBVolume, ChBVelocity and ChBFlow in CSCR patients and controls

7.6 Retinal function in CSCR

7.6.1 Static and dynamic fixation

I quantified the fixation in CSCR patients and controls using the static fixation test and dynamic microperimetry test. The bicurve ellipse area (BCEA) values representing the areas of 3 ellipses on which the eye fixates on the target for 68.2%, 95.4% and 99.6% of time were shown in **Table 7.17**. There were no statistically significant differences in fixation between CSCR eyes and controls. Interestingly, CSCR eyes demonstrated a small degree of unstable dynamic fixation and more stable static fixation when compared to that of controls.

Table 7.17: Dynamic and static fixation of CSCR patients and controls

	Controls	CSCR	P
<i>Dynamic fixation</i>			
68.2 % BCEA	1.0 (0.7 - 1.2)	1.0 (0.6 - 1.4)	0.70 [†]
95.4% BCEA	2.6 (1.8 - 3.4)	2.7 (1.5 - 3.9)	0.75 [†]
99.6% BCEA	4.7 (3.3 - 6.0)	4.8 (2.7 - 6.9)	0.71 [†]
Fixation within 2°	94.2 (91.5 - 97.0)	93.5 (87.4 - 99.6)	0.67 [†]
Fixation within 4°	99.4 (99.0 - 99.8)	99.2 (98.1 - 100.3)	0.91 [†]
<i>Static fixation</i>			
68.2 % BCEA	0.4 (0.2 - 0.6)	0.4 (0.1 - 0.8)	0.95 [†]
95.4% BCEA	1.2 (0.7 - 1.7)	1.1 (0.1 - 2.0)	0.60 [†]
99.6% BCEA	2.0 (1.1 - 2.9)	1.9 (0.3 - 3.5)	0.90 [†]
Fixation within 2°	98.8 (97.7 - 99.9)	99.4 (98.6 - 100.2)	0.81 [†]
Fixation within 4°	99.7 (99.4 - 100.0)	99.8 (99.3 - 100.3)	0.41 [†]

[†] Mann-Whitney Test

7.6.2 Retinal sensitivity

The mean total retinal sensitivity was 15.3 dB (95% CI: 13.0 - 17.5) and 19.6 dB (95% CI: 19.2 - 20.1) for CSCR patients and controls, respectively. The mean retinal sensitivity was approximately 15 – 23% lower in CSCR patients with the lowest at the central area of the macula where it could be reduced by as much as 59%. The mean retinal sensitivity over the macula of controls and CSCR patients is shown in **Table 7.18**.

The relationship between the retinal function determined as the sensitivity on microperimetry and the structural changes of the retina and choroid as found on autofluorescence imaging and EDI OCT was assessed in CSCR patients. There was no relationship between retinal sensitivity and choroidal structures at any of the ETDRS subfields. The retinal sensitivity correlated positively to the retinal thickness while being negatively correlated to the levels of FAF and NIR-AF as shown in **Table 7.19**.

Table 7.18: The mean retinal sensitivity at the macula of controls and CSCR patients

ETDRS subfields	Controls	CSCR	P
Central	19.5 (18.9 - 20.1)	12.2 (9.1 - 15.2)	<0.05 [†]
Nasal	19.5 (18.8 - 20.3)	16.9 (14.9 - 18.9)	<0.05 [†]
Temporal	19.9 (19.8 - 20.0)	16.9 (14.5 - 19.4)	<0.05 [†]
Superior	19.5 (19.0 - 20.1)	15.9 (12.8 - 19.0)	<0.05 [†]
Inferior	19.8 (19.5 - 20.1)	16.5 (14.4 - 18.6)	<0.05 [†]
Total	19.6 (19.2 - 20.1)	15.3 (13.0 - 17.5)	<0.05 [†]

[†] Mann-Whitney Test

Table 7.19: Pearson's correlation coefficients of retinal sensitivity and choroidal and retinal thickness and the level of FAF and NIR-AF in CSCR patients on each ETDRS subfield.

	Retinal sensitivity					
	Central	Nasal	Tempo ral	Superio r	Inferior	Total
Choroidal structure						
SfChT	-0.321					
Central subfield ChT	0.366					
Inner nasal		-0.454				
Inner temporal			-0.417			
Inner superior				0.072		
Inner inferior					-0.495	
Total ChT						-0.348
Retinal structure						
SfRT	0.222					
Central subfield RT	0.537					
Inner nasal		0.657*				
Inner temporal			0.506			
Inner superior				0.920**		
Inner inferior					0.240	
Total ChT						0.653*
FAF						
Central	-0.125					
Nasal		-0.804**				
Temporal			-0.521			
Superior				-0.801**		
Inferior					-0.019	
NIR-AF						
Central	-0.384					
Nasal		-0.832**				
Temporal			-0.727*			
Superior				-0.490		
Inferior					-0.347	

* $P < 0.05$, ** $P < 0.001$

7.7 Summary

In this chapter I have presented an investigation of the demographic characteristics and risk factors associated with CSCR. The changes in choroidal structure in ICGA and EDI OCT have been reported. The changes in choroidal function as measured by LDF have been studied. From the analyses I have demonstrated a reduced ability of the choroid to autoregulate morphologically and functionally in eyes with CSCR compared to normal healthy eyes.

The main complaint of CSCR patients during their hospital visit was reduced and/or blurred vision and transient seeing a grey/dark spot at the centre of their vision. Interestingly, nearly 30% of CSCR patients in my cohort experienced ocular pain and discomfort in the affected eye and a few patients reported migraine.

The risks of developing CSCR previously reported include systemic administration of steroid, pregnancy, alcohol use, antibiotic use, antihistamine use, autoimmune disease, untreated hypertension and tobacco use.²⁰⁰ My results partly supported these findings; previous use of steroid and hypertension were the main risk in our population. Hypertension was documented in 33% of my CSCR patients and 17% more of the CSCR patients had high BP (BP > 140/90 mmHg without medication) at study entry. No obvious risk association with tobacco use, urinary or gastrointestinal tract disorders in my CSCR patient cohort.

According to the previous literature, stress was reported as being associated with CSCR. In my studies, the information related to stress was developed further in 3 ways. First, the NS-SEC was used to determine the socio-economic class using patient occupation variations. This indicates work related stress. Second, patient stress profile was directly assessed using multifactorial questionnaires. Lastly, the level of cortisol which is related to the stress level was determined. My results showed that the majority of CSCR patients had level 4 NS-SEC which represents small employers and own account workers group. This was approximately 2 fold higher than the general population in the UK and Merseyside. Moreover, higher plasma cortisol level and higher scores in LEQ, PHQ-9, PHQ-15 and PSS were observed in CSCR patients compared with healthy controls. The mean PSS score of CSCR patients was 22.4 indicating a high level of stress among them.

Changes in choroidal structure were investigated with EDI OCT and ICGA in treatment naïve patients. Thicker and greater volume of the choroid was clearly observed in CSCR patients in symptomatic eyes. An approximately 30% increase in ChT and ChVolume compared to healthy eyes was observed in CSCR patients. The

comparative analysis between active and inactive CSCR showed that the choroid became thinner by 10% after the resolution of SRF. No significant differences in ChT and ChVolume were observed in either between acute and chronic CSCR, or between unilateral and bilateral CSCR.

The thickening of the choroidal structure was not only observed in the symptomatic eyes but also in the asymptomatic fellow eyes of patients with unilateral CSCR. Although no statistical significance was found between the asymptomatic fellow eyes and healthy controls, a thickening of around 8% was observed in the asymptomatic fellow eyes. The differences in ChT and ChVolume were greater if the asymptomatic fellow eyes had choroidal hyperpermeability seen on ICGA. In the affected eyes, the ChT within the hyperpermeability area was significantly thicker than that of the area without hyperpermeability. These morphological changes of the choroidal vasculature were also observed in the unaffected fellow eyes of unilateral CSCR.

The role of steroid use and hypertension as contributory factors for the increased ChT seen on EDI OCT was studied. The results showed that there were significant differences in ChT over the macular area in CSCR patients with and without hypertension compared to healthy controls while the overall ChT at the macula of CSCR patients with hypertension was the thickest. The history of steroid use did not affect ChTs.

These results confirm a choroidal structural abnormality in CSCR eyes. I further hypothesised that these changes reflected failure of choroidal autoregulation which in turn led to SRF accumulation at the macula. I studied this phenomenon by assessing the choroidal structure and function under physiological stress induced by isometric exercise (squatting). Following exercise, MAP increased by approximately 30% and OPP by approximately 40% whilst ChT increased significantly in CSCR patients but not in controls. More specifically, small but significant changes by approximately 2.5% of SfChT and 3% of total ChT were observed in CSCR patients.

The changes in choroidal function were evaluated by studying blood flow parameters using LDF. At the end of isometric exercise, the OPP increased by approximately 31% in CSCR and 40% in controls. When comparing the blood flow parameters between baseline and at the end of isometric exercise, no significant differences were observed in blood flow parameters in both of the groups. However, the mean change of ChBVolume from baseline in CSCR patients was significantly greater than that of healthy eyes (ChBVolume changed by -2% in CSCR and 1% in

healthy controls). No obvious associations were observed between changes in ChBFlow and in ChT after an increase in OPP. The change in ChBVolume in CSCR patients, however, was strongly negatively associated with the changes in the choroidal Rm.

In summary, my results provide further evidence that the choroid in CSCR eyes has not only structural alteration but also functional abnormality. These findings further support the choroidal dysfunction theory of the pathogenesis of CSCR.

Chapter

8 Discussions and conclusions

The study of choroidal structure and function using the latest imaging modalities available within our clinical setting has been the primary focus of this thesis. In this chapter I discuss my principle findings and relate them to the previous literature. I interpret my findings in understanding the role of the choroid in the pathogenesis of diabetic retinopathy and CSCR. I then go on to discuss future directions and research innovations in choroidal imaging.

8.1 Standardisation of choroidal thickness measurements

In Chapter 3, I described the development and validation of a standardised protocol to measure the choroidal thickness (ChT) on EDI OCT. The results presented in Section 3.2 showed that my protocol could achieve moderate ($K = 0.42$) and perfect ($K = 1$) inter- and intra-observer agreements on classifications of images from healthy eyes and substantial ($K = 0.66$) and almost perfect ($K = 0.86$) agreements from diabetic eyes. The proposed protocol also showed excellent inter- and intra-observer agreements for ChT measurements on both healthy and diabetic eyes ($ICC > 0.90$).

The measurement of ChT is challenging in part due to the fact that the measurements have to be done manually, often introducing considerable variation due to the poor definition of the transitional zone between the outer choroidal boundary and the sclera even in the absence of pathology. A clear standardised definition of the limits of the outer boundary of the choroid on EDI OCT images is

needed in order to allow a comparison across clinical studies as this can affect the reliability of measurements, especially for those scans taken from diseased eyes.

To address this, I developed a protocol based on the presence and/or absence of the suprachoroidal space (SCS) and the choroidal-scleral interface (CSI), seen as the hypo-reflective and the hyper-reflective bands respectively at the outer boundary of an EDI-OCT image. Variations in the topographical appearance of the choroidal posterior boundary have been known to affect ChT measurements. This has been shown in the results presented in this thesis as well as in a previous study.⁴⁴ Maul *et al* have used the presence of CSI alone to classify EDI OCT images into good, fair and poor. They found images with poor quality had the thickest ChT compared to fair and good quality images ($P < 0.001$). This study, however, did not mention the agreement on image classification. In my protocol, a relatively large variation in the choroidal measurement agreement was found in the group of scans in which the choroidal outer boundary structure was less visible, emphasising the importance of having a good technique to acquire and interpret ChT accurately.

Although I took great care during EDI OCT imaging, I was only able to make a ChT measurement in 95 – 98% of cases mainly due to the variation of choroidal outer boundary. The choroidal outer boundary could not always be observed for several reasons: 1) patient fixation, 2) choroidal anatomical variation such as the thick choroid typically seen in young people or CSCR patients and 3) variation across commercially available OCT instruments. Studies using Cirrus® HD OCT (~840 nm light source with axial resolution of 5µm), measured ChT in only 74 – 90% of cases.^{77, 247} The Heidelberg® Spectralis OCT (~870nm light source with axial resolution of 7µm) produces better images giving successful ChT measured in 92 - 96% of cases.^{56, 248} Using Topcon® 3D-OCT 1000 (~850 nm light source with axial resolution of 6 µm), Shin *et al*⁵⁰ reported ChT measurable rate of 63.3% on their population. Cirrus, Heidelberg and Topcon instruments are spectral domain (SD) OCTs. Swept source (SS) OCT technology uses a longer wavelength with a centred wavelength of 1050 - 1060 nm resulting in a better penetration into deeper structures. The outer boundary of the choroid was visualised in 100% of patients by SS OCT compared to 74.4% by Topcon® 3D-OCT²⁴⁹ and 73.6% by Cirrus® HD OCT with EDI function and 68.4% Cirrus® HD OCT without EDI function.⁶⁴ The standardised protocol I have developed could be applied to SS OCT to improve the reliability of ChT measurement.

In order to measure the ChT in a clinical setting, manual ChT measurement techniques require adequate inter- and intra-observer agreements. In Chapter 3 I have shown that using my protocol excellent inter- and intra-observer agreements for the ChT measurements on both, healthy eyes and diabetic eyes (ICC >0.90 in all image categories) could be achieved. The inter-observer ICC derived from this protocol was higher than reported in a previous study in subjects with diabetes (Pearson's coefficient $r = 0.81$) using the Heidelberg Spectralis OCT.¹⁷⁵

In addition to the correlation of the ChT measurement, coefficient of repeatability (CR) has also been used to determine the agreement of manual ChT measurements. I have shown that in patients with diabetic retinopathy, the inter-observer CR for SfChT was 54 μm using our proposed measurement protocol. The intra-observer CRs for ChT measurements in diabetic patients were generally smaller than the inter-observer CRs. The intra-observer CRs obtained were 18 μm (range: 9 – 22) for the total ChT and 36 μm (range: 21 – 47) for SfChT. These results are consistent with those of previous studies on the ChT measurement in other retinal diseases, such as AMD and CSCR.²⁵⁰

Inter- and intra-observer agreements on ChT measurements in diabetic eyes have been reported previously by Vujosevic *et al*¹⁷⁷ and Sim *et al*.⁴² Vujosevic reported the CR for inter-observer agreement on SfChT of 29 μm (95% CI: 24.8 – 32.8). Sim reported the 95% limits of agreement for the central ETDRS subfield of 53 μm . It is difficult to make a direct comparison between my results and those provided by previous reports for several reasons: 1) the different SD OCT device and choroidal segmentation method used in each study. The Vujosevic and Sim studies did not take into account the topographical variation in the outer boundary of the choroid on EDI OCT images, 2) the number of points measured and the methods used to measure the ChT were different and 3) the statistical methods used to report the measurement agreements.

In healthy eyes, Rahman *et al* reported a CR of 23.3 μm (95%CI, 18.7 – 27.9) for intra-observer and >32.1 μm (95%CI, 30.0 – 4.9) for inter-observer agreements on SfChT measurements.⁵⁹ In patients with chorioretinal diseases, the CRs were shown to increase from the normal range.²⁵⁰ This may suggest an increase in the variability of the ChT measurements as the choroidal outer boundary becomes less recognisable, possibly due to changes in retinal structures. This is supported by a higher CR from my results in patients with diabetes and a previous study by Kim *et al*.²⁵⁰ Kim studied the variability of SfChT measurement on 160 patients with various

eye diseases and reported the CR ranged between 24-26 μm for dry AMD, 30-36 μm for exudative AMD, 39-45 μm for polypoidal choroidal vasculopathy (PCV) and 46-50 μm for CSCR.²⁵⁰

My results have also shown that CR values increased for both, inter- and intra-observer as the choroidal outer boundary becomes less identifiable (with the smallest in group A). This suggests a direct impact of the image quality on the thickness measurements. Hence great care needs to be taken when interpreting the results of studies, including pre- and post-treatment comparisons that do not report image quality parameters at the outset. In recent years automation techniques for the segmentation of the choroid are becoming an active research topic and the validity is yet to be established.²⁵¹ To evaluate the performance of these automatic techniques, the manual annotations by experts are usually used as a reference standard and a standardised protocol such as I have developed will be preferred.

8.2 The choroidal thickness in healthy eyes

In Chapter 5, I have analysed data derived from a single horizontal line EDI OCT scan of 9 mm and the EDI OCT volume scan. My data allowed an estimation of the variation of the anatomical topography of the choroid in healthy eyes of a sample in the UK. The results obtained from Chapter 5 demonstrate the asymmetrical nature of the choroid in healthy eyes, seen in both horizontal and volumetric scans. In the single horizontal scan, the choroid displayed a bowl shaped appearance. The thickest point was found at the foveal centre with a mean ChT of 351 μm (95% CI: 321 – 381) in our normal eyes with mean age of 45 years (range: 29 - 67). The thickness decreased nasally and temporally, reaching a thinner point 3 mm temporal to the foveal centre and the thinnest point 3 mm nasal to the foveal centre. The mean total horizontal ChT was 304 (278 – 330) μm . These results are based on healthy eyes with a refractive error within ± 3.00 (spherical equivalent), without any previous eye disease, treatments or visual correction procedures. Various previous studies have used different selection criteria and definitions for normal. Margolis *et al*⁴⁷ defined their normal eyes as those with no pathological features seen on the selected scans regardless of pathology elsewhere or in the contralateral eyes. Others excluded participants with retinal or choroidal abnormalities seen on OCT⁷⁷ while some excluded participants with symptoms of a systemic disorder.⁵² The most commonly used criterion to define normal eyes is the refractive error, and in our case, ± 3.00 was used while others have used ± 6.00 .^{52, 77}

The SfChT obtained from my healthy participant cohort is in agreement with a previous study using the same SD OCT device with a similar populations age distribution.²¹² The SfChT results were also comparable to those using the more recent SS OCT technology.^{57, 65, 68} In a study of the UK population, Rahman *et al*⁵⁹ reported a mean SfChT of 332 μm (range: 172 – 550) and 332 μm (range: 142 – 563) for the right and the left eyes respectively in healthy participants with a mean age of 38 years (range: 30 – 49). Our results show, however, the mean SfChT was thicker in both eyes (mean SfChT of 363 μm [range: 169 – 546] for the right eye and 339 μm [range: 181 – 626] for the left eye). This discrepancy between mine and their results may derive from various sources, such as subject selection criteria, ChT measurement methods and ethnicity of participants, Caucasian in my healthy cohort as opposed to mixed race for Rahman. Karapetyan *et al*²⁵² estimated the interethnic variation of the ChT among 88 healthy participants (30 = Caucasians, 30 = Africans and 28 = Asians) with age ranging from 20 - 40 years. ChT was thickest in Caucasians (mean \pm SD; 403.62 \pm 37.4 μm) followed by Asians (383.64 \pm 40 μm) and Africans (372.47 \pm 31.4 μm).

When 2 eyes were compared, no significant differences were found between the right and left eyes from the centre of the fovea towards the temporal side. The differences, however, became significant towards the nasal side with the mean difference of 18.85 μm between the 2 eyes. These results were similar to those reported previously by Chen *et al*.⁵⁸ Chen *et al* reported no significant interocular differences between right and left at the foveal centre. The authors also suggested that there is a weak inverse relationship between age and interocular differences. The reason for interocular difference of the ChT at the nasal side is likely to be due to the refractive error as it has been shown in animal experiments.¹⁶ However, I did not determine this association.

Using the volume scan covering the ETDRS grid area, I have shown that the ChT gradually increases from the temporal side towards the foveal area. The ChT gradually decreases towards the nasal area, reaching the thinnest point close to the optic disc. I have also shown that the ChT gradually increases from the superior location towards the fovea and gradually decreases inferiorly. This can be summarised for the ETDRS overlay as central subfield > inner superior > inner temporal > inner inferior > outer superior > inner nasal > outer temporal > outer inferior > outer nasal. My results are comparable to previous reports.^{75,72, 74} This asymmetrical nature of the choroid at the macula differs from that observed in the

retina where the thinnest part was observed at the central area, becoming thicker towards the nasal part.

The reasons why the choroid becomes thinner towards the nasal part and thickest at the fovea are unclear but three possible reasons can be proposed based on the anatomical and vascular system of the choroid.

1) Narrower choriocapillaris diameters are found in the area surrounding the optic disc.¹⁵

2) The retina is partly supported by branches of the Circle of Zinn and short posterior ciliary arteries (PCA)s at the peripapillary and the nasal regions suggesting less choroidal blood supply is required in this area.²⁵³ This is in contrast to the vessel free zone in the retina at the fovea; hence the thicker choroid at the foveal region may serve as compensation for the lack of retinal blood supply.

3) The O₂ and nutrition requirements for the different retinal photoreceptors may also contribute to a thicker choroid at the fovea and thinner at the surrounding areas. This could be explained as follows: the retina consists of 2 types of photoreceptors, cones and rods. Cones concentrate at the foveal region and rods in the periphery.²⁵⁴ Rods demand high O₂ and produce higher heat compared to cones and any other cells in the body.^{255,256} The retinal blood supply has low flow and high O₂ exchange compared to the choroid which has a higher flow but less O₂ exchange.²⁵⁴ Hence, the retinal blood supply is more attuned to rod physiology whereas the choroidal system is suitable more for cone physiology. This suggests an evolution of the choroidal structure to serve the nutritional demand of the photoreceptors during embryogenesis.

Age was the main factor affecting the ChT in my healthy population. The effect of ageing on ChT started from the age of 50, predominantly at the foveal centre towards the temporal side. My results show that the decrease in ChT was 23% to 34% from age ≤40 years to >50 years. Regression analysis estimated that SfChT and total ChT decreased by 3.54 μm and 2.86 μm, respectively for each age year. The results derived from my model were higher than the 1.56 μm per year reported by Margolis *et al.*⁴⁷ The discrepancy between my model and their model might be on one hand due to the age range used in both studies and on the other to the participant selection criteria. The relationship between the age and the reduction of the ChT has also been reported by other studies on healthy eyes, for example Wei *et al.*⁴⁸ reported a decrease of SfChT by 4.1 μm per year among Chinese healthy

eyes and Ikuno *et al*⁶⁵ reported a decrease of SfChT by 4.32 μm per year in Japanese healthy eyes. These studies, however, only reported the reduction of ChT at one location and did not represent the volumetric structure of the choroid.

Other factors affecting the ChT include axial length (AxL)^{48, 55, 86} and refractive error.^{48, 55, 86} These two parameters are generally highly correlated; the greater the myopia, the greater the AxL. Several studies have established the association between the refraction and AxL on the ChT, however, other studies (including ours) did not observe this association.^{47, 52, 54} The main reason for not observing this correlation is likely to be the range of refractive error used in my study (within ± 3). Refractive error has been reported to be positively associated with ChT with estimates varying widely across reports: with estimates of thinning of ChT for every 1.00 D of myopia of 5.3 μm ,⁵⁷ 8.7 μm ,⁵⁵ 15.0 μm ,⁴⁸ 29.13 μm .⁶⁵ Similarly AxL has been reported to be negatively associated with ChT^{48, 86}: estimates of this effect are thinning of ChT for every 1 mm increase in AxL from 25.4 μm ⁶⁶ to 43.8 μm .²⁵⁷

8.3 Choroidal structure and function in diabetes

8.3.1 Changes of choroidal structure in DR

The results presented in Chapter 6 did not detect an association between choroidal structural changes and severity of DR. The presence of retinopathy and/or maculopathy within the retina seen on OCT did not appear to affect ChT as observed on EDI OCT scans.

Comparing the ChT of diabetic eyes to healthy eyes, my results showed (Chapter 6) a slight decrease in ChT in DM patients compared to controls (mean SfChT was 327.2 μm [95% CI; 301.5 - 360.4] for controls and 300.5 μm [95% CI; 238.2 - 362.8] for DM patients without DR). My results were in agreement with previous studies showing a slight decrease in ChT in DM patients without signs of DR.^{177, 178, 258, 259} My results, however, were in direct conflict with a study by Querques *et al*¹⁷⁵ who showed a 30% reduction in SfChT in DM patients without retinopathy. The difference between my results and those of Querques are likely to be due to the fact that they used a caliper to measure discrete points of the ChT. In addition, I have observed that in some cases they failed to include extravascular layers such as the choroidal-scleral interface in the pictures presented in their article.

Although I did not observe any significant differences in ChT between DR patients and healthy controls, the mean ChT in DR patients without CSMO was

greater than healthy and diabetic controls. The ChT of DR patients with CSMO/ischaemia, on the other hand, was slightly thinner than healthy and diabetic controls.

Using a similar SD OCT device (Heidelberg spectralis SD OCT), Kim *et al*²⁵⁹ observed no changes in SfChT in 24 DR patients with mild-to-moderate non-proliferative DR (NPDR) compared to 32 healthy controls ($P > 0.05$) while Lee *et al*²⁵⁸ observed a significant decrease in SfChT in this grade ($n = 56$) compared to healthy controls ($n = 48$; $P < 0.01$). Contradictory results from both studies were also observed in the DR patients with severe NPDR (Kim reported no changes whilst Lee reported a decrease in SfChT). These contradictory results are likely to arise from small samples in both clinical studies.

In more severe grades of DR (proliferative DR; PDR), a decrease in ChT has been reported varying from 40% by Vujosevic *et al*¹⁷⁷ using the RS-3000 SD OCT device and 45% by Lee *et al*²⁵⁸ using the Heidelberg SD OCT device. Kim *et al*²⁵⁹ studied 36 eyes of 20 patients with PDR, found a different pattern of ChT in PDR. In Kim's study, the mean SfChT eyes was $363.6 \pm 74.9 \mu\text{m}$. This was significantly thicker than that of diabetic controls, DR patients with mild-to-moderate NPDR and severe NPDR. The author also suggested a thickening of the choroid was associated with the increase in the severity of DR. Interestingly, Kim also observed a significant reduction of ChT in 40 eyes of 26 PDR patients who underwent panretinal photocoagulation treatment. The authors suggested that a decrease in ChT in their treated-PDR group was due to a decrease in the levels of Vascular Endothelial Growth Factor (VEGF).

The ChT has been studied in eyes with diabetic macular oedema (DMO) by ourselves as well as other groups. DMO is result from endothelial cell and pericytes dysfunction as well as the up-regulation of VEGF, and consequently, an increase in vascular permeability, leading to plasma fluid and protein leakage into extravascular spaces as observed on OCT.²³² In eyes with DMO, I observed that the ChT slightly increased in eyes without CSMO and slightly decreased in those with CSMO. These differences, however, did not reach a statistically significant level. My results, however, are in direct conflict with the previous study by Kim *et al*.²⁵⁹ Kim reported that when DMO occurs, the ChT increases by approximately 20%. The authors then sub-divided DMO into 3 sub-groups: cystoid, diffuse and serous retinal detachment (SRD) according to morphological appearances on the OCT scans. The SRD subtype had the thickest ChT. Based on their findings, Kim suggested that SRD may

appear at an early stage of DMO development, partly due to hyperpermeability of the choroid. These conclusions made by Kim, however, were based on a small number of patients and were also limited by an unequal distribution of DR grades: SRD occurred more frequently in patients with severe NPDR and PDR.

The sample size used for the choroidal structure analyses would be one of the limitations of my study. This sample size consisted of a relatively small number of patients for each DR group. The sample size may prevent significant findings and may invite type II error and thus, in future studies, a bigger sample size, involving a larger number of patients would be required in order to compare the ChT in DR. In addition to this, the sample size can be estimated in based on my inter- and intra-observer agreement findings in Chapter 3 (the mean difference of 33.1 μm and 54.4 μm for comparing total ChT and SfChT respectively).

In summary, the results obtained from my study in conjunction with the literature may suggest that the role of choroid is subtle and difficult to quantify in DM/DR certainly in early stages. My results detected no clear differences in ChT at any stages of DR that could be detected using EDI OCT. Whether or not there is a role of the choroid in the pathogenesis of DR is still debatable and warrants further study.

8.3.2 Choroidal blood flow regulation in DR

The results in Section 6.4 in Chapter 6 suggested that in DR, the autoregulation ability of the choroid is abnormal. In particular, a statistically significant increase in the ChBVelocity by 8% was observed in response to an increase of MAP of 18% in DR patients with CSMO/ischaemia ($P = 0.007$).

The effect of diabetes on the choroidal circulation is less well known compared to that to the retinal circulation. Experiments on animal models of induced diabetes by Braun *et al*²⁶⁰ reported evidence of lower RBC flow in the choriocapillaris in mildly hyperglycaemic rats (100.8 RBC/sec) and diabetic rats (105.8 RBC/sec) compared to the flow in healthy rats (124.7 RBC/sec). A lower velocity was associated with lower RBC flow in their animal model. These results suggested that choroidal circulation abnormalities may play a role in the DR.

In humans, Nagaoka *et al*¹⁸⁰ confirmed this hypothesis by evaluating ChBFlow parameters of the subfoveal choroid using LDF. ChBFlow parameters were directly compared between 36 healthy eyes, 33 DM with no DR eyes, 20 NPDR without CSMO eyes and 17 NPDR with CSMO eyes. Compared to healthy

eyes, lower ChBVelocity was found in every subgroup of diabetic patients (-9% for no DR, -18% for NPDR/-CSMO and -26% for NPDR/+CSMO). ChBVolume was lower in NPDR/+CSMO but not in other groups while ChBFlow was lower in every subgroup (-43% for no DR, -25% for NPDR/-CSMO and -58% for NPDR/+CSMO). Employing the same method, Schocket *et al*¹⁷⁹ found that patients with more severe DR (PDR) also had lower ChBVolume (-15%) and ChBFlow (-27%) compared to healthy eyes. These results provide supporting evidence to the animal model data but cannot be directly compared with my findings as the absolute ChBFlow is partially affected by the DC. There is a considerable amount of variation in the returning laser beam (being part of the DC) between experiments. This variation is often associated with an alteration of the optical property of the tissue.¹¹⁴ Changes in the DC level also rely on other factors such as the focus and position of the laser beam as shown in Section 3.3 in Chapter 3. Maintaining a similar DC level is essential for research using LDF and when reporting LDF results DC levels should always be reported especially under the pathological conditions. Neither Nagaoka nor Schocket mentioned the DC level in their studies.

In healthy eyes, the choroid is able to regulate a constant flow even after an increase of OPP up to approximately 67%.¹²² In eyes with AMD, an acute increase of OPP by 20% has been reported not to affect ChBFlow regulation in patients with dry AMD.²⁶¹ This level of increase in OPP, on the other hand, has been suggested to adversely affect the choroidal regulation in patients with wet AMD.²⁶²

For diabetic eyes, in our study, an increase of MAP by 18% caused the ChBVelocity to change by approximately 8% in patients with DR/+CSMO/ischaemia. This suggests that the choroid fails to regulate in this group of patients. Movaffaghy *et al*¹⁸¹ performed a similar experiment to mine. However, the paper was in French and only the abstract was accessible. They reported that an increase of 64% in OPP did not appear to affect the ChBFlow in diabetic patients without DR while an increase in OPP by 50% did affect the ChBFlow regulation in those with DR. We detected no changes in ChBVolume or ChBFlow during an increase of MAP in this group of patients. This might be due to the fact that these changes occurred below the minimum statistical detection limit or the sensitivity of the instrument. The sensitivity at the level of $P = 0.05$ based on healthy eyes would be 20.5% for ChBVolume, 7.2% for ChBVelocity and 20.2% for ChBFlow. These changes would be achieved by an increase in MAP to a higher level using different isometric exercise such as squatting (weight lifting was used in this study). This, however, would be difficult for patients with diabetes as the majority of patients are elderly.

Besides LDF, other methods, such as colour Doppler imaging and pulsatile ocular blood flow (POBF; recorded by Pneumotonometer) have been used to estimate the ChBFlow in patients with diabetes. The results obtained using these methods, however, show contradictory findings. For example, a decrease in POBF was found in patients with no DR/ mild NPDR by Geyer *et al*²⁶³ whereas no change in POBF was found by Savage *et al*²⁶⁴ and Schmidt *et al*.²⁶⁵ In severe PDR, three possible scenarios have been previously reported using POBF: an increase,²⁶⁴ a decrease,²⁶³ and no change²⁶⁵ suggesting an unclear role of choroid in the pathogenesis of DR. The results presented in this section using LDF, however, cannot be directly compared to these results derived from the POBF measurements for the following reasons:

1) The POBF is an estimation of the ChBVolume using the relationship between the changes in IOP and pulsatile components of the heartbeat. The main contribution to the changes found in POBF arises mainly from the large choroidal vessels. The signal measured by LDF, on the other hand, comes from the choriocapillaris⁹⁹ with less signal interfering from the retinal circulation and large choroidal circulation.

2) The POBF only provides the absolute change of the choroidal blood volume entering the eye not the autoregulation ability of the choroid. LDF is a technique suitable for assessing the autoregulation capability of the choroid. This is an essential mechanism of the choroid in order to maintain a stable ChBFlow under physiological stress and pathological conditions.

In summary, these results provide some insight into the role of the choroid in the pathogenesis of DR. My results using LDF suggest that there may be a loss of choroidal autoregulation in DR patients with CSMO/ischaemia; however, the choroidal structure remains unchanged as shown by EDI OCT. It is conceivable that the functional changes of the choroid might occur before the structural changes.

8.4 Choroidal structure and function in CSCR

CSCR is an important cause of visual disturbance in the middle-aged working population. In my cohort, the incidence of CSCR was 3.9 times higher in males compared to females. The gender ratio (male vs female) from our results was higher than the ratio of 2.8:1 from a previous study by Haimovici *et al*.²⁰⁰ Other population based studies have reported different gender ratios, 5.7:1 in a mainly Caucasian population,¹⁸⁶ 1.7:1 in Taiwanese population,¹⁸⁵ 3.1:1 in Korean population²⁶⁶ and

6.5:1 in African American population.²⁶⁷ These results indicate a diversity of the disease between races.

8.4.1 Changes in the choroidal structure in CSCR

The results presented in Section 7.3 of Chapter 7 showed that a general thickening of the choroid and an increase in ChVolume are the common morphological changes observed on EDI OCT in CSCR patients. An approximately 30% increase in the SfChT was observed in CSCR patients compared to healthy volunteers. Imamura *et al*²⁰⁴ observed a thickening of the SfChT by 75% and Maruko *et al*²⁰⁵ observed a 65% thickening of the SfChT. The smaller changes seen in my data may be due to racial differences since in my study more than 90% of patients were Caucasian while in their studies participants were mainly Asian.

The ChT at the macula was compared between different CSCR phenotypes. No significant differences were found regarding the duration of disease (acute vs chronic), the eye affected by CSCR (unilateral vs bilateral) or the presence of SRF (active vs inactive). This suggests that the choroid thickens in all CSCR phenotypes. A similar ChT between active and inactive cases suggests that the ChT change persists in CSCR patients even after the resolution of the fluid. This result agreed well with previous studies by Jirarattanasopa *et al*.²²⁰ Also, a longitudinal study by Kang *et al*²⁰⁹ showed that only a 9% decrease in ChT was observed after a complete SRF absorption without treatment.

The potential limitations of the ChT analyses of different CSCR phenotypes included: 1) In acute vs chronic cases, a 3 month period was used to define the duration of symptoms in acute and chronic phenotypes. There was a potential overlapping between these 2 phenotypes especially those with previous subclinical CSCR using this parameter. Hence, multimodal images including NIRAF and FAF should be used in conjunction with the symptom duration in order to determine the acute and chronic forms of the disease. 2) In active vs inactive cases, the main criteria used to judge active and inactive was the presence of SRF detected by OCT. Although OCT has been recommended to aid in diagnosing and monitoring CSCR, using OCT alone may not directly indicate the leaking of fluid into the subretinal space. Therefore, to confirm this finding, the FA may be needed.

In patients with unilateral CSCR, the ChT of symptomatic eyes was thicker than the asymptomatic fellow eye ($P < 0.01$ in all ETDRS subfields). These results were similar to the results reported previously.^{205, 206} Although no statistically significant difference in the ChT was observed between the asymptomatic fellow

eyes compared to healthy eyes, the ChT of asymptomatic fellow eyes was thicker than the normal values.

ICGA is now recognised by clinicians in aiding in the diagnosis and treatment in CSCR.¹⁹⁰ A unique feature of choroidal vascular hyperpermeability seen on ICGA in CSCR has been previously described.²²⁵ I noted that the choroidal vascular hyperpermeability of the symptomatic eyes occurs at approximately 1.5 minutes after injection (approximately 4 minutes for the asymptomatic fellow eyes). This visualisation time was earlier than that reported by Iida *et al*²²⁵ who suggested the visualisation time at approximately 5 minutes. This might be due to the improvements of imaging technology over the past decade from videotape to digital image with a confocal scanning laser ophthalmoscope (cSLO) system. The hyperpermeability on ICGA was observed in 100% of the symptomatic eyes and 56.5% of the asymptomatic fellow eyes.

The relationship between the choroidal vascular hyperpermeability seen on ICGA and the choroidal thickening observed on EDI OCT scans was further investigated in both the symptomatic and asymptomatic eyes. In the symptomatic eyes, the results showed that the area of thickest choroid coincided with the area of vascular hyperpermeability on ICGA. Similar results have been reported previously by Jirarattanasopa.²²⁰ Additionally, the results from my work also showed that there was an increase by approximately 8.35 μm of the ChT for every 10% increase in ICG hyperpermeability within 1 mm^2 area. Interestingly, there was no statistically significant difference in the ChT between the hyperpermeability area and surrounding area in 3 CSCR inactive eyes of bilateral patients. In these 3 eyes, a less active stage of CSCR was observed. Two possible explanations for this result could be explained as follows:

- 1) The focal thickening of the choroid may play an important part in the SRF accumulation during the active stage; this is supported by the findings in the symptomatic eyes.

- 2) The reduction of the focal thickening of the ChT to the level of surrounding areas after SRF resolution may suggest a healing process. In order to prove this hypothesis, however, a larger number of patients as well as longitudinal analyses would be required.

Among the asymptomatic fellow eyes of unilateral CSCR, 56.5% had ICG hyperpermeability. This was consistent with a previous report by Iida *et al*.²²⁵ They

reported 62% of the unaffected fellow eyes displayed choroidal hyperpermeability. I observed a slight thickening of ChT in unaffected eyes with hyperpermeability on ICGA compared to the symptomatic eyes without hyperpermeability. These findings were similar to those of Maruko *et al*²⁰⁵ who reported a significantly thicker choroid in unaffected fellow eyes with ICG hyperpermeability compared to those without ICG hyperpermeability. My analyses of the relationship between the choroidal vascular hyperpermeability in Chapter 7 also showed that the ChT at the hyperpermeability area was significantly thicker compared to the surrounding area ($P < 0.012$). Every 10% increase in amount of ICG hyperpermeability within the 1 mm² area caused the ChT to increase by 9.89 μm . The focal thickening in these patients with unilateral CSCR might suggest a subclinical abnormality of the hyperpermeability area of the unaffected eye and also indicate changes in the overlying RPE. This area of hyperpermeability with thickening of the choroid has been shown previously to co-localize with the area of leakage in recurrent CSCR of the affected eyes and new leakage areas of unaffected eyes of unilateral converting to bilateral CSCR.²²⁵

To my knowledge, the relationship between risk factors and ChT has not been explored previously. Hypertension and the use of corticosteroids are known risk factors contributing to the development of CSCR.^{199, 200} I have determined the effect of these known risk factors on the thickness of the choroid and found that CSCR patients with hypertension had the thickest choroid compared to healthy and CSCR patients with normotension. Moreover, this increase in ChT of CSCR patients with hypertension compared to those with normotension was clearly observed in CSCR eyes with SRF. Compared with hypertension, the ChT of CSCR patients with a history of steroid usage was thicker by 7.9 to 29.5 μm (2 – 8%) compared to those without a history of steroid usage. These differences of ChT in CSCR patients with and without history of steroid usage were not as significant as the changes in ChT caused by hypertension. This finding was similar to that of Han *et al*²⁴⁵ who reported no significant changes of ChT longitudinally during systemic high-dose corticosteroid administration.

CSCR is often considered as a self-limiting eye condition. However, CSCR patients with persistent accumulation of fluid and retinal detachment often require treatment. Although, verteporfin photodynamic therapy (VPDT) is considered to be a current standard for treating CSCR, a risk of developing choroidal neovascularisation (CNV) is a known complication as is the risk of recurrence.²⁶⁸ Thus, many investigators have investigated alternative treatments for CSCR such as intravitreal injections and pharmacological therapy. Recent reports have suggested

that CSCR may benefit from a mineralocorticoid receptor antagonist such as spironolactone and eplerenone.^{269, 270} These mineralocorticoid receptor antagonists are commonly used to treat hypertension. Therefore, controlling BP may be beneficial for CSCR patients and the BP should be monitored regularly in this group of patients.

Changes in ChT in response to treatment in CSCR have been reported by several groups. Although this was outside the scope of my work, a brief summary will be presented. Several published works have reported the use of VPDT to treat long standing CSCR patients. VPDT uses a light sensitive drug, verteporfin which is then activated by 689 nm laser light. Maruko *et al*^{207, 208} reported an increase in SfChT within 2 days after VPDT, followed by rapid reductions by 1 week and 4 weeks after. Similar findings were reported by other groups using the EDI OCT²⁰⁹ or with a longer wavelength SS OCT.²⁷¹ Patients with delayed resorption and unsuccessful resolution of SRF after VPDT showed a slower rate of decrease in ChT compared to patients with complete resolution.²⁷² Beside VPDT, Pitcher *et al*²⁷³ have reported that after using intravitreal aflibercept the SfChT significantly declined over a period of 6 months.

The reason behind the thickening of the choroid in CSCR is still unclear. In the next section, I will describe the proposed underlying mechanism of why the choroid becomes thicker in CSCR using the results from my work presented in Section 7.5 in Chapter 7.

8.4.2 Choroidal autoregulation in CSCR

In Section 7.5 of Chapter 7, the ability of the choroid to regulate its structure and function was investigated in CSCR patients and compared with that of healthy controls. The regulation of choroidal structure represented by ChT was assessed by EDI OCT while the regulation of choroidal function represented by ChBFlow parameters was assessed by LDF. To my knowledge, this work is the first to use the EDI OCT and LDF in conjunction to assess the changes in ChT in response to an increase in ocular perfusion pressure (OPP) in healthy and diseased eyes.

In healthy eyes, I observed no statistically significant changes in ChT using EDI OCT following an increase in OPP by 41%. These results were in agreement with Alwassia *et al*²⁷⁴ who measured the change in ChT in 15 healthy eyes using a portable OCT device. They reported that an increase in mean systolic BP over 30% did not alter the change of ChT ($P > 0.05$). In Alwassia's study a cardiac stress test was used, however, the authors failed to mention how this test was performed. On

the contrary, squatting, a recommended method to increase OPP, was used in my experiment. An acute increase of OPP by 40% was achieved using squatting compared to a 25% increase in OPP by Alwassia. Nonetheless, Alwassia's and my results suggest that there is a regulation mechanism of choroidal structure to maintain a constant thickness despite an acute OPP elevation in both low (Alwassia) and moderate (mine) levels in healthy eyes. On the other hand, in the choroidal blood flow autoregulation experiments using LDF, the moderate increase in OPP by 40% by squatting in healthy subjects did not affect the choroidal blood flow parameters. These results were in agreement with Riva *et al*¹²² even though the OPP was 20% lower than that achieved by Riva.

Isometric exercise is a type of static strength training wherein the muscle contracts but does not change in length. This type of exercise is known to stimulate the cardiovascular systems increasing heart rate and arterial BP. The sympathetic system is also known to be provoked resulting in vasoconstriction.

The mechanism of how the choroid regulates its structure and function remains unclear. One possible explanation might be the special cellular composition of the choroid. The choroid consists of a dense nerve plexus surrounding the vessel walls as well as specialised intrinsic choroidal neurons (as I have described in Chapter 1). These special neurons are highly concentrated at the fovea where there is high a concentration of non-vascular smooth muscle cells. These neurons are known to terminate at the muscle wall of the choroidal arterioles and to release nitric oxide (NO) which acts as a vasodilatation mediator.¹⁶ The regulation of choroidal blood circulation and choroidal structure during the acute increase of OPP in healthy eyes might be due to the activation of these neurons to maintain constant ChBFlow and ChT.

In CSCR patients, in contrast to healthy people, a dysregulation of choroidal structure and function was observed using EDI OCT and LDF, respectively (see Section 7.5). A significant increase in ChT in CSCR was observed using EDI OCT following an increase in OPP by 40% ($P < 0.05$). This significant increase in ChT after exercise is likely caused by the medium and large vessels not by the choriocapillaris. The resolution of a conventional SD OCT cannot give a clear visualisation of the choriocapillaris. Many have speculated that the 10 μm hyporeflective layer beneath the hyperreflective band of BM-RPE complex represents the choriocapillaris.²⁷⁵ Therefore if the increase in ChT occurs at the

choriocapillaris, it will need to dilate by as much as 2x the normal size to achieve the mean differences seen in this study.

The abnormality of choroidal function in CSCR has been shown by several groups using various methods. Kitaya *et al*²¹⁰ investigated the choroidal circulation of 36 acute CSCR patient using ICGA with a cSLO and reported a choroidal filling delay and a focal area of hypofluorescence. They also quantified the ChBFlow in a small subset of 11 patients using LDF and reported 45% lower in ChBFlow in symptomatic eyes (mean $6.27 \pm$ (SD) 4.64 AU) compared to fellow eyes (11.41 ± 4.09 AU) ($P < 0.01$). Using laser speckle flowgraphy (LSF), a technique used to determine a relative ChBVelocity, Saito *et al*²⁷⁶ reported a reduction of ChBVelocity with regression of SRF in 21 eyes of 20 acute CSCR (macular mean blur rate [MBR] decreased from 100% at baseline to 82.3% at 6 months of follow up). They also suggested that ChBFlow was elevated in acute CSCR. The difference between the 2 studies may be due to the fact that LDF is used to determine the ChBFlow from the choriocapillaris whereas the LSF determines ChBVelocity from the whole choroid. Moreover, the ChBVelocity from the LSF is often affected by large and medium sized vessels. Although, abnormalities of blood circulation are shown in both studies, the results from Kitaya and Saito cannot be used to explain the autoregulation of the choroidal function in CSCR.

To gain a better understanding of autoregulation capability of the choroid in CSCR, I used LDF for this purpose. In CSCR patients, an increase in OPP by 31% was achieved following squatting. This level of OPP increase did not affect the choroidal blood flow parameters when I compared between baseline and at the end of isometric exercise. However, the mean change of ChBVolume from baseline in CSCR patients was significantly greater than that of healthy eyes (ChBVolume changed by -2% in CSCR and 1% in healthy controls, $P = 0.03$) and these changes were negatively correlated with the change in choroidal vascular resistance. As mentioned above the LDF predominantly detects the moving red blood cells from the choriocapillaris, the results from Section 7.5.2 suggest that the function of this layer is impaired.

Dysregulation of ChBflow was previously demonstrated by Tillt *et al*.²¹¹ In this study, the LDF recordings were performed in 14 chronic inactive CSCR patients and compared with 14 healthy controls. The recruitment criteria for CSCR patients in Tillt's study included: 1) negative history of smoking or drug abuse, 2) positive history of chronic CSCR and a biomicroscopically inactive CSCR at study entry and

3) last episode of CSCR occurred at least 6 months to 2 years before enrolment. Using a compact LDF device, Tillt *et al* showed that the ChBFlow of CSCR patients was significantly increased following 6 minutes of squatting compared to controls ($P < 0.001$). An increase of OPP up to 85% caused the ChBFlow to increase by 2x that seen in healthy eyes. However, my work cannot be directly compared with Tillt *et al* mainly due to different patient selection criteria. CSCR patients with active SRF at the fovea were chosen in my work while chronic inactive CSCR patients were chosen in Tillt's study. Nevertheless, Tillt's findings and mine demonstrated failure of choroidal autoregulation in CSCR and the difference in results obtained from mine and theirs suggested a different mechanism may be involved during the active and inactive phases of CSCR.

So far, the results obtained in Section 7.5 indicate an impairment of choroidal autoregulation. This impaired choroidal regulation involved all the 3 main choroidal vascular layers, medium and large choroidal vascular layers and choriocapillaris as suggested by the results from EDI OCT and LDF.

Several factors have been shown to be involved in choroidal dysregulation in CSCR. CSCR patients have demonstrated autonomic dysfunction as shown on electrocardiogram during sympathetic and parasympathetic reactivity tests in a study.²⁷⁷ The main findings of this study included increased sympathetic activity, decreased parasympathetic activity and autonomic imbalance. CSCR patients also displayed several metabolic abnormalities such as high plasma cortisol (as shown in our result from Section 7.3) and tetrahydroaldosterone (THA) levels.²⁷⁸ THA is a metabolite product of mineralocorticoid and aldosterone associated with local BP and blood flow adjustments.²⁷⁹ In addition, as many CSCR patients tend to have high BP, the level of nitric oxide (NO) may play a role. NO is a potent vasodilator released by the local endothelial cells and plays an important role in choroidal blood flow regulation.²⁸⁰ These metabolic and autonomic imbalances lead to impaired choroidal autoregulation, a consequent choroidal vascular hyperpermeability and an increase in hydrostatic pressure allowing the fluid to leak into sub-retinal space.

I also observed that the degree of depression, somatic symptoms and perception of stress was higher in my cohort of CSCR patients. These factors have been shown to be related to developing CSCR. Emotional strain and stress may act as precursors for the neurogenic and metabolic disturbances. **Figure 8.1** shows a summary of the proposed pathogenesis of CSCR developed from current findings from my work and previous findings by other groups.

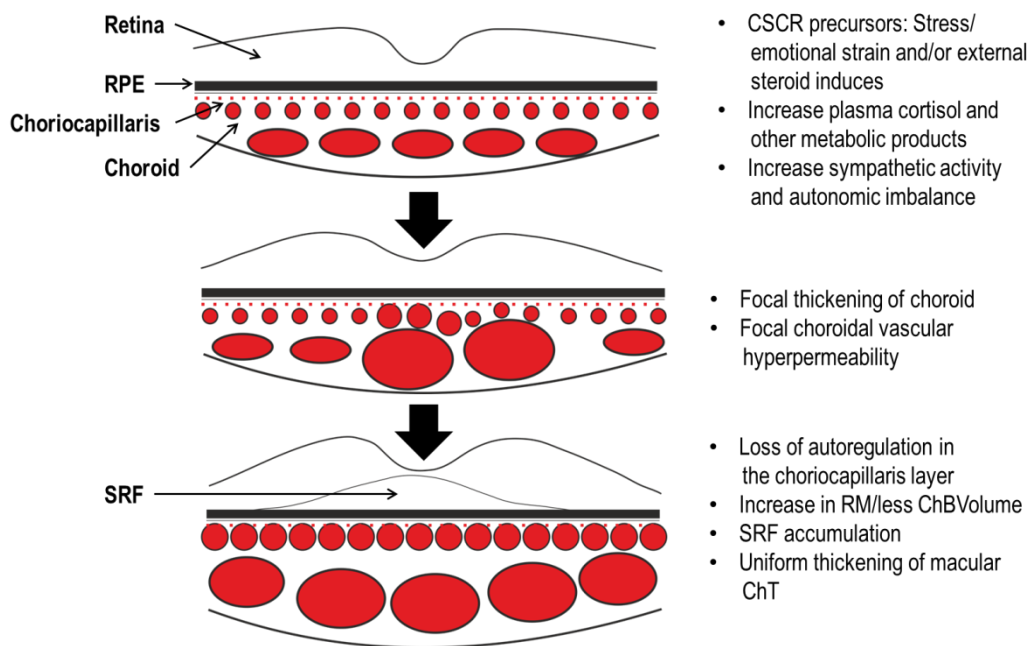


Figure 8.1: The proposed pathogenesis mechanism of CSCR from the results obtained from the work in this thesis

8.5 Future directions in choroidal ophthalmic imaging

In recent years, ophthalmic imaging has become more refined and more advanced. This has advanced the understanding and management of eye disease. OCT has become a standard imaging procedure. Since the development of EDI OCT, a better understanding of the role of the choroid in the pathogenesis of chorioretinal diseases is developing. Below I describe some of the current innovations in imaging.

8.5.1 *En face* imaging

En face images are a 3 dimensional visualisation of the OCT so that the retina is seen face on, or in coronal view. The superiority of *en face* images over the cross sectional B scan include 1) *en face* provides a layer by layer image and 2) *en face* viewing often picks up a small lesion which is missed by the distance setting between each of the cross sectional B scans.²⁸¹

En face OCT images can be produced by TD OCT and SD OCT. The 3D volume *en face* is constructed by C scans from TD OCT (each C scan is derived from several B scans) or several B scans for TD OCT and SD OCT (each B scan

derived from several A scans).²⁸² To acquire 3D volume images from conventional TD OCT and SD OCT, however, a longer time and better patient cooperation are required particularly when the EDI function is applied; to obtain 3D volume for *en face* using Heidelberg Spectralis® 197 B scans need to be acquired to cover a 6 × 6 mm (20 × 20 degree) area (30 µm gap between consecutive B scans).

A recent development of swept source (SS) OCT offers several advantages over SD OCT as described previously in Chapter 2. With a longer wavelength and higher tissue penetration, SS OCT has been shown to be more superior for *en face* 3D imaging than SD OCT, especially for choroidal imaging. SS OCT also has a faster scan rate (i.e. 100,000 A scans/sec of SS OCT vs 50000 A scans/sec of SD OCT, which enables the acquisition to be done within a few seconds.

En face imaging is useful in topographical analysis of the choroidal vasculature. Focal and diffuse choroidal dilatation have been described in patients with chronic CSCR using *en face* SS OCT.²⁸¹ The coronal view of *en face* image also allows directly comparison of each choroidal layer with other imaging modalities such as ICGA, FA and autofluorescence imaging.

8.5.2 Optical coherence tomography angiography

Optical coherence tomography angiography (OCTA) is a new image modality that detects motion of red blood cells within the vessels. The movement of blood cells creates a decorrelated signal. By calculating the decorrelation of signal amplitude between consecutive scans at the exact same location, the decorrelated pixels representing blood flow can be visualised. The decorrelation signal, however, can be interfered with by the bulk movement of the eye during the scan. The split-spectrum amplitude decorrelation angiography (SSADA) algorithm is one of the algorithms incorporated into commercially available OCTA to eliminate this effect as well as to improve the signal to noise ratio. The motion artefacts produced by saccadic and micro-saccadic eye movements are corrected by a motion correction algorithm.²⁸³ The result from these combined algorithms is a depth resolved volumetric map of retinal and choroidal vasculature.

The advantages of OCTA over conventional angiographic procedures (FA and ICG) are 1) OCTA is a non-invasive procedure 2) OCTA can provide *en face* visualisation of the distinctive flow map of various retinal and choroidal layers which can be colour coded compare to the 2D projection image obtained by FA and ICGA.

At the macula, images of the retinal vasculature obtained from OCTA show 2 distinct layers, an inner vascular plexus (start from ILM – outer border of IPL) and deep vascular plexus (outer border of IPL – midpoint of OPL).²⁸⁴ Flow index, a parameter used to represent blood flow, can be calculated using the average decorrelation value in the specified region. For the choroidal vasculature, the current commercially available system can detect only the choriocapillaris layer which is normally set at 10 µm below the RPE-Bruch's membrane complex. Because of a dense flow in the choriocapillaris, the signals from deeper and larger choroidal vessels are subject to interference artefact.²⁷⁵

AngioVue® by Optovue, Inc is currently the only OCTA commercially available in Asia and Europe. In the UK, it has been introduced in September 2014. AngioVue uses 840 nm light source and has a scan rate of 70,000 A scan/sec with axial resolution of 5µm. Other OCTA systems currently available as prototypes include Spectralis OCTA and Cirrus HD-OCT 5000.

8.6 Future work

Building on the research described in this thesis and the review of the literature, several aspects of choroidal structure and function could be investigated further.

1. Many CSCR patients display abnormalities of choroid and retina outside the normal routine 30° imaging such as the gravitational tract in autofluorescence due to the SRF. Thus looking at the wider choroid and retina should help to understand more about morphopathology. Currently available ultra-widefield imaging techniques in our clinic are Heidelberg Ultra-Widefield (covering angle view of 102° over the retina) and Optos.
2. Although, this current work has included a small but sufficient sample, a larger sample size may be required to determine various aspects of CSCR choroidal pathophysiology. For example, the effects of uncontrolled hypertension and antihypertensive medications on ChT in CSCR patients or a stress profile and psychological profile of patients with CSCR. The results produced from this current work can be used to estimate sample size for future studies.
3. My work only studied the changes of choroidal structure and function within the limit of a cross-sectional study. A longitudinal assessment of choroidal

structure and function should be considered in order to gain more insight into the pathogenesis of CSCR and DR.

4. At present, LDF remains the only method to determine ChBFlow at the fovea. The results obtained from LDF, however, do not give insights into changes in the medium and large choroidal vasculature layers. Thus, using LDF in combination with other techniques such as POBF could be considered.
5. As mentioned earlier, using the absolute values of LDF is considered inappropriate. This absolute LDF signal, however, contains other vascular components such as oscillations indicating the local regulation of blood flow. These can be analysed by mathematical models such as fractal dimensions and wavelet analysis if the LDF recording time is longer than 30s. Thus, this mathematical analysis could be considered for the future work.
6. Multimodal imaging will be the key for future research in the choroid. It would include FA, ICGA, multicolour imaging, autofluorescence imaging, EDI OCT, *en face* imaging, OCTA and adaptive optics (AO).

8.7 Conclusions

The choroid is a vital structure compartment of the posterior pole essential for retinal function. Until recently, histological study was the only way to assess changes of the choroid as real time visualisation in humans was not possible. With the growth in ophthalmic imaging technologies over the past decade, study of structure and function of the choroid has become possible and allows a better understanding of the role of the choroid in eye diseases.

The findings presented in this thesis give an insight into the role of the choroid in the pathogenesis of common eye problems seen in routine clinics. In patients with diabetes, no significant changes in the ChT were observed in any group of DR patients. ChBVelocity regulation was impaired in patients with severe DR. These findings suggest that functional changes of the choroid may occur before the structural changes. In CSCR patients, disruption of choroidal autoregulation was observed. All three choroidal vessel layers are believed to be affected in the impairment process. These findings highlight the significance of choroidal regulation in the pathogenesis of DR and CSCR.

References

1. Wybar KC. Vascular anatomy of the choroid in relation to selective localization of ocular disease. *Br J Ophthalmol* 1954;38(9):513-517.
2. Flowers RW, Hochheimer BF. Letter: Infrared fundus angiography. *Br J Ophthalmol* 1974;58(6):635.
3. Mrejen S, Spaide RF. Optical coherence tomography: imaging of the choroid and beyond. *Surv Ophthalmol* 2013;58(5):387-429.
4. Booij JC, Baas DC, Beisekeeva J, Gorgels TG, Bergen AA. The dynamic nature of Bruch's membrane. *Prog Retin Eye Res* 2010;29(1):1-18.
5. Goldbaum MH, Madden K. A new perspective on Bruch's membrane and the retinal pigment epithelium. *Br J Ophthalmol* 1982;66(1):17-25.
6. Mrejen S, Sarraf D, Mukkamala SK, Freund KB. Multimodal imaging of pigment epithelial detachment: a guide to evaluation. *Retina* 2013;33(9):1735-62.
7. Anand-Apte B, Hollyfield JG. Development anatomy of retinal and choroidal vasculature. In: Beshare J, Bok D, editors. *The retina and its disorders*. Oxford, UK: Elsevier Ltd, 2010:179-185.
8. Snell R, Lemp M. *Clinical anatomy of the eye*. Somerset: Wiley, 2013:505.
9. Chung SE, Kang SW, Kim JH, Kim YT, Park do Y. Engorgement of vortex vein and polypoidal choroidal vasculopathy. *Retina* 2013;33(4):834-40.
10. <http://www.oculist.net/downat0502/prof/ebook/duanes/pages/v7/v7c001.html>. Accessed November 2015
11. Remington L. Uvea, 3rd ed. In: Remington L, editor. *Clinical Anatomy and Physiology of the Visual System*. Saint Louis: Butterworth Heinemann, 2012:40-60.
12. Hayreh SS. Vascular pattern of the choriocapillaris. *Exp Eye Res* 1974;19(1):101-104.
13. Yoneya S, Tso MOM, Shimizu K. Patterns of the choriocapillaris - a method to study the choroidal vasculature of the enucleated human-eye. *International Ophthalmology* 1983;6(2):95-99.
14. Yoneya S, Tso MO. Angioarchitecture of the human choroid. *Arch Ophthalmol* 1987;105(5):681-687.
15. Fryczkowski AW. Anatomical and functional choroidal lobuli. *International Ophthalmology* 1994;18(3):131-141.
16. Nickla DL, Wallman J. The multifunctional choroid. *Prog Retin Eye Res* 2010;29(2):144-168.
17. Schroedl F, Brehmer A, Neuhuber WL, Kruse FE, May CA, Cursiefen C. The normal human choroid is endowed with a significant number of lymphatic vessel endothelial hyaluronate receptor 1 (LYVE-1)-positive macrophages. *Invest Ophthalmol Vis Sci* 2008;49(12):5222-5229.
18. Schmetterer L, Polak K. Role of nitric oxide in the control of ocular blood flow. *Prog Retin Eye Res* 2001;20(6):823-47.
19. Cherepanoff S, McMenamin P, Gillies MC, Kettle E, Sarks SH. Bruch's membrane and choroidal macrophages in early and advanced age-related macular degeneration. *Br J Ophthalmol* 2010;94(7):918-25.

20. Sharma S, Saxena S, Srivastav K, et al. Nitric oxide and oxidative stress is associated with severity of diabetic retinopathy and retinal structural alterations. *Clin Experiment Ophthalmol* 2015;43(5):429-36.
21. Weiter JJ, Schachar RA, Ernest JT. Control of intraocular blood flow. I. Intraocular pressure. *Invest Ophthalmol* 1973;12(5):327-331.
22. Linsenmeier RA, Padnick-Silver L. Metabolic dependence of photoreceptors on the choroid in the normal and detached retina. *Invest Ophthalmol Vis Sci* 2000;41(10):3117-3123.
23. Birol G, Wang S, Budzynski E, Wangsa-Wirawan ND, Linsenmeier RA. Oxygen distribution and consumption in the macaque retina. *Am J Physiol Heart Circ Physiol* 2007;293(3):H1696-H1704.
24. Parver LM. Temperature modulating action of choroidal blood flow. *Eye* 1991;5 (Pt 2):181-185.
25. Parver LM, Auker CR, Carpenter DO. The stabilizing effect of the choroidal circulation on the temperature environment of the macula. *Retina* 1982;2(2):117-120.
26. Parver LM, Auker CR, Carpenter DO, Doyle T. Choroidal blood flow II. Reflexive control in the monkey. *Arch Ophthalmol* 1982;100(8):1327-1330.
27. Tornquist P, Alm A. Retinal and choroidal contribution to retinal metabolism in vivo. A study in pigs. *Acta Physiol Scand* 1979;106(3):351-377.
28. Tornquist P, Alm A, Bill A. Permeability of ocular vessels and transport across the blood-retinal-barrier. *Eye* 1990;4 (Pt 2):303-309.
29. Booij J, Baas D, Beisekeeva J, Gorgels T, Bergen A. The dynamic nature of Bruch's membrane. *Prog Retin Eye Res* 2010;29(1):1-18.
30. Kiel JW, Shepherd AP. Autoregulation of choroidal blood flow in the rabbit. *Invest Ophthalmol Vis Sci* 1992;33(8):2399-2410.
31. Kogure K, David NJ, Yamanouchi U, Choromokos E. Infrared absorption angiography of the fundus circulation. *Arch Ophthalmol* 1970;83(2):209-214.
32. Spaide RF, Koizumi H, Pozonni MC. Enhanced depth imaging spectral-domain optical coherence tomography. *Am J Ophthalmol* 2008;146(4):496-500.
33. Huang D, Swanson EA, Lin CP, et al. Optical coherence tomography. *Science* 1991;254(5035):1178-1181.
34. Fercher AF, Hitzenberger CK, Drexler W, Kamp G, Sattmann H. In-Vivo optical coherence tomography. *Am J Ophthalmol* 1993;116(1):113-115.
35. Geitzenauer W, Hitzenberger CK, Schmidt-Erfurth UM. Retinal optical coherence tomography: past, present and future perspectives. *Br J Ophthalmol* 2011;95(2):171-177.
36. Costa RA, Skaf M, Melo LA, Jr., et al. Retinal assessment using optical coherence tomography. *Prog Retin Eye Res* 2006;25(3):325-353.
37. Adhi M, Duker JS. Optical coherence tomography-current and future applications. *Curr Opin Ophthalmol* 2013;24(3):213-221.
38. Wolf S, Wolf-Schnurbusch U. Spectral-domain optical coherence tomography use in macular diseases: a review. *Ophthalmologica* 2010;224(6):333-340.
39. Chhablani J, Barteselli G, Wang H, et al. Repeatability and reproducibility of manual choroidal volume measurements using enhanced

- depth imaging optical coherence tomography. *Invest Ophthalmol Vis Sci* 2012;53(4):2274-2280.
40. Potsaid B, Baumann B, Huang D, et al. Ultrahigh speed 1050nm swept source/Fourier domain OCT retinal and anterior segment imaging at 100,000 to 400,000 axial scans per second. *Opt Express* 2010;18(19):20029-20048.
 41. Staurengi G, Sadda S, Chakravarthy U, Spaide RF, International Nomenclature for Optical Coherence Tomography P. Proposed lexicon for anatomic landmarks in normal posterior segment spectral-domain optical coherence tomography: the IN*OCT consensus. *Ophthalmology* 2014;121(8):1572-8.
 42. Sim DA, Keane PA, Mehta H, et al. Repeatability and reproducibility of choroidal vessel layer measurements in diabetic retinopathy using enhanced depth optical coherence tomography. *Invest Ophthalmol Vis Sci* 2013;54(4):2893-2901.
 43. Branchini LA, Adhi M, Regatieri CV, et al. Analysis of choroidal morphologic features and vasculature in healthy eyes using spectral-domain optical coherence tomography. *Ophthalmology* 2013;120(9):1901-8.
 44. Maul EA, Friedman DS, Chang DS, et al. Choroidal thickness measured by spectral domain optical coherence tomography factors affecting thickness in glaucoma patients. *Ophthalmology* 2011;118(8):1571-1579.
 45. Ramrattan RS, van der Schaft TL, Mooy CM, de Bruijn WC, Mulder PG, de Jong PT. Morphometric analysis of Bruch's membrane, the choriocapillaris, and the choroid in aging. *Invest Ophthalmol Vis Sci* 1994;35(6):2857-2864.
 46. Curcio CA, Messinger JD, Sloan KR, Mitra A, McGwin G, Spaide RF. Human chorioretinal layer thicknesses measured in macula-wide, high-resolution histologic sections. *Invest Ophthalmol Vis Sci* 2011;52(7):3943-3954.
 47. Margolis R, Spaide RF. A pilot study of enhanced depth imaging optical coherence tomography of the choroid in normal eyes. *Am J Ophthalmol* 2009;147(5):811-815.
 48. Wei WB, Xu L, Jonas JB, et al. Subfoveal choroidal thickness: the Beijing Eye Study. *Ophthalmology* 2013;120(1):175-180.
 49. Benavente-Perez A, Hosking SL, Logan NS, Bansal D. Reproducibility-repeatability of choroidal thickness calculation using optical coherence tomography. *Optom Vis Sci* 2010;87(11):867-872.
 50. Shin JW, Shin YU, Cho HY, Lee BR. Measurement of choroidal thickness in normal eyes using 3D OCT-1000 spectral domain optical coherence tomography. *Korean J Ophthalmol* 2012;26(4):255-259.
 51. Ding X, Li J, Zeng J, et al. Choroidal thickness in healthy Chinese subjects. *Invest Ophthalmol Vis Sci* 2011;52(13):9555-9560.
 52. Fujiwara A, Shiragami C, Shirakata Y, Manabe S, Izumibata S, Shiraga F. Enhanced depth imaging spectral-domain optical coherence tomography of subfoveal choroidal thickness in normal Japanese eyes. *Jpn J Ophthalmol* 2012;56(3):230-235.
 53. Manjunath V, Goren J, Fujimoto JG, Duker JS. Analysis of choroidal thickness in age-related macular degeneration using spectral-domain optical coherence tomography. *Am J Ophthalmol* 2011;152(4):663-668.

54. Park KA, Oh SY. Choroidal thickness in healthy children. *Retina* 2013;33(9):1971-1976.
55. Kim M, Kim SS, Koh HJ, Lee SC. Choroidal thickness, age, and refractive error in healthy Korean subjects. *Optom Vis Sci* 2014;91(5):491-496.
56. Kim M, Kim SS, Kwon HJ, Koh HJ, Lee SC. Association between choroidal thickness and ocular perfusion pressure in young, healthy subjects: enhanced depth imaging optical coherence tomography study. *Invest Ophthalmol Vis Sci* 2012;53(12):7710-7717.
57. Ruiz-Medrano J, Flores-Moreno I, Pena-Garcia P, Montero JA, Duker JS, Ruiz-Moreno JM. Macular choroidal thickness profile in a healthy population measured by swept-source optical coherence tomography. *Invest Ophthalmol Vis Sci* 2014;55(6):3532-3542.
58. Chen FK, Yeoh J, Rahman W, Patel PJ, Tufail A, Da Cruz L. Topographic variation and interocular symmetry of macular choroidal thickness using enhanced depth imaging optical coherence tomography. *Invest Ophthalmol Vis Sci* 2012;53(2):975-985.
59. Rahman W, Chen FK, Yeoh J, Patel P, Tufail A, Da Cruz L. Repeatability of manual subfoveal choroidal thickness measurements in healthy subjects using the technique of enhanced depth imaging optical coherence tomography. *Invest Ophthalmol Vis Sci* 2011;52(5):2267-2271.
60. Kim JH, Kang SW, Ha HS, Kim SJ, Kim JR. Overestimation of subfoveal choroidal thickness by measurement based on horizontally compressed optical coherence tomography images. *Graefes Arch Clin Exp Ophthalmol* 2013;251(4):1091-1096.
61. Branchini L, Regatieri C, Flores-Moreno I, Baumann B, Fujimoto JG, Duker JS. Reproducibility of choroidal thickness measurements across three spectral domain optical coherence tomography systems. *Ophthalmology* 2012;119(1):119-123.
62. Yamashita T, Yamashita T, Shirasawa M, Arimura N, Terasaki H, Sakamoto T. Repeatability and reproducibility of subfoveal choroidal thickness in normal eyes of Japanese using different SD-OCT devices. *Invest Ophthalmol Vis Sci* 2012;53(3):1102-1107.
63. Copete S, Ruiz-Moreno JM, Cava C, Montero JA. Retinal thickness changes following photodynamic therapy in chronic central serous chorioretinopathy. *Graefes Arch Clin Exp Ophthalmol* 2012;250(6):803-808.
64. Adhi M, Liu JJ, Qavi AH, et al. Choroidal analysis in healthy eyes using swept-source optical coherence tomography compared to spectral domain optical coherence tomography. *Am J Ophthalmol* 2014;157(6):1272-1281.
65. Ikuno Y, Kawaguchi K, Nouchi T, Yasuno Y. Choroidal thickness in healthy Japanese subjects. *Invest Ophthalmol Vis Sci* 2010;51(4):2173-2176.
66. Li XQ, Larsen M, Munch IC. Subfoveal choroidal thickness in relation to sex and axial length in 93 Danish university students. *Invest Ophthalmol Vis Sci* 2011;52(11):8438-8441.
67. Ikuno Y, Maruko I, Yasuno Y, et al. Reproducibility of retinal and choroidal thickness measurements in enhanced depth imaging and high-penetration optical coherence tomography. *Invest Ophthalmol Vis Sci* 2011;52(8):5536-5540.

68. Ruiz-Moreno JM, Flores-Moreno I, Lugo F, Ruiz-Medrano J, Montero JA, Akiba M. Macular choroidal thickness in normal pediatric population measured by swept-source optical coherence tomography. *Invest Ophthalmol Vis Sci* 2013;54(1):353-359.
69. Read SA, Collins MJ, Vincent SJ, Alonso-Caneiro D. Choroidal thickness in childhood. *Invest Ophthalmol Vis Sci* 2013;54(5):3586-3593.
70. Li XQ, Jeppesen P, Larsen M, Munch IC. Subfoveal choroidal thickness in 1323 children aged 11 to 12 years and association with puberty: the Copenhagen Child Cohort 2000 Eye Study. *Invest Ophthalmol Vis Sci* 2014;55(1):550-555.
71. Karaca EE, Ozdek S, Yalcin NG, Ekici F. Reproducibility of choroidal thickness measurements in healthy Turkish subjects. *Eur J Ophthalmol* 2014;24(2):202-208.
72. Hirata M, Tsujikawa A, Matsumoto A, et al. Macular choroidal thickness and volume in normal subjects measured by swept-source optical coherence tomography. *Invest Ophthalmol Vis Sci* 2011;52(8):4971-4978.
73. Nagasawa T, Mitamura Y, Katome T, et al. Macular choroidal thickness and volume in healthy pediatric individuals measured by swept-source optical coherence tomography. *Invest Ophthalmol Vis Sci* 2013;54(10):7068-7074.
74. Agawa T, Miura M, Ikuno Y, et al. Choroidal thickness measurement in healthy Japanese subjects by three-dimensional high-penetration optical coherence tomography. *Graefes Arch Clin Exp Ophthalmol* 2011;249(10):1485-1492.
75. Tan CS, Cheong KX, Lim LW, Li KZ. Topographic variation of choroidal and retinal thicknesses at the macula in healthy adults. *Br J Ophthalmol* 2014;98(3):339-344.
76. Mapelli C, Dell'Arti L, Barteselli G, et al. Choroidal volume variations during childhood. *Invest Ophthalmol Vis Sci* 2013;54(10):6841-6845.
77. Manjunath V, Taha M, Fujimoto JG, Duker JS. Choroidal thickness in normal eyes measured using Cirrus HD optical coherence tomography. *Am J Ophthalmol* 2010;150(3):325-329.
78. Brown JS, Flitcroft DI, Ying GS, et al. In vivo human choroidal thickness measurements: evidence for diurnal fluctuations. *Invest Ophthalmol Vis Sci* 2009;50(1):5-12.
79. Tan CS, Ouyang Y, Ruiz H, Sadda SR. Diurnal variation of choroidal thickness in normal, healthy subjects measured by spectral domain optical coherence tomography. *Invest Ophthalmol Vis Sci* 2012;53(1):261-266.
80. Usui S, Ikuno Y, Akiba M, et al. Circadian changes in subfoveal choroidal thickness and the relationship with circulatory factors in healthy subjects. *Invest Ophthalmol Vis Sci* 2012;53(4):2300-2307.
81. Lee SW, Yu SY, Seo KH, Kim ES, Kwak HW. Diurnal variation in choroidal thickness in relation to sex, axial length, and baseline choroidal thickness in healthy Korean subjects. *Retina* 2014;34(2):385-393.
82. Chakraborty R, Read SA, Collins MJ. Diurnal variations in axial length, choroidal thickness, intraocular pressure, and ocular biometrics. *Invest Ophthalmol Vis Sci* 2011;52(8):5121-5129.
83. Grassi G, Bombelli M, Seravalle G, Dell'Oro R, Quarti-Trevano F. Diurnal blood pressure variation and sympathetic activity. *Hypertens Res* 2010;33(5):381-5.

84. Kanadani FN, Moreira T, Bezerra B, et al. Diurnal Curve of the Ocular Perfusion Pressure. *J Curr Glaucoma Pract* 2016;10(1):4-6.
85. Sarks SH. Senile choroidal sclerosis. *Br J Ophthalmol* 1973;57(2):98-109.
86. Sogawa K, Nagaoka T, Takahashi A, et al. Relationship between choroidal thickness and choroidal circulation in healthy young subjects. *Am J Ophthalmol* 2012;153(6):1129-1132 e1.
87. Takahashi S. [Studies on choroidal blood flow with a hydrogen clearance method. II. Comparison of blood flow in the choroid and other tissues (author's transl)]. *Nihon Ganka Gakkai Zasshi* 1981;85(9):1426-1431.
88. Yu DY, Alder VA, Cringle SJ. Measurement of blood flow in rat eyes by hydrogen clearance. *Am J Physiol* 1991;261(3 Pt 2):H960-968.
89. Nork TM, Kim CB, Shanmuganayagam D, Van Lysel MS, Ver Hoeve JN, Folts JD. Measurement of regional choroidal blood flow in rabbits and monkeys using fluorescent microspheres. *Arch Ophthalmol* 2006;124(6):860-868.
90. Shih YY, Wang L, De La Garza BH, et al. Quantitative retinal and choroidal blood flow during light, dark adaptation and flicker light stimulation in rats using fluorescent microspheres. *Curr Eye Res* 2013;38(2):292-298.
91. Mawatari Y, Hirata A, Fukushima M, Tanihara H. Choroidal dye filling velocity in patients with Vogt-Koyanagi-Harada disease. *Graefes Arch Clin Exp Ophthalmol* 2006;244(8):1056-1059.
92. Hirata Y, Nishiwaki H. The choroidal circulation assessed by laser-targeted angiography. *Prog Retin Eye Res* 2006;25(2):129-147.
93. Hirata Y, Nishiwaki H, Miura S, et al. Analysis of choriocapillaris flow patterns by continuous laser-targeted angiography in monkeys. *Invest Ophthalmol Vis Sci* 2004;45(6):1954-1962.
94. Emeterio Nateras OS, Harrison JM, Muir ER, et al. Choroidal blood flow decreases with age: an MRI study. *Curr Eye Res* 2014;39(10):1059-1067.
95. Rusia D, Harris A, Pernic A, et al. Feasibility of creating a normative database of colour Doppler imaging parameters in glaucomatous eyes and controls. *Br J Ophthalmol* 2011;95(9):1193-1198.
96. An L, Wang RK. In vivo volumetric imaging of vascular perfusion within human retina and choroids with optical micro-angiography. *Opt Express* 2008;16(15):11438-11452.
97. Sugiyama T, Araie M, Riva CE, Schmetterer L, Orgul S. Use of laser speckle flowgraphy in ocular blood flow research. *Acta Ophthalmol* 2010;88(7):723-729.
98. Zion IB, Harris A, Siesky B, Shulman S, McCranor L, Garzosi HJ. Pulsatile ocular blood flow: relationship with flow velocities in vessels supplying the retina and choroid. *Br J Ophthalmol* 2007;91(7):882-884.
99. Riva CE, Cranstoun SD, Grunwald JE, Petrig BL. Choroidal blood flow in the foveal region of the human ocular fundus. *Invest Ophthalmol Vis Sci* 1994;35(13):4273-4281.
100. Zhang Y, San Emeterio Nateras O, Peng Q, Rosende CA, Duong TQ. Blood flow MRI of the human retina/choroid during rest and isometric exercise. *Invest Ophthalmol Vis Sci* 2012;53(7):4299-4305.

101. Stalmans I, Vandewalle E, Anderson DR, et al. Use of colour Doppler imaging in ocular blood flow research. *Acta Ophthalmol* 2011;89(8):e609-630.
102. Yu BS, Lam AK. Technical note: How many readings are required for an acceptable accuracy in pulsatile ocular blood flow assessment? *Ophthalmic Physiol Opt* 2007;27(2):213-219.
103. Silver DM, Farrell RA. Validity of pulsatile ocular blood flow measurements. *Surv Ophthalmol* 1994;38 Suppl:S72-80.
104. Riva C, Ross B, Benedek GB. Laser Doppler measurements of blood flow in capillary tubes and retinal arteries. *Invest Ophthalmol* 1972;11(11):936-944.
105. Riva CE, Grunwald JE, Sinclair SH. Laser Doppler measurement of relative blood velocity in the human optic nerve head. *Invest Ophthalmol Vis Sci* 1982;22(2):241-248.
106. Riva CE, Feke GT, Eberli B, Benary V. Bidirectional LDV system for absolute measurement of blood speed in retinal vessels. *Appl Opt* 1979;18(13):2301-6.
107. Riva CE. Basic principles of laser Doppler flowmetry and application to the ocular circulation. *International Ophthalmology* 2001;23(4-6):183-189.
108. Bonner R, Nossal R. Model for laser Doppler measurements of blood flow in tissue. *Appl Opt* 1981;20(12):2097-2107.
109. Riva CE, Pournaras CJ, Poitry-Yamate CL, Petrig BL. Rhythmic changes in velocity, volume, and flow of blood in the optic nerve head tissue. *Microvasc Res* 1990;40(1):36-45.
110. Riva CE, Harino S, Petrig BL, Shonat RD. Laser Doppler flowmetry in the optic nerve. *Exp Eye Res* 1992;55(3):499-506.
111. Chamot SR, Movaffaghy AM, Petrig BL, Riva CE. Blood flow in the human iris measured by laser Doppler flowmetry. *Microvasc Res* 1999;57(2):153-161.
112. Riva CE, Cranstoun SD, Mann RM, Barnes GE. Local choroidal blood flow in the cat by laser Doppler flowmetry. *Invest Ophthalmol Vis Sci* 1994;35(2):608-618.
113. Palanisamy N, Riva CE, Rovati L, Cellini M, Gizzi C, Strobbe E. Does pupil dilation influence subfoveal choroidal laser Doppler flowmetry? *Acta Ophthalmol* 2013;91(7):e556-560.
114. Riva CE, Geiser M, Petrig BL. Ocular blood flow assessment using continuous laser Doppler flowmetry. *Acta Ophthalmol* 2010;88(6):622-629.
115. Petrig BL, Riva CE. Near-IR retinal laser Doppler velocimetry and flowmetry: new delivery and detection techniques. *Appl Opt* 1991;30(16):2073-2078.
116. Riva CE, Petrig BL. Choroidal blood-flow by laser-Doppler flowmetry. *Opt Eng* 1995;34(3):746-752.
117. Geiser MH, Diermann U, Riva CE. Compact laser Doppler choroidal flowmeter. *J Biomed Opt* 1999;4(4):459-464.
118. Geiser MH, Moret F, Riva CE. Helmet-mounted choroidal laser Doppler flowmeter. *P Soc Photo-Opt Ins* 2001;2(20):91-97.
119. Langhans M, Michelson G, Groh MJ. Effect of breathing 100% oxygen on retinal and optic nerve head capillary blood flow in smokers and non-smokers. *Br J Ophthalmol* 1997;81(5):365-369.

120. Kiel JW, van Heuven WA. Ocular perfusion pressure and choroidal blood flow in the rabbit. *Invest Ophthalmol Vis Sci* 1995;36(3):579-585.
121. Riva CE, Titze P, Hero M, Petrig BL. Effect of acute decreases of perfusion pressure on choroidal blood flow in humans. *Invest Ophthalmol Vis Sci* 1997;38(9):1752-1760.
122. Riva CE, Titze P, Hero M, Movaffaghy A, Petrig BL. Choroidal blood flow during isometric exercises. *Invest Ophthalmol Vis Sci* 1997;38(11):2338-2343.
123. Schmidl D, Boltz A, Kaya S, et al. Comparison of choroidal and optic nerve head blood flow regulation during changes in ocular perfusion pressure. *Invest Ophthalmol Vis Sci* 2012;53(8):4337-4346.
124. Polska E, Simader C, Weigert G, et al. Regulation of choroidal blood flow during combined changes in intraocular pressure and arterial blood pressure. *Invest Ophthalmol Vis Sci* 2007;48(8):3768-3774.
125. Lovasik JV, Kergoat H, Riva CE, Petrig BL, Geiser M. Choroidal blood flow during exercise-induced changes in the ocular perfusion pressure. *Invest Ophthalmol Vis Sci* 2003;44(5):2126-2132.
126. Geiser MH, Riva CE, Dorner GT, Diermann U, Luksch A, Schmetterer L. Response of choroidal blood flow in the foveal region to hyperoxia and hyperoxia-hypercapnia. *Curr Eye Res* 2000;21(2):669-676.
127. Leveque TK, Yu L, Musch DC, Chervin RD, Zacks DN. Central serous chorioretinopathy and risk for obstructive sleep apnea. *Sleep Breath* 2007;11(4):253-7.
128. Longo A, Geiser M, Riva CE. Subfoveal choroidal blood flow in response to light-dark exposure. *Invest Ophthalmol Vis Sci* 2000;41(9):2678-2683.
129. Arden GB, Gunduz MK, Kurtenbach A, et al. A preliminary trial to determine whether prevention of dark adaptation affects the course of early diabetic retinopathy. *Eye* 2010;24(7):1149-55.
130. Longo A, Geiser MH, Riva CE. Posture changes and subfoveal choroidal blood flow. *Invest Ophthalmol Vis Sci* 2004;45(2):546-551.
131. Kaeser P, Orgul S, Zawinka C, Reinhard G, Flammer J. Influence of change in body position on choroidal blood flow in normal subjects. *Br J Ophthalmol* 2005;89(10):1302-1305.
132. Grunwald JE, Hariprasad SM, DuPont J. Effect of aging on foveolar choroidal circulation. *Arch Ophthalmol* 1998;116(2):150-154.
133. Straubhaar M, Orgul S, Gugleta K, Schotzau A, Erb C, Flammer J. Choroidal laser Doppler flowmetry in healthy subjects. *Arch Ophthalmol* 2000;118(2):211-215.
134. Resch H, Weigert G, Karl K, Pemp B, Garhofer G, Schmetterer L. Effect of systemic moxaverine on ocular blood flow in humans. *Acta Ophthalmol* 2009;87(7):731-735.
135. Grunwald JE, Siu KK, Jacob SS, Dupont J. Effect of sildenafil citrate (Viagra) on the ocular circulation. *Am J Ophthalmol* 2001;131(6):751-755.
136. Grunwald JE, Iannaccone A, DuPont J. Effect of isosorbide mononitrate on the human optic nerve and choroidal circulations. *Br J Ophthalmol* 1999;83(2):162-167.
137. Weigert G, Berisha F, Resch H, Karl K, Schmetterer L, Garhofer G. Effect of unspecific inhibition of cyclooxygenase by indomethacin on retinal and choroidal blood flow. *Invest Ophthalmol Vis Sci* 2008;49(3):1065-1070.

138. Resch H, Zawinka C, Lung S, Weigert G, Schmetterer L, Garhofer G. Effect of histamine and cimetidine on retinal and choroidal blood flow in humans. *Am J Physiol Regul Integr Comp Physiol* 2005;289(5):R1387-R1391.
139. Boltz A, Schmidl D, Weigert G, et al. Effect of latanoprost on choroidal blood flow regulation in healthy subjects. *Invest Ophthalmol Vis Sci* 2011;52(7):4410-4405.
140. Schmidl D, Prinz A, Kolodjaschna J, et al. Effect of nifedipine on choroidal blood flow regulation during isometric exercise. *Invest Ophthalmol Vis Sci* 2012;53(1):374-378.
141. Simader C, Lung S, Weigert G, et al. Role of NO in the control of choroidal blood flow during a decrease in ocular perfusion pressure. *Invest Ophthalmol Vis Sci* 2009;50(1):372-377.
142. Weigert G, Resch H, Garhofer G, Fuchsjager-Mayrl G, Schmetterer L. Effects of topical clonidine versus brimonidine on choroidal blood flow and intraocular pressure during squatting. *Invest Ophthalmol Vis Sci* 2007;48(9):4220-4225.
143. Sugawara R, Nagaoka T, Kitaya N, et al. Choroidal blood flow in the foveal region in eyes with rhegmatogenous retinal detachment and scleral buckling procedures. *Br J Ophthalmol* 2006;90(11):1363-1365.
144. Samra WA, Pournaras C, Riva C, Emarah M. Choroidal hemodynamic in myopic patients with and without primary open-angle glaucoma. *Acta Ophthalmol* 2013;91(4):371-375.
145. Portmann N, Gugleta K, Kochkorov A, Polunina A, Flammer J, Orgul S. Choroidal blood flow response to isometric exercise in glaucoma patients and patients with ocular hypertension. *Invest Ophthalmol Vis Sci* 2011;52(10):7068-7073.
146. Kochkorov A, Gugleta K, Katamay R, Flammer J, Orgul S. Short-term variability of systemic blood pressure and submacular choroidal blood flow in eyes of patients with primary open-angle glaucoma. *Graefes Arch Clin Exp Ophthalmol* 2010;248(6):833-837.
147. Falsini B, Anselmi GM, Marangoni D, et al. Subfoveal choroidal blood flow and central retinal function in retinitis pigmentosa. *Invest Ophthalmol Vis Sci* 2011;52(2):1064-1069.
148. Chiquet C, Tonini M, Drillat P, Gaudry VV, Romanet JP, Geiser MH. Choroidal blood flow after isovolemic hemodilution in an eye with retinal vein occlusion and the contralateral healthy eye. *Retina* 2010;30(2):275-280.
149. Bosch MM, Merz TM, Barthelmes D, et al. New insights into ocular blood flow at very high altitudes. *J Appl Physiol* 2009;106(2):454-460.
150. Wimpissinger B, Resch H, Berisha F, Weigert G, Schmetterer L, Polak K. Response of retinal blood flow to systemic hyperoxia in smokers and nonsmokers. *Graefes Arch Clin Exp Ophthalmol* 2005;243(7):646-652.
151. Wimpissinger B, Resch H, Berisha T, Weigert G, Polak K, Schmetterer L. Effects of isometric exercise on subfoveal choroidal blood flow in smokers and nonsmokers. *Invest Ophthalmol Vis Sci* 2003;44(11):4859-4863.
152. Niknam RM, Schocket LS, Metelitsina T, DuPont JC, Grunwald JE. Effect of hypertension on foveolar choroidal haemodynamics. *Br J Ophthalmol* 2004;88(10):1263-1265.

153. Yannuzzi LA, Slakter JS, Sorenson JA, Guyer DR, Orlock DA. Digital indocyanine green videoangiography and choroidal neovascularization. *Retina* 1992;12(3):191-223.
154. Dithmar S, Holz FG. Fluorescence Angiography in Ophthalmology. Heidelberg: Springer Medizin Verlag 2008:224.
155. Owens SL. Indocyanine green angiography. *Br J Ophthalmol* 1996;80(3):263-266.
156. Sparrow JR, Dowling JE, Bok D. Understanding RPE lipofuscin. *Invest Ophthalmol Vis Sci* 2013;54(13):8325-8326.
157. Cuba J, Gomez-Ulla F. Fundus autofluorescence: applications and perspectives. *Arch Soc Esp Oftalmol* 2013;88(2):50-55.
158. Delori FC, Dorey CK, Staurengi G, Arend O, Goger DG, Weiter JJ. In vivo fluorescence of the ocular fundus exhibits retinal pigment epithelium lipofuscin characteristics. *Invest Ophthalmol Vis Sci* 1995;36(3):718-729.
159. Keilhauer CN, Delori FC. Near-infrared autofluorescence imaging of the fundus: visualization of ocular melanin. *Invest Ophthalmol Vis Sci* 2006;47(8):3556-3564.
160. Markowitz SN, Reyes SV. Microperimetry and clinical practice: an evidence-based review. *Can J Ophthalmol* 2013;48(5):350-357.
161. Rohrschneider K, Bultmann S, Springer C. Use of fundus perimetry (microperimetry) to quantify macular sensitivity. *Prog Retin Eye Res* 2008;27(5):536-548.
162. Klein R, Klein BE, Moss SE, Davis MD, DeMets DL. The Wisconsin epidemiologic study of diabetic retinopathy. II. Prevalence and risk of diabetic retinopathy when age at diagnosis is less than 30 years. *Arch Ophthalmol* 1984;102(4):520-526.
163. Klein R, Klein BE, Moss SE, Davis MD, DeMets DL. The Wisconsin epidemiologic study of diabetic retinopathy. III. Prevalence and risk of diabetic retinopathy when age at diagnosis is 30 or more years. *Arch Ophthalmol* 1984;102(4):527-532.
164. Cheung N, Mitchell P, Wong TY. Diabetic retinopathy. *Lancet* 2010;376(9735):124-36.
165. Younis N, Broadbent DM, Vora JP, Harding SP, Liverpool Diabetic Eye S. Incidence of sight-threatening retinopathy in patients with type 2 diabetes in the Liverpool Diabetic Eye Study: a cohort study. *Lancet* 2003;361(9353):195-200.
166. Organization WH. Prevention of blindness from diabetes mellitus 2006.
167. Wu L, Fernandez-Loaiza P, Sauma J, Hernandez-Bogantes E, Masis M. Classification of diabetic retinopathy and diabetic macular edema. *World J Diabetes* 2013;4(6):290-294.
168. Wong K. Defining diabetic retinopathy severity. In: Browning D, editor. Diabetic retinopathy evidence-based management, 2010.
169. Wilkinson CP, Ferris FL, 3rd, Klein RE, et al. Proposed international clinical diabetic retinopathy and diabetic macular edema disease severity scales. *Ophthalmology* 2003;110(9):1677-1682.
170. Sivaprasad S, Gupta B, Gulliford MC, et al. Ethnic variations in the prevalence of diabetic retinopathy in people with diabetes attending screening in the United Kingdom (DRIVE UK). *PLoS One* 2012;7(3):e32182.

171. McLeod DS, Lutty GA. High-resolution histologic analysis of the human choroidal vasculature. *Invest Ophthalmol Vis Sci* 1994;35(11):3799-3811.
172. Cao J, McLeod S, Merges CA, Lutty GA. Choriocapillaris degeneration and related pathologic changes in human diabetic eyes. *Arch Ophthalmol* 1998;116(5):589-597.
173. Gerl VB, Bohl J, Pitz S, Stoffelns B, Pfeiffer N, Bhakdi S. Extensive deposits of complement C3d and C5b-9 in the choriocapillaris of eyes of patients with diabetic retinopathy. *Invest Ophthalmol Vis Sci* 2002;43(4):1104-1108.
174. Fukushima I, McLeod DS, Lutty GA. Intrachoroidal microvascular abnormality: a previously unrecognized form of choroidal neovascularization. *Am J Ophthalmol* 1997;124(4):473-487.
175. Querques G, Lattanzio R, Querques L, et al. Enhanced depth imaging optical coherence tomography in type 2 diabetes. *Invest Ophthalmol Vis Sci* 2012;53(10):6017-6024.
176. Regatieri CV, Branchini L, Carmody J, Fujimoto JG, Duker JS. Choroidal thickness in patients with diabetic retinopathy analyzed by spectral-domain optical coherence tomography. *Retina* 2012;32(3):563-568.
177. Vujosevic S, Martini F, Cavarzeran F, Pilotto E, Midena E. Macular and peripapillary choroidal thickness in diabetic patients. *Retina* 2012;32(9):1781-1790.
178. Xu J, Xu L, Du KF, et al. Subfoveal choroidal thickness in diabetes and diabetic retinopathy. *Ophthalmology* 2013;120(10):2023-2028.
179. Schocket LS, Brucker AJ, Niknam RM, Grunwald JE, DuPont J, Brucker AJ. Foveolar choroidal hemodynamics in proliferative diabetic retinopathy. *International Ophthalmology* 2004;25(2):89-94.
180. Nagaoka T, Kitaya N, Sugawara R, et al. Alteration of choroidal circulation in the foveal region in patients with type 2 diabetes. *Br J Ophthalmol* 2004;88(8):1060-1063.
181. Movaffaghy A, Chamot SR, Dosso A, Pournaras CJ, Sommerhalder JR, Riva CE. Effect of isometric exercise on choroidal blood flow in type I diabetic patients. *Klinische Monatsblätter Fur Augenheilkunde* 2002;219(4):299-301.
182. Tarabishy AB, Ahn E, Mandell BF, Lowder CY. Central serous retinopathy. *Arthritis Care Res* 2011;63(8):1075-1082.
183. von Graefe A. Ueber centrale recidivirende retinitis. *Graefes Arch Clin Exp Ophthalmol* 1866;12:211-215.
184. Yannuzzi LA. Type-a behavior and central serous chorioretinopathy. *Retina* 1987;7(2):111-131.
185. Tsai DC, Chen SJ, Huang CC, et al. Epidemiology of idiopathic central serous chorioretinopathy in Taiwan, 2001-2006: a population-based study. *PLoS One* 2013;8(6):e66858.
186. Kitzmann AS, Pulido JS, Diehl NN, Hodge DO, Burke JP. The incidence of central serous chorioretinopathy in Olmsted County, Minnesota, 1980-2002. *Ophthalmology* 2008;115(1):169-173.
187. Quillen DA, Gass DM, Brod RD, Gardner TW, Blankenship GW, Gottlieb JL. Central serous chorioretinopathy in women. *Ophthalmology* 1996;103(1):72-79.

188. Cassel GH, Brown GC, Annesley WH. Central serous chorioretinopathy: a seasonal variation? *Br J Ophthalmol* 1984;68(10):724-726.
189. Ross A, Ross AH, Mohamed Q. Review and update of central serous chorioretinopathy. *Curr Opin Ophthalmol* 2011;22(3):166-173.
190. Wang M, Munch IC, Hasler PW, Prunte C, Larsen M. Central serous chorioretinopathy. *Acta Ophthalmol* 2008;86(2):126-145.
191. Ficker L, Vafidis G, While A, Leaver P. Long-term follow-up of a prospective trial of argon laser photocoagulation in the treatment of central serous retinopathy. *Br J Ophthalmol* 1988;72(11):829-834.
192. Fok AC, Chan PP, Lam DS, Lai TY. Risk factors for recurrence of serous macular detachment in untreated patients with central serous chorioretinopathy. *Ophthalmic Res* 2011;46(3):160-163.
193. Baran NV, Gurlu VP, Esgin H. Long-term macular function in eyes with central serous chorioretinopathy. *Clin Experiment Ophthalmol* 2005;33(4):369-72.
194. Loo RH, Scott IU, Flynn HW, Jr., et al. Factors associated with reduced visual acuity during long-term follow-up of patients with idiopathic central serous chorioretinopathy. *Retina* 2002;22(1):19-24.
195. Castro-Correia J, Coutinho MF, Rosas V, Maia J. Long-term follow-up of central serous retinopathy in 150 patients. *Doc Ophthalmol* 1992;81(4):379-386.
196. Garg SP, Dada T, Talwar D, Biswas NR. Endogenous cortisol profile in patients with central serous chorioretinopathy. *Br J Ophthalmol* 1997;81(11):962-964.
197. Cotticelli L, Borrelli M, D'Alessio AC, et al. Central serous chorioretinopathy and *Helicobacter pylori*. *Eur J Ophthalmol* 2006;16(2):274-278.
198. Carvalho-Recchia CA, Yannuzzi LA, Negrao S, et al. Corticosteroids and central serous chorioretinopathy. *Ophthalmology* 2002;109(10):1834-1837.
199. Tittl MK, Spaide RF, Wong D, et al. Systemic findings associated with central serous chorioretinopathy. *Am J Ophthalmol* 1999;128(1):63-68.
200. Haimovici R, Koh S, Gagnon DR, Lehrfeld T, Wellik S. Central serous chorioretinopathy case-control study g. Risk factors for central serous chorioretinopathy: a case-control study. *Ophthalmology* 2004;111(2):244-249.
201. Rouvas AA, Chatziralli IP, Ladas ID, et al. The impact of financial crisis on central serous chorioretinopathy in Greece: is there any correlation? *Eur J Ophthalmol* 2014;24(4):559-565.
202. Yoshioka H, Katsume Y. Experimental central serous chorioretinopathy. III: ultrastructural findings. *Jpn J Ophthalmol* 1982;26(4):397-409.
203. Prunte C, Flammer J. Choroidal capillary and venous congestion in central serous chorioretinopathy. *Am J Ophthalmol* 1996;121(1):26-34.
204. Imamura Y, Fujiwara T, Margolis R, Spaide RF. Enhanced depth imaging optical coherence tomography of the choroid in central serous chorioretinopathy. *Retina* 2009;29(10):1469-1473.

205. Maruko I, Iida T, Sugano Y, Ojima A, Sekiryu T. Subfoveal choroidal thickness in fellow eyes of patients with central serous chorioretinopathy. *Retina* 2011;31(8):1603-1608.
206. Kim YT, Kang SW, Bai KH. Choroidal thickness in both eyes of patients with unilaterally active central serous chorioretinopathy. *Eye* 2011;25(12):1635-1640.
207. Maruko I, Iida T, Sugano Y, Ojima A, Ogasawara M, Spaide RF. Subfoveal choroidal thickness after treatment of central serous chorioretinopathy. *Ophthalmology* 2010;117(9):1792-1799.
208. Maruko I, Iida T, Sugano Y, Furuta M, Sekiryu T. One-year choroidal thickness results after photodynamic therapy for central serous chorioretinopathy. *Retina* 2011;31(9):1921-1927.
209. Kang NH, Kim YT. Change in subfoveal choroidal thickness in central serous chorioretinopathy following spontaneous resolution and low-fluence photodynamic therapy. *Eye* 2013;27(3):387-391.
210. Kitaya N, Nagaoka T, Hikichi T, et al. Features of abnormal choroidal circulation in central serous chorioretinopathy. *Br J Ophthalmol* 2003;87(6):709-712.
211. Tittl M, Maar N, Polska E, Weigert G, Stur M, Schmetterer L. Choroidal hemodynamic changes during isometric exercise in patients with inactive central serous chorioretinopathy. *Invest Ophthalmol Vis Sci* 2005;46(12):4717-4721.
212. Branchini L, Regatieri C, Flores-Moreno I, Baumann B, Fujimoto J, Duker J. Reproducibility of choroidal thickness measurements across three spectral domain optical coherence tomography systems. *Ophthalmology* 2012;119(1):119-23.
213. Imamura Y, Iida T, Maruko I, Zweifel SA, Spaide RF. Enhanced depth imaging optical coherence tomography of the sclera in dome-shaped macula. *Am J Ophthalmol* 2011;151(2):297-302.
214. Younis N, Broadbent DM, Harding SP, Vora JR. Prevalence of diabetic eye disease in patients entering a systematic primary care-based eye screening programme. *Diabet Med* 2002;19(12):1014-1021.
215. Sahni J, Stanga P, Wong D, Harding S. Optical coherence tomography in photodynamic therapy for subfoveal choroidal neovascularisation secondary to age related macular degeneration: a cross sectional study. *Br J Ophthalmol* 2005;89(3):316-320.
216. Landis JR, Koch GG. The measurement of observer agreement for categorical data. *Biometrics* 1977;33(1):159-174.
217. Bland JM, Altman DG. Statistical methods for assessing agreement between two methods of clinical measurement. *Lancet* 1986;1(8476):307-310.
218. Fliess JL. The design and analysis of clinical experiments. New York: John Wiley & Sons, Inc, 1986:1-32.
219. Petrig B, Gehrig JP, Pompili P. New multi-channel DSP-based laser Doppler flowmetry analysis system for quantification of ocular blood flow. *Proceedings of SPIE* 2001;4156:318 - 327.
220. Jirarattanasopa P, Ooto S, Tsujikawa A, et al. Assessment of macular choroidal thickness by optical coherence tomography and angiographic changes in central serous chorioretinopathy. *Ophthalmology* 2012;119(8):1666-1678.

221. Kohn PM, Macdonald JE. The Survey of Recent Life Experiences: a decontaminated Hassles Scale for adults. *J Behav Med* 1992;15(2):221-36.
222. Brugha T, Bebbington P, Tennant C, Hurry J. The List of Threatening Experiences: a subset of 12 life event categories with considerable long-term contextual threat. *Psychol Med* 1985;15(1):189-94.
223. Kroenke K, Spitzer RL, Williams JB, Lowe B. The Patient Health Questionnaire Somatic, Anxiety, and Depressive Symptom Scales: a systematic review. *Gen Hosp Psychiatry* 2010;32(4):345-59.
224. Cohen S, Kamarck T, Mermelstein R. A global measure of perceived stress. *J Health Soc Behav* 1983;24(4):385-96.
225. Iida T, Kishi S, Hagimura N, Shimizu K. Persistent and bilateral choroidal vascular abnormalities in central serous chorioretinopathy. *Retina* 1999;19(6):508-512.
226. Bafiq R, Mathew R, Pearce E, et al. Age, Sex, and Ethnic Variations in Inner and Outer Retinal and Choroidal Thickness on Spectral-Domain Optical Coherence Tomography. *Am J Ophthalmol* 2015;160(5):1034-1043 e1.
227. <http://www.who.int/mediacentre/factsheets/fs312/en/>. Accessed March 2015.
228. https://www.diabetes.org.uk/About_us/News/diabetes-up-60-per-cent-in-last-decade/. Accessed July 2015.
229. Cheung N, Mitchell P, Wong T. Diabetic retinopathy. *Lancet* 2010;376(9735):124-36.
230. Semeraro F, Cancarini A, dell'Omo R, Rezzola S, Romano MR, Costagliola C. Diabetic retinopathy: vascular and inflammatory disease. *J Diabetes Res* 2015;2015:582060.
231. Kowluru RA, Chan PS. Oxidative stress and diabetic retinopathy. *Exp Diabetes Res* 2007;2007:43603.
232. Luttj GA. Effects of diabetes on the eye. *Invest Ophthalmol Vis Sci* 2013;54(14):ORSF81-7.
233. Spaide RF. Central serous chorioretinopathy. Berlin: Springer-Verlag, 2005:77-93.
234. Gackle HC, Lang GE, Freissler KA, Lang GK. Central serous chorioretinopathy. Clinical, fluorescein angiography and demographic aspects. *Ophthalmologe* 1998;95(8):529-533.
235. Wang M, Sander B, La Cour M, Larsen M. Clinical characteristics of subretinal deposits in central serous chorioretinopathy. *Acta Ophthalmologica Scandinavica* 2005;83(6):691-696.
236. Prunte C. Indocyanine green angiographic findings in central serous chorioretinopathy. *International Ophthalmology* 1995;19(2):77-82.
237. Scheider A, Nasemann JE, Lund OE. Fluorescein and indocyanine green angiographies of central serous choroidopathy by scanning laser ophthalmoscopy. *Am J Ophthalmol* 1993;115(1):50-56.
238. Nishiyama Y, Mori K, Murayama K, Yoneya S. Quantitative analysis of indocyanine green angiographic image in central serous chorioretinopathy. *Jpn J Ophthalmol* 2001;45(1):116.
239. Spaide RF, Hall L, Haas A, et al. Indocyanine green videoangiography of older patients with central serous chorioretinopathy. *Retina* 1996;16(3):203-213.
240. Piccolino FC, Borgia L. Central serous chorioretinopathy and indocyanine green angiography. *Retina* 1994;14(3):231-242.

241. Lafaut BA, De Laey JJ. Indocyanine green angiography in central serous chorioretinopathy. *Bull Soc Belge Ophthalmol* 1996;262:55-61.
242. Fuller PJ, Lim-Tio SS, Brennan FE. Specificity in mineralocorticoid versus glucocorticoid action. *Kidney Int* 2000;57(4):1256-1264.
243. Daruich A, Matet A, Dirani A, et al. Central serous chorioretinopathy: Recent findings and new physiopathology hypothesis. *Prog Retin Eye Res* 2015;48:82-118.
244. Zhao M, Celerier I, Bousquet E, et al. Mineralocorticoid receptor is involved in rat and human ocular chorioretinopathy. *J Clin Invest* 2012;122(7):2672-2679.
245. Han JM, Hwang JM, Kim JS, Park KH, Woo SJ. Changes in choroidal thickness after systemic administration of high-dose corticosteroids: a pilot study. *Invest Ophthalmol Vis Sci* 2014;55(1):440-445.
246. <http://www.ons.gov.uk/>. Accessed January 2015.
247. Ho J, Branchini L, Regatieri C, Krishnan C, Fujimoto JG, Duker JS. Analysis of normal peripapillary choroidal thickness via spectral domain optical coherence tomography. *Ophthalmology* 2011;118(10):2001-2007.
248. Mwanza J-C, Hochberg JT, Banitt MR, Feuer WJ, Budenz DL. Lack of association between glaucoma and macular choroidal thickness measured with enhanced depth-imaging optical coherence tomography. *Invest Ophthalmol Vis Sci* 2011;52(6):3430-3435.
249. Copete S, Flores-Moreno I, Montero JA, Duker JS, Ruiz-Moreno JM. Direct comparison of spectral-domain and swept-source OCT in the measurement of choroidal thickness in normal eyes. *Br J Ophthalmol* 2014;98(3):334-338.
250. Kim JH, Kang SW, Kim JR, Kim SJ. Variability of subfoveal choroidal thickness measurements in patients with age-related macular degeneration and central serous chorioretinopathy. *Eye* 2013;27(7):809-815.
251. Lu H, Boonarpa N, Kwong MT, Zheng Y. Automated segmentation of the choroid in retinal optical coherence tomography images. *Conf Proc IEEE Eng Med Biol Soc* 2013;2013:5869-72.
252. Karapetyan A, Ouyang P, Tang LS, Gemilyan M. Choroidal thickness in relation to ethnicity measured using enhanced depth imaging optical coherence tomography. *Retina* 2015.
253. Hayreh SS. The blood supply of the optic nerve head and the evaluation of it - myth and reality. *Prog Retin Eye Res* 2001;20(5):563-593.
254. Forrester JV. *The Eye: Basic Sciences in Practice*: Saunders, 2008.
255. Feke GT, Zuckerman R, Green GJ, Weiter JJ. Response of human retinal blood flow to light and dark. *Invest Ophthalmol Vis Sci* 1983;24(1):136-141.
256. Arden GB, Sidman RL, Arap W, Schlingemann RO. Spare the rod and spoil the eye. *Br J Ophthalmol* 2005;89(6):764-769.
257. Sanchez-Cano A, Orduna E, Segura F, et al. Choroidal thickness and volume in healthy young white adults and the relationships between them and axial length, ametropia and sex. *Am J Ophthalmol* 2014;158(3):574-583 e1.
258. Lee HK, Lim JW, Shin MC. Comparison of choroidal thickness in patients with diabetes by spectral-domain optical coherence tomography. *Korean J Ophthalmol* 2013;27(6):433-439.

259. Kim JT, Lee DH, Joe SG, Kim JG, Yoon YH. Changes in choroidal thickness in relation to the severity of retinopathy and macular edema in type 2 diabetic patients. *Invest Ophthalmol Vis Sci* 2013;54(5):3378-3384.
260. Braun RD, Wienczewski CA, Abbas A. Erythrocyte flow in choriocapillaris of normal and diabetic rats. *Microvasc Res* 2009;77(3):247-255.
261. Metelitsina TI, Grunwald JE, DuPont JC, Ying GS. Effect of isometric exercise on choroidal blood flow in patients with age-related macular degeneration. *Br J Ophthalmol* 2010;94(12):1629-1631.
262. Pournaras CJ, Logean E, Riva CE, et al. Regulation of subfoveal choroidal blood flow in age-related macular degeneration. *Invest Ophthalmol Vis Sci* 2006;47(4):1581-1586.
263. Geyer O, Neudorfer M, Snir T, et al. Pulsatile ocular blood flow in diabetic retinopathy. *Acta Ophthalmol Scand* 1999;77(5):522-525.
264. Savage HI, Hendrix JW, Peterson DC, Young H, Wilkinson CP. Differences in pulsatile ocular blood flow among three classifications of diabetic retinopathy. *Invest Ophthalmol Vis Sci* 2004;45(12):4504-4509.
265. Schmidt KG, von Ruckmann A, Kemkes-Matthes B, Hammes HP. Ocular pulse amplitude in diabetes mellitus. *Br J Ophthalmol* 2000;84(11):1282-1284.
266. Eom Y, Oh J, Kim SW, Huh K. Systemic factors associated with central serous chorioretinopathy in Koreans. *Korean J Ophthalmol* 2012;26(4):260-264.
267. Desai UR, Alhalel AA, Campen TJ, Schiffman RM, Edwards PA, Jacobsen GR. Central serous chorioretinopathy in African Americans. *J Natl Med Assoc* 2003;95(7):553-559.
268. Erikitoa OC, Crosby-Nwaobi R, Lotery AJ, Sivaprasad S. Photodynamic therapy for central serous chorioretinopathy. *Eye* 2014;28(8):944-57.
269. Herold TR, Prause K, Wolf A, Mayer WJ, Ulbig MW. Spironolactone in the treatment of central serous chorioretinopathy - a case series. *Graefes Arch Clin Exp Ophthalmol* 2014;252(12):1985-91.
270. Bousquet E, Beydoun T, Zhao M, Hassan L, Offret O, Behar-Cohen F. Mineralocorticoid receptor antagonism in the treatment of chronic central serous chorioretinopathy: a pilot study. *Retina* 2013;33(10):2096-102.
271. Razavi S, Souied EH, Cavallero E, Weber M, Querques G. Assessment of choroidal topographic changes by swept source optical coherence tomography after photodynamic therapy for central serous chorioretinopathy. *Am J Ophthalmol* 2014;157(4):852-860.
272. Kim YK, Ryoo NK, Woo SJ, Park KH. Choroidal thickness changes after photodynamic therapy and recurrence of chronic central serous chorioretinopathy. *Am J Ophthalmol* 2015;160(4):841-842.
273. Pitcher JD, Witkin AJ, DeCroos FC, Ho AC. A prospective pilot study of intravitreal aflibercept for the treatment of chronic central serous chorioretinopathy: the CONTAIN study. *Br J Ophthalmol* 2015;99(6):848-852.
274. Alwassia AA, Adhi M, Zhang JY, et al. Exercise-induced acute changes in systolic blood pressure do not alter choroidal thickness as measured by a portable spectral-domain optical coherence tomography device. *Retina* 2013;33(1):160-165.

275. Jia Y, Bailey ST, Hwang TS, et al. Quantitative optical coherence tomography angiography of vascular abnormalities in the living human eye. *Proc Natl Acad Sci U S A* 2015;112(18):E2395-402.
276. Saito M, Saito W, Hashimoto Y, et al. Macular choroidal blood flow velocity decreases with regression of acute central serous chorioretinopathy. *Br J Ophthalmol* 2013;97(6):775-780.
277. Tewari HK, Gadia R, Kumar D, Venkatesh P, Garg SP. Sympathetic-parasympathetic activity and reactivity in central serous chorioretinopathy: a case-control study. *Invest Ophthalmol Vis Sci* 2006;47(8):3474-3478.
278. Haimovici R, Rumelt S, Melby J. Endocrine abnormalities in patients with central serous chorioretinopathy. *Ophthalmology* 2003;110(4):698-703.
279. Marin Garcia PJ, Marin-Castano ME. Angiotensin II-related hypertension and eye diseases. *World J Cardiol* 2014;6(9):968-984.
280. Luksch A, Polska E, Imhof A, et al. Role of NO in choroidal blood flow regulation during isometric exercise in healthy humans. *Invest Ophthalmol Vis Sci* 2003;44(2):734-739.
281. Ferrara D, Mohler KJ, Waheed N, et al. En face enhanced-depth swept-source optical coherence tomography features of chronic central serous chorioretinopathy. *Ophthalmology* 2014;121(3):719-726.
282. Lumbroso B, Huang D, Romano A, Rispoli M, Coscas G. Clinical En Face OCT atlas. New Delhi: Jaypee Brothers Medical Publishers (P) Ltd, 2013.
283. Jia Y, Bailey ST, Wilson DJ, et al. Quantitative optical coherence tomography angiography of choroidal neovascularization in age-related macular degeneration. *Ophthalmology* 2014;121(7):1435-1444.
284. Spaide RF, Klancnik JM, Jr., Cooney MJ. Retinal vascular layers imaged by fluorescein angiography and optical coherence tomography angiography. *JAMA Ophthalmol* 2015;133(1):45-50.

Appendices

Appendix A. Ethic approval for Liverpool CSCR study



Health Research Authority

National Research Ethics Service

NRES Committee West Midlands - South Birmingham

HRA NRES Centre Manchester
3rd Floor
Barlow House
4 Minshull Street
Manchester
M1 3DZ

Telephone: 0161 625 7815
Facsimile: 0161 625 7299

18 July 2013

Mrs Jayashree Sahni
Consultant Ophthalmologist
Royal Liverpool University Hospitals NHS Trust
St Paul's Eye Unit
Liverpool
L7 8XP

Dear Mrs Sahni

Study title: The Liverpool Central Serous Chorioretinopathy Study
REC reference: 13/WM/0237
IRAS project ID: 129990

Thank you for your email of 15 July 2013, responding to the Committee's request for further information on the above research and submitting revised documentation.

The further information has been considered on behalf of the Committee by the Chair.

We plan to publish your research summary wording for the above study on the NRES website, together with your contact details, unless you expressly withhold permission to do so. Publication will be no earlier than three months from the date of this favourable opinion letter. Should you wish to provide a substitute contact point, require further information, or wish to withhold permission to publish, please contact the Co-ordinator Dr Ashley Totenhofer, nrescommittee.westmidlands-southbirmingham@nhs.net.

Confirmation of ethical opinion

On behalf of the Committee, I am pleased to confirm a favourable ethical opinion for the above research on the basis described in the application form, protocol and supporting documentation as revised, subject to the conditions specified below.

Ethical review of research sites

NHS sites

The favourable opinion applies to all NHS sites taking part in the study, subject to management permission being obtained from the NHS/HSC R&D office prior to the start of the study (see "Conditions of the favourable opinion" below).

Conditions of the favourable opinion

The favourable opinion is subject to the following conditions being met prior to the start of the study.

Management permission or approval must be obtained from each host organisation prior to the start of the study at the site concerned.

Management permission ("R&D approval") should be sought from all NHS organisations involved in the study in accordance with NHS research governance arrangements.

Guidance on applying for NHS permission for research is available in the Integrated Research Application System or at <http://www.rdforum.nhs.uk>.

Where a NHS organisation's role in the study is limited to identifying and referring potential participants to research sites ("participant identification centre"), guidance should be sought from the R&D office on the information it requires to give permission for this activity.

For non-NHS sites, site management permission should be obtained in accordance with the procedures of the relevant host organisation.

Sponsors are not required to notify the Committee of approvals from host organisations

It is the responsibility of the sponsor to ensure that all the conditions are complied with before the start of the study or its initiation at a particular site (as applicable).

Approved documents

The final list of documents reviewed and approved by the Committee is as follows:

Document	Version	Date
Advertisement	Flyer - Version 1	25 June 2013
Covering Letter		30 May 2013
Covering Letter		02 July 2013
GP/Consultant Information Sheets	1	18 April 2013
Investigator CV	Jayashree Sahni	29 May 2013
Letter from Sponsor	The Royal Liverpool and Broadgreen University Hospitals NHS Trust	03 June 2013
Letter of invitation to participant	1	25 June 2013
Participant Consent Form: Group B : Healthy Controls	1	24 June 2013
Participant Consent Form: Group A: CSCR Patients	2	24 June 2013
Participant Information Sheet: Group B : Healthy Controls	2	24 June 2013
Participant Information Sheet: Group A: CSCR Patients	2	24 June 2013
Participant Information Sheet: Fluorescein Angiography		
Protocol	1	21 April 2013
Questionnaire: Participant Questionnaire	1	24 June 2013
REC application	3.5	30 May 2013
Response to Request for Further Information		15 July 2013

Statement of compliance

The Committee is constituted in accordance with the Governance Arrangements for Research Ethics Committees and complies fully with the Standard Operating Procedures for Research

Ethics Committees in the UK.

After ethical review

Reporting requirements

The attached document "*After ethical review – guidance for researchers*" gives detailed guidance on reporting requirements for studies with a favourable opinion, including:

- Notifying substantial amendments
- Adding new sites and investigators
- Notification of serious breaches of the protocol
- Progress and safety reports
- Notifying the end of the study

The NRES website also provides guidance on these topics, which is updated in the light of changes in reporting requirements or procedures.

Feedback

You are invited to give your view of the service that you have received from the National Research Ethics Service and the application procedure. If you wish to make your views known please use the feedback form available on the website.

Further information is available at National Research Ethics Service website > After Review

13/WM/0237

Please quote this number on all correspondence

We are pleased to welcome researchers and R & D staff at our NRES committee members' training days – see details at <http://www.hra.nhs.uk/hra-training/>

With the Committee's best wishes for the success of this project.

Yours sincerely



Signed on behalf of:
Professor Simon Bowman
Chair

Email: nrescommittee.westmidlands-southbirmingham@nhs.net

Enclosures: "After ethical review – guidance for researchers"

Copy to: Mr Nattapon Boonarpa - The University of Liverpool

Mrs Heather Rogers - Royal Liverpool University Hospital

Appendix B. The Liverpool CSCR study questionnaires

Liverpool CSCR Study
Participant Questionnaire

The Royal Liverpool and 
Broadgreen University Hospitals
NHS Trust

Royal Liverpool University Hospital
Prescot Street
Liverpool
L7 8XP

Tel: 0151 706 2000
Fax: 0151 706 5806

The Liverpool Central Serous Chorioretinopathy Study (Liverpool CSCR Study)

Trust R&D Study Number: 4571

Questionnaires

Names of Lead Researchers:

Mrs Jayashree Sahni (Principal Investigator), Mr Nattapon Boonarpha

What is the purpose of this questionnaire?

This questionnaire is a part of the research project that is being carried out at St. Paul's Eye Unit, Royal Liverpool University Hospital. The purpose of this questionnaire is to assess the relationship of stress and determine the psychological profile support to the central serous chorioretinopathy disease. The information that we receive from you will be valuable for future diagnosis, treatment and management of this disease.

What are the procedures?

You will be asked to complete all the questions in this questionnaire. Please take your time to be familiar with all the questions within this questionnaire and feel free to ask if there any doubts occur during your time with the questionnaire.

What are the possible disadvantages and risks of taking part?

Since these are the questionnaire that widely use in research, there are no risk of upsetting of participant.

What are the possible benefits of taking part?

There will be no immediate benefit to you as an individual person. However, we hope that the study will help us to clarify some aspects of the CSCR disease. This will help us making a better assessment of your eye, allowing a more precise diagnosis and management where the CSCR is present.

Will my taking part in this study be kept confidential?

The questionnaire will be coded with a unique identifier numbers and letters and will not contain your name or any identification.

- 24. Decisions about intimate relationship(s).....
- 25. Not enough time to meet your obligations.....
- 26. Dissatisfaction with your mathematical ability.....
- 27. Financial burdens.....
- 28. Lower evaluation of your work than you think you deserve.....
- 29. Experiencing high levels of noise.....
- 30. Adjustments to living with unrelated person(s) (e.g., roommate).....
- 31. Lower evaluation of your work than you hoped for.....
- 32. Conflicts with family member(s).....
- 33. Finding your work too demanding.....
- 34. Conflicts with friend(s).....
- 35. Hard effort to get ahead.....
- 36. Trying to secure loan(s).....
- 37. Getting "ripped off" or cheated in the purchase of goods.....
- 38. Dissatisfaction with your ability at written expression.....
- 39. Unwanted interruptions of your work.....
- 40. Social isolation.....
- 41. Being ignored.....
- 42. Dissatisfaction with your physical appearance.....
- 43. Unsatisfactory housing conditions.....
- 44. Finding work uninteresting.....
- 45. Failing to get money you expected.....
- 46. Gossip about someone you care about.....
- 47. Dissatisfaction with your physical fitness.....
- 48. Gossip about yourself.....
- 49. Difficulty dealing with modern technology (e.g., computers).....
- 50. Car problems.....
- 51. Hard work to look after and maintain home.....

Life Events Questionnaire (LEQ)

Instruction: Please check the box or boxes corresponding to the event or events which have happened to you during the last six months. Please also check the box or boxes corresponding to the month or months of the event or events that have happened to you.

Event	Time						
		1 month ago	2 months ago	3 months ago	4 months ago	5 months ago	6 months ago
1. Have you suffered from a serious illness, injury or an assault?	<input type="checkbox"/> Yes <input type="checkbox"/> No						
2. Has a serious illness, injury or assault happened to a close relative?	<input type="checkbox"/> Yes <input type="checkbox"/> No						
3. Has a parent, spouse (or partner), child, brother or sister of yours died?	<input type="checkbox"/> Yes <input type="checkbox"/> No						
4. Has a close family friend or other relative (such as an aunt, cousin or grandparent) died?	<input type="checkbox"/> Yes <input type="checkbox"/> No						
5. Have you had a separation due to marital difficulties or break off a steady relationship?	<input type="checkbox"/> Yes <input type="checkbox"/> No						
6. Have you had a serious problem with a close friend, neighbour or relatives?	<input type="checkbox"/> Yes <input type="checkbox"/> No						

Event	Time						
		1 month ago	2 months ago	3 months ago	4 months ago	5 months ago	6 months ago
7. Have you been made redundant or fired from your job?	<input type="checkbox"/> Yes <input type="checkbox"/> No						
8. Have you been seeking work without success for more than a month?	<input type="checkbox"/> Yes <input type="checkbox"/> No						
9. Have you had a major financial crisis?	<input type="checkbox"/> Yes <input type="checkbox"/> No						
10. Have you had problems with the police involving a court appearance?	<input type="checkbox"/> Yes <input type="checkbox"/> No						
11. Has something you valued been lost or stolen?	<input type="checkbox"/> Yes <input type="checkbox"/> No						
12. Have you/your wife or partner given birth to a child?	<input type="checkbox"/> Yes <input type="checkbox"/> No						

Patient Health Questionnaire – 9 (PHQ-9)

Instruction: Please indicate how often have you been bothered by any of the following problems over *the last 2 weeks*

	Not at all	Several days	More than half the days	Nearly every day
1. Little interest or pleasure in doing things	0	1	2	3
2. Feeling down, depressed, or hopeless	0	1	2	3
3. Trouble falling or staying asleep, or sleeping too much	0	1	2	3
4. Feeling tired or having little energy	0	1	2	3
5. Poor appetite or overeating	0	1	2	3
6. Feeling bad about yourself — or that you are a failure or have let yourself or your family down	0	1	2	3
7. Trouble concentrating on things, such as reading the newspaper or watching television	0	1	2	3
8. Moving or speaking so slowly that other people could have noticed? Or the opposite - being so fidgety or restless that you have been moving around a lot more than usual	0	1	2	3
9. Thoughts that you would be better off dead or of hurting yourself in some way	0	1	2	3

If you checked off **any problems**, how **difficult** have these problems made it for you to do your work, take care of things at home, or get along with other people?

Not difficult at all	Somewhat difficult	Very difficult	Extremely difficult
<input type="checkbox"/>	<input type="checkbox"/>	<input type="checkbox"/>	<input type="checkbox"/>

Patient Health Questionnaire – 15 (PHQ-15)

Instruction: Please indicate how much have you been bothered by any of the following problems over *the last 4 weeks*

	Not bothered at all (0)	Bothered a little (1)	Bothered a lot (2)
A. Stomach pain			
B. Back pain			
C. Pain in your arms, legs, or joints (knees, hips, etc.)			
D. Menstrual cramps or other problems with your periods (WOMEN ONLY)			
E. Headaches			
F. Chest pain			
G. Dizziness			
H. Fainting spells			
I. Feeling your heart pound or race			
J. Shortness of breath			
K. Pain or problems during sexual intercourse			
L. Constipation, loose bowels, or diarrhea			
M. Nausea, gas, or indigestion			
N. Feeling tired or having low energy			
O. Trouble sleeping			

Perceived Stress Scale (PSS)

Instruction: Please indicate *how often* you felt or thought a certain way to each question during the last month. The best approach is to answer each question fairly quickly. That is, don't try to count up the number of times you felt a particular way, but rather indicate the alternative that seems like a reasonable estimate. To answer the question, please circle the appropriate number using the following estimation scale.

0 = Never 1 = Almost Never 2 = Sometimes 3 = Fairly Often 4 = Very Often

	Never	Almost Never	Sometimes	Fairly Often	Very Often
1. In the last month, how often have you been upset because of something that happened unexpectedly?	0	1	2	3	4
2. In the last month, how often have you felt that you were unable to control the important things in your life?	0	1	2	3	4
3. In the last month, how often have you felt nervous and "stressed"?	0	1	2	3	4
4. In the last month, how often have you dealt successfully with irritating life hassles?	0	1	2	3	4
5. In the last month, how often have you felt that you were effectively coping with important changes that were occurring in your life?	0	1	2	3	4
6. In the last month, how often have you felt confident about your ability to handle your personal problems?	0	1	2	3	4
7. In the last month, how often have you felt that things were going your way?	0	1	2	3	4
8. In the last month, how often have you found that you could not cope with all the things that you had to do?	0	1	2	3	4

9. In the last month, how often have you been able to control irritations in your life?	0	1	2	3	4
10. In the last month, how often have you felt that you were on top of things?	0	1	2	3	4
11. In the last month, how often have you been angered because of things that happened that were outside of your control?	0	1	2	3	4
12. In the last month, how often have you found yourself thinking about things that you have to accomplish?	0	1	2	3	4
13. In the last month, how often have you been able to control the way you spend your time?	0	1	2	3	4
14. In the last month, how often have you felt difficulties were piling up so high that you could not overcome them?	0	1	2	3	4

Appendix C. Lists of publications

Peer reviewed publications

- Boonarpa N, Zheng Y, Stangos AN, *et al.* **Standardization of choroidal thickness measurements using enhanced depth imaging optical coherence tomography.** International journal of ophthalmology 2015; 8
- Lu H, Boonarpa N, Kwong MT, Zheng Y. **Automated segmentation of the choroid in retinal optical coherence tomography images. Conference proceedings :** Annual International Conference of the IEEE Engineering in Medicine and Biology Society IEEE Engineering in Medicine and Biology Society Annual Conference 2013

Published abstracts

- **Interactive and automated segmentation of the choroid in enhanced depth optical coherence tomography** (ARVO/ISIE Imaging Conference 2013)
- **Improving the analysis of choroidal laser Doppler flowmetry** (ARVO 2013)
- **Impact of hypertension on choroidal thickness in central serous chorioretinopathy** (ARVO 2015)

Standardization of choroidal thickness measurements using enhanced depth imaging optical coherence tomography

Nattapon Boonarpa^{1,2}, Yalin Zheng^{1,2}, Alexandros N. Stangos², Huiqi Lu^{1,2}, Ankur Raj^{1,2}, Gabriela Czanner^{1,3}, Simon P. Harding^{1,2}, Jayashree Nair-Sahni^{1,2}

¹Department of Eye and Vision Science, Institute of Ageing and Chronic Disease, University of Liverpool, Liverpool L69 3GA, United Kingdom

²St. Paul's Eye Unit, Royal Liverpool University Hospital, Liverpool L7 8XP, United Kingdom

³Department of Biostatistics, University of Liverpool, Liverpool L69 3GS, United Kingdom

Correspondence to: Jayashree Nair-Sahni. Department of Eye and Vision Science, Institute of Ageing and Chronic Disease, University of Liverpool, 3rd Floor, UCD Building, Daulby Street, Liverpool L69 3GA, United Kingdom. j.sahni@liverpool.ac.uk

Received: 2014-11-01

Accepted: 2014-12-15

Abstract

• **AIM:** To describe and evaluate a standardized protocol for measuring the choroidal thickness (ChT) using enhanced depth imaging optical coherence tomography (EDI OCT).

• **METHODS:** Single 9 mm EDI OCT line scans across the fovea were used for this study. The protocol used in this study classified the EDI OCT images into four groups based on the appearance of the choroidal-scleral interface and suprachoroidal space. Two evaluation iterations of experiments were performed: first, the protocol was validated in a pilot study of 12 healthy eyes. Afterwards, the applicability of the protocol was tested in 82 eyes of patients with diabetes. Inter-observer and intra-observer agreements on image classifications were performed using Cohen's kappa coefficient (κ). Intraclass correlation coefficient (ICC) and Bland-Altman's methodology were used for the measurement of the ChT.

• **RESULTS:** There was a moderate ($\kappa=0.42$) and perfect ($\kappa=1$) inter- and intra-observer agreements on image classifications from healthy eyes images and substantial ($\kappa=0.66$) and almost perfect ($\kappa=0.86$) agreements from diabetic eyes images. The proposed protocol showed excellent inter- and intra-observer agreements for the ChT measurements on both, healthy eyes and diabetic eyes (ICC >0.90 in all image categories). The Bland-

Altman plot showed a relatively large ChT measurement agreement in the scans that contained less visible choroidal outer boundary.

• **CONCLUSION:** A protocol to standardize ChT measurements in EDI OCT images has been developed; the results obtained using this protocol show that the technique is accurate and reliable for routine clinical practice and research.

• **KEYWORDS:** choroid; enhanced depth imaging; choroidal thickness; optical coherence tomography; diabetes

DOI:10.3980/j.issn.2222-3959.2015.03.09

Boonarpa N, Zheng Y, Stangos AN, Lu H, Raj A, Czanner G, Harding SP, Nair-Sahni J. Standardization of choroidal thickness measurements using enhanced depth imaging optical coherence tomography. *Int J Ophthalmol* 2015;8(3):484-491

INTRODUCTION

There is a growing interest in the role of the choroid in various chorioretinal diseases. Abnormalities of the choroidal integrity have been associated with the pathogenesis of several retinal diseases, such as age-related macular degeneration (AMD)^[1], central serous chorioretinopathy (CSCR)^[2] and diabetic maculopathy^[3].

New optical coherence tomography (OCT) image modalities, including enhanced depth imaging OCT (EDI OCT)^[4] and a longer wavelength swept source OCT^[5], enable a better visualization of the choroid in contrast to conventional techniques such as indocyanine green angiography and ultrasonography. Measuring the choroidal thickness (ChT) may become one of the determinants in the pathogenesis of several eye disease conditions^[2,6-8] as well as in healthy eyes during the aging process^[9-11].

The precise location of the choroidal-scleral interface (CSI) is essential for the accurate measurement of the ChT. Histologically, the choroid consists of 4 layers: Bruch's membrane, choriocapillaris, choroidal stroma and suprachoroid, which consists of the suprachoroidal lamina and the suprachoroidal space (SCS)^[12]. These choroidal histological structures are not clearly demarcated on the OCT images. Usually, the anterior boundary of the choroid is

easily identifiable in normal OCT and EDI OCT images as the outer limit of the hyper-reflective band representing the retinal pigment epithelium (RPE) and Bruch's membrane complex. The outer boundary of the choroid, on the other hand, appears to vary depending on the image quality. On EDI OCT images, the outer boundary of the choroid has been previously described by Spaide *et al*^[11] as the hypo-reflective space underneath the choroid SCS while Maul *et al*^[12] described it as a well demarcated hyper-reflective band between the large choroidal vessels and the sclera CSI. However, the clarity of the outer boundary of the choroid on EDI OCT images often suffer from the limitations of the penetration power of the OCT device and it might be further affected by the status and types of disease. This limitation may prevent the ability to visualize the choroidal structures on the EDI OCT images, resulting in the variability of manual measurements of the ChT, which in turn limit the applicability of EDI OCT measurements to identify and monitor pathology.

Different groups have defined the posterior boundary of the choroid as either the inner surface of the sclera or as the area demarcated by the hyper-reflective margin between the end of large choroidal vessels and the sclera^[9,10,14,15]. To date, there is a lack of clarity in the definition of the outer boundary of the choroid in ChT measurements which in turn may lead to problems in comparative studies.

In this study, we propose a standardized protocol for defining the variation in the topographical appearance of the choroidal posterior boundary in patients with eye disease using diabetes as a disease model. We have validated this standardized protocol by determining the inter- and intra-observer agreements in the classification of EDI OCT images and the inter- and intra-observer agreements of ChT measurements.

SUBJECTS AND METHODS

Subjects Subjects, including normal healthy volunteers with no known previous eye diseases and patients with diabetes, were recruited into this cross-sectional prospective observational study. The study was conducted in accordance with the Declaration of Helsinki. Informed consents were obtained from all subjects prior to their participation in the study.

All subjects underwent slit lamp biomicroscopy, best corrected visual acuity (BCVA) test using Bailey-Lovie logMAR (logarithm of the minimum angle of resolution) chart and EDI OCT scan on the Spectralis SD OCT system (Heidelberg Engineering, Heidelberg, Germany). For patients with diabetes, the inclusion criteria were men and women aged 18 or over with Type 1 or 2 diabetes mellitus, with or without any stage of diabetic retinopathy (DR). The degrees of retinopathy and maculopathy were graded by trained graders using the Liverpool Diabetic Eye Study (LDES) grading protocol^[16]. The exclusion criteria for patients with

diabetes included pregnancy, previous macular or pan-retinal laser treatment, contraindication to dilatation, history of intraocular injection or surgery and other significant eye diseases.

Horizontal EDI OCT images were taken using the Spectralis SD OCT system (Heidelberg Engineering, Heidelberg, Germany) by an externally accredited imaging scientist (Lu H). The EDI acquisition was done using the protocol previously described by Margolis and Spaide^[10]. An automatic real-time (ART) averaging of 100 was applied to each section using the built-in automatic averaging and real time eye-tracking features in order to obtain images of adequate quality for visualization and to maximize the signal-to-noise ratio. The images were exported at a 1:1 pixel ratio for analyses.

Standardized Protocol for Defining Choroidal Margins

Single 9 mm horizontal EDI OCT line scan passing through the center of the fovea was used for analysis. The foveal center was defined as the point of maximum depression within an area of 500 μ m in diameter^[17]. When both the SCS and the CSI were identified in the image, the CSI was seen as a clear intermediate hyper-reflective band outer to the vascular-like structure of the choroid and the SCS was seen as a hypo-reflective band posterior to the CSI (Figure 1). The images were first classified into four sub-groups depending on the presence or the absence of the SCS and the CSI at the posterior boundary of the choroid (Figure 2).

Group A: both structures (CSI and SCS) were present and more than 80% of the CSI and SCS layers were identifiable across the length of the scan. Group B: 2 image categories were included within this group 1) both structures (CSI and SCS) were observed in the scan, however, it was in less than 80% of the length of the scan; 2) scans where only one of the structures were observed, either CSI or SCS. Group C: neither SCS nor CSI were observed in the scan, however, a distinct smooth line indicating the outer limit of the large choroidal vessels with the sclera was seen. Ungradable: scans showed either no identifiable posterior boundary of the choroid or a portion of the choroidal structure was missing.

The anterior boundary of the choroid in each image was defined as the hyper-reflective band corresponding to the RPE-Bruch's membrane complex. The posterior boundary was defined and based on the classification as follows: for group A, the outer limit of the CSI was used; for group B, the outer limit of the CSI was used where both SCS and CSI were visible in the image. Where only one of the two were identifiable, the posterior boundary was drawn at either the outer limit of the CSI or the inner limit of the SCS. For group C, the smooth band signifying the outer limit of the large choroidal vessels was used.

easily identifiable in normal OCT and EDI OCT images as the outer limit of the hyper-reflective band representing the retinal pigment epithelium (RPE) and Bruch's membrane complex. The outer boundary of the choroid, on the other hand, appears to vary depending on the image quality. On EDI OCT images, the outer boundary of the choroid has been previously described by Spaide *et al*^[11] as the hypo-reflective space underneath the choroid SCS while Maul *et al*^[12] described it as a well demarcated hyper-reflective band between the large choroidal vessels and the sclera CSI. However, the clarity of the outer boundary of the choroid on EDI OCT images often suffer from the limitations of the penetration power of the OCT device and it might be further affected by the status and types of disease. This limitation may prevent the ability to visualize the choroidal structures on the EDI OCT images, resulting in the variability of manual measurements of the ChT, which in turn limit the applicability of EDI OCT measurements to identify and monitor pathology.

Different groups have defined the posterior boundary of the choroid as either the inner surface of the sclera or as the area demarcated by the hyper-reflective margin between the end of large choroidal vessels and the sclera^[9,10,14,15]. To date, there is a lack of clarity in the definition of the outer boundary of the choroid in ChT measurements which in turn may lead to problems in comparative studies.

In this study, we propose a standardized protocol for defining the variation in the topographical appearance of the choroidal posterior boundary in patients with eye disease using diabetes as a disease model. We have validated this standardized protocol by determining the inter- and intra-observer agreements in the classification of EDI OCT images and the inter- and intra-observer agreements of ChT measurements.

SUBJECTS AND METHODS

Subjects Subjects, including normal healthy volunteers with no known previous eye diseases and patients with diabetes, were recruited into this cross-sectional prospective observational study. The study was conducted in accordance with the Declaration of Helsinki. Informed consents were obtained from all subjects prior to their participation in the study.

All subjects underwent slit lamp biomicroscopy, best corrected visual acuity (BCVA) test using Bailey-Lovie logMAR (logarithm of the minimum angle of resolution) chart and EDI OCT scan on the Spectralis SD OCT system (Heidelberg Engineering, Heidelberg, Germany). For patients with diabetes, the inclusion criteria were men and women aged 18 or over with Type 1 or 2 diabetes mellitus, with or without any stage of diabetic retinopathy (DR). The degrees of retinopathy and maculopathy were graded by trained graders using the Liverpool Diabetic Eye Study (LDES) grading protocol^[16]. The exclusion criteria for patients with

diabetes included pregnancy, previous macular or pan-retinal laser treatment, contraindication to dilatation, history of intraocular injection or surgery and other significant eye diseases.

Horizontal EDI OCT images were taken using the Spectralis SD OCT system (Heidelberg Engineering, Heidelberg, Germany) by an externally accredited imaging scientist (Lu H). The EDI acquisition was done using the protocol previously described by Margolis and Spaide^[10]. An automatic real-time (ART) averaging of 100 was applied to each section using the built-in automatic averaging and real time eye-tracking features in order to obtain images of adequate quality for visualization and to maximize the signal-to-noise ratio. The images were exported at a 1:1 pixel ratio for analyses.

Standardized Protocol for Defining Choroidal Margins

Single 9 mm horizontal EDI OCT line scan passing through the center of the fovea was used for analysis. The foveal center was defined as the point of maximum depression within an area of 500 μ m in diameter^[17]. When both the SCS and the CSI were identified in the image, the CSI was seen as a clear intermediate hyper-reflective band outer to the vascular-like structure of the choroid and the SCS was seen as a hypo-reflective band posterior to the CSI (Figure 1). The images were first classified into four sub-groups depending on the presence or the absence of the SCS and the CSI at the posterior boundary of the choroid (Figure 2).

Group A: both structures (CSI and SCS) were present and more than 80% of the CSI and SCS layers were identifiable across the length of the scan. Group B: 2 image categories were included within this group 1) both structures (CSI and SCS) were observed in the scan, however, it was in less than 80% of the length of the scan; 2) scans where only one of the structures were observed, either CSI or SCS. Group C: neither SCS nor CSI were observed in the scan, however, a distinct smooth line indicating the outer limit of the large choroidal vessels with the sclera was seen. Ungradable: scans showed either no identifiable posterior boundary of the choroid or a portion of the choroidal structure was missing.

The anterior boundary of the choroid in each image was defined as the hyper-reflective band corresponding to the RPE-Bruch's membrane complex. The posterior boundary was defined and based on the classification as follows: for group A, the outer limit of the CSI was used; for group B, the outer limit of the CSI was used where both SCS and CSI were visible in the image. Where only one of the two were identifiable, the posterior boundary was drawn at either the outer limit of the CSI or the inner limit of the SCS. For group C, the smooth band signifying the outer limit of the large choroidal vessels was used.

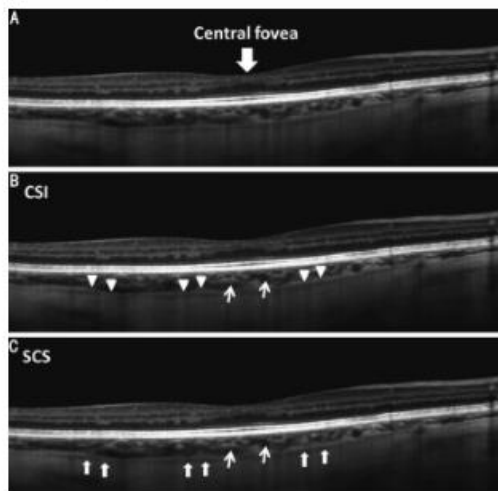


Figure 1 A single 9 mm horizontal line scan with enhanced depth imaging obtained from the right eye of a 55-year-old healthy male. A: The choroidal-scleral interface (CSI); B: Is indicated by a well demarcated hyper-reflective band (triangle heads) and the supra-choroidal space (SCS); C: Is indicated by the hypo-reflective band (arrows). The narrow arrows indicate the cross section of large choroidal vessels.

Measurement of Choroidal Thickness All EDI OCT images were classified and delineated using the proposed protocol by two masked expert observers (Boonarpa N and Stangos AN). In addition, observer Boonarpa N repeated the classification and measurement tasks one week later, masked from the previous measurements. The anterior and posterior boundaries of the choroid were manually delineated using Image J software version 1.45S (National Institutes of Health, USA). The ChT was then measured as the perpendicular distance between the anterior and posterior boundary at 500 μm intervals up to 3 mm nasal and 3 mm temporal from the foveal center using a program developed in MATLAB R2012a (The Mathworks Inc., Natick, USA). The total ChT was calculated from the average ChT from the 13 locations measured. The subfoveal ChT was used to represent the ChT at the foveal center.

Two evaluation iterations were performed: in the pilot study, the images from healthy volunteers were analyzed to test if the standardization methodology was valid. The second experiment was performed to evaluate whether the protocol was applicable for the management of disease represented by images from patients with diabetes.

Statistical Analysis Statistical analyses were performed using the Statistical Package for Social Scientists (SPSS) program version 20 (SPSS Inc., IBM, USA).

In order to determine the level of agreement between observers on the evaluation of the choroidal topographic

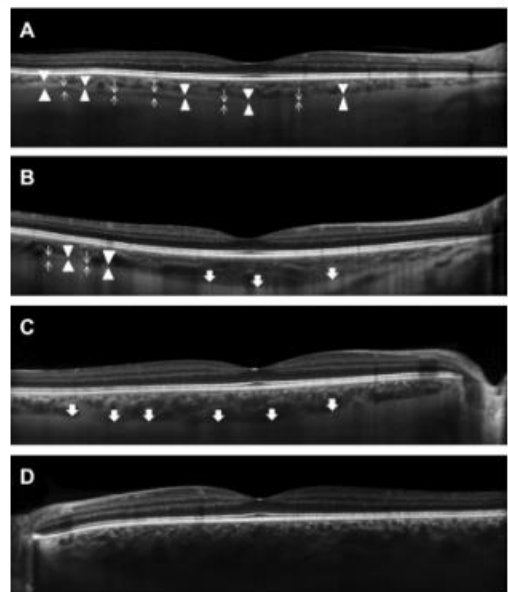


Figure 2 Example of EDI OCT image classifications categories. Group A (A), the choroidal outer boundary consists of more than 80% of the CSI (triangle heads) and the SCS (narrow arrows) across the length of the scan. Group B (B) consists of less than 80% of the CSI and the SCS across the length of the scan. Group C (C) consists of a smooth line between the outer limit of large choroidal vessels and the sclera (wide arrows) and ungradable (D) when the outer choroidal boundary is not identifiable on the scan.

appearances on EDI OCT scans, the Cohen's kappa coefficient (κ) was calculated (less than 0.20 signifies poor agreement, $\kappa=0.21-0.40$ fair, $\kappa=0.41-0.60$ moderate, $\kappa=0.61-0.80$ substantial, $\kappa=0.81-1.00$ almost perfect agreement)^[19].

Inter- and intra-observer agreements for the thickness measurements were shown using Bland and Altman plot^[20]. The coefficient of repeatability (CR) was defined as $1.96 \times$ standard deviation (SD) between two measurements. These analyses were done separately on 5 sets of images (*i.e.* group A, group B, group C, group agreed as ungradable and non-agreed images) for the total ChT and the subfoveal ChT. Intraclass correlation coefficient (ICC) was used to determine the reliability of the measurements. An ICC value below 0.40 represents poor agreement, 0.40-0.75 represents fair to good agreement and above 0.75 represents excellent agreement^[20]. A 5% level of significance was considered.

RESULTS

A total of 58 subjects (46 patients with diabetes and 12 healthy volunteers) were recruited in this study. The mean age of the 12 healthy volunteers (5 males) was 43.3 (± 12)y (range 28-67). The mean age of the 46 subjects with diabetes

Table 1 Summary of inter-observer agreements on the total and subfoveal choroidal thickness measurements

Inter-observer agreement	Total ChT			Subfoveal ChT		
	ICC (95%CI)	Mean difference (95%CI) (µm)	CR (µm)	ICC (95%CI)	Mean difference (95%CI) (µm)	CR (µm)
Group A	0.985 (0.873-0.996)	7.1 (4.1-10.2)	14.1	0.986 (0.965-0.994)	4.4 (-0.4-9.2)	22.2
Group B	0.963 (0.913-0.984)	5.8 (-3.5-15.0)	40.7	0.916 (0.778-0.967)	18.5 (2.7-34.3)	69.8
Group C	0.971 (0.912-0.990)	10.7 (-0.2-21.6)	41.4	0.959 (0.880-0.985)	15.1 (-1.0-31.2)	61.4
Overall	0.972 (0.944-0.985)	7.6 (3.4-11.9)	33.1	0.949 (0.900-0.972)	12.2 (5.2-19.2)	54.4
Non-agreement	0.964 (0.878-0.988)	15.7 (3.4-28.0)	49.9	0.918 (0.747-0.971)	27.4 (5.5-49.3)	89.2

ICC: Intraclass correlation coefficient; CI: Confidence interval; CR: Coefficient of repeatability; ChT: Choroidal thickness.

Table 2 Summary of intra-observer agreements on the total and subfoveal choroidal thickness measurements

Intra-observer agreement	Total ChT			Subfoveal ChT		
	ICC (95%CI)	Mean difference (95%CI) (µm)	CR (µm)	ICC (95%CI)	Mean difference (95%CI) (µm)	CR (µm)
Group A	0.996 (0.985-0.999)	2.9 (1.1-4.8)	8.8	0.989 (0.975-0.995)	2.0 (-2.4-6.4)	21.2
Group B	0.989 (0.973-0.996)	-4.2 (-9.3-1.0)	22.1	0.984 (0.961-0.993)	-4.5 (-13.0-4.1)	36.8
Group C	0.996 (0.991-0.998)	-0.5 (-4.4-3.4)	18.0	0.982 (0.958-0.992)	-0.6 (-10.7-9.5)	46.8
Overall	0.995 (0.991-0.997)	-0.3 (-2.4-1.8)	17.5	0.985 (0.975-0.990)	-0.8 (-5.1-3.6)	35.9
Non-agreement	0.981 (0.912-0.996)	6.3 (-4.9-17.4)	26.1	0.927 (0.686-0.985)	4.4 (-21.3-30.0)	60.1

ICC: Intraclass correlation coefficient; CI: Confidence interval; CR: Coefficient of repeatability; ChT: Choroidal thickness.

(36 males) was 54.4 (±15)y (range 20-76). Eighty-two EDI OCT images from both eyes of the 46 subjects were included in this study. In this group, EDI OCT scans could not be obtained from one of the eyes of 10 patients due to poor fixation. On clinical examination, 24 eyes were graded with M1 diabetic maculopathy and 1 eye had M0.5 maculopathy^[9]. Five OCT scans passing through the fovea showed intraretinal fluid. There was no statistically significant difference in ChT measurements between the scans with maculopathy and without maculopathy ($P>0.05$, data not shown). The visual acuity (logMAR) was -0.01 (±0.11). In the pilot study on 12 eyes of 12 healthy volunteers (one eye per subject), the inter- and intra-observer agreements on the choroidal posterior boundary classification were $\kappa=0.42$ and $\kappa=1$, respectively. The ICC for inter-observer agreement on the total ChT on the scans in which the image classification was agreed was 0.960 [95% confidence interval (CI), 0.684-0.994] and 0.992 (95% CI, 0.972-0.998) for intra-observer agreement.

This protocol was then applied to the 82 EDI OCT images of the 46 diabetic subjects. The inter-observer agreement on the image classifications was $\kappa=0.66$ (95% CI, 0.53-0.79; $P<0.001$). Both observers agreed on the classification of 63 EDI OCT scans: 24 scans (38.1%) were classified as group A, 22 (34.9%) as group B, and 17 (27.0%) as group C. The intra-observer agreement on the image classification was $\kappa=0.86$ -95% CI, 0.76-0.95; $P<0.001$) where 74 EDI OCT scans were given the same classification: 26 scans (35.1%) group A, 21 scans (28.4%) group B, 24 scans (32.4%) group C and 3 scans (4.1%) were ungradable.

There were excellent inter- and intra-observer agreements of ChT measurements in patients with diabetes on both, the total

ChT and subfoveal ChT, for scans that received the same classification from the observers. The inter-observer ICC values ranged from 0.963 to 0.985 with an overall ICC value of 0.972 (95% CI, 0.944-0.985) for the total ChT and from 0.916 to 0.986 with an overall ICC of 0.949 (95% CI, 0.900-0.972) for subfoveal ChT (Table 1). The ICC for intra-observer measurement agreement ranged from 0.989 to 0.996 with the overall ICC value of 0.995 (95% CI, 0.991-0.997) for the total ChT and 0.982 to 0.989 with the overall ICC of 0.985 (95% CI, 0.975-0.990) for subfoveal ChT (Table 2). The EDI OCT scans classified as group A showed greater reliability for both the total ChT and subfoveal ChT (as shown by the ICC value) than those EDI OCT scans containing less identifiable structures (groups B and C).

Figure 3 shows Bland and Altman plots of the inter-observer and intra-observer differences versus the mean of total ChT for each EDI OCT image classification. Figure 4 shows Bland and Altman plots^[10] of the inter-observer and intra-observer differences versus the mean of subfoveal ChT for each image classification. The inter-observer CRs for the total ChT in EDI OCT scans classified as group A, B and C were 14.1 µm, 40.7 µm and 41.4 µm respectively with an overall CR value of 33.1 µm. The intra-observer CRs for the total ChT were 8.8 µm, 22.1 µm and 18.0 µm for groups A, B and C respectively with an overall CR value of 17.5 µm. The inter- and intra-observer CRs of the subfoveal ChT were approximately 2 times higher than those of the total ChT in each image classification (Tables 1, 2).

DISCUSSION

Measuring the ChT has proven to be challenging, as there is a considerable variation in the transitional zone between the

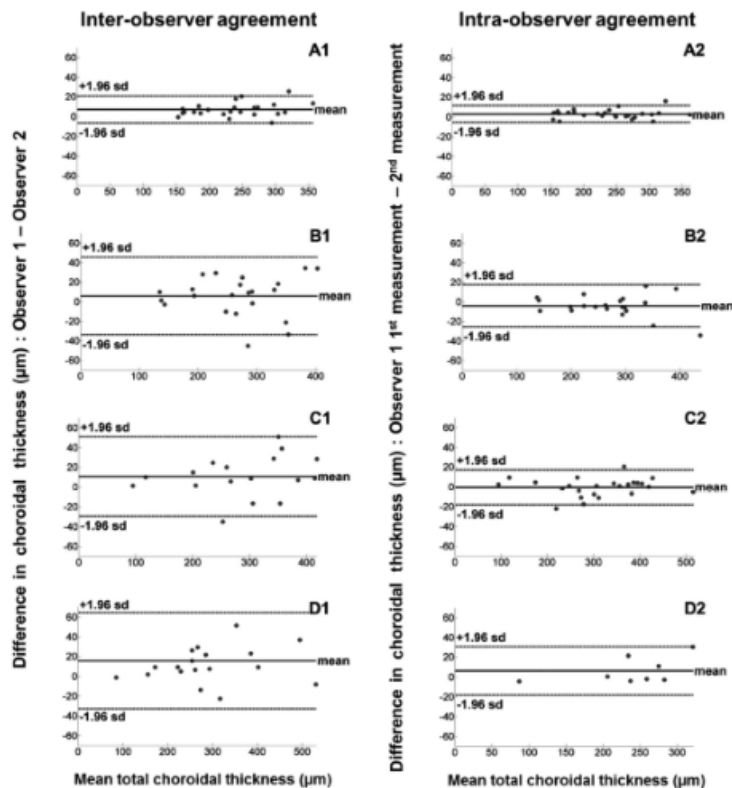


Figure 3 Bland-Altman plots showing inter-observer (right hand column) and intra-observer agreements (left hand column) with mean difference (thick line) and 95% limits of agreement (dashed lines) for the total ChT measurements by classification A1, A2: Group A; B1, B2: Group B; C1, C2: Group C; D1, D2: Non-agreement.

outer choroidal boundary and the sclera even in the absence of pathology. A clear standardized definition of the limits of the outer boundary of the choroid on EDI OCT images is needed in order to allow a comparison across clinical studies as this can affect the reliability of measurements, especially for those scans taken from diseased eyes.

To address this issue, we have developed a standardized protocol based on the presence and/or absence of the SCS and the CSI, seen as the hypo-reflective and the hyper-reflective bands respectively at the outer boundary of an EDI-OCT image. Using these criteria, we have classified the images into 4 groups: A, B, C and ungradable. To our knowledge this detailed descriptive definition of the outer boundary of the choroid has not been reported previously. We have demonstrated good agreement in grading the images by using the proposed protocol and excellent user concordance in evaluating the ChT on images taken from healthy eyes and those taken from eyes with diabetes. Additionally, although a single horizontal EDI OCT line scan passing through the center of the fovea was used in this

study, our standardized definitions of the choroidal outer boundaries could also be applied for the volumetric analysis of the choroid since the protocol has accounted for irregularities of the choroidal outer boundary.

The variation in the topographic appearances of the choroidal posterior boundary has been known to affect ChT measurements. An example of the variation of the topographic appearances was shown by Maul *et al*^[13], who graded the EDI OCT images obtained from glaucoma subjects using the criteria of presence or absence of CSI. Their results suggested a significant association between the variability in appearance of the choroidal outer boundary and the ChT measurement. The results presented in this study not only show an agreement with those presented by Maul *et al*^[13] but also suggest that the variability of the choroidal outer boundary affect the reliability of the total ChT and subfoveal ChT measurements. In particular, there was a relatively large variation in the choroidal measurement agreement found in the group of scans in which the choroidal outer boundary structure was less visible (groups B and C).

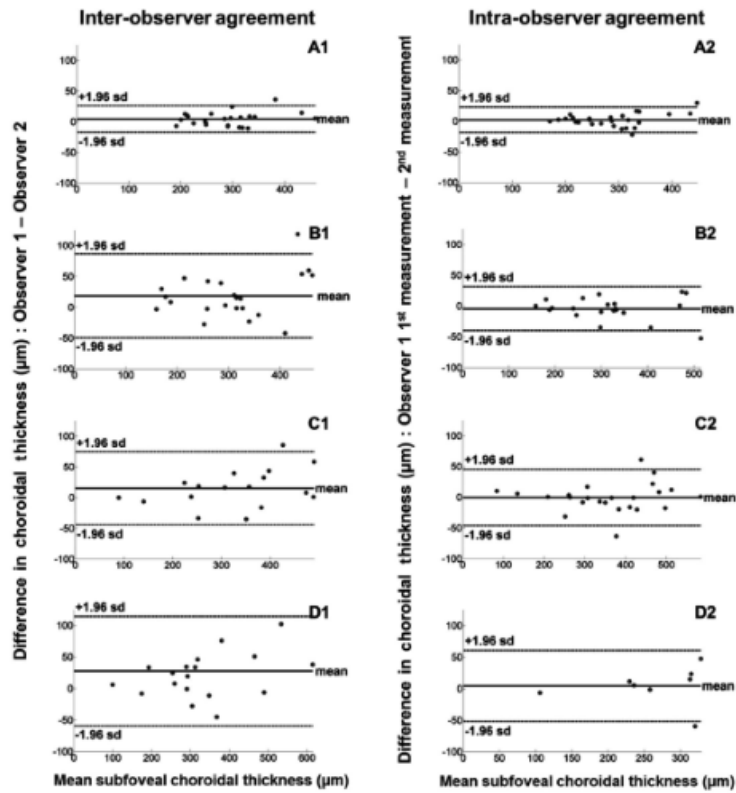


Figure 4 Bland–Altman plots showing inter–observer (right hand column) and intra–observer agreements (left hand column) with mean difference (thick line) and 95% limits of agreement (dashed lines) for ChT measurements at the foveal center by classification A1, A2: Group A; B1, B2: Group B; C1, C2: Group C; D1, D2: Non-agreement.

Other factors that may influence the ability to visualize the choroidal posterior boundary include patients' fixation and the type of commercial OCT instruments used. There is a wide variation in the reports: Using Cirrus OCT, Ho *et al*^[21] could measure the ChT in 90% of the scans while Manjunath *et al*^[22] could delineate the choriocleral boundary from only 34 of 46 (74%) of the OCT scans. Using Heidelberg Spectralis OCT, previous reports have shown variations between 92% and 96% as reported by Kim *et al*^[23] and Mwanza *et al*^[24] respectively.

In order to be used in a clinical setting, manual ChT measurements require adequate inter- and intra-observer agreements. In healthy subjects, Spaide *et al*^[4] previously reported a high inter-observer correlation of 34 eyes from 17 healthy volunteers ($r > 0.90$). Rahman *et al*^[25] showed high intra-observer, inter-observer and intra-session correlations on ChT measurements. In subjects with diabetes, the inter-observer correlation of the ChT has been reported at 0.81 using Heidelberg Spectralis OCT^[24]. These authors, however, only reported the measurement agreement at the

central fovea whereas in our study we have used the entire length of the scan. Another important point to note is that the majority of the studies published report the ChT measurement reliability using Pearson's correlation coefficient^[4,22,25,26]. Pearson's correlation coefficient only illustrates the linear association of two variables but not the agreement between the measurements^[27,28] and thus, it would be inappropriate to use Pearson's coefficient. Inappropriate statistical methods used for assessing the reliability may be misleading and lead to unreliable conclusions. In this study we have used the ICC and the kappa coefficient, which are the most appropriate methods to measure the reliability of continuous and categorical data respectively^[20,27]. We have shown that higher measurement agreements can be achieved using our measurement protocol for both healthy eyes and eyes with diabetes (all ICC > 0.9).

CR has also been used to determine the agreement of the ChT measurement. A previous study has reported that the CR of manual caliper measurements on the subfoveal ChT in healthy eyes is 23.3 µm (95% CI, 18.7-27.9 µm) for

Standardizing choroidal thickness measurements

intra-observer and $>32.1 \mu\text{m}$ (95% CI, 30.0–4.9 μm) for inter-observer agreements [25]. In patients with chorioretinal diseases, the CRs were shown to increase from the normal range. This may suggest that the variability of ChT measurements increase as the choroidal outer boundary becomes less recognizable due to the changes in the ChT or retinal structures. The inter-observer CR values at the center of the fovea in patients with nonexudative AMD, exudative AMD, polypoidal choroidal vasculopathy (PCV) and CSCR ranged between 24–26 μm , 30–36 μm , 39–45 μm and 46–50 μm respectively [29]. We have shown that in patients with DR, the inter-observer CR at the central foveal ChT was 54 μm using our proposed measurement protocol. This result was comparable to that obtained by Sim *et al* [30] who reported the CR for inter-observer agreement on the subfoveal ChT was 53 μm . The inter-observer CR for the total ChT obtained using our measurement protocol, however, provided a much smaller CR value than that obtained by Sim *et al* [30] (33 μm vs 42 μm) which is an indication of a better agreement between observers for the total ChT.

The intra-observer CRs for ChT measurements in diabetic patients were generally smaller than the inter-observer CRs. The intra-observer CRs obtained were 18 μm for the total ChT and 36 μm for subfoveal ChT. These results agree with those of previous investigations on the ChT measurement in other retinal diseases, such as AMD and CSCR [30]. Although these intra-observer CRs were better compared to a previous report [30] (26 μm for total ChT and 48.3 μm for the subfoveal ChT), it is difficult to make a comparison between our CRs and those provided by the previous reports for several reasons: firstly, these reports did not take into account the topographical variation in the outer boundary of the choroid on EDI OCT images and secondly, the number of points measured and the methods used to measure the ChT were different. Our measurements include the extra vascular layers of the choroid into the measurements while other protocols may fail to include the extra vascular choroidal structure.

Our results have also shown that the CR values increased for both, the inter- and intra-observer measurements as the choroidal outer boundary becomes less identifiable (with the smallest in group A). This suggests a direct impact of the image qualities on the thickness measurements. Hence great care needs to be taken while interpreting the results of the studies that do not report image quality parameters at the outset. This can also have implications in obtaining meaningful results for example while comparing the ChT measurements pre- and post-treatment. In addition, automation techniques for the segmentation of the choroid are becoming an active research topic [31–33]. To evaluate the performance of these automatic techniques, the manual annotations by experts are usually used as a reference

standard. Thus, our standardized protocol can be used to study the reliability and accuracy of the automatic techniques.

In conclusion, we have introduced standardized definitions of the outer and inner boundaries of the choroid in EDI OCT images and we have demonstrated its significance in accurate measurements of ChT.

ACKNOWLEDGEMENTS

Foundation: Supported by Foundation for the Prevention of Blindness.

Conflicts of Interest: Boonarpa N, None; Zheng Y, None; Stangos AN, None; Lu H, None; Raj A, None; Czanner G, None; Harding SP, None; Nair –Sahni J, None.

REFERENCES

- 1 Luty G, Grunwald J, Majji AB, Uyama M, Yoneya S. Changes in choriocapillaris and retinal pigment epithelium in age-related macular degeneration. *Mol Vis* 1999;5:35–38
- 2 Imamura Y, Fujiwara T, Margolis R, Spaide RF. Enhanced depth imaging optical coherence tomography of the choroid in central serous chorioretinopathy. *Retina* 2009;29(10):1469–1473
- 3 Vujosevic S, Martini F, Cavazzera F, Pilotto E, Midena E. Macular and peripapillary choroidal thickness in diabetic patients. *Retina* 2012;32(9):1781–1790
- 4 Spaide RF, Koizumi H, Pozzoni MC. Enhanced depth imaging spectral-domain optical coherence tomography. *Am J Ophthalmol* 2008;146(4):496–500
- 5 Mansouri K, Medeiros FA, Marchese N, Tatham AJ, Auerbach D, Weinreb RN. Assessment of choroidal thickness and volume during the water drinking test by swept-source optical coherence tomography. *Ophthalmology* 2013;120(12):2508–2516
- 6 Fong AHC, Li KKW, Wong D. Choroidal evaluation using enhanced depth imaging spectral-domain optical coherence tomography in vogt-koyanagi-harada disease. *Retina* 2011;31(3):502–509
- 7 Fujiwara T, Imamura Y, Margolis R, Slakter JS, Spaide RF. Enhanced depth imaging optical coherence tomography of the choroid in highly myopic eyes. *Am J Ophthalmol* 2009;148(3):445–450
- 8 Reibaldi M, Boscia F, Avitabile T, Uva MG, Russo V, Zagari M, Bonfiglio V, Reibaldi A, Longo A. Enhanced depth imaging optical coherence tomography of the choroid in idiopathic macular hole: a cross-sectional prospective study. *Am J Ophthalmol* 2011;151(1):112–117
- 9 Fujiwara A, Shiragami C, Shirakata Y, Manabe S, Izumibata S, Shiraga F. Enhanced depth imaging spectral-domain optical coherence tomography of subfoveal choroidal thickness in normal Japanese eyes. *Jpn J Ophthalmol* 2012;56(3):230–235
- 10 Margolis R, Spaide RF. A pilot study of enhanced depth imaging optical coherence tomography of the choroid in normal eyes. *Am J Ophthalmol* 2009;147(5):811–815
- 11 Ding X, Li J, Zeng J, Ma W, Liu R, Li T, Yu S, Tang S. Choroidal thickness in healthy chinese subjects. *Invest Ophthalmol Vis Sci* 2011;52(13):9555–9560
- 12 Remington LA. Uvea. In Remington LA, ed. *Clinical Anatomy and Physiology of the Visual System* 3rd ed. Saint Louis: Butterworth-Heinemann;2012:40–60
- 13 Maul EA, Friedman DS, Chang DS, Boland MV, Ramulu PY, Jampel HD, Quigley HA. Choroidal thickness measured by spectral domain optical

- coherence tomography factors affecting thickness in glaucoma patients. *Ophthalmology* 2011;118(8):1571-1579
- 14 Branchini L, Regatieri CV, Flores-Moreno I, Baumann B, Fujimoto JG, Duker JS. Reproducibility of choroidal thickness measurements across three spectral domain optical coherence tomography systems. *Ophthalmology* 2012;119(1):119-123
- 15 Inamura Y, Iida T, Maruko I, Zweifel SA, Spaide RF. Enhanced Depth Imaging Optical Coherence Tomography of the Sclera in Dome-Shaped Macula. *Am J Ophthalmol* 2011;151(2):297-302
- 16 Younis N, Broadbent DM, Harding SP, Vora JR. Prevalence of diabetic eye disease in patients entering a systematic primary care-based eye screening programme. *Diabet Med* 2002;19(12):1014-1021
- 17 Sahni J, Stanga P, Wong D, Harding S. Optical coherence tomography in photodynamic therapy for subfoveal choroidal neovascularisation secondary to age related macular degeneration: a cross sectional study. *Br J Ophthalmol* 2005;89(3):316-320
- 18 Landis JR, Koch GG. The measurement of observer agreement for categorical data. *Biometrics* 1977; 33(1):159-174
- 19 Bland JM, Altman DG. Statistical methods for assessing agreement between two methods of clinical measurement. *Lancet* 1986;1 (8476): 307-310
- 20 Fleiss JL. Reliability of Measurement. *The Design and Analysis of Clinical Experiments* Hoboken, NJ, USA, John Wiley & Sons Inc.:1999; 1-32
- 21 Ho J, Branchini L, Regatieri C, Krishnan C, Fujimoto JG, Duker JS. Analysis of normal peripapillary choroidal thickness via spectral domain optical coherence tomography. *Ophthalmology* 2011;118(10):2001-2007
- 22 Manjunath V, Taha M, Fujimoto JG, Duker JS. Choroidal thickness in normal eyes measured using Cirrus HD optical coherence tomography. *Am J Ophthalmol* 2010;150(3):325-329
- 23 Kim M, Kim SS, Kwon HJ, Koh HJ, Lee SC. Association between choroidal thickness and ocular perfusion pressure in young, healthy subjects: enhanced depth imaging optical coherence tomography study. *Invest Ophthalmol Vis Sci* 2012;53(12):7710-7717
- 24 Mwanza JC, Hochberg JT, Banitt MR, Feuer WJ, Budenz DL. Lack of association between glaucoma and macular choroidal thickness measured with enhanced depth-imaging optical coherence tomography. *Invest Ophthalmol Vis Sci* 2011;52(6):3430-3435
- 25 Rahman W, Chen FK, Yeoh J, Patel P, Tufail A, Da Cruz L. Repeatability of manual subfoveal choroidal thickness measurements in healthy subjects using the technique of enhanced depth imaging optical coherence tomography. *Invest Ophthalmol Vis Sci* 2011;52(5):2267-2271
- 26 Querques G, Lattanzio R, Querques L, Del Turco C, Forte R, Piaro L, Souied EH, Bandello F. Enhanced depth imaging optical coherence tomography in type 2 diabetes. *Invest Ophthalmol Vis Sci* 2012;53(10): 6017-6024
- 27 Bartko JJ. Measurement and reliability: statistical thinking considerations. *Schizophrenia Bull* 1991;17(3):483-489
- 28 Bland JM, Altman DG. Measuring agreement in method comparison studies. *Stat Methods Med Res* 1999;8(2):135-160
- 29 Kim JH, Kang SW, Kim JR, Kim SJ. Variability of subfoveal choroidal thickness measurements in patients with age-related macular degeneration and central serous chorioretinopathy. *Eye (Lond)* 2013;27(7):809-815
- 30 Sim DA, Keane PA, Mehta H, Fung S, Zarranz-Ventura J, Fruttiger M, Patel PJ, Egan CA, Tufail A. Repeatability and reproducibility of choroidal vessel layer measurements in diabetic retinopathy using enhanced depth optical coherence tomography. *Invest Ophthalmol Vis Sci* 2013;54(4): 2893-2901
- 31 Lu H, Boonarpa N, Kwong MT, Zheng Y. Automated segmentation of the choroid in retinal optical coherence tomography images. *Conf Proc IEEE Eng Med Biol Soc* 2013;2013: 5869-5872
- 32 Hu Z, Wu X, Ouyang Y, Ouyang Y, Sadda SR. Semiautomated segmentation of the choroid in spectral-domain optical coherence tomography volume scans. *Invest Ophthalmol Vis Sci* 2013;54(3):1722-1729
- 33 Zhang L, Lee K, Niemeijer M, Mullins RF, Sonka M, Abramoff MD. Automated segmentation of the choroid from clinical SD-OCT. *Invest Ophthalmol Vis Sci* 2012;53(12):7510-7519